Sedimentology and sediment dynamics in tidally dominated areas influenced by anthropogenic utilization

Fakultät für Mathematik und Naturwissenschaften der Carl von Ossietzky

Universität Oldenburg

zur Erlangung des Grades und Titels eines

Doktors der Naturwissenschaften (Dr. rer. nat.)

angenommene Dissertation von

Anna-Lena Geßner
Geboren am 30.05.1996 in Hamburg

Gutachter:	Dr. Thomas H. Badewien
Zweitgutachter:	Prof. Dr. Oliver Zielinski
Tag der Disputation:	19. Mai 2025

Für meinen Vater

Abstract

Climate change, coastal erosion and the need for effective flood protection present significant global challenges. In particular, vulnerable regions are exposed to extreme weather events, characterized by high population densities, sensitive ecosystems, or low elevations above sea level. Historically, hard coastal protection measures, such as groynes have been widely implemented to mitigate erosion and regulate hydrodynamic conditions. However, their long-term effects on hydrodynamics, sediment transport, and ecological systems, especially in tide-dominated environments, remain inadequately understood. Due to the increasing need for coastal protection infrastructure, a comprehensive understanding of its impacts and interactions with natural coastal processes is essential. This is particularly critical for the long-term planning of coastal defense strategies and the design of specific protection measures. The more accurately these effects are understood, the more reliable numerical simulations and predictive models become.

This study investigates the influence of coastal protection measures on sedimentology, hydrodynamics, and the distribution of contaminants. A tide-dominated inlet serves as a case study due to its complex system and variable hydrodynamic conditions.

The research focuses on the tidal inlet Harle, located along the German North Sea coast between the East Frisian Islands of Spiekeroog and Wangerooge. A prominent groyne extending from Wangerooge significantly alters the natural exchange between the North Sea and the Wadden Sea. Its influence on sediment transport processes and the morphological evolution of the tidal inlet is substantial, as the structure modifies current velocities and transport processes. To assess these changes, sedimentological analyses were conducted, identifying seven distinct surface facies within the Harle, which were classified into three spatially defined realms. A comprehensive facies map, derived from sediment samples and integrated multibeam backscatter data, illustrates the sedimentological development of the inlet in response to coastal protection measures. In order to create a comparison, the results for the Harle were compared with those of the Otzumer Balje, a neighboring tidal inlet that remains largely unaffected by anthropogenic interventions.

The results indicate that both tidal inlets undergo seasonal sediment redistributions driven by storm-induced transport and biological activity. The Otzumer Balje exhibits natural sedimentary dynamics, characterized by coarser material in summer and finer, mudflat-derived sediments in winter. In contrast, the Harle exhibits a more diverse composition of bioclastic sediments, including bryozoan-encrusted shell fragments, suggesting that the presence of the groyne has contributed to local more stable sedimentation patterns. Geomorphologically, the Otzumer Balje is distinguished by a single, dynamic main channel with an active subaquatic dune system, whereas the Harle features a two-channel system, shaped by localized erosion and deposition processes directly influenced by the groyne. Additionally, the Harle supports a more diverse benthic community, likely resulting from reduced sediment deposition in certain areas and the presence of habitat-forming species such as *Lanice conchilega*.

Beyond sedimentological and ecological changes, this study also examines the spatial distribution of heavy metal contamination in the Harle, highlighting the heterogeneity of sedimentary and geochemical properties. Grain size variations play a critical role in pollutant distribution, with fine-grained sediments accumulating higher concentrations of heavy metals, particularly in areas near the harbor and along shallow channels. While most heavy metals remain below Effect Range-Low thresholds, arsenic exhibits

significant enrichment, likely associated with pyrite-rich peat layers and anthropogenic inputs from industrial and agricultural sources. Hydrodynamic measurements near the groyne reveal altered current patterns, contributing to localized erosion, sediment redistribution, and the formation of depositional zones, which in turn affect the spatial distribution of contaminants.

Zusammenfassung

Im Zuge des Klimawandels stellen Küstenerosion und die Notwendigkeit eines wirksamen Hochwasserschutzes weltweit erhebliche Herausforderungen dar. Besonders betroffen sind Regionen, die von Extremwetterereignissen beeinflusst werden, eine hohe Bevölkerungsdichte haben, empfindlichen Ökosystemen umfassen oder eine geringe Höhe über dem Meeresspiegel aufweisen. Zum Schutz dieser Küsten wurden in der Vergangenheit häufig harte Küstenschutzmaßnahmen wie Buhnen eingesetzt, um Erosion zu verhindern und Strömungen zu regulieren. Ihre langfristigen Auswirkungen auf die Hydrodynamik, den Sedimenttransport und die Ökosysteme sind jedoch, insbesondere in tidedominierten Bereichen, noch unzureichend erforscht. Angesichts der zunehmenden Bedeutung von Küstenschutz ist ein umfassendes Verständnis der Auswirkungen und Wechselwirkungen mit der natürlichen Umwelt essenziell. Dies gilt insbesondere für die langfristige Planung von Küstenschutzmaßnahmen im Allgemeinen und den Bau spezifischer Schutzstrukturen im Besonderen. Je besser die Auswirkungen verstanden sind, desto präzisere Simulationen und Prognosen können erstellt werden.

Diese Studie untersucht daher den Einfluss von Küstenschutzmaßnahmen auf Sedimentologie, Hydrodynamik und Schadstoffverteilung. Als Fallstudie dient ein gezeitendominiertes Seegat, da es ein komplexes System mit wechselnden hydrodynamischen Bedingungen darstellt.

Im Fokus steht das Seegat Harle, das an der deutschen Nordseeküste zwischen den Ostfriesischen Inseln Spiekeroog und Wangerooge liegt. Eine markante Buhne auf Wangerooge ragt in das Seegat hinein und beeinflusst den natürlichen Austausch zwischen der Nordsee und dem Wattenmeer erheblich. Insbesondere die Sedimenttransportprozesse und die Morphologie des Seegats sind betroffen, da die Buhne einen großen Einfluss auf die Strömung und damit auf den Stofftransport hat. Um diese Veränderungen zu erfassen, wurden sedimentologische Analysen durchgeführt. Dabei konnten sieben unterschiedliche Oberflächenfazies in der Harle identifiziert werden, die sich drei spezifischen Bereichen zuordnen lassen. Eine umfassende Fazieskarte, basierend auf Sedimentproben und der Integration von Multibeam-Daten, verdeutlicht die sedimentologische Entwicklung des Seegats als Folge der Küstenschutzmaßnahmen. Zur besseren Einordnung der Ergebnisse wurde die Harle mit der Otzumer Balje, einem weitgehend unbeeinflussten benachbarten Seegat, verglichen.

Die Ergebnisse zeigen, dass beide Seegatten saisonalen Sedimentverlagerungen unterliegen, die durch sturmbedingten Transport und biologische Aktivitäten gesteuert werden. Die Otzumer Balje weist eine natürliche Sedimentdynamik auf, mit gröberem Material im Sommer und feinkörnigen, teils aus Schlickwatt stammenden Sedimenten im Winter. Im Gegensatz dazu zeigt die Harle eine größere Vielfalt bioklastischer Sedimente, darunter Schalenfragmente die mit Bryozoen bewachsen sind, was auf stabilere Sedimentationsbedingungen durch die Buhnenkonstruktion hindeutet. Geomorphologisch unterscheidet sich die Otzumer Balje durch einen einzelnen, dynamischen Hauptkanal mit aktiven subaquatischen Dünen, während die Harle ein zweikanaliges System aufweist, das durch strömungsbedingte Erosion und Sedimentation im direkten Bereich der Buhne beeinflusst wird. Zudem unterstützt die Harle eine vielfältigere Benthos-Gemeinschaft, was auf eine geringere Sedimentation in einigen Bereichen und das Vorkommen habitatbildender Organismen wie *Lanice conchilega* zurückzuführen ist.

Neben den sedimentologischen und ökologischen Veränderungen untersucht diese Studie auch die Verteilung von Schwermetallkontaminationen in der Harle und hebt die

räumliche Heterogenität sedimentärer und chemischer Eigenschaften hervor. Variationen in der Korngröße beeinflussen die Schadstoffverteilung, wobei feinkörnige Sedimente in Hafennähe und entlang flacher Kanäle höhere Schwermetallkonzentrationen aufweisen. Während die meisten Schwermetalle unter den Grenzwerten bleiben, zeigt Arsen eine signifikante Anreicherung. Diese wird mit pyritreichen Torfschichten sowie anthropogenen Einträgen aus Industrie und Landwirtschaft in Verbindung gebracht. Hydrodynamische Messungen nahe der Buhne verdeutlichen veränderte Strömungsmuster, die zu lokaler Erosion, Sedimentumlagerung und der Bildung von Ablagerungszonen führen und somit auch die Schadstoffverteilung beeinflussen.

Table of content

Chapter 1

General introduction

Coastal areas are among the most densely populated regions globally, rendering them particularly vulnerable to the impacts of climate change, particularly rising sea levels. Coastal population densities are significantly elevated compared to inland areas. For example, approximately 41% of the European population resides within coastal zones (European Environment Agency, 2020). This demographic concentration has facilitated extensive development of critical socioeconomic infrastructure, including harbors, industrial complexes, and agriculture, many of which are strategically positioned near coastlines to capitalize on maritime access.

However, these assets are increasingly at risk by climate-induced stressors. Projections indicate a rise in the frequency and intensity of extreme weather events, such as hurricanes and storm surges, which exacerbate vulnerabilities in these regions. Catastrophic storm surges, in particular, pose substantial risks to coastal settlements, infrastructure, and ecosystems, frequently culminating in significant physical damage, accelerated erosion, and irreversible land loss (Bouwer, 2019; McGregor et al., 2005).

Efforts to protect coastal settlements and populations from storm surges have a long and well-documented history. Complex protective structures have been recorded in regions such as the Mediterranean, China, and Japan since the Middle Ages (Pranzini, 2018). Along the North Sea coast, the earliest artificial coastal protection strategies were dwelling mounds, or terps, constructed along the lowland coasts of the Netherlands, Germany, and Denmark. These mounds were progressively enhanced to address rising sea levels, with their use documented as far back as Roman times, including references by Pliny the Elder (Niemeyer et al., 2011). Today, these dwelling mounds, known locally as Warften, remain iconic landmarks along the North Sea coast. In some instances, they continue to serve as functional flood protection measures. Over time, various strategies for coastal protection have been implemented, broadly categorized into hard protection measures and soft protection measures (Fig. 1.1).

Hard protection measures, such as dikes and seawalls, are well-established solutions designed to mitigate flooding along coastlines and riverbanks. These structures serve as physical barriers, protecting inland areas from storm surges and tidal inundation. Breakwaters, a form of hard protection, are constructed to shield harbor berths, maneuvering zones, and port facilities from extreme wave action by dissipating wave energy through wave breaking or partial reflection back to the sea. In shallow waters near beaches, breakwaters are often deployed to reduce wave energy, thereby minimizing sand erosion and preserving beach stability (Fairley et al., 2009; Lorenzoni et al., 2016; Pranzini et al., 2018).

Groynes are another common hard protection measure. These elongated, shore-perpendicular structures, typically made of timber, concrete, or rock, extend from the beach into the water. Their primary purpose is to interrupt longshore sediment transport and mitigate beach erosion. Beach groynes are designed to trap littoral drift sediment and prevent sand loss from beaches, whereas stream groynes are installed in areas with strong currents to control erosion forces by modifying current flow (Kunz, 1997; Wheeler et al., 2010). The blockage caused by a groyne typically results in sediment accretion on the updrift side and erosion on the downdrift side. To manage these effects, groynes are often installed in sequences, forming groyne fields. Proper design of groynes, including their length, height, and permeability, is critical to their effectiveness. Short groynes are ineffective at retaining sediment due to bypassing at their tips, while excessively long or impermeable groynes can obstruct sediment flow to downdrift areas, causing severe erosion (Coghlan et al., 2013; Hanson et al., 2009; Valsamidis and Reeve, 2020).

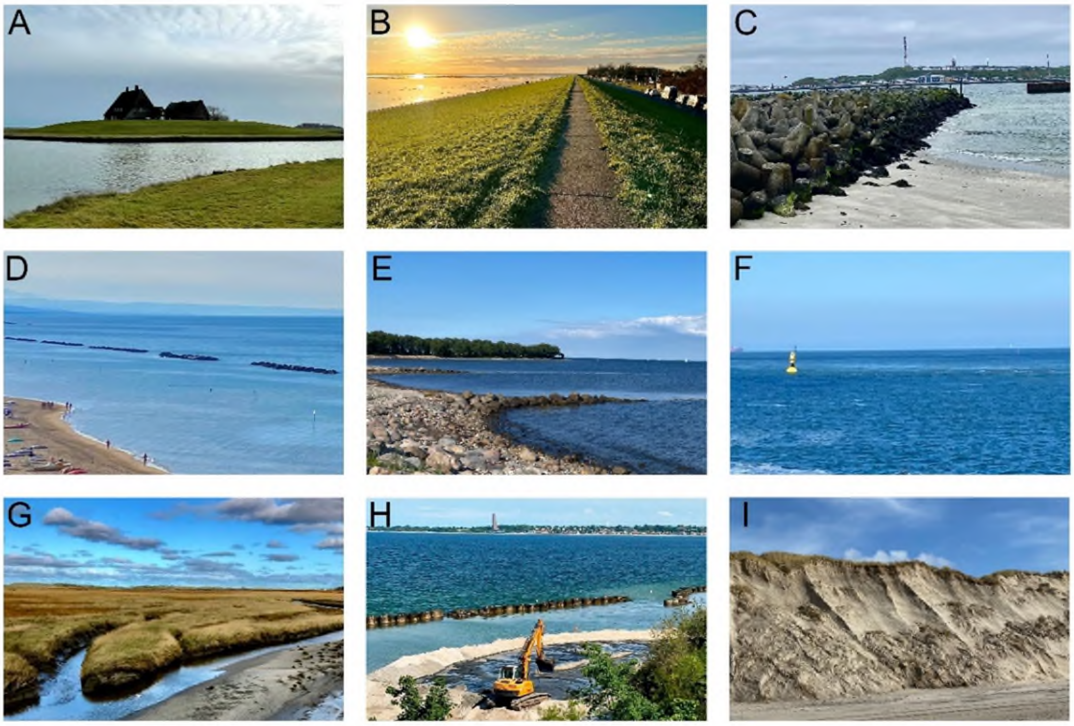

Figure 1.1: Illustration of various examples of coastal protection strategies. Panel A depicts a dwelling mound (terp/warft) on the island of Hallig Hooge in the German North Sea, showcasing a traditional method of flood resilience. Panel B shows a dike along the German North Sea coast, representing a primary hard protection measure against coastal flooding. Panel C features a breakwater installation protecting the harbor of Heligoland Island in the German North Sea. Panel D illustrates a breakwater formation in shallow waters off a beach along the Italic Adriaic Sea, designed to reduce wave energy. Panel E highlights a groyne field along a Baltic Sea beach, implemented to minimize sediment drift and support beach stabilization. Panel F depicts a submerged stream groyne with a yellow head buoy along the German North Sea coast on the island of Wangerooge, showcasing measures to regulate water flow. Panel G shows an active saltmarsh along the Eiderstedt Peninsula in the German North Sea, demonstrating nature-based protection strategies. Panel H illustrates beach nourishment as a soft protection measure along a Baltic Sea beach in Kiel, Germany. Panel I presents a dune formation along the Danish coastline, after a storm surge in 2020, as an example of natural coastal defense enhancement.

Soft coastal protection strategies focus on working with natural processes to reduce flooding and erosion. These strategies often aim to enhance or restore natural habitats while providing coastal protection, particularly because human activities have significantly degraded coastal environments on a global scale. Thus, overfishing and dredging have profoundly altered marine ecosystems, leading to reduced biodiversity and the depletion of critical marine resources (Coleman and Williams, 2002; Erftemeijer and Lewis, 2006; Lee et al., 2010; Lotze, 2007; Perissi et al., 2017; Robinson et al., 2005; Stronkhorst et al., 2003; Vikas and Dwarakish, 2015). Globalization has further intensified these issues, particularly with the rise of invasive species. Alien species, often transported via ship hulls or ballast water, establish themselves in new regions, outcompeting native species and disrupting local ecosystems (Hulme et al., 2008; Sanchirico et al., 2009; Turbelin et al., 2022). The necessity for integrative coastal management practices that address both environmental and socio-economic drivers, respectively, is to be addressed by soft management measures.

The implementation of soft protection measures, such as beach nourishment involves adding sand to beaches to replace material lost through erosion. While effective, beach nourishment requires regular maintenance, as strong erosion forces can displace the added sand over time (Hanson et al., 2002). Salt marsh restoration reduces wave energy and erosion through the friction created by the rough surface of the salt marsh (Adam, 2019; Castagno et al., 2021; Currin et al., 2017). Dune stabilization protects the mainland from flooding by maintaining and strengthening natural dune systems. Dune chains act as buffers against storm surges and waves. Stabilization techniques include installing fences to reduce wind erosion, using artificial sand traps, or planting vegetation such as *Ammophila arenaria* (marram grass), which stabilizes dunes by trapping sediment and anchoring it with roots (Durán and Moore, 2013; Sigren et al., 2014).

Soft coastal protection measures are widely recognized for their ecological benefits, including the enhancement of biodiversity, habitat restoration, and the reinforcement of natural processes that mitigate coastal erosion and flooding. Despite these advantages, their efficacy is often limited in high-risk areas where immediate and robust protection is critical. In such scenarios, soft protection strategies typically require integration with either additional soft measures or engineered hard protection structures to provide comprehensive and reliable defense against extreme events.

However, the reliance on hard coastal defenses, while effective in providing immediate and dependable protection, introduces significant and insufficiently understood long-term environmental consequences. Hard coastal protection measures are hypothesized to exert adverse impacts on coastal ecosystems by disrupting natural sedimentary and hydrodynamic processes, as well as natural habitats (Morris et al., 2018). While short-term effects, such as localized changes, are typically more observable and manageable, the systemic consequences of hard protection measures, such as permanent alterations to hydrological, sedimentary, and ecological dynamics, are complex and difficult to predict. In particular, how the altered dynamics will affect the environment in the long term? These challenges highlight the critical need for a more nuanced and integrated understanding of the ecological trade-offs associated with hard protection measures, especially in their interconnected and cumulative interactions.

The North Sea Coast is a distinctive laboratory for case studies due to its complexity and dynamic geology and hydrodynamics. Understanding the interplay between these natural systems and the anthropogenic interventions along this coastline requires a thorough insight of its unique geological and hydrodynamic background. The Wadden Sea, located in the back-barrier region of protective islands within the Southern North Sea, is recognized as a UNESCO Natural Heritage site. In this ecologically sensitive region, it is particularly important to implement coastal protection strategies that can enhance and sustain ecosystem resilience while also assessing the impacts of recent strategies.

1.1 Geological background of the Southern North Sea

During the Pliocene and Pleistocene epochs, the North Sea Basin experienced alternating phases of regression during glacial periods and transgression during interglacial periods. The sedimentary sequences from this time are marked by transitions between glacio-fluvial and marine deposits. Advancing ice sheets caused significant erosion, while meltwater runoff carved anastomosing valleys that were subsequently infilled with meltwater deposits, intersecting the pre-existing marine sediments (Eisma et al., 1981; Phillips et al., 2017; Streif, 1989).

During the Holocene, rising sea levels driven by the permanent melting of ice sheets and eustatic adjustments led to widespread transgression. This process began with the erosion of surface sediments and was followed by the deposition of marine sediments, reshaping the basins stratigraphy and facilitating the landward migration of the coastline (Behre and Menke, 1969; Streif, 1989). Offshore, fine- to medium-grained sands were deposited under high-energy conditions, forming the foreshore zone and shaping the dynamic sedimentary environment of the region. Further inland, the sedimentary sequence is dominated by sand and clay deposits associated with tidal flats, overlain by peat layers formed in coastal bogs. These peat layers are intersected by gully deposits associated with tidal flats (Chang et al., 2006; Streif, 1989; Streif, 1990). The development of fen peat occurred as a result of rising groundwater levels. Streif (2004) identified a stratigraphic sequence along the Southern North Sea coast comprising six distinct peat layers, each separated by interbedded clastic coastal sediments, reflecting alternating phases of sedimentation and peat formation driven by coastal dynamics and hydrological changes.

Outcrops along the coastline provided the basal Pleistocene structure for most barrier islands. Sedimentation and wave action facilitated the formation of spit bars along the outcrops, which were subsequently stabilized by vegetation. The presence of vegetation on these spit bars enhanced sediment retention, promoting the accumulation of material and leading to the development of dune systems. As the tidal amplitude transitioned from microtidal to mesotidal conditions, these spit bars evolved into elongated, detached barrier islands (Streif, 1989; Niemeyer, 1995).

The shape of islands in the Southern North Sea is largely determined by tidal amplitude (Fig. 1.2). The West Frisian Islands of the Netherlands and the East Frisian Islands along the German coast are influenced by mesotidal conditions, resulting in the development of elongated barrier islands. Farther north, in the innermost part of the German Bight, between Jade Bay and the Eider Estuary, macrotidal conditions prevail, resulting in rounded to crescent-shaped islands. Moving further north, the tidal amplitude decreases again to mesotidal conditions, leading to the elongated morphology of the North Frisian Islands (Streif, 1989).

The complex interplay of semidiurnal tides, wave dynamics, and coastal currents further drives the widening of tidal inlets, enhancing the morphological complexity of the coastal system (Eitner, 1996b; FitzGerald et al., 1988; Lüders, 1952; Niemeyer, 1995; Sha, 1989; Streif, 1989). The interaction between the natural longshore current in the North Sea and tidal currents generates an eastward littoral drift. This drift leads to the continuous redeposition of sediments and drives the eastward migration of the West and East Frisian Islands. Additionally, catastrophic storm surges during the Middle Ages caused significant erosion, mainland land loss, the fragmentation and separation of island and landmasses. These relict sediments have served as a sediment source for islands located east of the relict sands, facilitating the general eastward migration of the barrier islands along the Southern North Sea.

In areas lacking relict sediments, the western parts of the islands are more susceptible to erosion, with the resulting material being transported eastward and redeposited. This eastward erosion is primarily influenced by the dynamics of inlet channels. During high tide, the longshore drift is interrupted, leading to the formation of a circulation cell that exposes the western beaches of the islands to increased erosion. The proximity of these channels to the western ends of the islands directly affects the intensity of erosion, with shorter distances resulting in stronger erosive forces (Eitner, 1996b; Fleming and Davies, 1994; Homeier, 1973; Kunz, 1997; Luck, 1978; Lüders, 1952; Niemeyer et al., 1996; Witte, 1970).

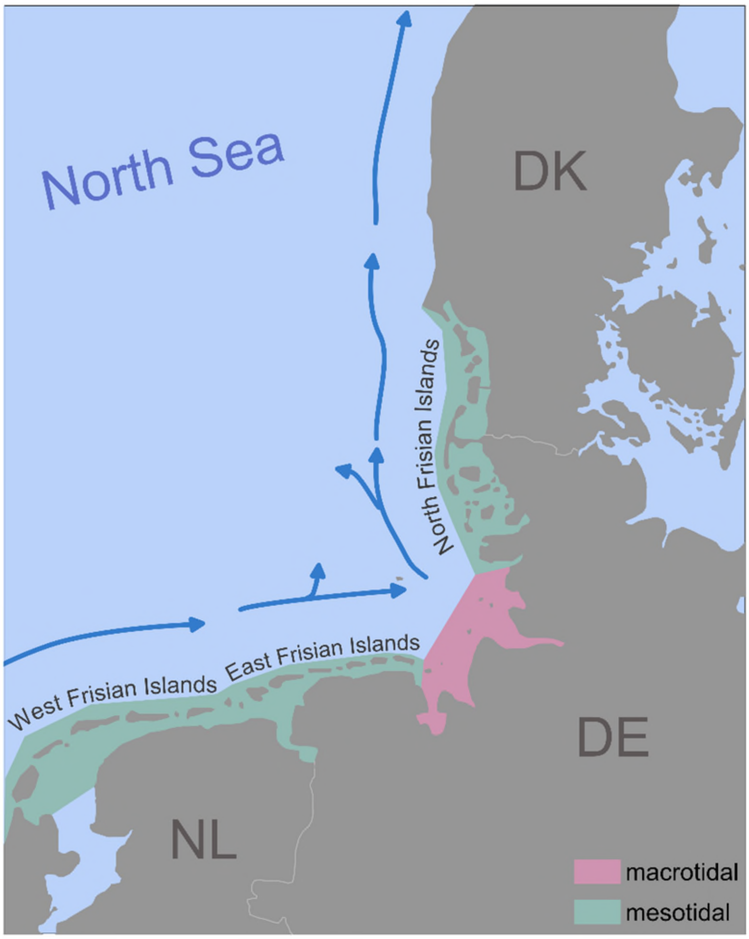

Figure 1.2: Map of the Southern North Sea and the relevant Frisian Islands. The prevailing coastal longshore currents are represented by blue arrows, while tidal conditions are indicated with mesotidal regions in green and macrotidal regions in red. NL: The Netherlands, DE: Germany, DK: Denmark.

To mitigate further erosion along the islands and limit the eastward migration, coastal protection measures have been implemented.

1.2 Hydrodynamics of the Southern North Sea

The North Sea is a shallow shelf sea, with water depths gradually increasing toward the north. In the German Bight, depths typically range from 20 to 40 meters, with maximum depths reaching approximately 58 meters near Heligoland. The relatively shallow depths in this area lead to the dominance of nearshore hydrodynamic processes. Consequently, the influence of large-scale oceanic circulations along the coastline is reduced. This results in a complex interplay of tidal forces, wind-driven currents, riverine inputs, and seasonal variations **(**Huthnance, 1991; Schramkowski et al., 2002).

The North Sea exhibits a general anticlockwise circulation pattern. Water enters through the Dover Strait, flows northeastward toward the German Bight, and then shifts northward, continuing toward the Skagerrak. Longshore transport along the coastline is strongly influenced by a semidiurnal tidal regime. Due to the influence of the Coriolis force, the Kelvin wave propagating through the Dover Strait undergoes an anticlockwise rotation around these amphidromic points. These amphidromic points located in the central Southern Bight, near the Netherlands, and the central North Sea, offshore Denmark, result in areas with low mesotidal to microtidal ranges. According to Hayes (1979), this is observed along the West Frisian Islands and the North Frisian Islands. Moving toward the German Bight, the tidal range increases (Fig. 1.2). Along the East Frisian Islands, the mean tidal range of 2.9 meters defines a mesotidal coast characterized by mixed energy dynamics, reflecting the combined influences of tidal forces and wave action (Huthnance, 1991; Ladage et al., 2007; Niemeyer, 1997).

The East Frisian Islands are separated by narrow tidal inlets, which facilitate the exchange of water between the North Sea and the tidal basins of the Wadden Sea. The tidal wave traverses these inlets at current velocities exceeding 1 ms^{-1} (Albinus et al., 2025, in prep). Stanev et al. (2003) demonstrated that tidal range significantly influences tidal flow asymmetry. Along the East Frisian Islands, this asymmetry manifests as ebb dominance, where the ebb flow is shorter in duration but stronger than the flood flow. The flood flow begins earlier in the tidal cycle and lasts longer, while the ebb flow occurs closer to slack water. This asymmetry is amplified during spring tides due to nonlinear and frictional effects (Stanev et al., 2007).

The hydrodynamic regime of the backbarrier basins is controlled by the tidal prism, which determines the exchange of water between the basin and the open North Sea. Small tidal prisms are associated with wave-dominated systems, where sediment transport is primarily driven by wave action, whereas larger tidal prisms correspond to tide-dominated environments with stronger bidirectional flows. The drainage of the backbarrier basin influences the distribution of sediment and the formation of tidal channels, which, in turn, affect the stability and morphology of the adjacent inlets.

For the East Frisian Islands, wind-driven waves generally propagate eastward, adding an eastward component to sediment transport and shaping the morphology of the ebb deltas. The tidal prism plays a crucial role in determining the orientation of these deltas. Westward-oriented ebb deltas are associated with large tidal prisms, while eastward-oriented deltas indicate wave dominance and are linked to smaller tidal prisms (Ladage et al., 2007; Nummedal and Penland, 1981; Sha, 1989).

Vertical density gradients arise from the lower salinity of the Wadden Sea water, which is influenced by terrestrial runoff. The gradients facilitate the downward movement of denser North Sea water beneath the less dense Wadden Sea water, resulting in an accelerated surface-layer flow (Burchard and Badewien, 2015).

Coastal defense structures constructed along the western sides of the islands aim to mitigate erosion and prevent the littoral drift that erodes the western parts of the islands (Fig. 1.3). However, these structures modify current patterns and sediment transport dynamics, altering the natural sedimentology and morphology of the tidal inlets and basins. The construction of hard coastal protection measures tends to reduce the tidal prism of the Harle Inlet.

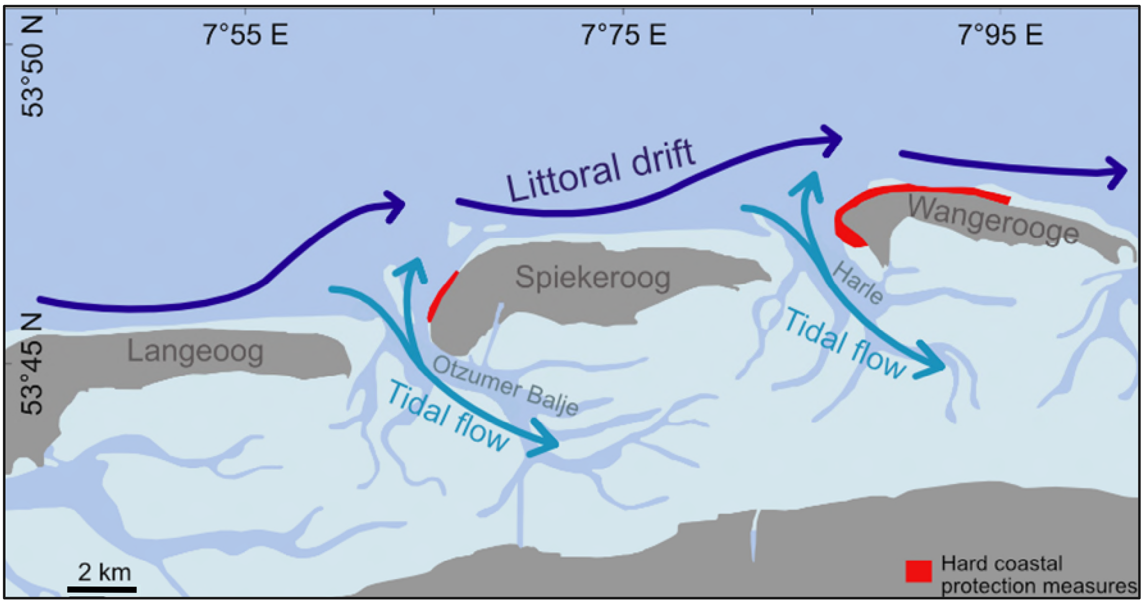

Figure 1.3: Map of the East Frisian Islands Langeoog, Spiekeroog, and Wangerooge. The blue arrows indicate the dominant direction of littoral drift, which significantly influences sediment transport and contributes to coastal erosion. Red areas denote regions where hard coastal protection measures have been implemented along the islands. Spiekeroog has fewer hard protection structures compared to Wangerooge, leading to a more pronounced impact of coastal defense measures in the Harle inlet, while the Otzumer Balje inlet remains largely unaffected with minimal anthropogenic influence.

Since the construction of these defense structures, the drainage area of the Harle Inlet has decreased from 154 km² in 1650 to 62 km² in 1960. Conversely, the drainage area of the Otzumer Balje increased from 57 km² in 1650 to 73 km² in 1960 (Fitzgerald et al., 1984).

1.3 Objectives of the thesis

The implementation of hard coastal protection measures is often inevitable in specific locations to mitigate erosion or safeguard infrastructure. However, the long-term impacts of such measures remain inadequately understood, particularly in highly dynamic systems such as tidal inlets. These environments are characterized by intricate hydrodynamic processes, including complex interactions of currents with varying directions and velocities, which can magnify the effects of coastal engineering interventions.

This study aims to investigate the long-term consequences of sustained coastal protection measures within a tidal inlet environment, focusing on the island of Wangerooge in the German North Sea. Wangerooge has been selected as the focal area due to its dynamic interaction with the Harle tidal inlet channel, which lies between the islands of Spiekeroog and Wangerooge. Over time, the Harle inlet has migrated eastward, encroaching closer to the western part of Wangerooge and prompting the implementation of hard coastal protection measures to mitigate erosion and stabilize the shoreline.

To address these challenges, a series of beach groynes (A - H) was installed along the northern and western shores of Wangerooge between 1875 and 1884 (Fig. 1.4). These groynes were designed to trap sediments and prevent further shoreline erosion. However, their implementation resulted in unintended consequences. Scouring near Groyne A eventually connected with a pre-existing gully, leading to the formation of the Dove Harle channel. Over time, this channel expanded and deepened, significantly altering the morphology of the inlet and its surrounding areas (Lüders, 1952).

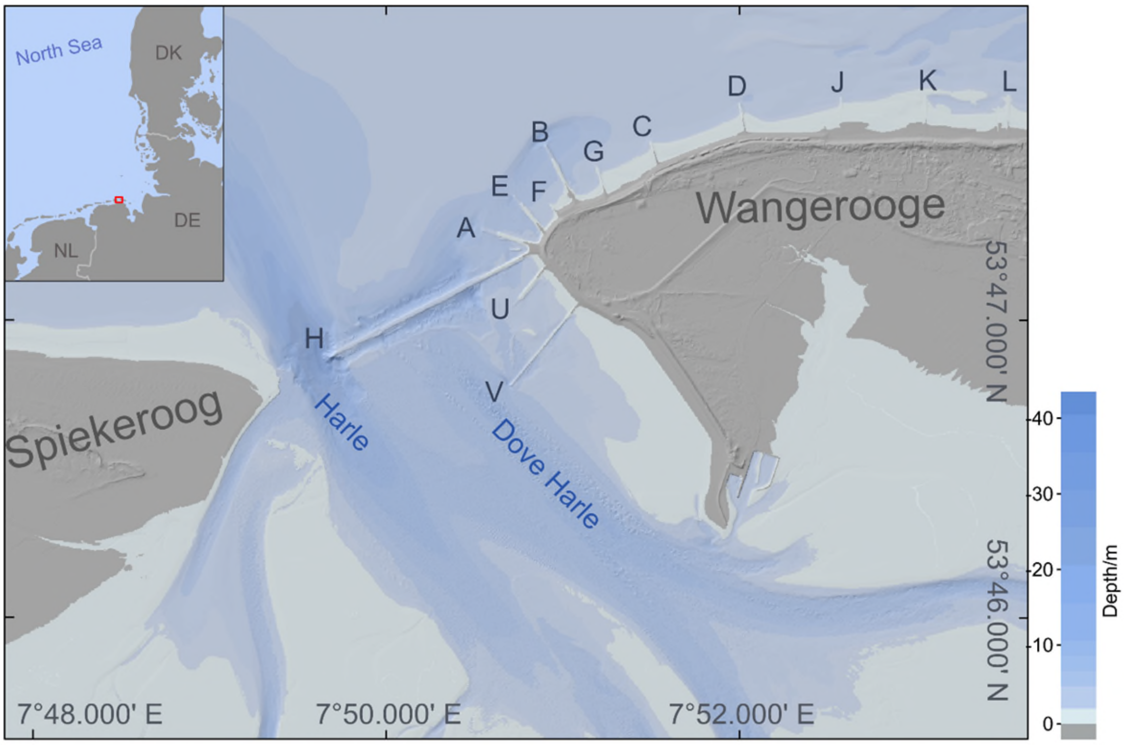

Figure 1.4: Map of the Harle tidal inlet, featuring the two main channels, Harle and Dove Harle, located between the East Frisian Islands of Spiekeroog and Wangerooge. Along Wangerooge, specific groynes (A-H, U, V) are marked. The extended Groyne H reduces the exchange area between the North Sea and the back-barrier basin. NL: The Netherlands, DE: Germany, DK: Denmark.

In 1940, Groyne H was extended into a 1,400 m long submerged stream groyne to counteract the ongoing erosion and hydrodynamic disruptions. This modification narrowed the width of the Harle tidal inlet by approximately two-thirds, substantially altering its natural configuration. These structural changes disrupted the hydrodynamic conditions of the inlet, further influencing its sedimentary processes and morphology (Kunz, 1997; Ladage et al., 2006; Ladage and Stephan, 2004; Lüders, 1952; Mascioli et al., 2022).

The project “Gute Küste Niedersachsen” explores an innovative approach by creating real-world laboratories to address the inclusive design of ecosystem-based coastal protection with the focus on ecosystem strengthening coastal protection (Kempa et al., 2023). As part of these real-world laboratories, the island of Spiekeroog and its tidal inlets, Otzumer Balje and Harle, were selected due to their combination of hard protection measures and large natural reservation areas. The Harle inlet serves as a critical case study for examining how such measures affect hydrodynamic, sedimentological, and ecological processes.

By focusing on the impacts of these long-term interventions, this study aims to understand the complex interactions between hard coastal protection measures and the natural dynamics of tidal inlet systems. To achieve these objectives, sedimentological and hydrodynamic analyses were conducted. The specific research objectives addressed are as follows:

1. **Development of a surface facies map for the Harle inlet**: Construction of a detailed map displaying the sedimentological properties and spatial distribution of sedimentary facies in the back-barrier area.

2. **Identification of deposition and erosion zones**: Assessing the locations and dynamics of depositional and erosional areas in the Harle inlet in response to hydrodynamic alterations caused by the groyne.

3. **Comparison with an almost natural inlet**: Highlighting sedimentological differences between the Harle inlet and an almost natural tidal inlet to understand the effects of anthropogenic modifications.

4. **Development of a comparative facies map for the Otzumer Balje**: Create a facies map of the Otzumer Balje, an inlet with minimal anthropogenic impact, to serve as a reference for natural inlet conditions

5. **Transport process analysis**: Examine sediment transport dynamics within the Harle inlet and identify deviations from natural transport processes.

6. **Seasonal shift in surface sediments**: Investigate seasonal changes in sediment composition and distribution across the inlet.

7. **Heavy metal analysis**: Analyze the concentration and spatial distribution of heavy metals within the Harle inlet to evaluate potential contamination associated with altered sedimentary processes.

8. **Identification of heavy metal sinks and sources:** Assess the potential of sedimentary deposits to function as sinks for heavy metals, contributing to ecosystem services. Additionally, identify potential sources of heavy metal contamination within the inlet.

This work provides a comprehensive understanding of the long-term geomorphological, sedimentological, and environmental impacts of hard coastal protection measures in tidal inlets. The findings aim to inform future coastal management strategies by highlighting the broader implications of such interventions.

1.4 List of publications

This thesis comprises an introduction in Chapter 1, a summarizing conclusion in Chapter 5, and three core chapters based on individual manuscripts. Chapter 2 presents a manuscript that has been fully published, Chapter 3 a manuscript currently under review, and Chapter 4 contains a manuscript ready to submit. While all three manuscripts have been reformatted to align with the stylistic requirements of this thesis, their original content remains unchanged.

Chapter 2 investigates the impact of a submerged stream groyne on the morphology and sedimentology of the Harle tidal inlet in the Southern North Sea. Through sedimentological and statistical analyses, the study identifies distinct facies patterns shaped by tidal currents influenced by the groyne. A detailed facies map, developed using multibeam data, reveals significant morphological changes in the inlet. Comparative analysis with the Otzumer Balje highlights the effects of coastal protection structures on sediment dynamics in high-energy tidal systems. This chapter is based on the published manuscript:

I. Geßner, A.-L., Wollschläger, J., Giebel, H.-A., Badewien, T.H. (2024). Impact of a submerged stream groyne on morphology and sedimentology on a tidal inlet, Harle (Southern North Sea, Germany). Frontiers in Earth Science, 12, 1292462. DOI: 10.3389/feart.2024.1292462

Authors contribution:

A-LG conducted fieldwork, performed data analysis, and prepared the initial draft of the manuscript. JW was responsible for conceptualization, funding acquisition, project administration, supervision, and manuscript review and editing. H-AG contributed to manuscript review and editing. TB provided funding acquisition, project administration, supervision, and manuscript review and editing. All authors actively contributed to the conception and the revision of the manuscript.

Chapter 3 presents a comprehensive facies map of the Otzumer Balje tidal inlet in the Southern North Sea to assess the impact of coastal protection measures. The analysis highlights differences between the impacted Harle inlet and the naturally evolving Otzumer Balje inlet. The chapter also investigates seasonal variations in surface sediments for both the Otzumer Balje and Harle inlets, addressing the significant influence of biological and physical factors throughout the year. The findings provide critical insights into the impact of coastal protection infrastructure on the tidal inlet system. The chapter is based on the submitted manuscript:

II. Geßner, A.-L.; Albinus, M.; Giebel, H.-A.; Wollschläger, J.; Mascioli, F.; Badewien, T. H. (2025). Facies Mapping and Seasonal Sediment Shift of Tidal Inlets: Impacts of coastal protection measures. Sedimentary Environments (in review).

Authors contribution:

A-LG conducted fieldwork, carried out data analysis, and drafted the initial version of the manuscript. MA conducted fieldwork and carried out data analysis. H-AG led the conceptualization, managed project administration, supervised the work, and contributed to manuscript review and editing. JW supported the conceptualization and participated in manuscript review and editing. FM contributed data essential to the study. TB provided funding, managed project administration, and supervised the work. All authors were actively involved in the manuscript's conception and contributed to its revision.

Chapter 4 investigates heavy metal concentrations in the Harle inlet and examines the interplay between hydrodynamics, sediment transport, and chemical composition, with a focus on sedimentary and chemical heterogeneity. The chapter highlights variations in sediment grain size, the distribution of heavy metals, and the influence of altered current patterns near a coastal defense structure on erosion and deposition processes. The findings underscore the critical role of sediment texture in contaminant distribution and offer valuable insights into the combined effects of natural processes and anthropogenic activities on tidal inlet dynamics. The chapter is based on the submitted manuscript:

III. Geßner, A.-L., Kalmbach, C., Albinus, M., Bunzel, D., Wollschläger, J., Badewien, T.H., Giebel, H.-A. (2025): Influence of Coastal Protection Measures on Sediment Transport and Heavy Metal distribution in surface sediments in the tidal inlet Harle (Southern North Sea).

Authors contribution

A-LG conducted fieldwork, performed data analysis, and prepared the initial draft of the manuscript. CK carried out laboratory work and statistical analysis. MA contributed by conducting fieldwork and processing data. DB participated in fieldwork activities and data analysis, while JW performed measurements onboard. TB provided funding, managed project administration, and supervised the work. H-AG led the conceptualization, oversaw project administration, supervised the work, and contributed to the manuscript review and editing. All authors actively participated in the manuscript's conception and contributed to its critical revision.

Chapter 2

Impact of a submerged stream groyne on morphology and sedimentology on a tidal inlet, Harle (Southern North Sea, Germany)

This chapter is based on the publication:

Geßner, A.-L., Wollschläger, J., Giebel, H.-A., Badewien, T.H. (2024). Impact of a submerged stream groyne on morphology and sedimentology on a tidal inlet, Harle (Southern North Sea, Germany). Frontiers in Earth Science, 12, 1292462. DOI: 10.3389/feart.2024.1292462

Abstract

Coastal erosion and the need for flood protection present globally significant challenges. To address these challenges, hard coastal protection structures, such as groynes, are employed worldwide to safeguard coastal areas and regulate currents. However, their specific effects on current dynamics and sediment properties, particularly within tidal inlets, remain inadequately investigated, especially in regions like the North Sea characterized by prevalent tidal currents. This study aims to address the knowledge gap by examining the long-term impacts of coastal protection measures on sedimentology, with a focus on the environment of a tidal inlet. The Southern North Sea coast is subject to mesotidal conditions. It presents a mixed-energy coast with an erosive eastward littoral drift, providing an ideal setting for this investigation. On the island of Wangerooge, a prominent groyne extends into the Harle inlet, significantly restricting the exchange area between the North Sea and the Wadden Sea. Consequently, the changes in flow dynamics and sediment transport resulting from the construction significantly affect sediment distribution and morphology within the inlet. Sedimentological analysis was employed to characterize surface sediment properties and statistical analysis identified seven distinct facies associated with three realms, which were shaped by the tidal currents affected by the groyne to a distinct pattern. Additionally, the integration of multibeam data from existing literature facilitated the creation of a comprehensive facies map. These findings suggest alterations in the morphology of the inlet. By comparing the results with an unaffected inlet, the Otzumer Balje, this study provides valuable insights into the complex interplay between coastal protection infrastructure and coastal sedimentology within a high-dynamic tidal inlet system

2.1 Introduction

Coastal erosion and flood protection represent globally acknowledged challenges, particularly amid the escalating risks of climate change and rising sea levels (Linham and Nicholls, 2010; Masselink and Russell, 2013; Vousdoukas et al., 2018). Small islands and flat coastal areas exhibit heightened vulnerability due to their geographical characteristics, presenting challenges in terms of limited adaptation options. Additionally, regions with substantial natural and cultural heritage necessitate protection against these challenges, given that relocation is frequently impractical, and the very existence of these areas is imperiled. A spectrum of coastal protection has been developed ranging from hard structures like dikes, seawalls, breakwaters, and groynes to softer, more natural approaches such as beach nourishment, reef restoration, and the restoration of seagrass meadows and salt marshes. While natural methods tend to offer positive ecological impacts, the utilization of hard coastal protection measures may be indispensable for ensuring effective and resilient protection (De Ruig, 1998; Narayan et al., 2016; Morris et al., 2018). Typically, the implementation of hard coastal protection structures is considered in areas where there is a high infrastructure and asset risk or where relocation and adaptation options are unfeasible. Moreover, these structures offer distinct advantages in regions with high protection value, such as densely populated cities or heavily utilized waterways. The need for immediate and reliable protection is crucial, and hard structures are capable of providing such results (Schoonees et al., 2019). It is often intended for hard structures to undergo periodic renewal or modification during their protective period.

The North Sea stands out as an area where coastal protection measures are prevalent. The concept of “building with nature” has emerged as a scientific approach where conventional coastal protection methods are adapted and substituted with innovative strategies that encompass greater socio-economic functions (Van Slobbe et al., 2013). However, most areas along the North Sea coast rely on conventional structures like groynes, dykes, and seawalls for protection (Kunz, 1997). Characterized by a mesotidally influenced coastline with a flat mainland, fronted by islands, the North Sea coast features the East Frisian Islands, a chain of barrier islands located in the southern German North Sea. These islands formed during the Holocene transgression, driven by the rapid rise in global sea level resulting from the melting of global ice sheet. The transgression causes the coastline to shift landward, forming predominantly sandy islands. The process involved the gradual rise in sea level, reaching river valleys and transform the previously elevated Pleistocene sand into elongated spit bars through wave action. Over time, these spit bars migrated inland, developing into coastal dunes. As the tidal amplitude transitioned from microtidal to mesotidal, the spit bars underwent a transformative process, evolved into elongated detached barrier islands (Fig. 2.1). The continuous widening of the tidal inlets, influenced by the intricate interplay of semidiurnal tides, wave action, and currents, has engendered a persistent littoral drift and consequential erosion force in the west-to-east direction (Streif, 1989; Niemeyer, 1995). Presently, the East Frisian Islands are subject to the enduring effects of semidiurnal tides, dynamic wave action, and strong currents within the tidal inlets, leading to an ongoing littoral drift and a prevailing erosion force in the west-to-east direction. This drift instigates a migration of the inlet channels, with erosion predominantly manifesting on the western side of the islands, while sediment deposition occurs on the eastern side. In the early 20th century, groynes were constructed to counteract this shift (Witte, 1970; Flemming and Davies, 1994; Niemeyer et al., 1996; Kunz, 1997). The general significance of barrier islands as a protective barrier for the mainland and wetlands, mitigating erosion and storm impacts, has been emphasized by Fritz et al. (2007) and Penland et al. (1988).

Initially, beach groynes were constructed as a measure to safeguard the northern beaches of the East Frisian Islands. However, due to their limited effectiveness in preventing sand erosion and detrimental generating of scours, the beach groynes were transformed into stream groynes through the addition of underwater extensions. This modification successfully prevented further erosion. Nevertheless, during storm events, the northern beaches are subject to significant damage, resulting in the removal of sand. To mitigate this, artificial beach nourishment is employed to replenish the eroded material and maintain existing structures. The construction of stream groynes serves to prevent further migration and facilitates the stabilization of the islands. Overall, the groyne protection measures on the East Frisian Islands aims to safeguard the island settlements, stabilize waterways and inlets, and provide protection against storm flood events (Eitner, 1996b; Kunz, 1997).

The majority of the East Frisian Islands are protected by groynes to defend their northern beaches. However, specific inlets exhibited a significant tendency to migrate eastward and endanger the settlements. In part, this migration is so extensive that settlements that were located at the former eastern side of the island are nowadays located at its western side. Thus, further migration of the island threatens the very existence of the settlements (Lüders, 1952; Homeier, 1973; Fitzgerald and Penland, 1987). To address this, modifications were made to the western inlets of the islands Borkum, Norderney, Baltrum, and Wangerooge using groynes. Notably, the tidal inlet between Spiekeroog and Wangerooge (Harle inlet) is heavily influenced by a stream groyne. Conversely, the tidal inlet between Langeoog and Spiekeroog (Otzumer Balje) remains unprotected, with a groyne field developed solely along the northern beach of Spiekeroog.

The Spiekeroog Coastal Observatory (SCO; Zielinski et al., 2022) and its integrated Time Series Station (TSS; Badewien et al., 2009; Reuter et al., 2009) provides a robust scientific infrastructure for conducting various investigations in the Otzumer Balje. Through the utilization of this infrastructure, Son et al. (2011) discovered evidence of sediment recirculation within the ebb tidal delta. The transport of sediments in this area is primarily driven by the combined forces of tidal currents and wave action. Noormets et al. (2006) conducted research on local scouring within the tidal inlet, focusing on hydrodynamic flow changes due to the presence of the TSS pile and the interaction of currents with existing bedforms such as megaripples and compound dunes. analyze the morphological, sedimentological, and hydrodynamic conditions of the Otzumer Balje (Wang et al., 1995; Bartholomä et al., 2009; Lettmann et al., 2009; Wang et al., 2012; Wang et al., 2014). The aforementioned investigations along the Otzumer Balje inlet describe a high dynamic system with crucial interactions between tidal currents, waves, morphology and sediments. Interrupting the natural system in the Harle inlet by the construction of groynes leads on the one hand to the required termination of the natural shifting and migration of the inlet channels. On the other hand, the natural equilibrium is disrupted and depending on the varying condition the effects are various. To gain a better understanding of the interactions between environment and construction the Harle inlet between Spiekeroog and Wangerooge is investigated.

Their study explored seasonal variations in ripple dimensions and the influence of neap-spring tidal cycles. Additionally, numerous numerical models have been employed

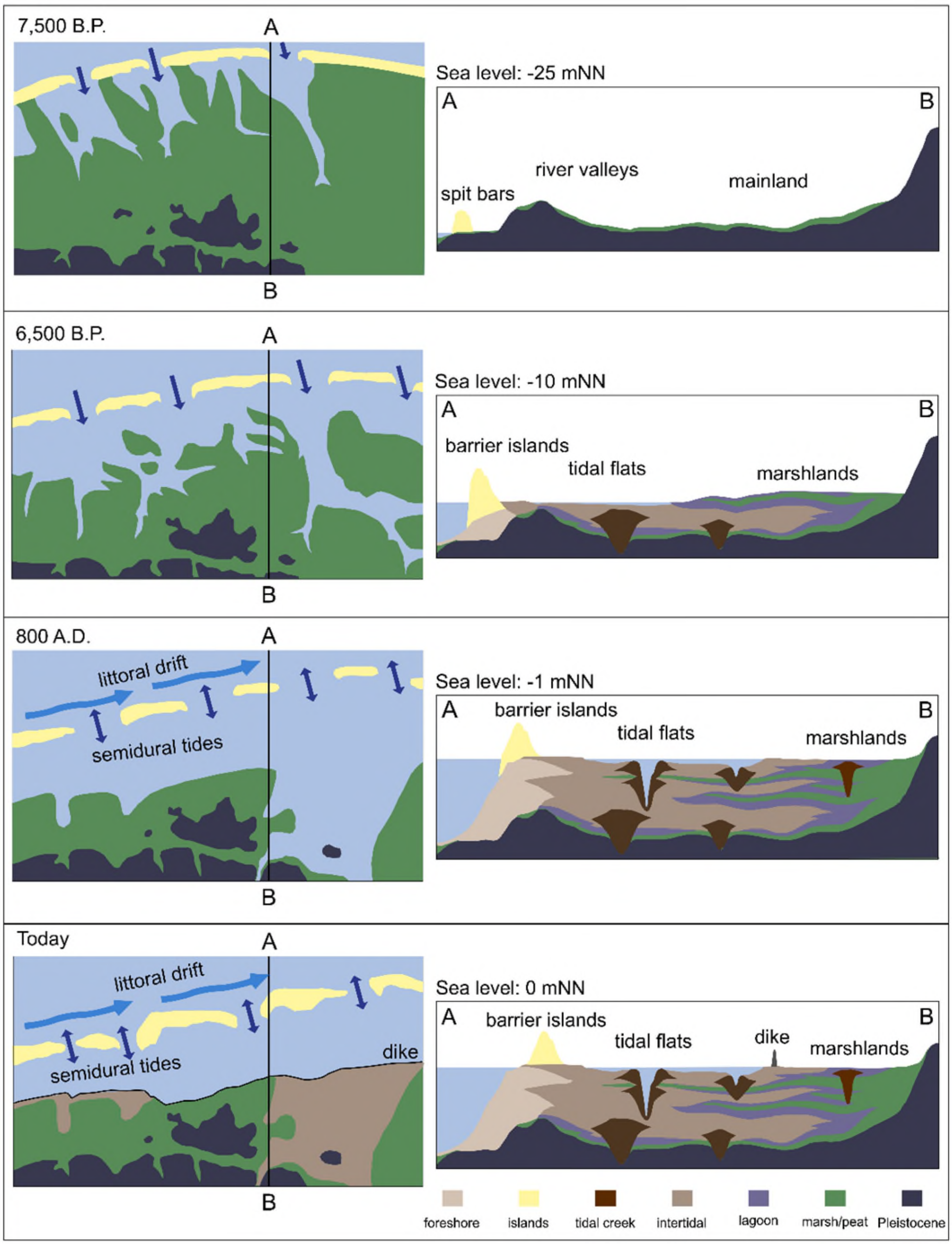

Figure 2.1: Schematic development of the coastline along the East Frisian Islands, modified after Flemming and Davies (1994), begins around 7,500 B.P. with a sea level of −25 mNN. This area is characterized by spit banks and primarily consists of marsh/peat sediments and Pleistocene sands. A cross-section along line AB illustrates the evolution of the subsurface in the region. As the sea level rose, the spit banks transformed into islands around 6,500 B.P. and migrated inland. The higher sea level resulted in tidal currents, giving rise to mudflats and marshes in the backshore area. By 800 AD, the development of semidiurnal tides and littoral drift was complete. With the implementation of today's coastal protection measures, such as dikes, the landward migration of the islands was halted, and the littoral drift led to an eastward transport.

to Mascioli et al. (2022) present sedimentological maps and hydroacoustic data obtained from the Harle inlet. The maps delineate four distinct sediment types within the inlet and describe its primary bedforms. The authors emphasize the erosive forces caused by the interaction between an anthropogenic element, a groyne, and tidal currents. However, their study lacks detailed sedimentological surface facies with component analysis, as well as information on alteration and deposition processes. The primary aim of our study is to investigate the impact of the groyne on sedimentology to comprehend the interactions of currents and transport within the Harle. Additionally, the study aims to interpret morphological alterations through notable features observed within the inlet, as reflected in maps and data.

2.2 Material and methods

2.2.1 Study area

The barrier island system along the southern North Sea serves as a crucial protective barrier for the Wadden Sea, spanning the Dutch, German, and southern Danish coasts. This study focusses on the northwest coast of the German Wadden Sea, specifically the vicinity of the East Frisian Island of Spiekeroog within this barrier island system. The presence of tidal inlet systems between the islands facilitates the connection and exchange of water between the tidal flats and the open sea. In the case of Spiekeroog, the island is confined by two tidal inlet systems, namely, “Otzumer Balje” to the west, separating the islands Langeoog and Spiekeroog, and “Harle” to the east, separating Spiekeroog from Wangerooge (Fig. 2.2).

2.2.2 Sedimentological situation

On the seaward side of the tidal inlets, sediment accumulation has resulted in the formation of ebb-tidal deltas northeast of the island (Hayes, 1980). This process is driven by a strong littoral drift, tidal currents, and waves action. Sediment bypassing along the ebb-tidal deltas forms swash-bar migration around the outer edge. Additionally, the hypothesis proposed by Burchard et al. (2008) suggests that density gradients contribute to the accumulation of Suspended Particular Matter (SPM) in the Wadden Sea. The prevailing understanding, as postulated by FitzGerald (1988) and FitzGerald et al. (1984; 2000), identifies longshore sediment movement as the primary driver of easterly sediment transport. This sediment transport exerts a considerable influence on the East Frisian Islands, prompting an eastward shift (Kunz, 1997).

The island of Wangerooge has historically borne the brunt of intense storm surges during the 19th century, resulting in severe consequences. The impact of these storm surges included the destruction of villages on Wangerooge and eroded the dunes along the western coast. Subsequent to dune breaching, a sand beach formed above the high-water level in the western part of Wangerooge. Notably, storm surge events caused the dune edge in the western part of Wangerooge to shift approximately 1,370 m eastward. Over the period from 1650 to 2004, the west side of Wangerooge shifted eastward by 2,010 m, while the east side extended by 3,030 m. A parallel eastward sediment transport from the neighboring island Spiekeroog led to a reduction of the width of the Harle from 5.5 km to about 2 km. Simultaneously, the orientation of the Harle estuary shifted from north to northeast, forming the “Dove Harle.” The formation of the Dove Harle can be attributed to the connection of a tidal channel and a scour caused by the ebb current in the area of Groyne A (Fig. 2.2). With the formation of the Dove Harle, the western beach of Wangerooge underwent erosion and shifted to the southwest (Lüders, 1952; Homeier, 1973; Ladage and Stephan, 2004).

To counteract further erosion on the west side of Wangerooge, the beach groyne, Groyne H, was constructed. Subsequent to its implementation, a limited redeposition of sands stabilized in the southwest region, although no re-sedimentation occurred in the west. The extension of Groyne H aimed to prevent the formation of Dove Harle and mitigate siltation, achieving partial success. Furthermore, the groyne contributed to stabilizing the course of the Harle estuary. Between 1950 and 2002, a bar formed, separating the channels of the Harle and the Dove Harle. This bar, aligned orthogonally to the Groyne H and parallel to the channel, is situated the tip of the Groyne H (Lüders, 1952; Homeier, 1973; Ladage and Stephan, 2004).

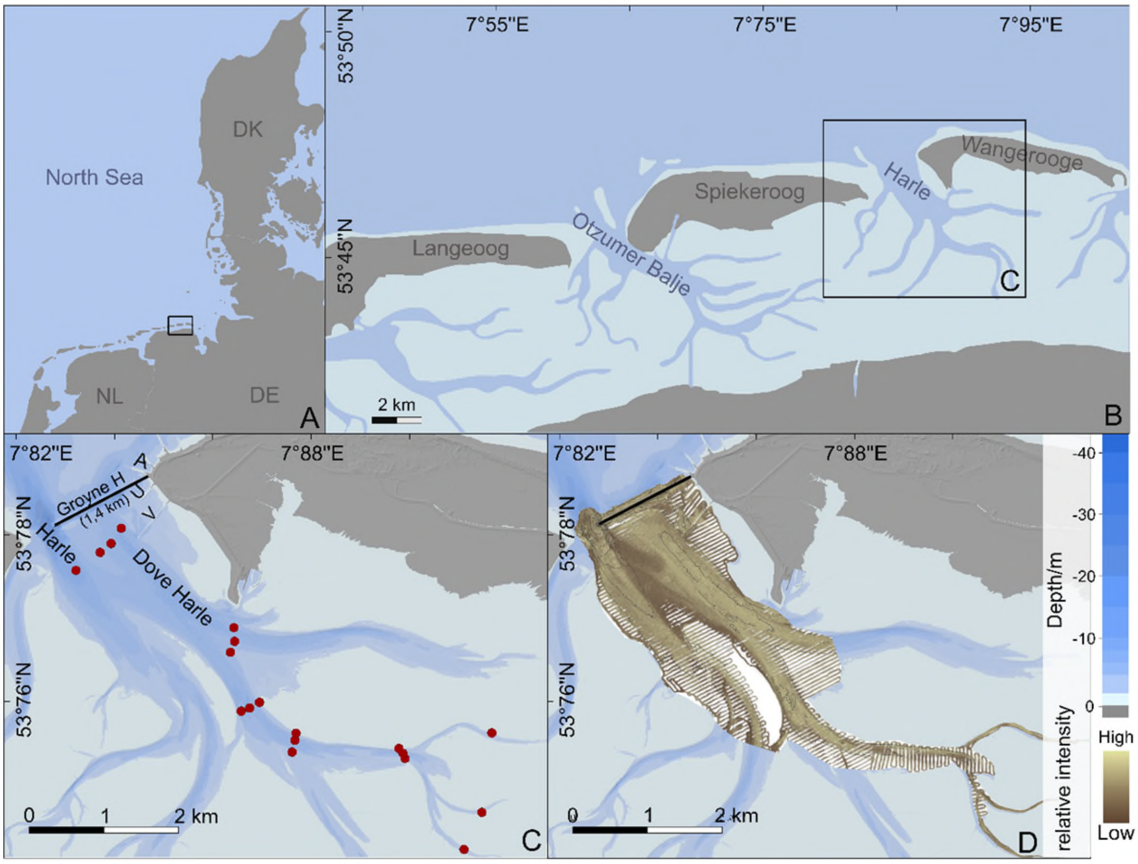

Figure 2.2: Overview map in (A) (DK: Denmark; DE: Germany; NL: Netherlands) of the working area along the German North Sea coast (WSV, 2021). (B) shows the islands Langeoog, Spiekeroog and Wangerooge and the tidal inlets “Otzumer Balje” and “Harle.” In (C) a detailed map of the sampling stations (red dots) along the Harle is shown with the marked groynes A, H, U, and V. The modified multibeam echo sounder backscatter data from Mascioli et al., 2022 are shown in (D). Dark colors indicate low backscatter intensity and light colors indicates high intensity.

2.2.3 Hydrodynamic situation

The hydrodynamic conditions along the Harle inlet exhibit characteristics that are instrumental to the overall understanding of the study area. The tidal regime is predominantly semidiurnal, marked by a mean range of 2.9 m. Annual wave heights, as reported by Ladage et al. (2007), vary significantly within the range 0.7–1.0 m. This coastal area, as classified by Hayes (1979), can be characterized as a mesotidal, mixed-energy coast with tidal influence (Ladage et al., 2007). In this region, the ebb current emerges as the primary tidal current around the East Frisian Islands. The flow passes through the inlet channels, showcasing a strong north-westerly sediment transport that notably exceeds the strength of the south-easterly sediment transport during the flood flow. The flood current, as observed by Niemeyer (1990), endures a comparatively shorter duration, creating an asymmetry in the tidal patterns. The temporal dynamics of tidal currents, as highlighted by Stanev et al. (2007), indicate an early occurrence of the flood current, while the ebb current commences shortly before slack tide. This temporal asymmetry contributes to the overall tidal behavior. Generally, the maximum tidal current is more than 1 ms^{-1}, ushering dense North Sea water with higher salinity into the comparatively lighter brackish Wadden Sea water. A noteworthy phenomenon arises in the Harle due to the constrained discharge of the stream groyne on the downstream side during low tide of the Groyne H. This restriction gives rise to a counteracting dynamic eddy, resulting in a low-velocity zone at the center of the eddy. The clockwise rotation of the eddy with a speed of 0.2 ms^{-1} is confined by the Groyne H and Groyne V (Albinus, 2021). This intricate interplay of tidal currents, sediment transport, and eddy formation plays a crucial role in shaping the hydrodynamic conditions of the Harle inlet, necessitating careful consideration in the broader context of the study.

2.2.4 Methods

Following the storm flood season in March 2022, sediment samples were collected in the Harle inlet with a 1 m^2 Van Veen grab sampler at several stations along the tidal channel (Fig. 2.2). The same sampling stations were approached again after the fair-weather season in September 2022. The deployment of the grab sampler from RV Senckenberg targeted subtidal stations, while RV Otzum was employed for shallower stations in both intertidal and subtidal areas during high water tide.

For comprehensive analysis bulk samples (250 mL) extracted from the grab sampler were used for grain size analysis after Udden and Wenthwoth scale, and semi-quantitative component analysis. Grain size analysis were involved wet sieving (>2,000 µm; 2,000-1,000 µm; 1,000–200 µm; 200–63 µm and 63 µm were analyzed with a binocular of a scatter sample. These components were classified based on their abundances: present (1%–2%), rare (2%–5%), abundant (5%–10%), very abundant (10%–24%) and dominant (>24%). The combination of grain size distribution and component analysis, is utilized to determine the sedimentological facies (Reading, 1996; Miall, 2022). The facies along the Harle inlet are classified and categorized by statistical analysis into facies groups. The multibeam data presented by Mascioli et al. (2022), depict the seafloor characteristics within the study area. Bathymetric information facilitated the identification of morphological features such as ripples and slope angles, while the backscatter intensity could give more insights into sediment characteristics and distribution.

Hence, the correlation of that backscatter data with the sedimentological results of our study facilitated the precise mapping of facies on to distinct backscatter intensity zones, culminating in the development of a detailed facies map of the sample sites. This systematic approach ensures the most comprehensive coverage in characterizing the sedimentology of the Harle inlet and extended the work of Mascioli et al. (2022) by the detailed facies map to reveal the impact of the longstanding groyne.

To thoroughly investigate the long-term impacts of coastal protection measures on the Harle inlet, a comparative analysis is conducted with the Otzumer Balje inlet. The Otzumer Balje, situated between the islands of Langeoog and Spiekeroog, experiences minimal impact from coastal protection measures and is well described in the literature. Consequently, any significant deviations, particularly in morphology and sediment distribution, observed in the Harle may indicate the influence of groynes.

2.3 Results

The sedimentological characteristics of the sample locations along the inlet system of the Harle have been analyzed. Overall, seven facies groups have been identified: clayey sands, organic-rich clayey sands, very fine sands, bioclastic organic-rich fine sands, bioclastic fine sands, bioclastic middle sands, and shill sands (Fig. 2.3). In combination with the backscatter intensity of the multibeam data from Mascioli et al. (2022), the facies of the sample locations have been expanded due to their associated backscatter intensity area and led to a facies map of the Harle (Fig. 2.4).

2.3.1 Facies F1: clayey sands

Facies F1, characterized by clayey sands, exhibits very fine sands with a fine fraction (< 63 µm) content of 35 wt %. The grain size distribution displays a well sorted sand with the median (D50) of 79 µm. Within the sediment grains (> 63 µm), a diverse composition includes silicates, bivalve shell debris and plant detritus. Minor occurrences of echinoid spines are observed, while gastropod remains and the benthic foraminifera *Haynesina sp.*, *Elphididae sp.*, and *Ammonia sp.* are comparatively less present.

The spatial distribution of clayey sands occurs in the southernmost gully, situated closest to the mainland and farthest from the inlet. Utilizing multibeam backscatter data, the precise area of the facies has been identified along the end of the southernmost gully at water depth between 1 and 2 m.

2.3.2 Facies F2: organic-rich clayey sands

Dominated by a higher amount of plant detritus, the organic-rich clayey sands facies F2 consists of very fine sand with a fine fraction of 19 wt %, in contrast to F1. The D50 of the F2 facies is 83 µm and the sediment is well sorted. This facies is predominantly composed of plant fragments and silicates. F2 also contains of present echinoid fragments, mainly echinoid spines, the foraminifera *Haynesina sp.*, *Ammonia sp*, and *Elphididae sp*, as well as bivalve fragments.

Located in the northern gully of the Harle inlet, close to Wangerooge, the facies F2 is in the multibeam data depicted as patches along the end of the norther gully. Water depths associated with this facies range between 1 and 2 m.

2.3.3 Facies F3: very fine sands

Comprising well sorted very fine sands with a D50 of 91 µm and a fine fraction of 3 wt %, facies F3 primarily consists of silicates and bivalve fragments. Gastropoda, plant fragments, echinoid fragments and the foraminifera *Ammonia sp.*, *Haynesina sp.*, and *Elphididae sp.* are also present.

Facies F3 is located along the shallow flanks of the channels, with water depths ranging between 2 and 6 m. Additionally, the very fine sands of this facies occur also in the middle of the inlet area, approximately 730 m south of Groyne H, forming the sand bar between the Harle and the Dove Harle at a water depth of around 5 m.

2.3.4 Facies F4: bioclastic organic-rich fine sands

Characterized by a composition mainly of silicates and bivalve shell debris, the F4 bioclastic organic-rich fine sands exhibit a D50 of 96 µm and a minor fine fraction of

4 wt %. The grain size distribution varies from well to poor sorted, and additional sediment forming components include gastropods, plant fragments, with minor amounts of bryozoan, *Lanice sp.*, tube fragments, echinoid fragments, and foraminifera.

Covering the flanks of the main channel and the transition zone between the Wadden area and the inlet system, facies F4 is present at water depths ranging between 2 and 7 m.

2.3.5 Facies F5: bioclastic sands

Distinguished by fine-grained, poor sorted sands, facies F5 is composed of a coarser grain size with a D50 of 128 µm. Made primarily of silicates and bivalve shell debris, facies F5 contains a lesser amount of fine fraction, 3 wt %. Other components are gastropods, while echinoid fragments, foraminifera, and bryozoan are underrepresented, and plant fragments are absent.

Similar to facies F4, the coarser bioclastic sands of facies F5 occur along the main channels and in the transition zone between the intertidal zone and the subtidal zone, with water depths ranging between 2 and 8 m.

2.3.6 Facies F6: medium bioclastic sands

Facies F6 is composed of bivalve shell debris and silicate grains with present echinoid fragments and less present bryozoans, foraminifera, *Lanice* tubes, and plant fragments. The medium-grained sands are poorly sorted with a D50 of 281 µm. The fine fraction content is 3 wt %, and gastropods are present in equal amounts

Facies F6 is notably found in the main channels of the Harle and Dove Harle, with water depths exceeding 5 m.

2.3.7 Facies F7: shill sands

Comprised mainly of silicate grains and bivalve fragment shill, facies F7 is made of a poorly sorted coarse-grained sand with a D50 of 820 µm. Gastropods are the abundant sediment former, and fragments of bryozoan occur. Less present are plant fragments, echinoid fragments and foraminifera. A distinctive feature is the preservation of bivalve shells, covered with encrusting bryozoans, with their calcific shells being micritic.

Distributed along the inner channel of the Dove Harle, the facies F7 is exclusive to this area, with water depths ranging between 5 and 10 m.

The sediment type changes along the morphology of the inlet system. In the shallow gullies of the Wadden shoals between the islands and the mainland, is mud, while at higher water depths on the flanks and surfaces of the narrower channels, are finer sands. As the water depths increase closer to the inlet and the exchange area between the North Sea and the Wadden Sea, the deep main channels are composed of medium to coarse-grained sands. The main channels are separated by a shallow sandbar, which interrupts the coarse facies with finer facies.

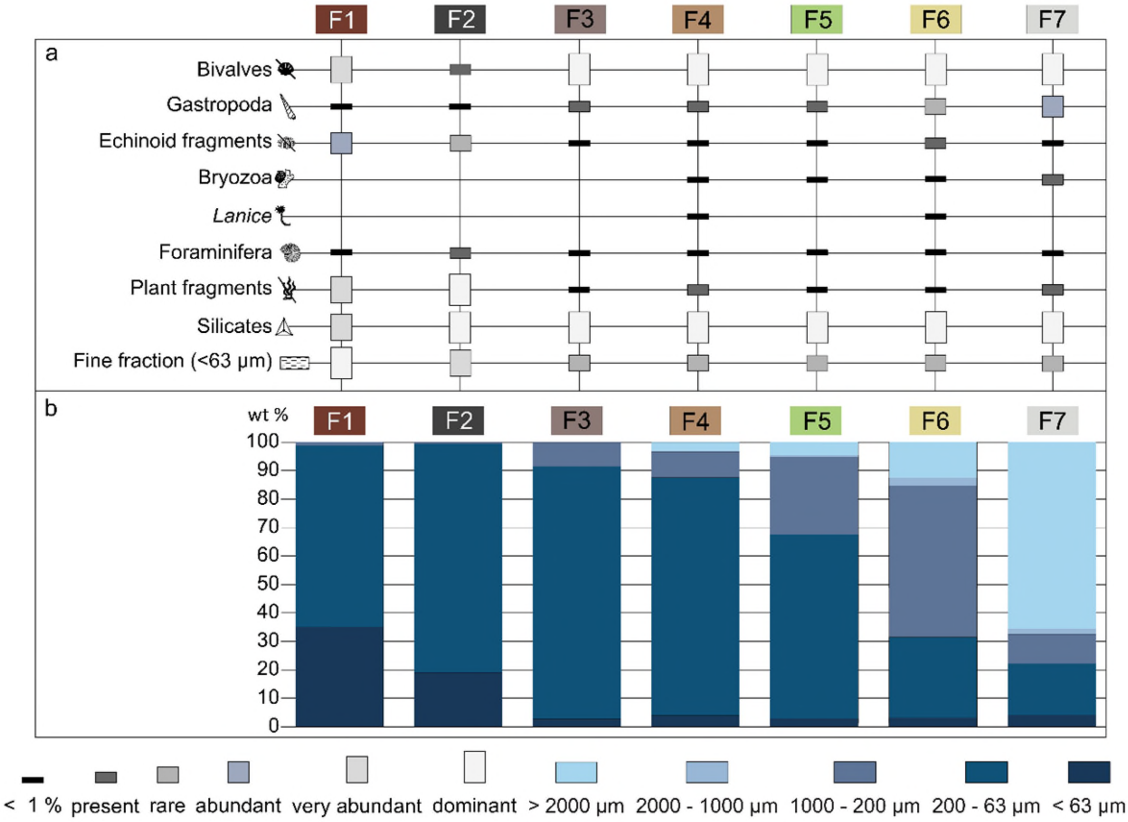

Figure 2.3: In (A) the relative abundance of the major components of the seven identified facies is shown. Silicates contain quartz minerals and flint stone. Abundance ranges from dominant (>24%) to very abundant (10%–24%), to abundant (5%–10%), to rare (2%–5%) to present (1%–2%), to under represent with <1%. The combination of the different sediment formers defines the facies. In (B) the mean grain size distribution is shown. Lighter blueish colors indicate a coarser material. Thus, the grain size increases from facies F1 to F7.

2.4 Discussion

The inlet system of the Harle provides a distinctive case study for investigating the impact of longstanding hard coastal protection measure in tidal environments. The implementation of such measures has resulted in significant alterations in flow dynamics and a constriction in the exchange between the North Sea and the adjacent Wadden Sea. Consequently, discernible perturbations can be observed in the inherent morphology of the inlet and the sedimentological facies characteristics.

2.4.1 Facies distribution

In a comprehensive classification, the sedimentary facies within the Harle inlet can be grouped into three distinct realms, encompassing a total of seven facies. The first realm, the Wadden realm, is represented by facies F1 and F2, predominantly occurring within the gullies of the intertidal shoals, exhibiting a high content of fine sediment and organic detritus. The second realm comprises facies F3, F4, and F5, constituting the channel beds and flanks. Within these subtidal areas, the sediment is predominantly fine-grained, with a minor portion of fine fraction. Silicate grains and bivalve shell debris are the primary constituents of these facies. A sandbar present towards the southern region of Groyne H, composed of facies F3, F4, and F5, shares sedimentological characteristics with the channel beds and flanks. The third realm is the main channel realm, characterized by facies F6 and F7. These facies exhibit a sediment composition of medium to coarse-grained sands, containing significant amounts of silicate grains and bivalve shell debris. This realm is distinguished by the largest water depths in the main channels, and the flow energy during tidal exchanges is most pronounced. Surface sediment structures are constituted of sand ripples and sand waves (Mascioli et al., 2022).

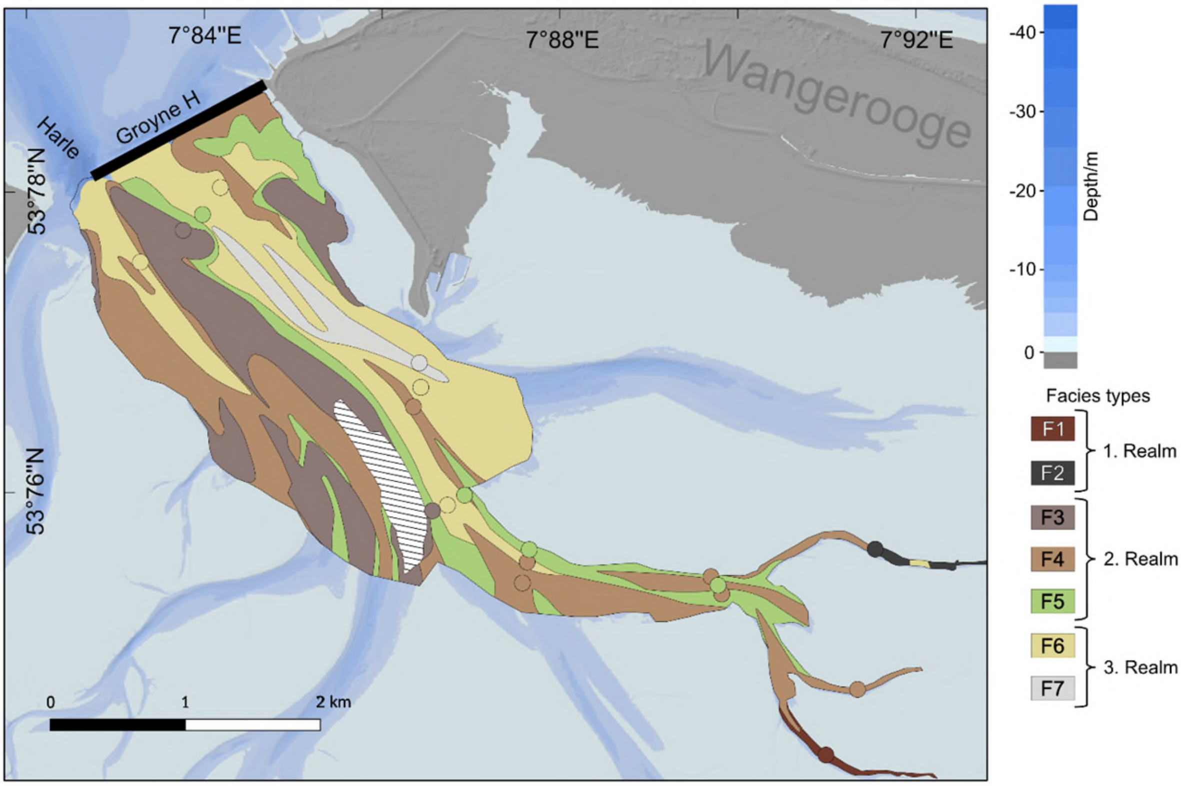

Figure 2.4: Facies map of the working area. Dark brownish colors represent the first realm of facies F1 and F2 in the channels. Brownish and greenish colors in the main channels and on the flanks represent facies F3, F4, and F5 of the second realm. Yellowish and grayish colors in the main channels represent the third realm of facies F6 and F7. The colored points show the sample station and the associated facies.

Mascioli et al. (2022) proposed a similar classification for the Harle, identifying an additional realm characterized by Holocene peat or clay outcrops. This realm consists of hard substrate from the Holocene, surrounded by sands, and is situated along the slope of the main Harle channel. However, due to the limited spatial extent of this realm and the lack of ground truthing, its presence is solely based on the interpretation of hydroacoustic data. Observations by Streif (2004) indicate the occurrence of a peat layer along the slopes of the tidal inlets representing the termination of Pleistocene morainic and glaciofluvial deposits overlain by Holocene marine sediments. This peat layer suggests the erosion forces exerted by the current flow and provides insights into the maximum depth of channel deepening and the reworking of underlying coarse sediments in the inlets.

Conspicuous features observed in Facies F7 include bivalve shells encrusted by bryozoans (Fig. 2.5).

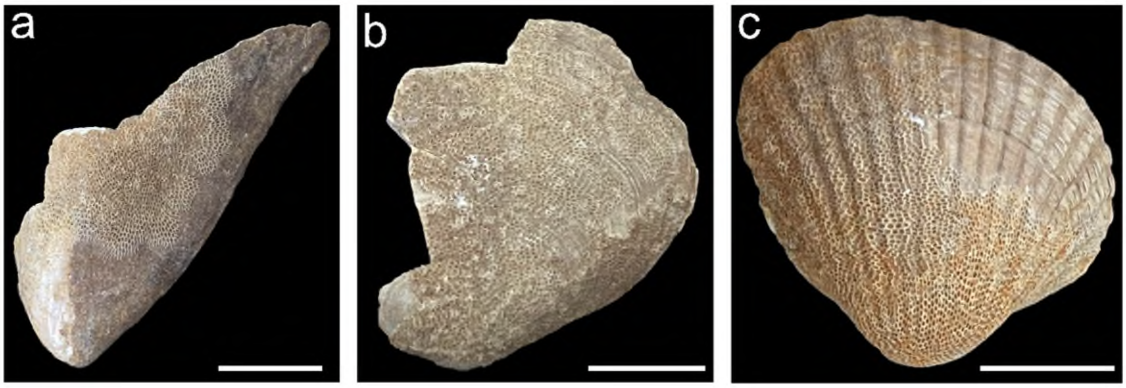

Figure 2.5: Disarticulated bivalve shells of Mytilidae (A), *Mya* (B) and Cardiidae (C) and with overgrown bryozoans. Scale bar shows 1 cm.

While bryozoans are present in Facies F4, F5, and F6, their abundance is less than 1 %, indicating their underrepresentation. The primary occurrence of bryozoans is found in Facies F7 along the channel of the Dove Harle. Bryozoans, known to require hard substrates for larval settlement only on solid surfaces (Kuklinski and Barnes, 2005; Ward and Thorpe, 1989). In unconsolidated sediment, sessile organisms can utilize mollusk shells as hard substrates. Encrusting and boring bryozoans are particularly prevalent on disarticulated bivalve shells in diverse marine coastal environments (Almeida et al., 2018a; Almeida et al., 2018b; Brett et al., 2011; de Blauwe, 2006; de Blauwe 2020; Denisenko et al., 2017; Kuklinski et al., 2005; McKinney, 1996). The most stable position for shells in high-velocity regimes is with the convex side facing upwards (Allen, 1984). In intertidal regimes, encrusting bryozoans, as described by Almeida et al. (2015) and de Blauwe (2006), generally grow on disarticulated bivalve shells on their convex side. Amini et al. (2004) observed that areas with high sedimentation rates tend to have fewer bryozoans. Disturbances such as substrate movement and bioturbation can also decrease the bryozoan abundance (Kelly and Horowitz, 1987; Smith, 1995).

In Facies F7, bryozoans are predominantly found on the convex side of bivalve shells, suggesting a stable position. The presence of encrusting bryozoans implies a low sedimentation rate in this area, while the orientation indicates a stable substrate movement with low grain movement. Lüders (1952) described a sediment deposition process of an infill in the Dove Harle. Investigations by Homeier (1973) and Ladage and Stephan (2004) indicated a termination of the deposition, discussing the non-attainment of dynamic equilibrium. The occurrence of bryozoans on the bivalve shells also suggests restricted sedimentation within the Dove Harle. Currently, it is assumed that 66 % of the ebb current flows through the Dove Harle (Ladage and Stephan, 2004). This indicate changes in the hydrographic conditions, which caused the termination of deposition in the Dove Harle channel.

2.4.2 Morphological structures

Groynes, in general, exert significant influence on various environmental factors, including changes in bathymetry through erosion and the formation of scours, alteration of flow patterns, velocity, and turbulence sediment transport, deposition and erosion processes, as well as impacting bed shear stress (Kristensen et al., 2016; Walker et al., 1991; Wu and Qin, 2020; Zhou et al., 2021). Ladage and Stephan (2004) documented a bisection of the main channel, resulting in the establishment of a dual channel system since 1998. The modification appears stable, accompanied by the development of a sand barrier between the main channels of the Harle and Dove Harle.

Scouring and sediment deposition are the primary effects of groynes on sediment dynamics. The sedimentation rate is influenced by the length, angle, and crest elevation of a groyne, lower crest heights resulting in higher erosion forces and a negative sedimentation rate (Henning and Hentschel, 2013). Several investigations have been conducted to examine altered flow characteristics along groynes and groyne fields (Biria et al., 2015; Henning and Hentschel, 2013; Higham et al., 2017; Sukhodolov et al., 2004). Overall, flow velocity is increased at the tip of the groyne. The specific characteristics of the groyne, whether emerged or submerged, lead to variations in flow patterns and resulting sedimentation patterns. On the downstream side of an emerged groyne, flow velocity decreases, resulting in the development of a mixed shear layer along the streamline and the formation of a recirculation eddy near the groyne. Depending on the topography, the number of recirculation eddies differs, with a single eddy occurring in deep flows and a counteracting second recirculation eddy occurring in shallow flows (Armaly et al., 1983; Talstra et al., 2005). Based on sediment composition, larger grains settle along the mixed shear layer due to decreased flow energy, while finer sediment is transported by the eddy into the groyne field and subsequently settles. Very fine sediments tend to be transported to the attached corner of the groyne. In the case of submerged groynes, a vertical eddy forms at the leeside, leading to erosion on the downstream side. Lower flow velocities within the groyne field result in sediment deposition in the center of the field (Carling et al., 1994; Henning and Hentschel, 2013).

In the specific case of the tidal inlet of the Harle and Groyne H, the main flow direction undergoes semidiurnal changes, with the groyne being submerged during flood and partially emerged during ebb, resulting in scouring north and south of the groyne during flood conditions (Fig. 2.6). The intensity of the scours is greater in areas where the groyne crest is lower. South of Groyne H, a sand barrier composed of Facies F3 is formed orthogonally to the groyne and parallel to the channels, permanently separating the channels of the Harle and Dove Harle. The presence of groynes can lead to the formation of sandbars, which induce changes in flow behavior. Along the mixed shear layer, where flow velocity decreases, sediment load settles. It can be assumed that the distance of 700 m is determined by the flow dynamics of vertical circulation cell which occurs during the overflow of the groyne at flood. The shape of the sand barrier follows the flow edge, which can be observed as breaking water in aerial photographs. The facies distribution indicates the presence of finer grained sediments of facies F4 and F5 in the area between Groyne H, Groyne U, and Groyne V. The recirculation eddy may transport these fine-grained sediments to the corner, where they settle and deposit.

Considering the tidal influences, it is reasonable to infer that sediment deposits and erosion areas are influenced by both submerged and emerged groyne characteristics of Groyne H. The scours observed during flood conditions are the outcome of the vertical eddy generated when the groyne is submerged. Conversely, the formation of the sand barrier and the presence of finer grained sands in the attached corner of the groyne field are the result of ebb conditions when the Groyne H is partially emerged, and the recirculation eddies and mixed shear layers are formed (Fig. 2.6).

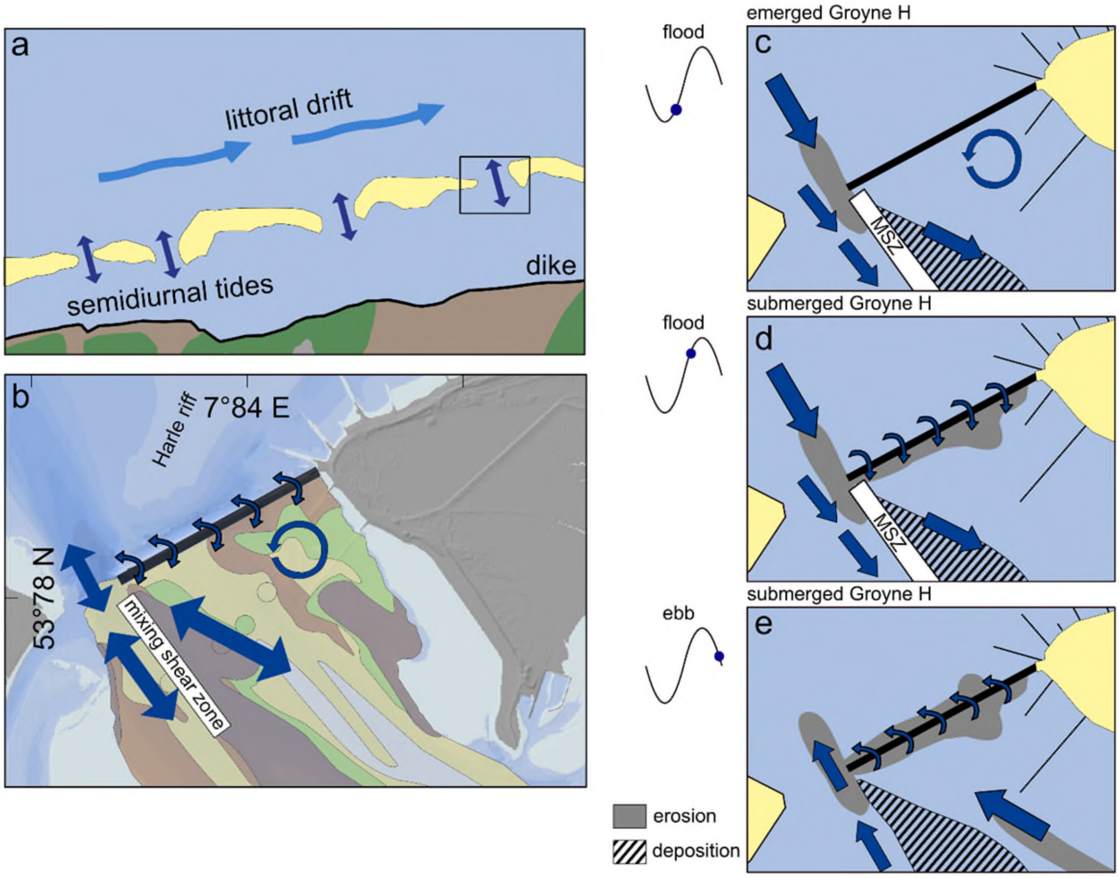

Figure 2.6: (A) shows an overview of the East Frisian Islands and the tidal directions and the direction of the littoral drift. (B) shows schematically the prevailing currents over the facies map, influenced by Groyne H (black line). During the onset of the flood current, the water flows into the inlet around the partially emerged Groyne H (C). An eddy forms in the downstream area. A strong current develops at the tip of the groyne, leading to erosion. Behind, a mixed shear zone develops where sediment is deposited. During high tide (D), the groyne is submerged and a vertical circulation cell develops, leading to scour erosion south of Groyne H. During the onset of the ebb current (E), the groyne is submerged and the vertical circulation cell leads to scour erosion north of the groyne. The strong current along the Dove Harle channel leads to erosion along the main channel.

2.4.3 Comparison with a natural inlet

To assess the impacts caused by the longstanding coastal protection measures in the Harle, a comparison with a tidal inlet system minimally affected is necessary. The tidal inlet system between the islands Langeoog and Spiekeroog, respectively the Otzumer Balje, provides a suitable basis for such a comparison, being only protected by groynes along its northern coastline, leaving the inlet itself unaffected. Given the short distances between the Harle and Otzumer Balje, as well as the similar geographic and oceanographic conditions, a comparative analysis between these two systems can offer valuable insights into the extent of the impacts resulting from coastal protection measures. The sediment dynamics of the inlet channel in the Otzumer Balje are characterized by anticlockwise shifting due to sediment transport in the ebb delta, with recirculation of sediments occurring within the delta (Son et al., 2011; Valle-Levison et al., 2018). The tidal flats of the Otzumer Balje are dominated by a single main channel (Fig. 2.7). In contrast to the Harle, where the main channel is divided into the Harle and the Dove Harle. The split-up of the main channel in the Harle was a semi natural process that has been influenced and restricted by human activities. However, the altered current energies and bedload capacities have led to the formation of a sandbar between the Harle and the Dove Harle. This sandbar has developed as a result of the modified flow patterns and sediment transport dynamics (Ladage and Stephan, 2004). In the Harle, the formation of the sandbar acts as a barrier, whereas a similar sand bar has not formed in the Otzumer Balje. Consequently, the current energy in the Otzumer Balje is not restricted.

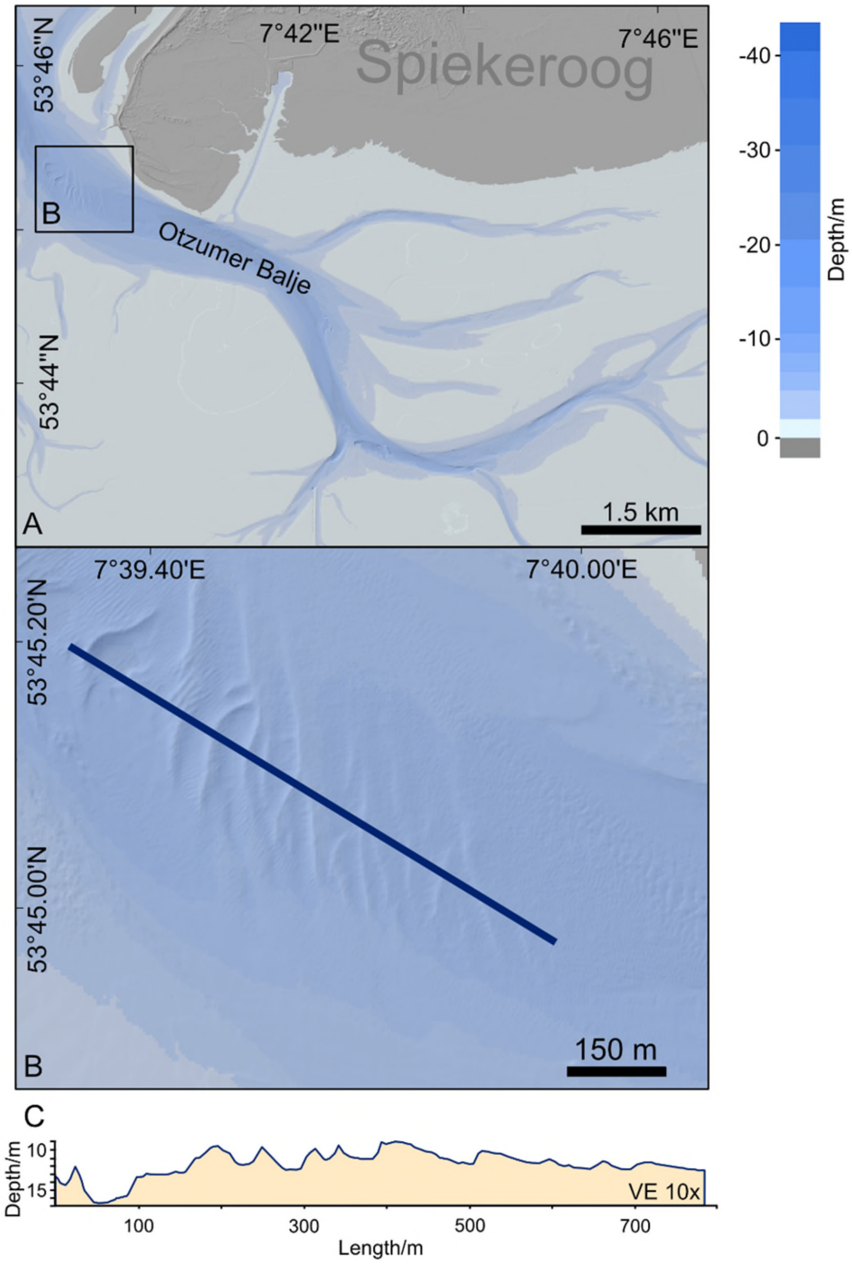

Figure 2.7: Overview map of the Otzumer Balje (A), with the subaqueous dune field in (B) and the marked cross section (blue line). Cross-section through the subaqueous dunes (C) with a 10x vertical exaggeration (WSV, 2021).

Digital Elevation Model data from the Waterways and Shipping Authority Germany (WSA) show the main channel of the Otzumer Balje. Here a subaquatic dune field has developed at the widest section. These compound subaquatic dune field reach a maximum height of 3.5 m and is extended to a length of 1,280 m (Fig. 2.7). Literature states that subaquatic dunes typically form under high current velocity conditions ranging from 0.6 to 1.5 ms^{-1} (Ashley, 1990; Boothroyd, 1985; Reineck and Singh, 1980). Megaripples can be observed within the tidal flats along the area of the Time Series Station (Noormets et al., 2006). Subaquatic dunes are commonly found in tidal inlets, as seen in the inlet channel between islands Skallingen and Fanø, respectively, where they migrate at a rate of 0.07 m per day (Bartholomä et al., 2004). In contrast, the dominant bedforms in the Harle are ripples to megaripples, with subaquatic dunes being absent. The maximum currents in the Harle reach a speed of 1 ms^{-1} at the tip of the groyne, but on the downstream side, the flow velocity decreases to 0.2 ms^{-1} (Albinus, 2021). This results in sediment deposition along the mixed shear layer in the sand barrier. Large sand waves, rather than dunes, are observed by Mascioli et al. (2022) in the Harle, particularly on the sand barrier between the main channels. The height of these sand waves increases with distance from Groyne H. Factors such as current energy and water depth can influence the formation and height of subaquatic dunes (Allen, 1968; Flemming, 1978), and in the Otzumer Balje, the water depth along the dune catchment area ranges from 19 m to 25 m, whereas in the Harle, the water depth in the sand wave areas is < 10 m.

The sediment grain size in the Otzumer Balje varies between 350 µm in the inlet channel and 88 µm in the back-barrier intertidal basin (Antia, 1994; Flemming and Nyandwi, 1994; Son et al., 2011). Notably, sediments corresponding to Facies F7 are absent in the literature about Otzumer Balje. Unlike the Harle, the Otzumer Balje does probably not exhibit shill sediments characterized by disarticulated shells overgrown by bryozoan colonies. As previously hypothesized, the channel of the Dove Harle is covered with this facies, indicating a low sediment bedload within the channel. However, despite these conditions, no distinct bedforms such as megaripples and sand waves are observed in the Dove Harle channel.

Data on the northern side of Groyne H, specifically regarding the “Harle Riff”, are currently lacking. However, it is reasonable to assume that an ebb stream recirculation eddy occurs in this area. This eddy would interact with the natural system, similar to the observed recirculation of sediments along the northern shoals in the Otzumer Balje and it may assume that the sublittoral sediment transport is restricted to a minimum.

2.5 Conclusion

Overall the sedimentary facies within the Harle inlet can be classified into three realms:

- Wadden realm (Facies F1 and F2): Found in intertidal shoal gullies, this realm is characterized by fine sediment and organic detritus.
- Channel realm (Facies F3, F4, and F5): Predominantly consisting of fine-grained sediment with silicate grains and bivalve shell debris. This realm encompasses the channel beds and flanks
- Main channel realm (Facies F6 and F7): Characterized by medium to coarse-grained sands with high flow energy and sand ripples. This realm is situated at the greatest depths within the main channels.

The construction of groynes in the Harle has led to various morphological changes, which are not observed in the natural neighboring tidal inlet, Otzumer Balje. Depending on the semidiurnal tides, resulting in the periodic emerge and submerge of the groyne, contribute to morphological alterations in the Harle erosion along the groyne flanks is likely induced by vertical circulation cells at high water tides. Furthermore, erosion is evident at the tip of the groyne, where increased flow exerts higher erosion forces. Conversely, specific deposition areas emerge, such as the occurring eddy during low water tides and in the mixing shear zone, where flow decreases, and sediment load is lower. These dynamics result in the separation of the two main channels, Harle and Dove Harle, in the Harle inlet. Additionally, notable differences in sediment bedforms are observed between the Harle and the natural system of the Otzumer Balje. In the natural system, bedforms are dominated by ripples and megaripples, with occasional subaquatic dunes. In contrast, the Harle exhibits only ripples and megaripples, subaquatic dunes are absent.

To enhance the comparison between the Harle and the Otzumer Balje, it is imperative to generate a facies map for the Otzumer Balje using the methodology outlined in this study. The existing literature on the Otzumer Balje referenced in this research provides a comprehensive overview of prior investigations, offering valuable insights into the general disparities between the tidal inlets. However, to enable a direct and robust comparison, the creation of a comprehensive facies map is essential. Such a map would illustrate variations in sediment distribution and surface sediment influences across a broad expanse for the Otzumer Balje, facilitating a more evident demonstration of the impacts of coastal protection measures on the Harle inlet. Unlike individual sampling points used as references, a facies map created with multibeam backscatter data provides a holistic depiction of the overall surface sediments, thereby offering a more nuanced understanding of the differences between the two inlet systems.

This study highlighted the combination of hydroacoustic backscatter data with sedimentological characteristics as grain size and component analysis to interpret morphological alterations, sedimentation and transport processes in relation to tidal currents and coastal protection structures, which could be easily applied at other study sites.

Chapter 3

Facies Mapping and Seasonal Sediment Shift of Tidal Inlets: Impacts of Coastal Protection Measures

This chapter is based on the publication:

Geßner, A.-L.; Albinus, M.; Giebel, H.-A.; Wollschläger, J.; Mascioli, F.; Badewien, T. H. (2025) Facies Mapping and seasonal sediment variation analysis of tidal inlets: Impacts of coastal protection measures. Journal of Sedimentary Environments. (in review)

Abstract

Coastal areas play a vital role in the face of climate change, especially concerning sea level rise, coastal protection, and ecosystem preservation. This study investigates the impacts of hard coastal protection on mesotidal inlets, focusing also on seasonal sediment shift and comparing natural versus modified systems. A surface facies map was compiled for the almost natural tidal inlet of the East Frisian Islands Otzumer Balje to contrast to the Harle inlet, which is influenced by long-term coastal protection measures. Sediment samples were collected after storm season and fair-weather season to analyze grain size and composition. Results show that both inlets experience seasonal changes in sediment characteristics due to biological factors like benthos growth and physical factors such as storm induced sediment transport. The Otzumer Balje exhibits seasonal sediment shift, with coarser materials prevailing in summer and allochthonous mudflat sediments accumulating during winter storms. In contrast, the Harle features a higher diversity of bioclastic materials, including bryozoan-encrusted shell fragments, indicative of more stable sediment conditions. Geomorphologically, the Otzumer Balje is characterized by a single-channel system with active subaquatic dunes, whereas the Harle consists of two main channels influenced by groyne-induced scouring and sediment deposition. Biological activity differs between the inlets, with the Harle displaying more diverse benthic communities and pronounced bryozoan colonization due to lower sedimentation rates. The study underscores the role of coastal protection measures in shaping these tidal inlets and highlights the necessity of coastal management strategies that account for the interaction between human interventions and natural dynamics.

3.1 Introduction

Over the last few decades, seasonal variability has become more significant, and extreme weather events have increased in frequency. Societal vulnerability in coastal areas is expected to rise due to coastal migration, urbanization, limited habitable space, and population growth. Additionally, climate change is contributing to more frequent extreme weather events in an increasing number of areas. Key factors include temperature extremes, precipitation extremes, storms, and severe weather (Morss et al., 2011).

Temperature extremes significantly impact the marine environment. Hot summer events lead to higher sea surface temperatures, and especially in shallow areas, the temperature differences between the seasons become substantial. Higher water temperatures can increase mortality rates among benthic organisms (Soon and Zheng, 2020). Benthic organisms are important for the sediment stability. Microalgae, which produce extracellular polymeric substances, stabilize the sediment (Decho, 2000; Lubarsky et al., 2010; Spears et al., 2008). Microbenthic organisms can also stabilize the sediment through bioturbation and mucous-binding of sediment (Montserat et al., 2008; Mouritsen et al., 1998, Probert, 1984). Short term effects of benthos mortality include an increase in coarse sediment grains and decreased fine faction content (Mouritsen et al., 1998). The shells of the dead benthic organisms are damaged by wave energy and transport mechanisms, forming smaller bioclastic components. With increasing transport length and time before deposition, these components become more damaged, finer, and rounded (Leighton et al., 2016; Zuschin et al., 2003) and can be an indicator for transport length.

Storm events play a crucial role in sediment transport and erosion. Storms with strong winds and high wave action significantly impact sediment morphology and movement. Changes in grain size, morphology, and transport mechanisms can alter benthos communities. Human settlements are also at risk from severe storm events, as intense erosion can have fatal consequences for land use and settlements. The impacts of storms are well documented, with significant consequences recognized in various coastal areas (Costanza et al., 2021; Dolan and Davies, 1994; Leonardi et al., 2017; Liu and Wang, 2019; Mather and Stretch, 2012; Potter, 2014; Rangel-Buitrago and Anfuso, 2011).

Historically records documented extensive damages along the North Sea coast since the Middle Ages on (Behre, 2004; Mauelshagen, 2007; Meier, 2011; Meier, 2012; Soens et al, 2011). Several flood events reshaped the entire German North Sea coastline, creating tidal basins and the Wadden Sea area, isolating settlements from the mainland, forming islands, and submerge islands (Fig. 3.1; Meier 2012; Meurer, 2000). To protect remaining land and settlements, coastal defense measurements were developed (Niemeyer et al., 1996).

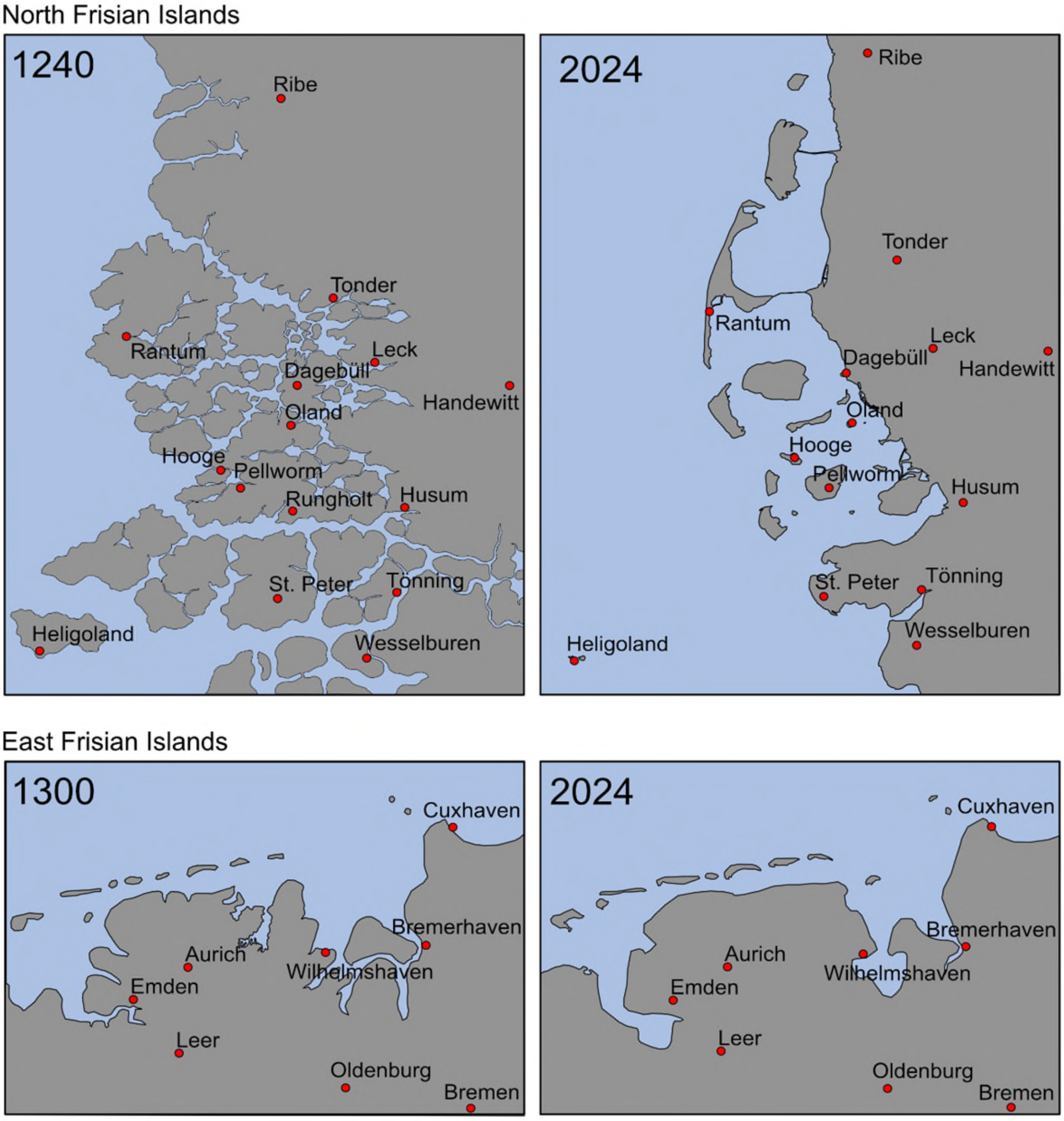

Figure 3.1: Historical maps of the North and East Frisian Islands along the Southern North Sea coast. These maps illustrate the geographic conditions before the catastrophic storm floods of 1362. The maps depict the North Frisian Islands in 1240 (based on Mejer, 1649) and their current state. For the East Frisian Islands, the maps show the situation in 1300 (based on Behre, 2004; Folckers, 1722; Ladage et al., 2007; and Sello et al., 1966) and their current state. The extent of land loss has been significant and dramatic.

Coastal management has been well-established for decades, incorporating a range of hard protection measures such as dikes, seawalls, breakwaters, and groynes along coastlines and islands. Among these, groynes play a particularly significant role in shaping coastal dynamics, as they directly influence hydrodynamic conditions, sediment transport, and deposition patterns, ultimately modifying shoreline morphology. By disrupting longshore drift, groynes affect sediment redistribution along the coast. The construction of a groyne causes sediment to accumulate on the updrift side, offering protection to that area from erosion. However, this sediment blockage often results in erosion on the downdrift side due to the reduced sediment supply (Coghlan et al., 2013; Hanson et al., 2009). To prohibit the erosion, groynes are installed in sequences to form a groyne field.

In areas with bidirectional tidal flows, hydrodynamic patterns are affected in two directions, which may lead to both erosion and sedimentation upstream and downstream of the groyne. These bathymetric changes can result in sediment scouring, channel migration, and channel infilling (Wheeler et al., 2010). Investigations by Ladage et al. (2006) and Mascioli et al. (2022) have shown how the construction of a stream groyne influences sedimentology and morphology in tidal inlets in the Southern North Sea. Albinus et al. (2025, in prep.) and Geßner et al. (2024) highlight the hydrodynamic alterations caused by these structures. The construction of groynes can disrupt natural tidal flows by increasing flow velocities, leading to erosion and scouring in the immediate vicinity. Additionally, changes in flow dynamics can produce mixed shear zones, where sediment is deposited, creating shallower areas that form barriers. These changes can significantly alter the local coastal environment, emphasizing the need for detailed and informed design considerations in coastal management practices.

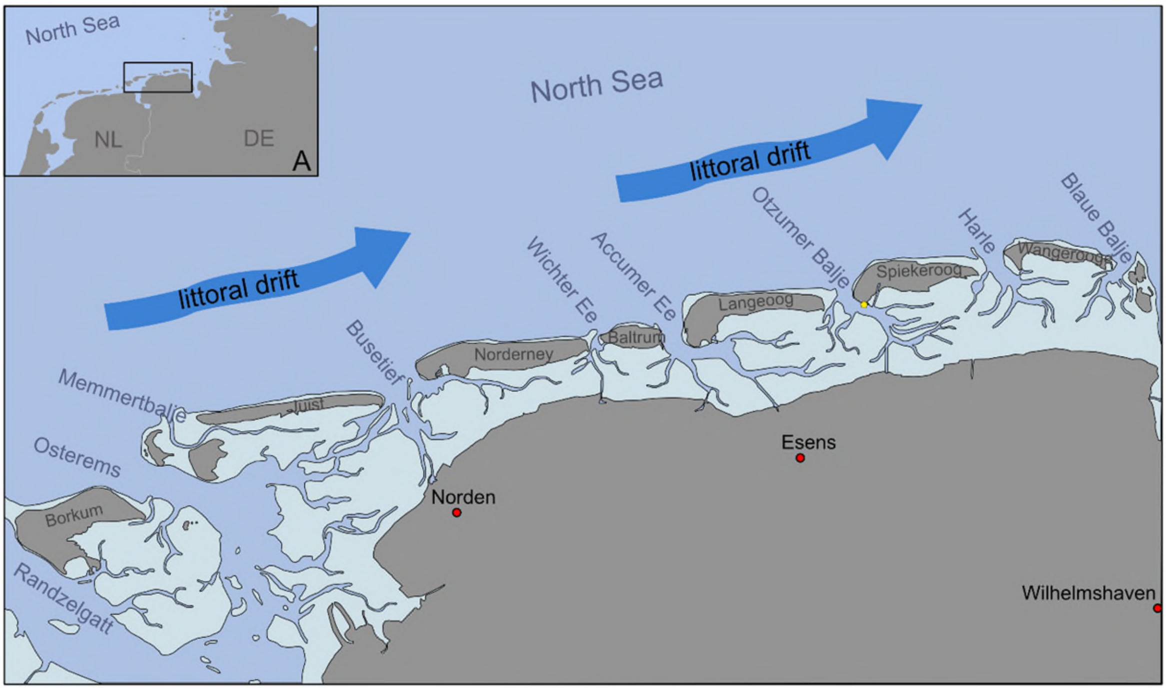

Figure 3.2: Overview map of the East Frisian Islands. This map highlights the main littoral drift along the North Sea coast, which transports sediments from west to east. The Time Series Station (TSS; marked by a yellow dot) is situated in the tidal inlet of Otzumer Balje. NL: The Netherlands, DE: Germany.

In the Southern North Sea, an eastward directed littoral drift transports sediment from west to east, resulting in the eastward migration of the East Frisian Islands (Niemeyer, 1995). To prevent further eastward migration, groynes have been established along the inlets Randzelgat, Busetief, Wichter Ee, and Harle (Fig. 3.2; Lüders, 1952; Homeier, 1973; Fitzgerald and Penland, 1987). Most of the other inlets are in relative pristine condition.

The Harle inlet, located between the islands of Spiekeroog and Wangerooge, is significantly affected by the presence of a particular anthropogenic structure, the Groyne H. This groyne restricts the exchange area between the North Sea and the Wadden Sea, extending from the western end of the island Wangerooge to Spiekeroog and narrows the inlet channel from 5.5 km to about 2 km. Studies by Mascioli et al. (2022) and Geßner et al. (2024) in the Harle inlet investigate the morphological and sedimentological features.

The results indicate an important impact of Groyne H on sediment distribution, deposition areas, and tidal currents. These findings have been compared to the conditions of the inlet Otzumer Balje, which is also located along the East Frisian Islands between the islands of Langeoog and Spiekeroog. However, this inlet is almost unaffected by groynes. The existing groynes on the island Spiekeroog are present to defend the northern beach. Several studies have been conducted in the Otzumer Balje, focusing on tidal currents (Niesel, 1999; Valle-Levinson et al., 2018), benthos (Reiss and Kröncke, 2001), sediment (Herrling and Winter, 2014; Noormets et al., 2006; Son et al. 2011), and the Wadden flats (Bungenstock et al., 2021).

Geßner et al. (2024) have outlined significant disparities between the Harle and Otzumer Balje inlets, including differences in morphological characteristics, sediment composition, water depth, and tidal current patterns. However, they identified a critical gap in the availability of a comprehensive facies map, which could better illustrate variations in sediment distribution and surface sediment characteristics between the two inlets, particularly to emphasize the influence of Groyne H on the Harle inlet.

This study aims to address this gap by creating a detailed facies map of the Otzumer Balje, elucidating the differences between the two inlets and highlighting the impacts of coastal protection measures in a tidally dominated environment by bidirectional currents. Additionally, sediment samples collected from fixed locations in both the Harle and Otzumer Balje inlets after the storm season in March and the fair-weather season in September provide insights into seasonal variations of the surface sediments. These data underscore the different sediment dynamics in the two inlets and further illustrate the influence of coastal protection structures like Groyne H on tidally influenced systems.

3.2 Study area

Along the North Sea, the coasts of the Netherlands, Germany, and Denmark, as well as the tidal basins of the Wadden Sea, are protected by the seaward barrier of the Frisian Islands (Fig. 3.3A). In the southernmost region, these islands form a chain of barrier islands separated by tidal inlets, known as the West and East Frisian Islands. The study area is situated in the Southern North Sea, specifically within the tidal inlets of Spiekeroog, an island along the eastern end of the East Frisian Islands of the northwest coast of Germany. Spiekeroog is delimited by the tidal inlet "Otzumer Balje" to the west and "Harle" to the east (Fig. 3.3B). These tidal inlets serve as connection and exchange areas between the open North Sea and the tidal basins. Due to the influence of tides, winds, and waves, these areas are highly dynamic systems.

The tidal inlets of the island Spiekeroog have a semidiurnal average tidal range of 2.9 m (Dittmer, 1999; Niemeyer and Kaiser, 1994). Described after Hayes (1980), mesotidal conditions prevail in this area with a mixed energy tidal regime (Herrling and Winter, 2014; Ladage et al., 2007). The annual significant wave height in the inlet ranges from 0.7 to 1.0 m (Ladage and Stephan, 2004; Niemeyer, 1995). The dominant tidal current is the ebb current (Niemeyer, 1990), also evident by subaquatic dunes, which orientation reflects ebb dominance (Geßner et al., 2024). The current velocity is up to 1.3 ms^{-1} in the Otzumer Balje and 1.0 ms^{-1} in the Harle (Albinus et al., 2025, in prep.; Valle-Levinson et al., 2018). Stanev et al. (2007) describes the asymmetry of the tidal currents. With the flood current dense North Sea water with a higher salinity is intruding in the relatively lighter Wadden Sea water. This density gradients are described by Burchard et al. (2008) as well as Burchard and Badewien (2015) and result in the accumulation of suspended particular matter (SPM) in the Wadden Sea area.

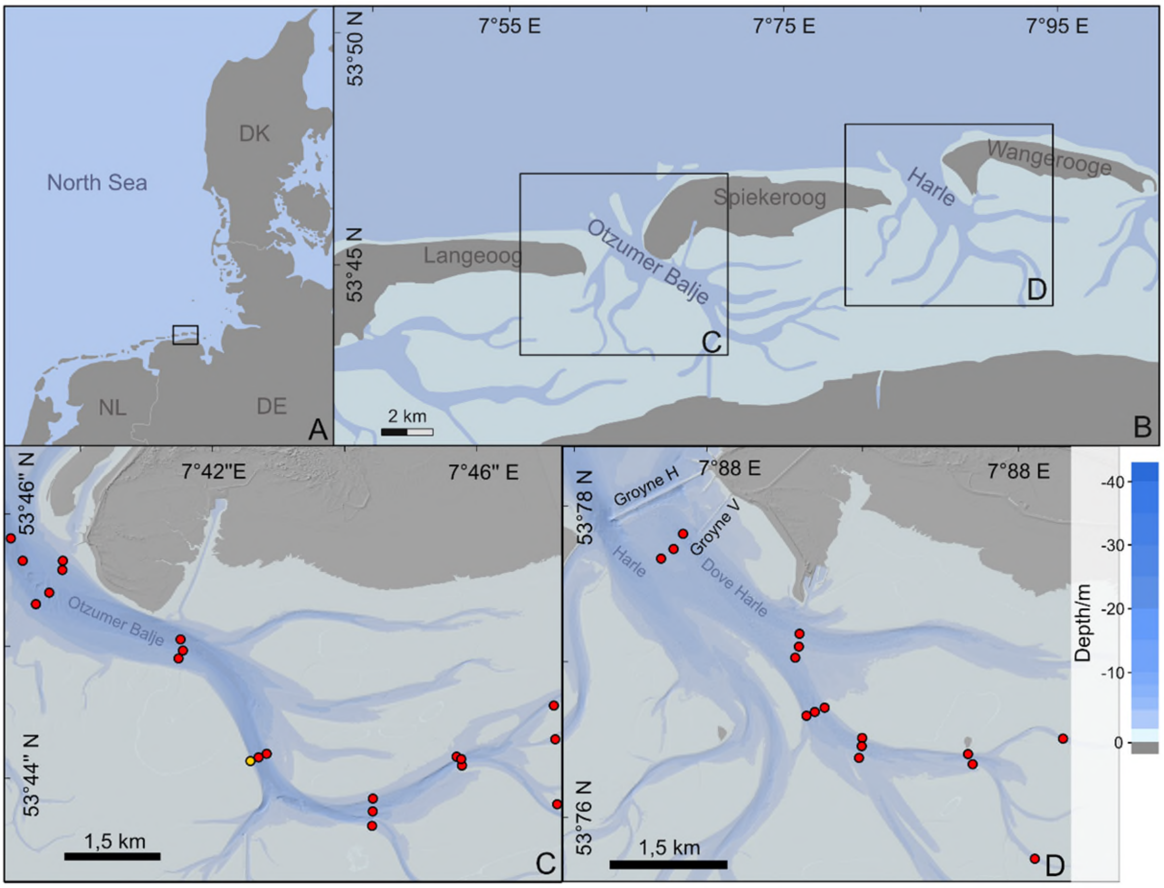

Figure 3.3: Map of the study area. Map A provides an overview of the North Sea, highlighting Denmark (DK), Germany (DE), and The Netherlands (NL). Map B shows the locations of the tidal inlets Otzumer Balje and Harle. Map C displays the sampling stations in Otzumer Balje from March and September (marked by red dots), including station In12 (marked by a yellow dot). Map D illustrates the sampling stations from the study by Geßner et al. (2024) in March, which were resampled in September as part of this study. The groynes H and V are situated along the western end of the Island Wangerooge.

The Otzumer Balje between the islands of Langeoog and Spiekeroog is characterized by a single main channel, which is divided into gullies in the tidal flats (Fig. 3.3C). In the literature, the sediments of the gullies are described as fine-grained sands with a D50 of 88 µm, and the channel beds are medium to coarse-grained sands with a D50 of 350 µm (Antia, 1994; Flemming and Nyandwi, 1994; Son et al., 2011). Morphologically, the Otzumer Balje is mainly characterized by rippels and megaripples. In the main channel occurs a field of subaquatic compound dunes of a size of 0.210 km^2. The dunes have a height of max 3.5 m at a water depth of around 12 m (Geßner et al., 2024). Son et al. (2011) discover a recirculation of sediment within the ebbtidal delta of the Otzumer Balje.

Small beach groynes are attached to the northwestern part of island of Spiekeroog, which protrude 200 m in the northern branch channel of the Otzumer Balje and are not supposed to affect the main channel.

The Harle is an ebb-dominated tidal inlet characterized by two main channels, namely the Harle and the Dove Harle (Fig. 3.3D). These channels constitute the primary transport channels for tidal flows. In the backbarrier basin there are tidal flats interspersed with channels. Geßner et al. (2024) provide a detailed map of the sediment and facies within the main inlet body, which extends from the inlet to an end of a channel. Three distinct realms are generally observed in the Harle inlet.

The sediments within the gullies primarily consist of fine-grained materials and a high proportion of plant detritus, forming the Wadden realm. The smaller channels and the channel flanks are composed of fine to medium silicate sands with bivalve fragments, constituting the channel beds and flanks realm. In contrast, the beds of the main channels are characterized by medium to coarse silicate grains and bivalve fragments, defining the main channel realm.

The construction of a series of groynes along the island of Wangerooge strongly influences the Harle inlet. The long groyne, Groyne H, situated within the exchange area between the open North Sea and the tidal basin, results in the deepest depression with a water depth of 34 m among the Frisian Islands (Fig. 3.3D). However, the main channel depths range from 5 to 10 m. As a consequence of the groyne construction, a fine to medium-grained sandbar formed in the inlet, separating the Harle and Dove Harle channels (Geßner et al., 2024; Homeier, 1973; Ladage and Stephan, 2004; Lüders, 1952).

Coastal protection measures significantly impact the natural currents, with a maximum tidal current exceeding 1 ms^{-1}. Due to the restricted discharge of the stream groyne on the downstream side during low tide of Groyne H, a counteracting dynamic eddy is generated. This results in a low-velocity zone in the center of the eddy, rotating clockwise at a speed of 0.2 ms^{-1}. The eddy is constrained by Groyne H and the further southeast located Groyne V (Fig. 3.3D; Albinus et al., 2025, in prep.; Geßner et al., 2024).

3.3 Methods

Sedimentological sampling and facies mapping

Samples of sediment were obtained from various energetic zones within the channels of the tidal inlets Otzumer Balje and Harle (Fig. 3.3). Utilizing a 1 m^2 Van Veen grab sampler, collection occurred both after the storm flood season in March 2022 and following the fair-weather season in September 2022. In the course of two ship-based field campaigns, samples from the subtidal regions were acquired aboard the *RV Senckenberg*, while those from the shallower intertidal regions were obtained using the *RV Otzum* during high tide.

For the grain size analysis and the semiquantitative component analysis bulk samples (250 ml) were extracted from the grab samples. To gain the grain size distribution after the Udden and Wenthwoth scale, the samples were wet sieved in the fractions > 2000 µm; 2000 – 1000 µm; 1000 – 200 µm; 200 – 63 µm and <63 µm and dried in a drying oven at 38 °C for 72 h. Scatter samples of the fractions > 2000 µm to 63 µm were analysed with a binocular to determine the semiquantitative component analysis. Depending on the corresponding weight percentage of each grain size fraction, the abundances were classified in: under represent (< 1 %), present (1-2 %), rare (2-5 %), abundant (5-10 %), very abundant (10-24 %), and dominant (> 24 %).

Geßner et al. (2024) published a sedimentological facies map of the Harle based on the sediment samples collected in March 2022. Grain size and component analyses were conducted, and the results underwent statistical analysis to categorize the facies groups.

Following the methodology outlined by Geßner et al. (2024), the samples in this study were analyzed using the same approach. Overall statistical analysis allowed for the identification of facies occurring in March and September in the Otzumer Balje, as well as in September in the Harle.

To generate a sedimentological facies map, multibeam backscatter data from 2019 obtained through regular monitoring campaigns in the Otzumer Balje were provided by the Lower Saxony Water Management, Coastal and Nature protection Agency (NLWKN). The intensity of the backscatter signal depends on various factors such as seafloor roughness and grain size (Hamilton, 1980). By integrating the backscatter intensity with the results of the facies analysis, a facies map was compiled.

Comparison of samples collected at the different seasons (March and September) addressed variances in the samples attributed to seasonal variations like the growth of benthic organisms and storm-induced erosion and transport forces.

Current velocity measurements in the Harle and Otzumer Balje

Current velocity data were collected during research cruises SE202106-1 (Otzumer Balje, June 2021), SE202203-1 and SE202203-2 (Otzumer Balje, Harle, March 2022), and SE202206-1 (Harle, June 2022) aboard RV *Senckenberg*. The vessel was anchored south of the west beach of Spiekeroog for measurements in the Otzumer Balje and south of the tip of Groyne H for the Harle. Data acquisition was conducted using an RD Instruments Teledyne Workhorse Sentinel II 1200 kHz ADCP, mounted on the starboard hull of the vessel at a depth of 1.3–1.5 m below the waterline. The ADCP operated in single-ping broadband mode with a bin size of 0.25 m, providing a data output frequency of 1–2 Hz. A compass calibration was performed to align the internal ADCP compass with the navigation data from a GPS Trimble Receiver. Each time series measurement spanned approximately 12 hours.

3.4 Results

Based on distinct sedimentological characteristics, the samples were systematically categorized into groups. The classification was conducted employing grain size distribution and component analysis data. After Geßner et al. (2024) the classified facies were used and extended by new occurring facies. Within the two distinct inlets, Otzumer Balje and Harle, a total of nine facies types were discerned: clay (F0), clayey sands (F1), organic-rich clayey sands (F2), very fine sands (F3), bioclastic organic-rich fine sands (F4), bioclastic fine sands (F5), bioclastic middle sands (F6), shill sands (F7) and submarine dune sands (F8). The seasonal variations in the facies of the two inlets are shown in figure 3.4 and the extended facies map of the Otzumer Balje in figure 3.5.

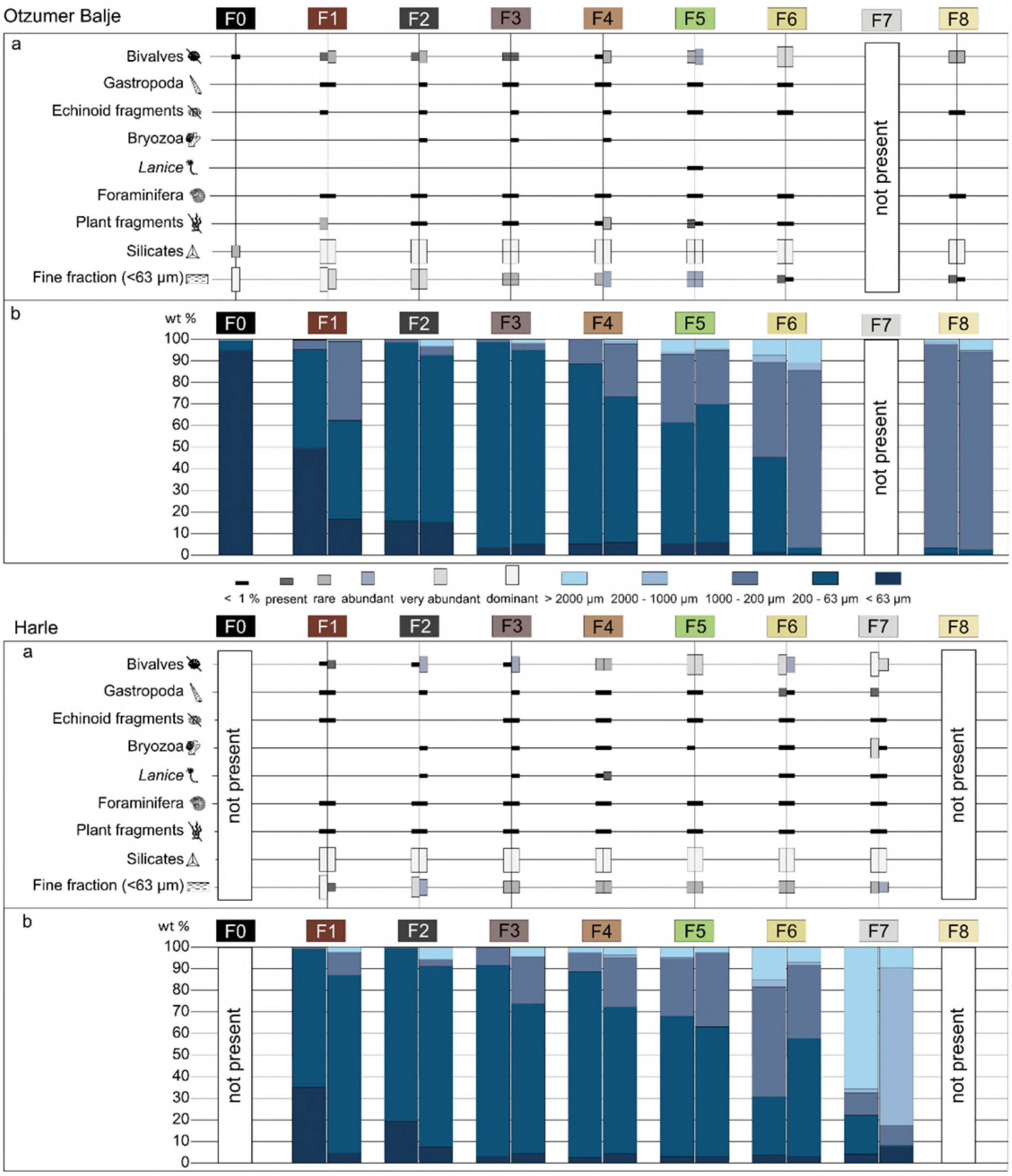

Figure 3.4: Component composition (a) and grain size (b) distribution for each facies. The results from March are presented on the left column, while the results from September are presented on the right column. For facies F0, no comparable samples were collected in September; therefore, only the March data are displayed.

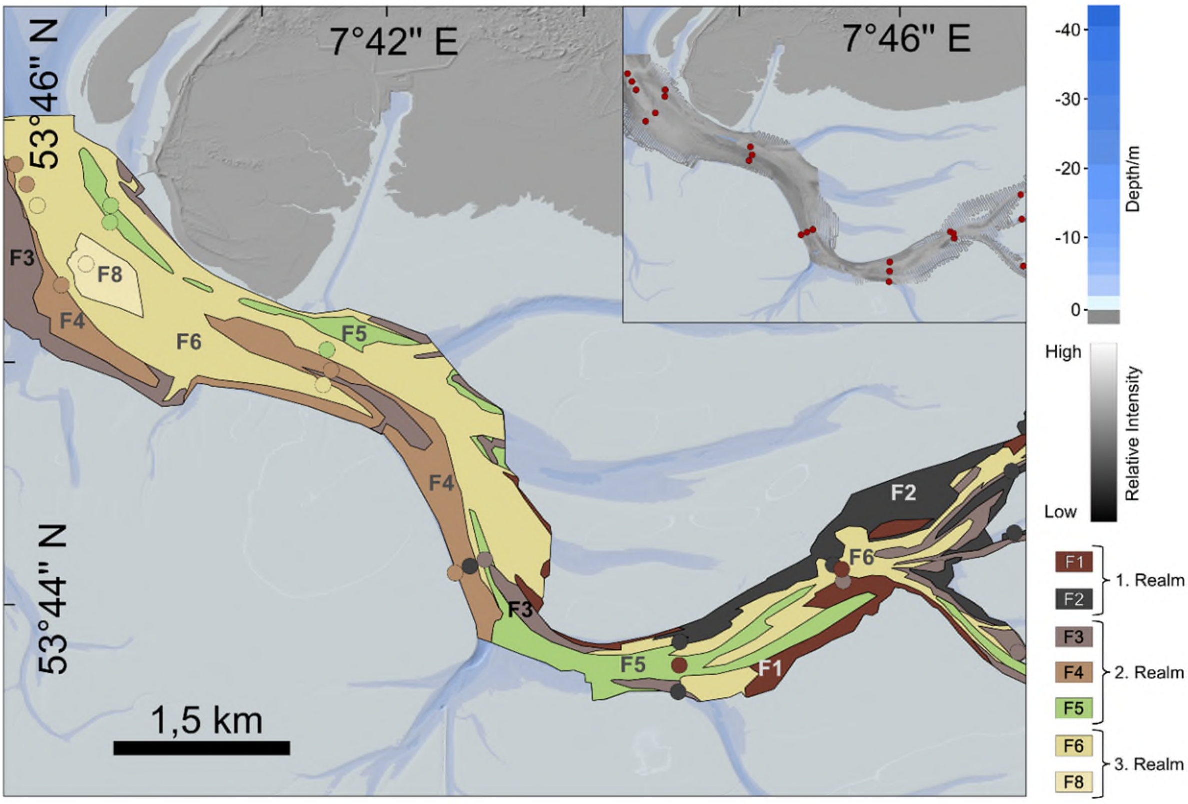

Figure 3.5: Facies map of the Otzumer Balje inlet. The top right corner displays backscatter data along with the sample stations. Dark colors indicate relatively low backscatter intensity, while lighter colors indicate high intensity.

3.4.1 Facies 0: Clay

Otzumer Balje: The facies F0 comprises fine fraction (< 63 µm) constituting 95 weight percent (wt%) of the total. Grains larger than 63 µm consist primarily of silicate grains and include present bivalve fragments. The sediment exhibits very well sorting characteristics with a median grain size (D50) of 63 µm.

Facies F0 is exclusively found in March on the western flank of the main channel in the Otzumer Balje, occurring at water depths ranging between 1 and 2 meters. In the backscatter data the facies could not be observed.

3.4.2 Facies 1: Clayey sands

Otzumer Balje: In March, facies F1 in the Otzumer Balje is composed of 50 wt% fine fraction, with dominant occurrences of silicates in fractions larger than 63 µm. Plant fragments are rare, while bivalve fragments are present. Less present components include foraminifera and echinoid fragments. During summer, the fine fraction constitutes 17 wt %, with dominant occurrences of silicates and abundant bivalve fragments, and less present foraminifera, plant fragments, and gastropods. The sediment is moderately sorted in March, with a D50 of 64 µm, and becomes moderately to poorly sorted in September with a D50 of 105 µm.

Facies F1, characterized by high backscatter intensity and a planar surface, is located in the backbarrier area along the flanks and branch channels near the intertidal mudflats at water depths between 7 and 10 m.

Harle: In March, the fine fraction in facies F1 is 35 wt%, with dominant grain components of silicates. Bivalve fragments, plant fragments, foraminifera, echinoid fragments, and gastropods are less present. In summer, the fine fraction is 4 wt%, dominated by silicates grains larger than 63 µm, with present bivalve fragments and less present plant fragments, foraminifera, echinoid fragments, and gastropods. The sediment is moderately sorted in March with a D50 of 83 µm and poorly sorted in September with a D50 of 119 µm.

Facies F1 is found in the southernmost gully of the Harle at water depths between 1 m and 2 m.

3.4.3 Facies 2: Organic-rich clayey sands

Otzumer Balje: Facies F2 in the Otzumer Balje consists of 16 wt% fine fraction in March, with silicates grains being dominant and bivalve fragments are present, and less present plant fragments, echinoid fragments, and foraminifera. In summer, the fine fraction content is 15 wt%, with dominant silicates and rare bivalve fragments. Less present components include bryozoans, plant fragments, foraminifera, echinoid fragments, and gastropods. The moderately well-sorted sand has a D50 of 102 µm in March and 105 µm in summer.

Facies F2 shares a similar distribution like F1, found along channel surfaces and flanks in intertidal areas primarily at water depths between 2 m and 6 m, but occasionally reaching depths of 14 m, including gullies. It exhibits the highest backscatter intensity with a planar surface.

Harle: In March, facies F2 in the Harle contains 19 wt% fine fraction, with dominant silicates grains and less present bivalve fragments, plant fragments, and foraminifera. In summer, the fine fraction is 7 wt%, larger components are dominated by silicates with abundant bivalve fragments and less present *Lanice*, plant fragments, foraminifera, and gastropods. The moderately well-sorted sand has a D50 of 98 µm in March and is poorly sorted in September with a D50 of 114 µm.

Facies F2 is found in the northernmost gully of the Harle at water depths between 1 m and 2 m.

3.4.4 Facies 3: Very fine sands

Otzumer Balje: Facies F3 in the Otzumer Balje consists of 4 wt% fine fraction in March, dominated by silicates grains with present bivalve fragments. Less present components include foraminifera, plant fragments, and gastropods. In summer, the fine fraction is 5 wt%, with dominant silicate grains, rare bivalve fragments, and less present plant fragments, foraminifera, bryozoa, echinoid fragments, and gastropods. The sediment is moderately well-sorted with a D50 of 111 µm in March, and similarly sorted in September with a D50 of 112 µm.

Facies 3 is located at the southernmost gully in the Otzumer Balje and on the flanks of the channel, at water depths between 1 and 10 meters. The facies is characterized by high to moderate backscatter intensity with surface ripples.

Harle: In March, the fine fraction rate for F3 is 3 wt%, with dominant silicate grains and less present bivalve fragments, foraminifera, echinoid fragments, and plant fragments. In summer, the fine fraction rates are 4 wt%, dominated by silicates with abundant bivalve fragments. Less present are *Lanice*, bryozoa, foraminifera, plant fragments, echinoid fragments, and gastropods. The sorting is moderate in March and poor in September. The D50 is 117 µm in March and 138 µm in September.

Facies F3 is found at the flanks of the channels in the Harle, at water depths between 2 m and 6 m, and on the inner part of the inlet on a sand barrier between the main channels Harle and Dove Harle, around a water depth of 5 m.

3.4.5 Facies 4: Bioclastic organic-rich fine sands

Otzumer Balje: Facies F4 in the Otzumer Balje consists of 5 wt% fine fraction in March, composed predominantly of dominant silicates with present bivalve fragments and less present foraminifera, and plant fragments. In summer, the fine fraction is 6 wt%, with dominant silicate grains, rare bivalve fragments and present plant fragments, and less present foraminifera, echinoid fragments, gastropods and bryozoa. The moderately sorted sand has a D50 of 127 µm in March and 209 µm in September.

Facies F4 occurs at the western flanks of the inlet channel in the Otzumer Balje, near the island of Langeoog, at water depths between 9 m and 10 m. The facies have a high to moderate backscatter intensity with surface ripples, in general with a lower intensity as facies F3

Harle: In March, the fine fraction of F4 consists of 3 wt%, with dominant silicate grains, rare bivalve fragments, and less present bryozoa, foraminifera, *Lanice*, plant fragments, gastropods, and echinoid fragments. In summer, the wt% of fine fraction is 4 %, with dominant silicates, abundant bivalve fragments, present *Lanice*, and less present bryozoa, gastropods, plant fragments, echinoid fragments, and foraminifera.

The moderate to poorly sorted sand of facies F4 is found along the flanks of the channels in the Harle, at water depths between 2 m and 7 m.

3.4.6 Facies 5: Bioclastic sands

Otzumer Balje: The sediments of F5 consist of 4 wt% fine fraction in March, with dominant silicate grains, rare bivalve fragments, and present plant fragments. Less present are foraminifera, gastropods, and echinoid fragments. In summer, F5 comprises 4 wt% fine fraction, with dominant silicates and abundant bivalve fragments, and less present plant fragments, *Lanice*, foraminifera, echinoid fragments, and gastropods. The poorly sorted sand has a D50 of 208 µm in winter and 209 µm in summer.

Facies F5 is part of the main Otzumer Balje channel and the northeastern flanks in the inlet, with water depths between 5 and 18 meters. The facies shows a backscatter signal ranging from moderate to low intensity, featuring a mottled distribution and the presence of megaripples.

Harle: The F5 facies in the Harle consists of 3 wt% fine fraction in March, dominated by silicates with abundant bivalve fragments and less present foraminifera, gastropods, bryozoa, plant fragments, and echinoid fragments. In summer, F5 comprises 3 wt% fine fraction, with dominant silicate grains, abundant bivalve fragments, and less present foraminifera, gastropods, and echinoid fragments. The poorly sorted sediment has a D50 of 143 µm in winter and 175 µm in summer.

Facies F5 occurs along the main channels and in the transition zone between the intertidal zone and the subtidal zone, with water depths ranging between 2 m and 8 m.

3.4.7 Facies 6: Medium bioclastic sands

Otzumer Balje: In March, facies F6 in the Otzumer Balje consists of 2 wt% fine fraction, with dominant silicate components. Bivalve fragments are very abundant, and echinoid fragments, plant fragments, and gastropods are less present. In summer, F6 comprises 1 wt% fine fraction, with dominant silicates and very abundant bivalve fragments, and less present gastropods, echinoid fragments, foraminifera, and plant fragments. The sediment is moderate to poorly sorted, with a D50 of 483 µm in winter and 486 µm in summer.

Facies F6 occurs in the inner part of the inlet, describing the seafloor of the Otzumer Balje main channel at water depths between 10 and 20 meters. The facies displays variable bedforms, from ripples and megaripples to plane grounds, with backscatter intensity ranging from very low to low, and some areas exhibiting a mottled medium intensity

Harle: Facies F6 in the Harle consists of 4 wt% fine fraction in March, with dominant silicates grains and very abundant bivalve fragments, and present gastropods. Less present are echinoid fragments, plant fragments, *Lanice*, foraminifera and bryozoa. In summer, the fine fraction is 3 wt%, with dominant silicates, abundant bivalve fragments, and less present gastropods, plant fragments, foraminifera, echinoid fragments, *Lanice*, and bryozoa. In winter, the poorly sorted sand has a D50 of 398 µm, and in summer, it is 246 µm.

Facies F6 is prominent in the main channels of the Harle and Dove Harle, with water depths higher than 5 m.

3.4.8 Facies 7: Shill sands

Facies F7 is not present in the Otzumer Balje.

Harle: Facies F7 consists of 4 wt% fine fraction in March, primarily composed of dominant silicates grains and dominant bivalve fragments. Bryozoa are very abundant, and gastropods are present, while less present components include plant fragments, echinoid fragments, foraminifera and *Lanice*. Encrusting bryozoans cover most surfaces of the bivalve fragments and other fragments. In September, the fine fraction is at 9 wt%. Dominant components are silicate grains with very abundant bivalve fragments. Less present are *Lanice*, echinoid fragments, bryozoa, foraminifera and plant fragments. The poorly sorted sand has a D50 of 1696 µm in winter and 120 µm in summer.

Distributed along the inner channel of the Dove Harle, F7 occurs only in the Harle and in water depths ranging between 5 m and 10 m.

3.4.9 Facies 8: Submarine dune sands

Otzumer Balje: In March, facies F8 consists of 1 wt% fine fraction. The facies is composed of primarily dominant silicate grains with abundant bivalve fragments, as well as less present echinoid fragments and foraminifera. In September, the facies is composed of < 1 wt% fine fraction and dominated by silicate grains. Bivalve fragments are abundant and less present components are gastropods, echinoid fragments, foraminifera and plant fragments. The moderately sorted coarse sand has a D50 of 443 µm in March and in September the coarse sand is moderately sorted with a D50 of 461 µm.

The facies F8 occurs only in the Otzumer Balje along the widest section of the channel, where submarine dunes with ripples dominate the surface. The backscatter intensity varies from low to medium, with dune crests showing medium intensity and dune valleys showing low intensity.

3.5 Discussion

3.5.1 Facies map Otzumer Balje:

By integrating facies data along the Otzumer Balje with multibeam backscatter data, a detailed facies map has been constructed (Fig. 3.5). Eight distinct facies were identified for the Otzumer Balje and organized into specific realms, corresponding to those described for the Harle by Geßner et al. (2024).

The first realm in the Otzumer Balje inlet, the Wadden Realm, comprises facies F1 and F2. This realm is closest to the intertidal flats and has the shallowest water depths in the inlet. The second realm encompasses the channel beds and flanks, including facies F3, F4, and F5. The third realm comprises facies F6 and F8, representing the beds of the main channel and the deepest parts of the smaller branch channels.

The clay of facies F0 represents the characteristic sediment composition of mudflats. These mudflats are not part of the inlet system but rather delineate the inlet channels, as described by Bungenstock et al. (2021), who documented a range of sandy to clayey sediments within *Mytilus*-beds in this region. The proximity of these mudflats suggests an allochthonous origin of the sediment. A storm surge intensifies hydrodynamic forces, increasing wave action and current velocity, which enhances bed shear stress and leads to the erosion of fine sediments from the mudflat surface (Liu et al., 2023). The occurrence exclusively in the March samples and at a single location along the western flank of the main channel (station In12) further supports this interpretation. Consequently, facies F0 is not a typical component of the inlet system but represents clay-rich mudflats of allochthonous origin.

Facies F7, as described by Geßner et al. (2024) in the Harle, is absent in the Otzumer Balje. Instead, the Otzumer Balje features coarse shell sediment, which covers the surface in the area of direct exchange between the North Sea and the Otzumer Balje inlet, located between the islands Langeoog and Spiekeroog. Unlike the bivalve shells in the Harle, the shells in the Otzumer Balje are classified as facies F6 and are not encrusted with bryozoans. Generally, the occurrence of bryozoans in the Otzumer Balje is underrepresented. Amini et al. (2004) observed a correlation between sedimentation rates and the abundance of bryozoans. Areas with high sedimentation rates tend to have fewer bryozoans, indicating ongoing transport processes and movement of finer sediments within the Otzumer Balje inlet system.

Facies F8 is occurring in the Otzumer Balje, where a subaqueous dune field covering an area of 0.210 km² is observed, exhibiting ebb dominance (Fig. 3.6). These dunes can be observed in the backscatter data, as well as in digital elevation data. The slip face is northwest directed, towards the open North Sea. With the ebb flow the sediment is moving in northwesterly direction and the dunes are shifting inside the dune field. Subaqueous dunes of this nature are common in tidal inlets and occur at various locations. In general, these dune fields have a fixed expansion area (Allen, 1968; Belleney et al., 2022; Cuadrado and Gómez, 2011; Ernstsen et al., 2006; Flemming, 2000; Gonzales and Eberli, 1997; Svenson et al., 2009; Toso et al., 2019). This facies is absent in the Harle and subaquatic dunes were not detected by Geßner et al. (2024) at all. This absence is likely due to the shallow water depth in the Harle as well as its narrowness, respectively, which may limit dune formation and migration.

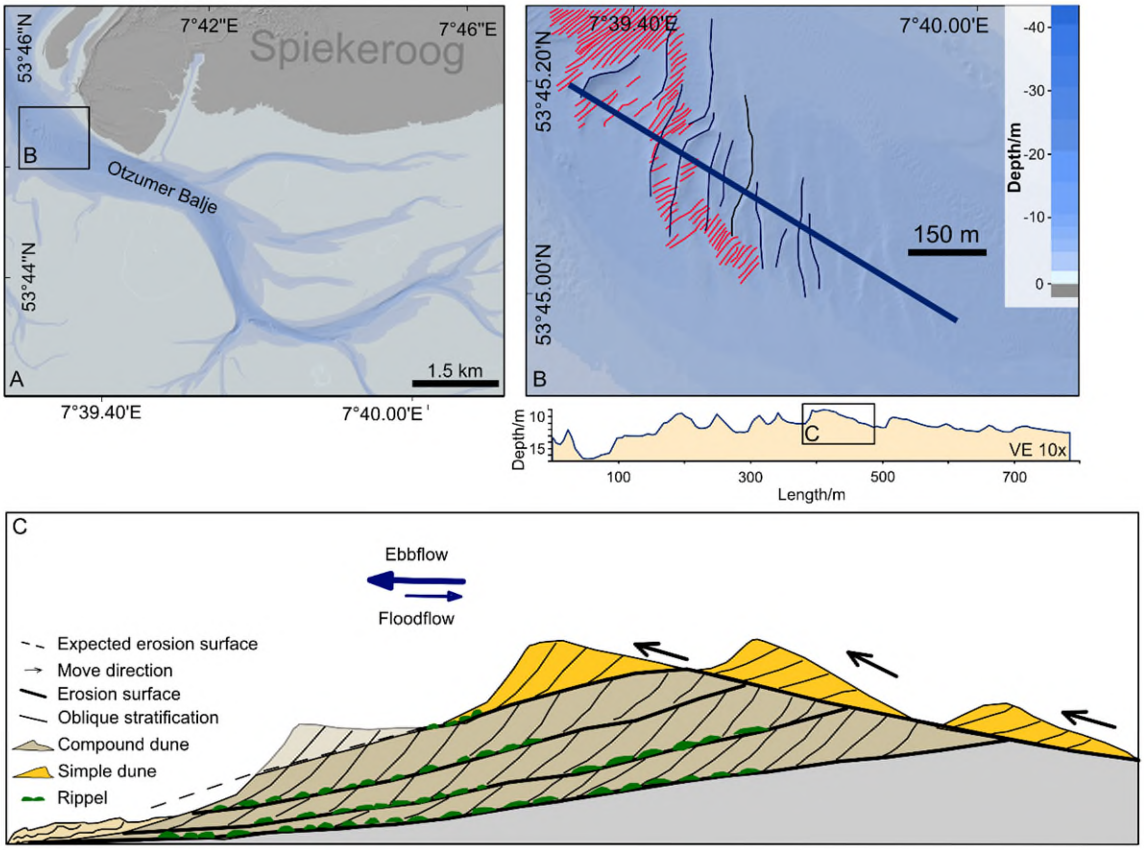

Figure 3.6: Subaquatic dunes in the Otzumer Balje. Panel A shows the overall area of the subaquatic dunes. Panel B provides a detailed map of the dunes, highlighting the dunes (black lines) and the ripples on them (red lines). The cross-section of the dunes is located along the bold blue line. Panel C illustrates the schematic formation of the dunes, depicting the shifting of simple dunes in the ebb flow direction (after Olariu, 2012).

3.5.2 Seasonal shift

The geographical location of the East Frisian Islands experiences several seasonal variations throughout the year. In winter, the area is strongly influenced by cooler temperatures, storms, and storm surges. While in summer, the temperatures are higher and the weather is calmer (Fig. 3.7). These seasonal differences result in variations in flow and transport energy, wave heights, and temperature.

For the Harle tidal inlet, seasonal wind patterns significantly affect circulation. During the storm season, southwesterly winds induce a deflection of surface circulation (upper 5 m) toward a more northeasterly orientation. In contrast, during fair weather conditions, flow across all water layers aligns more closely with the main axis of the inlet channel. Additionally, fair weather conditions lead to enhanced ebb and flood velocities due to minimal wind interference, allowing flow to propagate more efficiently along the inlet axis. At the Otzumer Balje inlet, seasonal variations also shape hydrodynamic behavior. In fair weather conditions (June), the surface and mid-column layers exhibit a narrower range of deviation from the main flow direction, whereas near-bottom flow shows increased scattering. This is due to a larger gradient between the open North Sea and the Wadden Sea, driven by increased stratification resulting from calmer weather and surface heating (Burchard and Badewien, 2015). In contrast, during the storm season (March), increased mixing mobilizes finer sediments more effectively than in summer. In comparison to the Harle, observations from June 2021 along the Otzumer Balje reveal that ebb flow is directed into a secondary gully, a feature that is only faintly visible in surface flow during March (Fig. 3.7).

For the Harle tidal inlet, seasonal wind patterns significantly affect circulation. During the storm season, southwesterly winds induce a deflection of surface circulation (upper 5 m) toward a more northeasterly orientation. In contrast, during fair weather conditions, flow across all water layers aligns more closely with the main axis of the inlet channel. Additionally, fair weather conditions lead to enhanced ebb and flood velocities due to minimal wind interference, allowing flow to propagate more efficiently along the inlet axis. At the Otzumer Balje inlet, seasonal variations also shape hydrodynamic behavior. In fair weather conditions (June), the surface and mid-column layers exhibit a narrower range of deviation from the main flow direction, whereas near-bottom flow shows increased scattering. This is due to a larger gradient between the open North Sea and the Wadden Sea, driven by increased stratification resulting from calmer weather and surface heating (Burchard and Badewien, 2015). In contrast, during the storm season (March), increased mixing mobilizes finer sediments more effectively than in summer. In comparison to the Harle, observations from June 2021 along the Otzumer Balje reveal that ebb flow is directed into a secondary gully, a feature that is only faintly visible in surface flow during March (Fig. 3.7).

Seasonal biological variations further influence sediment composition, as benthic growth, mortality, and predation fluctuate throughout the year. These biological and physical factors contribute to observable changes in surface sediment composition, as documented in previous studies (Andersen et al., 2005; Beukema, 1987; Kröncke et al., 2001; Reiss and Kröncke, 2001; Wheatcroft et al., 2013).

To determine the seasonal variances within the surface sediments of the Otzumer Balje and the Harle, the same sampling stations from March 2022 were resampled and analyzed in September 2022. Seasonal variability of the study area is influenced by factors like benthos growth, predation, mortality, and temperature, wind speeds, and hydrodynamic forces. These factors affect the grain sizes of the bioclastic material and the transport properties, which change with the seasons and the transport potential. In general, the samples show a decrease in the fractions of < 200 µm and an increase of the coarser fractions > 200 µm from winter to summer. Additionally, the abundance of bioclastic material increase during summer. Some facies in the Otzumer Balje and Harle show significant differences attributable to seasonal influences. Especially F1, F2, F4 F6 and F7.

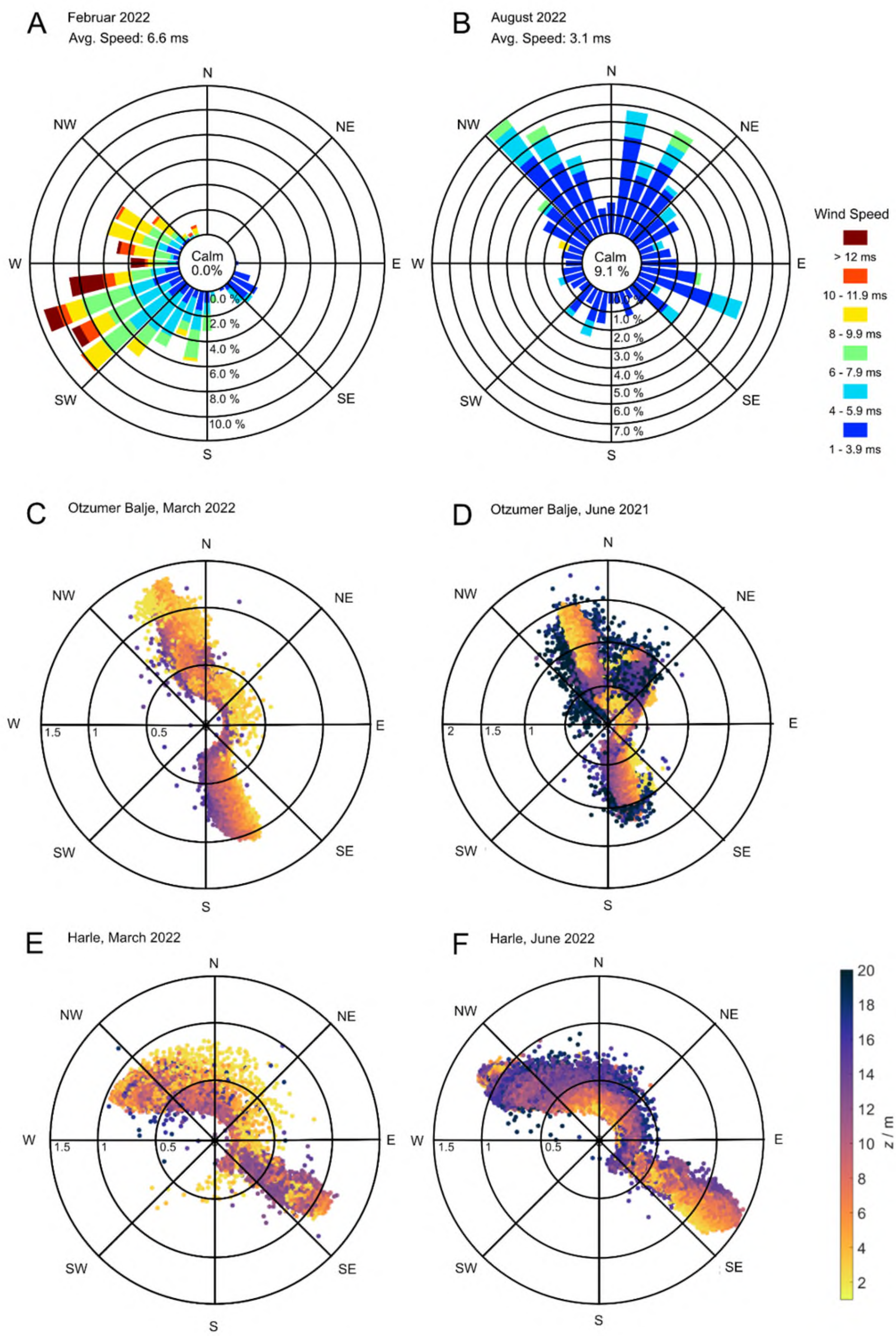

Figure 3.7: Wind roses and polar plots illustrating wind and current velocity patterns. Panels A and B depict wind roses for February and August, respectively. In February, wind speeds reached up to 12 ms^{-1}, predominantly from the southwest, directed toward the northeast. In August, 9.1% of the winds were calm, with a maximum recorded speed of 7.9 ms^{-1}. The dominant winds originated from the northwest and northeast, moving toward the southeast and southwest. Panels C–F display current velocity magnitude and direction as polar plots over depth zzz, where yellow represents near-surface layers and violet indicates deeper layers. Data were collected from anchor stations in the Otzumer Balje (March 2022, Panel C; June 2021, Panel E) and in the Harle (March 2022, Panel D; June 2022, Panel F).

Facies F0 occurs only in the March samples in the Otzumer Balje and is interpreted as allochthonous mudflat sediments. As shown in figure 3.7, storms and storm surges in February 2022 were northeast directed, with wind speeds up to 37.5 ms^{-1}. These strong winds lead to a high erosion potential and caused significant damage along the entire North Sea coast (Kendon et al., 2023; Mühr et al., 2022). The northern beaches of the East Frisian Islands also experienced substantial damage and beach erosion. The high erosion force during these storms transported both coarser and clayey sediments from the mudflats into deeper areas of the backbarrier region and the inlet channels, where they are deposited. At station In12 of the Otzumer Balje inlet (Fig. 3.3) the eroded material from the approximately 40 m distant mudflats were deposited in the inlet channel. Due to the strong cohesion forces of the mud material the transport width is limited during calmer flow situations, so the further erosion takes longer times (Hjulström, 1935; McCave, 1984). During summer, the sediment composition at station In12 has changed, with facies F4 emerging. This facies is likely the original sedimentary unit in this area, as suggested by backscatter intensities, surrounding sediment characteristics, comparative samples, and baseline data from Mascioli et al. (2021).

In both inlets, facies F1 shows an increase in the occurrence of benthic organisms from winter to summer, causing a shift in grain size distribution. The sediment becomes coarser, with the fine fraction decreasing and the coarser fraction significantly increases. This trend is also observed in the facies F2, F3, and F4. Benthic organisms grow during summer and predation and mortality lead to more available larger shell material. Additionally, longer transport durations result in mechanical damage of shells, producing shattered components, which are still part of the coarse fraction (Leighton et al., 2016; Zuschin et al., 2003). In the Harle, there is an increase in the occurrence of *Lanice conchilega* for the mentioned facies types. *L. conchilega* propagate during winter and grow during summer. The tubeworm is also observed in the sandy areas of the intertidal backbarrier flats (Bungenstock et al., 2021) and live in patch colonies. Their abundance is pronounced in subtidal areas to create a niche for other benthic organisms and reduces the near bottom flow velocity (Heuers et al., 1998; Rabaut et al., 2007; Van Hoey, 2006).

Facies F5 exhibits a fining trend in sediment composition in both inlets. Despite an increase in benthic organisms during summer, the proportion of sediment fractions >63µm increases in the Otzumer Balje, while fractions >200 µm increase in the Harle. Facies F5 is primarily located along the flanks and smaller branch channels. In the Harle, it is also present within the mixed shear zone and an area influenced by a circulation eddy (Geßner et al., 2024). It is hypothesized that higher hydrodynamic energy during storm surges transports larger shell fragments over greater distances and intensifies the fragmentation of bioclastic material. In contrast, calmer summer conditions reduce transport energy and erosion potential, allowing finer sediments to settle and accumulate. Geßner et al. (2024) suggest that the mixed shear zone and circulation eddy in the Harle result from the influence of Groyne H within the inlet. In the Otzumer Balje, facies mapping shows no evidence of similar facies arrangements in the direct exchange zone, supporting the hypothesis that the sandbarrier along the mixed shear zone in the Harle is a consequence of coastal protection measures.

Facies F6 of the Harle shows a significant decrease in the coarser fraction and an increase in the 200 – 63 µm fraction, with notable decrease in bivalve shells and gastropods during late summer (Fig. 3.4). This pattern suggests the relocation of coarser grained material in inlet transported by the tidal currents, driven and intensified by storm activity (Papili et al., 2014). Facies F6 of the Otzumer Balje shows minimal changes throughout the seasons.

Facies F7 in the Harle displays a high variance in grain size due to the varying sizes of bivalve shells and fragments. In March, samples were dominated by *Cardioidea* shells overgrown with encrusting bryozoans. By summer, *Mytilus* shells dominated the samples, with *Cardioidea* shells still present (Fig. 3.8). The shells of *Mytilus* from September were smaller and not overgrown by bryozoans. This suggests increased mortality of juvenile *Mytilus* during summer. Incze et al. (1980) observed a similar rise in mussel mortality in late summer in Maine, USA, attributed to a combination of high temperatures, with energy balance issues in the mussels, and the decline of phytoplankton. These factor combinations may also be relevant in the case of the Harle. Additionally, the presence of mud trapped between the shells suggests that the sediment is relatively recent and that the shells likely originate from mussel beds in the backbarrier area, which are part of the backbarrier flats of the Wadden Sea (Bungenstock et al., 2021). Notably, Facies F7 is absent in the Otzumer Balje.

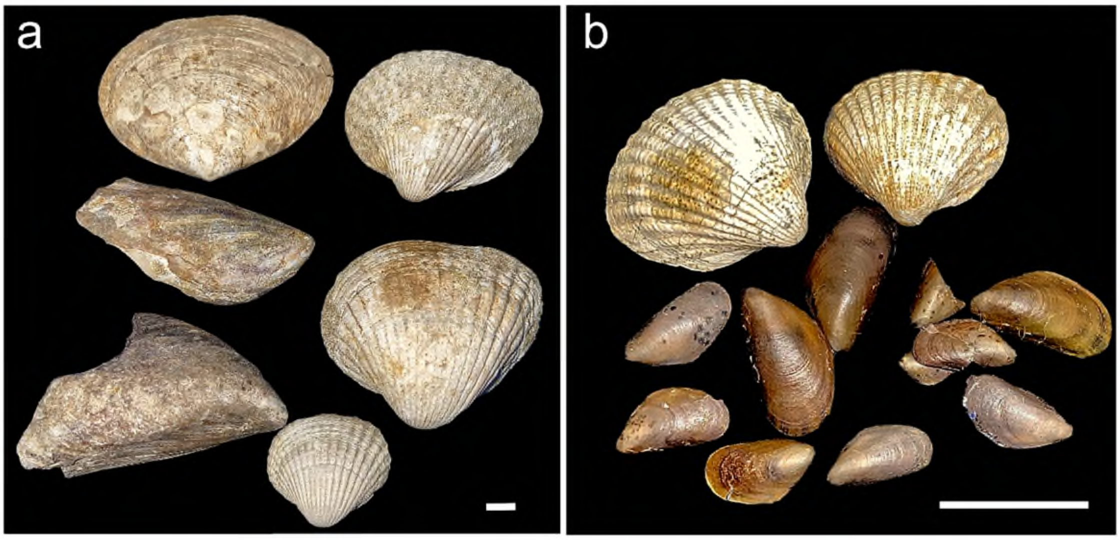

Figure 3.8: Bivalve shells of facies F7. Panel a shows the overgrown bivalve shells collected in March. Panel b displays both overgrown bivalve shells and smaller shells that are not overgrown by encrusting bryozoans. The scale bar represents 1 cm.

Facies F8 along the subaquatic dune field in the Otzumer Balje generally has low proportions of fine fraction, which decrease further in summer. Sampling subaquatic dunes is challenging, as grain sizes vary depending on the sample location within the dune field. Dune crests are generally finer grained than the dune valleys, where coarser fractions are deposited (Allen, 1968). Also, the dune field is a dynamic system, with dunes shifting over time. In the case of the tidal inlet between Skallingen and Fanø, the movement has been observed with 0.07 m per day (Bartholomä et al., 2006). Furthermore, fine fraction in subaquatic dunes are generally low because the finer sediments remain in wash load (Einstein and Chien, 1940; Khulllar 2007; Woo et al., 1986). Facies F8 is absent in the Harle due to the lack of subaqueous dunes.

3.5.3 Comparison of Harle and Otzumer Balje:

Distinct differences between the tidal inlets Otzumer Balje and Harle were previously identified by Geßner et al. (2024) based on a facies map of the Harle and existing literature on the Otzumer Balje, including studies by Antia (1994), Flemming and Nyandwi (1994), Son et al. (2011), and Valle-Levinson et al. (2018). This study deepens these findings by highlighting differences in sedimentology and seasonal shifts between these two closely situated tidal inlet systems. By utilizing the newly developed facies map of the Otzumer Balje along with seasonal data from both inlets, a direct comparison is now possible. This comparison provides insights into the effects of human activities by the influence of coastal protection measures on tidal inlet dynamics. Additionally, the data indicate that both tidal inlets display high heterogeneity in their surface sediments, with significant seasonal shift between early spring and summer.

Geomorphological key features distinguished the two inlets include the sandbar separating the main channels Harle and Dove Harle in the Harle inlet, and the subaquatic dunes present in the Otzumer Balje (Eitner, 1996a; Eitner, 1996b; Geßner et al., 2024; Herrling and Winter, 2016; Lüders 1952; Ladage and Stephan, 2004; Mascioli et al., 2022). The absence of dunes in the Harle is due to general shallow water depths, which suppressed the formation of subaquatic dunes. The formation of the sandbar interior of the Harle inlet, separating the main channels, is caused by the construction of Groyne H.

The spatial facies distribution of the inlets is nearly equal distributed, with the three realms of the Wadden area, the channels and flanks, and the main channels present in both inlets. However, their facies combinations vary, notably due to the presence of the facies F7 in the Harle and F8 in the Otzumer Balje. As described by Ladage and Stephan (2004) and Geßner et al. (2024), the ebb current is strongest in the Dove Harle, and the seafloor is dominated by shill fragments overgrown by bryozoans. This feature is unique among the two tidal inlets. The strong tidal currents in the Dove Harle tend to prohibit sedimentation and arranges the shell fragments in a stable position where encrusting bryozoans grow. In contrast, facies F7 is entirely absent in the Otzumer Balje, where the occurrence of bryozoan is generally low. Amini et al. (2015) noted that overgrown bryozoan are reliant to stable conditions without sedimentation and served as an indicator for that process in the Dove Harle.

In contrast to facies F7 in the Harle, the Otzumer Balje features facies F8 along the inlet. Facies F8 describes the sediment of subaquatic dunes found in the Otzumer Balje, but which do not occur in the Harle. Bathymetric data indicate the presence of subaquatic dunes in other Frisian Islands inlets. However, these dunes remain within a fixed area. The formation of subaquatic dunes is influenced by both water depth and flow velocity (Flemming, 2000; Yalin, 1976). In the Otzumer Balje, the flow velocities of both flood and ebb currents are sufficient to generate these bedforms, which typically develop under velocities ranging from 0.6 to 1.5 ms^{-1} (Reineck and Singh, 1980; Boothroyd, 1985; Ashley, 1990). Although flow velocities in the Harle inlet can also reach up to 1.0 ms^{-1}, subaquatic dunes are absent. This absence is primarily attributed to the shallower water depths in the Harle inlet, which remain below 10 m, preventing the formation of these dune structures.

The finer grained facies of the Wadden realm have a broader spatial distribution in the Otzumer Balje. In the Otzumer Balje, the facies of the channel and flank realm exhibit an elongated shape, whereas in the Harle, these facies display a circular distribution directly south of Groyne H (Geßner et al., 2024). This circular alignment in the Harle is attributed to the presence of a circular eddy. The absent of such a facies alignment in the Otzumer Balje highlights the significant anthropogenic impact of the Groyne H on the Harle inlet.

Overall, both inlets exhibit seasonal variations in their surface sediments, driven by a combination of biological and physical factors. Observations indicate that benthos growth plays a significant role in both inlets. However, the presence of the tubeworm *L. conchilega* is notably higher in the Harle inlet, particularly during the summer months.

While *L. conchilega* is distributed across the tidal flats of the Frisian Islands (Bungenstock et al., 2021), its abundance is more pronounced in the Harle samples than in the sediment samples of the Otzumer Balje. Additionally, the occurrence of encrusting bryozoan is also higher in the Harle. These observations may reflect lower sedimentation rates in the Dove Harle and reduced bottom flow velocities in the shallower area, caused by the presence of *L. conchilega* patches, which promote the flourishing of organisms while limiting sediment relocation. In general, the sediment in the Harle inlet is composed of a more divers bioclastic material compared to the Otzumer Balje (Fig. 3.4).

Despite their geographical proximity and several similarities, the two inlets are very different from each other. Therefore, environmental results must be recorded and interpreted separately to obtain a comprehensive and nuanced understanding.

3.6 Conclusion

This study presents a comprehensive comparison of the Otzumer Balje and Harle tidal inlets, focusing on sedimentological and seasonal variations through the application of a newly constructed facies map for the Otzumer Balje. The findings reveal significant differences in sediment composition, geomorphological features, and biological activity between the two inlets, driven by both natural processes and anthropogenic influences.

Sediment composition:

The sediment composition in the Otzumer Balje shows clear seasonal variability, with coarser sediments dominating in summer. This seasonal shift is characterized by a marked reduction in fine fractions smaller than 200 µm and a corresponding increase in coarser fractions above this threshold. In contrast, the Harle exhibits a greater diversity of bioclastic materials, including larger bivalve shells and fragments that often show mechanical damage. Certain sediment facies are unique to each inlet: for example, facies F7, characterized by bryozoan-encrusted shell fragments, is exclusive to the Harle, while facies F8, representing subaquatic dunes, is confined to the Otzumer Balje. Allochthonous mudflat sediments (facies F0) are present in the Otzumer Balje during winter storms, which are transported into the channel.

The sedimentation patterns highlight further distinctions: the Otzumer Balje is marked by active sediment transport, especially within its dynamic subaquatic dune system, whereas the Harle demonstrates localized sediment stability largely due to restricted sedimentation along the Dove Harle. Notably, in the Dove Harle, bryozoan colonization on disarticulated shells is prominent. Additionally, deposition in the Harle is influenced by the construction of Groyne H, which forms a sandbarrier along the mixing shear zone due to differential current energies, as well as local eddy formation that traps sediments.

Geomorphological features:

The Harle consists of two main channels, with a deep scour at the tip of Groyne H. The Harle consists of two main channels, with a deep scour at the tip of Groyne H reaching depths of 34 m, shaped by Groyne H. The morphology is further influenced by scouring along the flanks of the groyne. Additionally, deposition south of Groyne H results in the formation of a sandbar in the mixed shear zone. Subaquatic dunes dominate the Otzumer Balje, confined to specific areas due to the dynamic equilibrium between erosion and deposition processes. In the Harle, shallower water depths prevent the formation of such dunes, but a sandbar forms in the mixing shear zone, separating the main channels. The presence of strong tidal currents in the Dove Harle leads to a reduction in sedimentation rates, which contributes to the maintenance of the two primary channels within the Harle inlet. Additionally, the Harle displays a circular alignment of facies near the groyne fields of Groyne H and Groyne V, driven by a circular eddy caused by the groynes. In contrast, the Otzumer Balje exhibits elongated facies distributions along its channels and flanks.

Biological activity:

Biological activity in the two inlets is also distinct. Both systems experience seasonal increases in benthic organism abundance, such as *Lanice conchilega*, but the Harle demonstrates more pronounced growth during the summer months. The Harle also supports a more diverse array of bioclastic material, including shell fragments from various benthic organisms. Bryozoans play a key role in the Harle, with extensive encrustation of shell fragments in facies F7, indicative of stable, low-sedimentation conditions within the Dove Harle channel. In contrast, bryozoan activity in the Otzumer Balje is constrained by higher sedimentation rates and dynamic sediment transport.

This study highlights the necessity of sustainable coastal management strategies that prioritize the preservation of natural sediment dynamics. The sedimentological and ecological characteristics of tidal inlets are significantly influenced by the presence or absence of large-scale coastal protection measures. Naturally dominated inlets, like the Otzumer Balje, facilitate stronger sediment transport between open marine and coastal environments, a phenomenon observed in tidal systems worldwide. While this process supports dynamic sediment exchange, it can also lead to increased erosion of intertidal zones during extreme weather events. However, as long as natural sediment dynamics enable redeposition and the preservation of coastal features, these systems remain resilient. In contrast, human interventions, such as those observed in managed tidal inlets like the Harle, restrict sediment exchange, leading to localized erosion and a diminished capacity to adapt to storm impacts. With the increasing frequency of extreme weather events due to climate change, such constraints can pose significant challenges to long-term coastal resilience. Maintaining this balance is crucial not only for the protection of barrier islands but also for ensuring the long-term stability of tidal environments in the face of sea level rise. These findings contribute to a broader understanding of human-nature interactions in tidal systems, offering valuable insights for global coastal management and adaptation strategies.

Chapter 4

Influence of Coastal Protection Measures on Sediment Transport and Heavy Metal distribution in surface sediments in the tidal inlet Harle (Southern North Sea)

This chapter is based on the manuscript:

Geßner, A.-L.; Kalmbach, C.; Albinus, M.; Bunzel, D.; Wollschläger, J.: Badewien, T.H.; Giebel, H.-A. (2025): Influence of Coastal Protection Measures on Sediment Transport and Heavy Metal distribution in surface sediments in the tidal inlet Harle (Southern North Sea).

Abstract

This study examines the interplay between hydrodynamics, sediment transport, and trace metal contamination in the Harle tidal inlet, highlighting the strong influence of human interventions and natural processes on sediment dynamics. Sediment grain sizes vary from fine-grained deposits in harbors and shallow channels to sand-dominated areas in deeper channels, with SiO_2 as the dominant mineral component. Heavy metal concentrations of Cr, Zn, Cu, and Pb generally remain below threshold levels, but arsenic shows significant enrichment due to both natural, pyrite-rich peat layers, and anthropogenic sources, industrial and agricultural inputs. The construction of Groyne H has altered current patterns, accelerating erosion, sediment redistribution, and the exposure of arsenic rich peat, leading to localized arsenic mobilization. Fine-grained sediments exhibit higher heavy metal concentrations, emphasizing the critical role of sediment texture and organic content in contaminant distribution. However, the dynamic tidal regime prevents long-term heavy metal accumulation in the inlet, contrasting with nearby salt marshes, which act as temporary sinks for contaminants. These findings underscore the substantial impact of coastal engineering on sedimentary and chemical processes in tidal inlets. Understanding these interactions is crucial for assessing environmental risks and developing sustainable coastal management strategies in regions affected by anthropogenic and natural sediment dynamics.

4.1 Introduction

Coastal regions are among the most densely populated areas worldwide. Many of the world's largest cities are situated along coastlines, reflecting the enduring appeal and strategic importance of these locations. It is estimated that a substantial proportion of humanity resides in coastal areas, with some studies suggesting that approximately 60% of the global population lives within 100 km of the coast (Neumann et al., 2015; Small and Nicholls, 2003). The advantages of coastal regions are multifaceted, encompassing trade opportunities, abundant food resources, and tourism, which has grown considerably in recent decades. Historically, coastal and riverside areas have been favored for settlement due to their access to resources and transportation routes (Iberall et al., 1988). However, in recent decades, these areas have faced increasing socio-economic pressures and environmental challenges due to intensified human activity (Neumann et al., 2015).

Specifically, pollution poses a major challenge to coastal environments. In addition to natural processes, such as rock weathering and the mobilization of heavy metals, coastal regions are highly impacted by industrial, agricultural and urban activities. Waste generated in these areas, often transported directly or indirectly through river systems and estuaries, contributes to the contamination of coastal ecosystems, threatening their ecological health and sustainability. The pollutants range from macro- and microplastics to metals, rubber, and processed wood, contributing to the degradation of marine habitats (Herdiansyah et al., 2021; Jambeck et al., 2015; Sudarmadji et al., 2019; Xuemei and Hawkins, 2002). But additionally, heavy metal contamination is a pressing issue. Sources of heavy metals (Fig. 4.1) include industrial activities such as ore mining, energy production, trade, transport and manufacturing (e.g., textiles, electronics, pigments, and coatings), urbanization, as well as agricultural practices that rely on fertilizers, pesticides, and synthetic chemicals containing these metals (Bradl, 2005; Vikas and Dwarakish, 2015).

The transport and accumulation of heavy metals in aquatic systems further compound environmental risks. These pollutants are carried by rivers, drainage systems, and groundwater, ultimately entering coastal waters via estuaries. In aquatic environments, heavy metals are typically transported as hydroxides, oxides, silicates, or sulfides, and they adsorb onto clay minerals, silica, or organic matter (Pintilie et al., 2007; Uddin, 2016). Adsorption processes are influenced by factors such as pH, which increases adsorption capacity as it rises, and the composition of cations and anions in the electrolyte background, where competition for adsorption sites occurs (Arias et al., 2005; Gray et al., 1999; Jing et al., 2018).

Sediment type also plays a critical role in the adsorption and mobility of heavy metals. Fine-grained sediments with high proportions of clay minerals or organic matter exhibit greater adsorption capacity compared to coarse-grained sediments (Jing et al., 2018). While some heavy metals are relatively immobile and persist within sediments, others are more mobile, transferring into groundwater or being taken up by plant roots (Sherene, 2010). The remobilization of heavy metals between sediments and water is influenced by chemical changes such as variations in salinity, redox conditions, pH, the presence of organic complexing agents, and biodegradation processes (Gregor, 1972; Forstner and Wittmann, 1983; Walker et al., 2006; Pachana et al., 2010). These changes are particularly common along tidal flats and coastal regions.

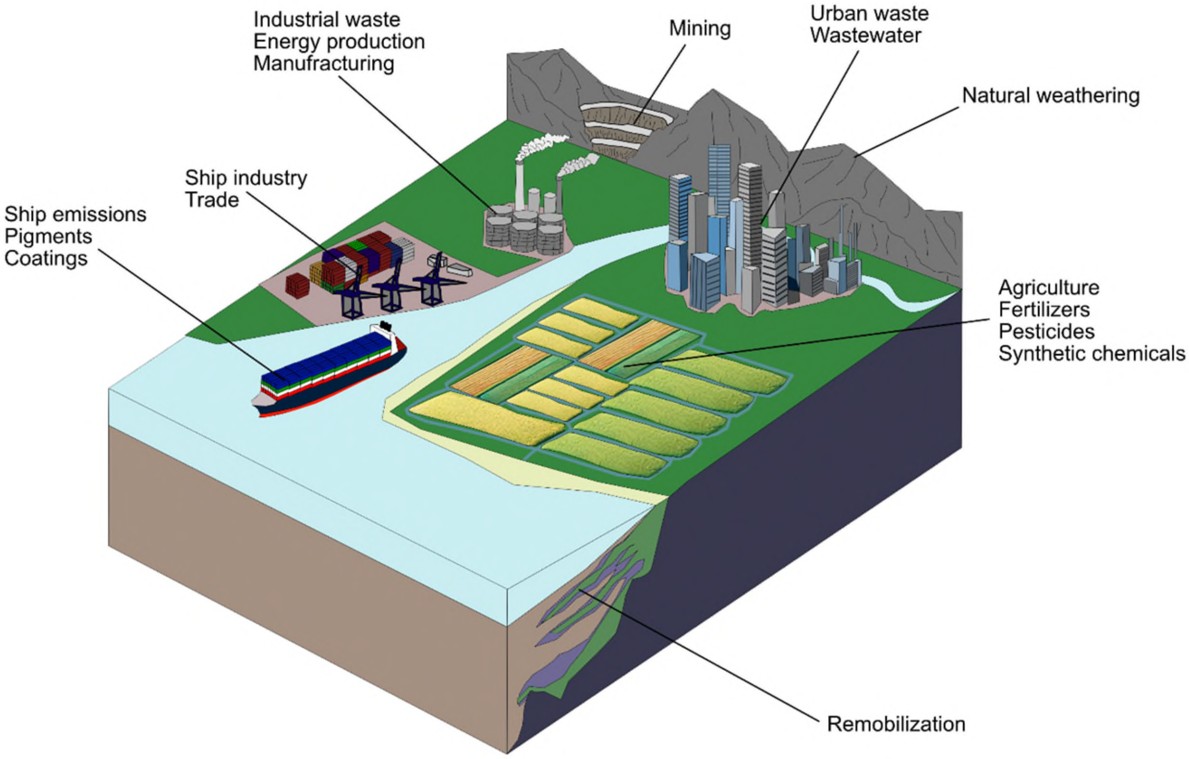

Figure 4.1: Scheme of heavy metal sources and transport pathways to marine environments. Heavy metals are imported into the sea by groundwater transport and riverine flow. Additionally, heavy metal remobilization occurs in subsurface environments, where sediment layers may be enriched with heavy metals.

Once in the aquatic environment, heavy metals pose severe risks to marine and terrestrial biodiversity, with cascading impacts on ecosystems and human health. While trace amounts of certain metals, such as cobalt, copper, iron, manganese, molybdenum, vanadium, strontium, and zinc, are essential for biological functions, excessive concentrations become toxic. Moreover, metals such as mercury, lead, arsenic, cadmium, and chromium are toxic even in trace amounts, posing acute and chronic health risks (Zhang et al., 2012). Heavy metals enter the food web primarily through bioaccumulation in marine benthos and fish, which subsequently leads to their biomagnification through higher trophic levels. Fish and other aquatic organisms, integral to human diets, act as vectors for heavy metal pollution, indirectly exposing humans to these toxins (Sonone et al., 2021). In humans, exposure to these toxic metals can result in endocrine disruption, damage to the circulatory and nervous systems, and an increased risk of cancer (Yang et al., 2002; Żukowska and Biziuk, 2008; Zhang et al., 2012).

Given the high risks associated with pollution, various guidelines have been established to mitigate its impact on the environment. In Europe, the conventions under the Oslo and Paris Commission (OSPAR) play a critical role in pollution monitoring and regulation. These conventions provide frameworks for setting baseline values, monitoring environmental thresholds, and establishing limit values (Nijenhuis et al., 2000; Nielsen et al., 2022; Sanz-Prada et al., 2022). One key metric used by OSPAR is the Effects Range-Low (ERL), which evaluates the environmental status of affected areas. When the concentration of heavy metals exceeds the ERL, the potential for adverse environmental impacts increases considerably, and occasional toxic biological effects on marine organisms cannot be excluded. This highlights the importance of adhering to these guidelines to protect marine ecosystems.

However, pollution is not the only environmental pressure threatening marine and coastal ecosystems. Climate change further exacerbates existing challenges, particularly in coastal regions where rising sea levels intensify the strain on both natural habitats and human infrastructure. To mitigate these risks, a diverse array of coastal protection measures is actively implemented, particularly in regions most vulnerable to such challenges (Linham and Nicholls, 2010; Masselink and Russell, 2013; Vousdoukas et al., 2018). Coastal protection strategies span a broad spectrum, ranging from rigid and hard engineering structures, such as sea dikes, seawalls, revetments, breakwaters, or groynes, to soft nature-based approaches, such as coastal dunes, seagrass meadows or salt marshes. Hard structures are often preferred in regions with high-value infrastructure and critical assets. These hard structures are especially advantageous in densely populated urban areas and heavily trafficked waterways, where reliable, immediate protection is indispensable (De Ruig, 1998; Narayan et al., 2016; Morris et al., 2018; Schoonees et al., 2019). However, achieving a balance between engineering efficiency and environmental sustainability remains essential. In tidally influenced coastal areas, these traditional coastal protection measures strongly affect tidal current patterns, sedimentology, and morphology (Albinus et al., 2025, in prep.; Geßner et al., 2024; Geßner et al., 2025 in review; Kunz, 1997; Ladage et al., 2006; Mascioli et al., 2023). As a result, they can also impact sedimentation dynamics and thus the potential accumulation of heavy metals. However, nature-based approaches such as salt marshes can also affect the local hydrodynamic and sedimentation (Allen, 2000). Here, the vegetation friction ensures wind wave and storm surge attenuation and thus reduces the wave run-up height on the dike (John et al., 2015; Möller et al., 2014), which is why salt marshes are often used as complementary coastal protection measures, particularly on the Wadden Sea mainland coast (Marin-Diaz et al., 2023; Narayan et al., 2016; van Loon-Steensma, 2015). Consequently, ecosystem-based coastal protection measures can also represent a sink for heavy metals. The specific impacts of various coastal protection structures on the accumulation of sediments enriched with heavy metals have, however, been insufficiently investigated to date. Hence, further scientific investigations are necessary to improve our understanding of the underlying processes and to support the implementation of more environmentally sustainable coastal protection measures. This study aims to elucidate the relationship between the effect of coastal protection measures on the transport and accumulation of heavy metals in tidally dominated inlets. Tidal basins and inlets are highly dynamic systems characterized by considerable heterogeneity in surface sediment grain size and composition, as well as by their role as unique habitats for marine organisms (Alp and Le Pichon, 2021; Becking et al., 2011; De la Vega et al., 2018; Desmond et al.,2000; Escapa et al., 2008; Reise, 2004). Understanding the spatial distribution of polluted areas within such tidal-influenced coastal areas, identifying the types and concentrations of heavy metals present, and examining how anthropogenic pollution is manifested allows for the identification of pollutant sources and sinks. Furthermore, this study seeks to assess the influence of existing coastal protection measures on the patterns of heavy metal accumulation and distribution. Insights gained will contribute to a deeper understanding of how such measures interact with sediment dynamics and pollutant transport, informing future strategies for sustainable coastal management and pollution mitigation.

4.2 Study area

The Southern North Sea coast along the Netherlands, Germany, and Denmark is characterized by the Wadden Sea. The Wadden Sea, the largest contiguous natural area under constant tidal influence, developed during the Holocene and is a key habitat for various organisms (Behre, 2004; Karle et al., 2021; Wang et al., 2012). A system of barrier islands protects the Wadden Sea, namely the West Frisian Islands along the Netherlands, the East Frisian Islands along Germany and the North Frisian Islands along the northern part of Germany and the southern Part of Denmark (Fig. 4.2A). Narrow channels, the tidal inlets, separate the barrier islands and represent the area of water exchange between the North Sea and the Wadden Sea. Tidal inlets play a crucial role in coastal ecosystems by facilitating water and nutrient exchange, supporting biodiversity, improving water quality, and transporting sediments. Due to the influence of tides, waves, and wind, these inlets are highly dynamic systems. Hard coastal protection measures along barrier islands of the East Frisian islands significantly alter the natural system (Mascioli et al., 2023; Ladage & Stephan, 2004; Ladage et al., 2006; Lüders, 1952), creating new zones of erosion and sediment deposition that may serve as potential accumulation sites for heavy metals. This phenomenon is observed in the study area, specifically in the tidal inlet known as "Harle," which is located between the barrier islands of Spiekeroog and Wangerooge (Fig. 4.2B).

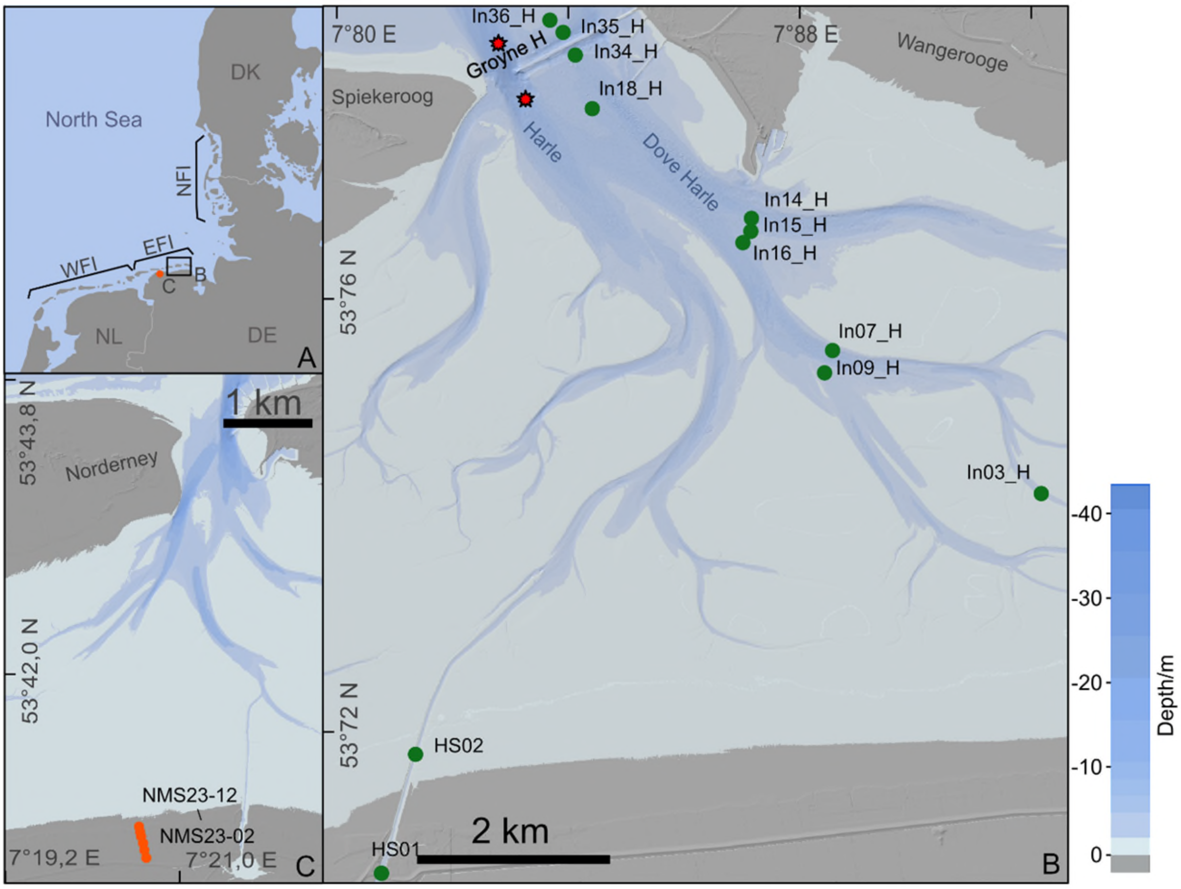

Figure 4.2: (A) Map of the study area, showing the West Frisian Islands (WFI), East Frisian Islands (EFI), and North Frisian Islands (NFI) located along the coasts of the Netherlands (NL), Germany (DE), and Denmark (DK). (B) Sample locations within the Harle Inlet, where green dots indicate sites for sediment and heavy metal sampling, and red stars mark locations of ADCP time-series measurements. (C) Sampling locations in a reference area within the saltmarsh along the coast of Neßmersiel.

The North Sea is influenced by semidiurnal tides. The conditions along the East Frisian Islands are mesotidal with a tidal range of about 2.9 m (Ladage et al., 2007). The mesotidal regime has an asymmetry of the currents. The flood current occurs early in the tidal cycle and the ebb current starts shortly before slack tide, resulting in an ebb dominance in the regional tidal inlets (Niemeyer, 1990; Stanev et al., 2007).

The Southern North Sea Coast is under the influence of a littoral drift, which transports sediments from West to East, especially along the sandy Frisian Islands (Wang et al., 2012). This causes massive changes along the island shoreline, because the western ends of the islands are eroded and transported to the east. Thus, the islands migrate eastward and the settlements are endangered. To prohibit further erosion and protect the islands against storm surges, overwash, and rising sea levels, many of the islands are nowadays secured by coastal protection measures such as dikes, groynes, and sand nourishment (Doughty et al., 2006; Feagin et al., 2010; Oost et al., 2012). Within the Harle inlet, a longstanding groyne, the so-called "Groyne H", was built and restricts the exchange area of the North Sea and Wadden Sea. Originally installed in 1877 as a beach groyne to trap sediment, Groyne H was later modified into a 1400 m stream groyne in 1940 following the development of the secondary channel, Dove Harle (Lüders, 1952; Witte, 1970). This Groyne H has a massive and longstanding impact on the natural habit of the inlet, strongly affecting its flow patterns. The tidal flow is accelerated at the tip of the groyne and the flow velocity is increasing rapidly as the stream passes the narrow point. Depending on the tide, the groyne is submerged during high water and partially emerged during low tide. Circular eddies occur during low tide, caused by the attached the groyne field on Wangerooge (Albinus et al., 2025, in prep.). Geßner et al., 2024 and Geßner et al., 2025 (in review) describe the morphological and sedimentological impacts caused by Groyne H by the development of a sedimentological facies map.

In general, the Harle inlet is dominated by two tidal channels, the Harle and the Dove Harle (Fig. 4.2B). The predominant ebb tide is primarily streaming out of the secondary channel, the Dove Harle, near Wangerooge and prohibits sedimentation in this channel. Consequently, the main Harle channel experiences a shrinking in its drainage area, altering the tidal dynamics of the inlet. The altered flood currents result in a mixed shear zone where fine sediment precipitate and form a sediment bar, separating the channels of the Harle and the Dove Harle. In general, characteristic sediment patterns can be found in the Wadden Sea are, whereby the grain size typically decreases towards the mainland. However, coarser sediments can also be transported and deposited within the deeper tidal inlets by strong currents, while fine-grained sediments are deposited on the tidal flats with calmer currents (Nyandwi and Flemming, 1995). Accordingly, Geßner et al. (2024) defined three different realms for the sediment deposition area of the tidal inlet, from (1) the Wadden realm to (2) the flanks and channel realm to (3) the main channel realm. The bedform interior the Harle is limited to megaripples. Although subaquatic dunes occur in other East Frisian Island inlets, these kind of bedforms are completely absent in the Harle inlet.

In order to investigate the relationships between sediment attributes and potential heavy metal accumulation under the influence of various coastal protection measures and local anthropogenic and natural factors, however, sediment samples were taken from sites located in the area of influence of contrasting coastal protection elements. This included not only a groyne crossing a tidal inlet with adjacent tidal flats, but also a coastal salt marsh with a dike in the hinterland. Ship traffic is limited to ferries, small motorboats and crab cutter within the Wadden Sea and the tidal inlet. Furthermore, by taking sediment samples That anthropogenic impact is represented by samples from the harbor basin of Harlesiel and its entrance, this allows the anthropogenic impact on the sediment characteristics to be investigated. Because for the purpose of hinterland drainage, there is a tidal gate in Harlesiel that allow the water to discharge into the Wadden Sea through the harbor basin at low tide.

For the investigation of a vegetated coastal ecosystem, the salt marsh called "Westernessmerheller" (WNH) was chosen. This salt marsh is located on the mainland coast of the central Wadden Sea and west of the harbor Neßmersiel (Fig. 4.2C). The investigated salt marsh is situated on the seaward side of the dike line and is exposed to comparatively hydrodynamically calmed conditions, as the nearest barrier islands Norderney and Baltrum provide sufficient shelter. Most parts of the Wadden Sea National Park in 1986, i.e., largely left to natural processes. In contrast, a restricted area of the WNH was actively restored in the summer of 2022 as part of a compensation measure. In the course of this measure, artificial drainage ditches were refilled with clayey soils and the area was recontoured through topsoil removal to recreate a more natural landscape with greater topographic heterogeneity. In addition, a meandering tidal creek system was constructed in the salt marsh to enable more natural tidal flooding and drainage of the salt-marsh area and the associated introduction of marine sediments. The restoration of salt marshes by removing topsoil and recreating natural tidal creeks improves hydrodynamic connectivity, promotes natural sediment accretion and enables the reintroduction of site-specific halophytes (Chang et al., 2015; Reed et al., 1999). This not only strengthens biodiversity and habitat function, but also increases coastal protection through wave energy attenuation and long-term resilience to sea level rise (Hudson et al., 2021; Taylor-Burns et al., 2024; Vuik et al., 2019).

4.3 Methods

4.3.1 Hydrodynamic measurements

Data acquisition took place in June 28th 2022 with an Acoustic Doppler Current Profiler (ADCP), a Teledyne RD Instruments Workhorse 1200 kHz ADCP on the *RV Senckenberg* cruise SE202206-1 The ADCP was mounted starboard at a depth of 1.25 m. The position was given every minute by a Differential Global Positioning System (DGPS) from Trimble. The ADCP operated in broadband mode with bin size set to 0.25 m. Data were collected during a 11 hours permanent measuring site south of Groyne H from 05:00 UTC slightly after low tide until 16:00 UTC slightly before low tide. The same approach was used on June 29th 2022 north of Groyne H (Fig. 4.2B). For the correction of the speed of sound, conductivity and temperature data from a Ferrybox Pocketbox by 4H-JENA engineering GmbH were used to calculate the mean salinity data. Suspended Sediment Concentration (SSC) was calculated from the acoustic backscatter signal obtained by the ADCP after Deines (1999). To calibrate the calculation coefficients, Suspended Particular Matter (SPM) samples of two depths were taken with a water sampler, connected to a Conductivity Temperature Depth sensor (CTD) over the measurement period. Meridional and zonal velocities were rotated to the geographical orientation of Groyne H (60.56 °), resulting in an along-groyne (u) component and an across-groyne (v) component.

4.3.2 Sediment sampling

A total of 12 marine sediment samples were collected during a ship-based field campaign in April 2023 with a 1 m^2 van-Veen grab sampler with the *RV Otzum.* The sampling was conducted during a period of high-water levels, spanning a duration of two hours following the low tide until two hours prior to the subsequent low tide. Samples for grain size analysis (50 mL) and heavy metal analysis were taken from the material retrieved with the grab sampler and freeze-dried.

Salt marsh sampling was carried out on April 4th 2023. A total of six surface sediment samples were taken along a defined transect, with the transect extending from the seaward dike toe, across the salt-marsh platform, to the tidal flats adjacent to the seaward edge of the salt marsh. The samples were taken using a cylindrical frame (Ø ~10 cm). By sampling along a transect perpendicular to the coast, it was possible to take three samples within the actively restored area as well as two samples on the adjacent passively restored areas and one sample in the tidal flats. The two passively restored sampling sites were selected because they represent the most common salt-marsh appearance along the coastline of Lower Saxony. Sampling of the actively restored area, on the other hand, allows the effects of ecosystem-strengthening dike foreshore management approaches on the presence of heavy metals to be assessed. The respective geodetic x-, y-, and z-positions of the individual samples were measured with a real time kinematic (RTK) u-blox F9P module GNSS (global navigation satellite system) receiver.

Sediment grain size distribution were determined by wet sieving of 50 mL samples through the fractions > 2000 µm; 2000 – 1000 µm; 1000 – 200 µm; 200 – 63 µm and <63 µm, ffollowed by drying for 72 hours in a drying oven at 38 °C.

Minerogenic grain-size determination by laser diffraction was carried out by using the HORIBA LA-950 analyzer. The samples were first mechanically homogenized by carefully mixing the sediment material with a plastic spatula to disaggregate sediment aggregates. Coarse particles such as plant debris, shells, and stones were removed manually to avoid measurement artifacts. The samples were then gently dried in a drying oven at 38 °C for at least 24 hours. From each dried subsample, approx. 5 mL of sediment was taken and subjected to chemical pretreatment to remove all organic components. For this purpose, a 10-30 mL solution of 30% hydrogen peroxide (H_2O_2) was added in steps and the samples were then cooked at 60-70 °C for at least 24 hours until the organic remnants were completely reacted. Subsequently, all carbonate components were dissolved by adding 10 mL of 32% hydrochloric acid (HCl) in order to measure only the minerogenic grain-size signal. Excess liquids were removed after the reaction was complete by multiple centrifugation and subsequent pipetting. However, as some samples consisted mainly of fine-grained material (including cohesive clays), all samples were additionally treated in a final step with approx. 1 mL of 2% sodium metaphosphate solution $(NaPO_3)_n$ and homogenized in an overhead shaker for 2 hours to disperse any remaining clayey aggregates. A small amount was then fed into the laser-diffraction device for wet dispersive particle-size analysis. Further descriptions of sample pretreatments for laser-diffraction analysis can also be found in Blott et al. (2004).

Prior to the heavy metal analysis, the samples were homogenized using an agate mill (Fritsch Planetary Mill Pulverisette 5). An X-ray fluorescence (XRF) spectrometer Panalytical Axios max (Panalytical, Malvern, England) was utilized to analyze the chemical sediment composition and concentration of the samples. For the element analysis, the samples were mixed with di-lithium tetrabonate and ammonium nitrate and were preheated in a muffle oven (Thermo Fisher Scientific, Waltham, USA) at 500 °C. The annealed materials were fused to glass lenses using a melt fusion device (HD Elektronik und Elektrotechnik GmbH, Kleve, Deutschland) and subsequently analyzed by XRF. The following chemical compounds and elements were analyzed in the study: the major Al_2O_3 and the minor elements arsenic (As), chromium (Cr), copper (Cu), lead (Pb), and zinc (Zn).

To determine the concentration of organic carbon in sediment samples, total carbon (TC) and inorganic carbon (TIC) were measured separately and subsequently utilized to calculate the total organic carbon (TOC) through subtraction. The TC and TIC measurements were conducted using a carbon-sulfur determinator (CS-580 Eltra, software version Uni 2.4.3.7a40-4920, Haan, Germany). For the measurement of TC, sediment samples were mixed with vanadium pentoxide and subsequently subjected to combustion at 1,350 °C in the determinator. The resulting carbon concentration was recorded as TC. For the TIC measurement, sediment samples were placed in Erlenmeyer flasks with magnetic stirring bars and heated to 70 °C. Perchloric acid was added to the samples to acidify them. The concentration of TIC was then measured. The total organic carbon (TOC) was calculated by subtracting the measured TIC from the TC. Furthermore, the mercury (Hg) concentration was directly measured using a direct mercury analyzer (DMA-80, 2009, Milestone Inc., Shelton, USA). The samples were first weighed, then subjected to drying and thermal decomposition in an oxygen-rich atmosphere. The released mercury was captured through amalgamation and quantified using an optical spectrometer. The accuracy of the measurements was validated through participation in interlaboratory ring tests and comparison with international reference materials such as DORM-3 and DORM-4. Trace metal concentrations derived from the XRF were normalized to Aluminium (Al). Normalization to Al balances the dilution effect and allows for the comparison of sediment samples from different stations and different grain sizes or genesis. For further analysis the data were statistical analysed and the enrichment factors were calculated with the lithogenic background data from Beck et al., (2013).

For further analysis the data were statistical analysed with a Pearson correlation and the enrichment factors were calculated with the lithogenic background data of the Jade bay from Beck et al. (2013).

4.4 Results and Discussion

4.4.1 Hydrodynamic conditions

Time-series measurements using ADCP data provided detailed insights into current velocities and directions across the groyne at two specific locations. At the site north of Groyne H, the analysis revealed that the flood current begins earlier relative to slack water, while the ebb current shortly after high slack tide (Fig. 4.3). Notably, the slack water at low tide persists longer than at high tide. Although the ebb current is shorter in duration, it exhibits a higher average velocity. These observations align with hydrodynamic patterns reported in previous studies, such as Niemeyer (1990) and Stanev et al. (2007). Analysis of along-groyne velocities and directions (App. Fig. 1) highlights the transport dynamics along the groyne flanks, characterized by a pronounced west-east directional flow pattern both north and south of Groyne H. During the flood tide, the flow exhibits a strong eastward-directed component, while during the ebb tide, the flow reverses to a westward direction. This bidirectional flow pattern reflects the influence of tidal dynamics and the structural impact of the groyne on local hydrodynamics.

Suspended sediment concentrations (SSC) are highest during the ebb current, particularly between water depths of 5 and 15 m. Sediment transport is most prominent along the seafloor (14 mgL^{-1}) during ebb flow, where particles are assumed to be mobilized primarily by rolling, saltation, and suspension due to the enhanced shear stress between velocities in the upper and lower layers of the water column. Finer sediment grains, forming the wash load, are transported at depths of 5 to 10 m and remain mobilized during the later stages of the ebb current, albeit with reduced transport energies and velocities. In contrast, sediment transport during the flood current is generally lower. The highest sediment concentrations during the flood current occur at its onset, with transport observed along both the seafloor and in the water column as wash load between depths of 5 and 10 m.

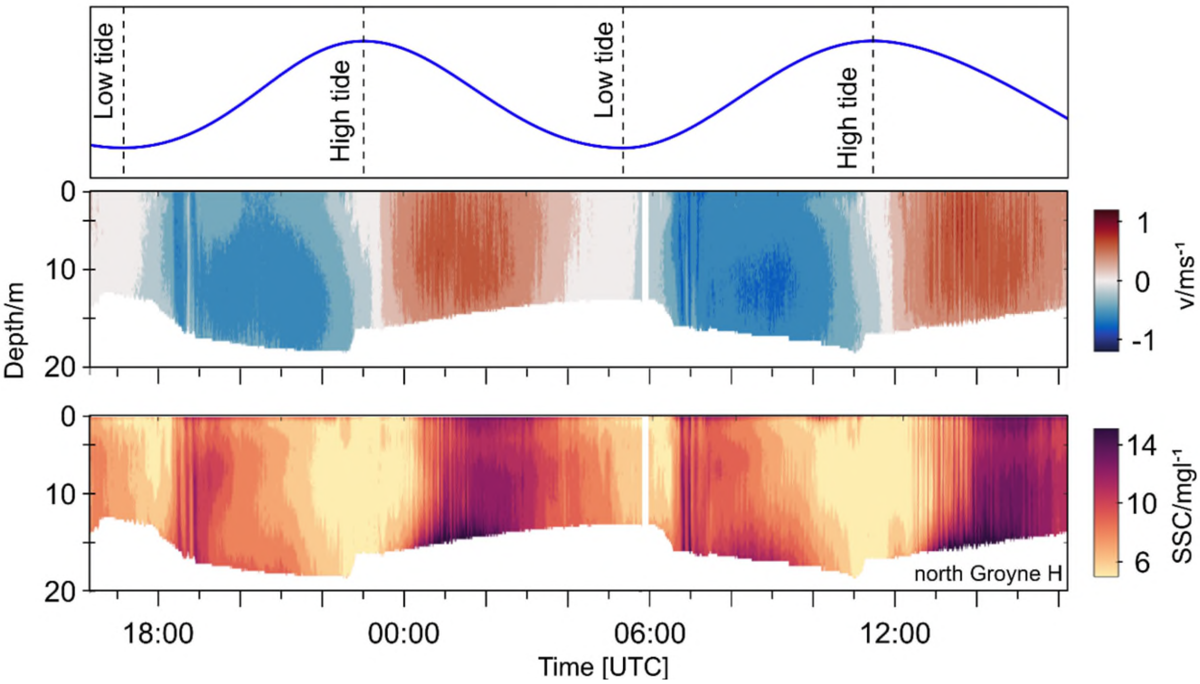

Figure 4.3: ADCP data from the time-series station located north of Groyne H. The top panel depicts the tidal cycle during the measurement period on June 28th and 29th 2022. The middle panel presents meridional velocity data, while the bottom panel illustrates SSC over the same time frame.

Data from the site located south of Groyne H indicate a different SSC distribution and reduced current velocities (Fig. 4.4). Notably, the ebb current here exhibits diminished velocities. Sediment transport is primarily concentrated within the water column at depths of 5 to 10 m, with SSC ranging from 10 to 14 mgL^{-1}. Near-seafloor transport occurs predominantly during the flood current, with SSC increasing between depths of 5 and 17 m, peaking near the seafloor.

The observed differences in current velocities and SSC between the sites north and south of Groyne H are attributed to hydrodynamic effects induced by the groyne. As described by Geßner et al. (2024) and Albinus et al. (2025, in prep.), the tidal current intensifies around the tip of the groyne. Beyond this narrow point, the current decelerates in the downstream groyne field, resulting in sediment deposition within the mixing shear zone. North of Groyne H, flood flow exhibits vertical zonation, with the highest velocities occurring after low tide and progressively decreasing until slack water. In contrast, south of Groyne H, flood velocities are intermixed and lack distinct zonation. During the ebb current, this pattern is reversed: south of Groyne H, the flow appears more stratified, while north of the groyne, zonation is less distinct.

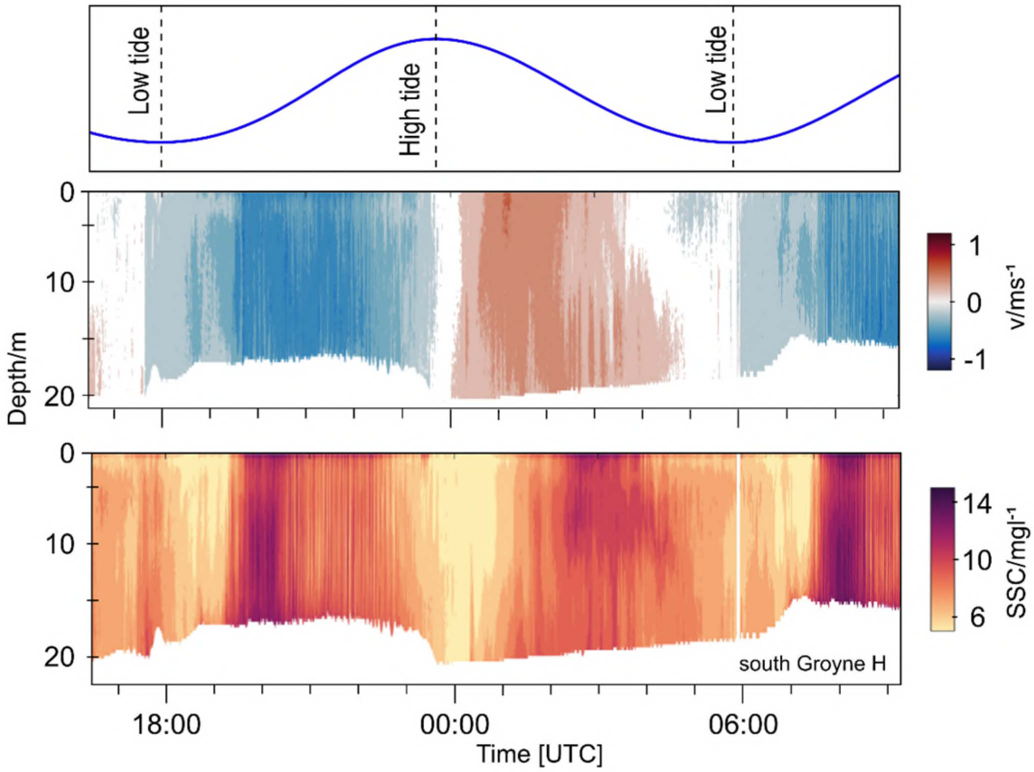

Figure 4.4: ADCP data recorded during the night of June 28th and day of 30th, 2022. The upper panel displays the tidal cycle, while the middle panel presents meridional velocity data from the time-series station located south of Groyne H. The lower panel illustrates the SSC measured during the same period.

It can be assumed that the variations in SSC are similarly influenced by changes in current velocities. The ebb current south of Groyne H mobilizes and erodes previously during slack tide deposited sediments, transporting them out of the inlet. During flood flow, SSC is well-mixed throughout the water column south of Groyne H. In contrast, north of the groyne, two primary sediment transport zones are evident: a near-seafloor zone characterized by rolling, saltation, and suspension, and a wash load zone between 5 and 10 m. As water passes the tip of the groyne, these two zones become intermixed, leading to the absence of a clear distinction between the wash load and near-seafloor transport zones, probably due to the narrowing of the flow area. During ebb flow, the near-seafloor transport zone appears earlier than the wash load zone both north and south of Groyne H. This phenomenon is driven by the vertical density gradient, where lighter Wadden Sea water overlays denser North Sea water. The resulting vertical stratification accelerates the near-surface layer, enhancing the zonation of SSC (Buchard et al., 2008). During the flood tide, the inflow of denser North Sea water occupies the mid-water column. The shear stress generated at the seabed induces turbulence, mobilizing sediment from the seafloor. SSC is notably higher north of the groyne, where stronger currents, accelerated by the groyne tip, generate higher erosion forces. This elevated sediment load is attributed to the intensified mixing and the active erosion of sediments near the groyne tip, as observed by Geßner et al. (2024). Similar processes occur south of Groyne H, where the accelerated flow at the groyne tip enhances sediment mobilization and erosion during both ebb and flood tides.

Figure 4.5 illustrates the net SSC transport observed during the measurement period. The data indicate that north of Groyne H, SSC transport is greater during ebb flow than during flood flow, meaning that more SSC is exported from the Harle. South of Groyne H, transport is higher during flood flow. Additionally, transport patterns exhibit irregular fluctuations, with pronounced spikes at the northern station occurring during ebb tide, whereas south of the groyne, these irregular transport patterns emerge during flood tide, further supporting the described processes. Overall, at the time of measurement, SSC transport was higher during ebb tide than during flood tide.

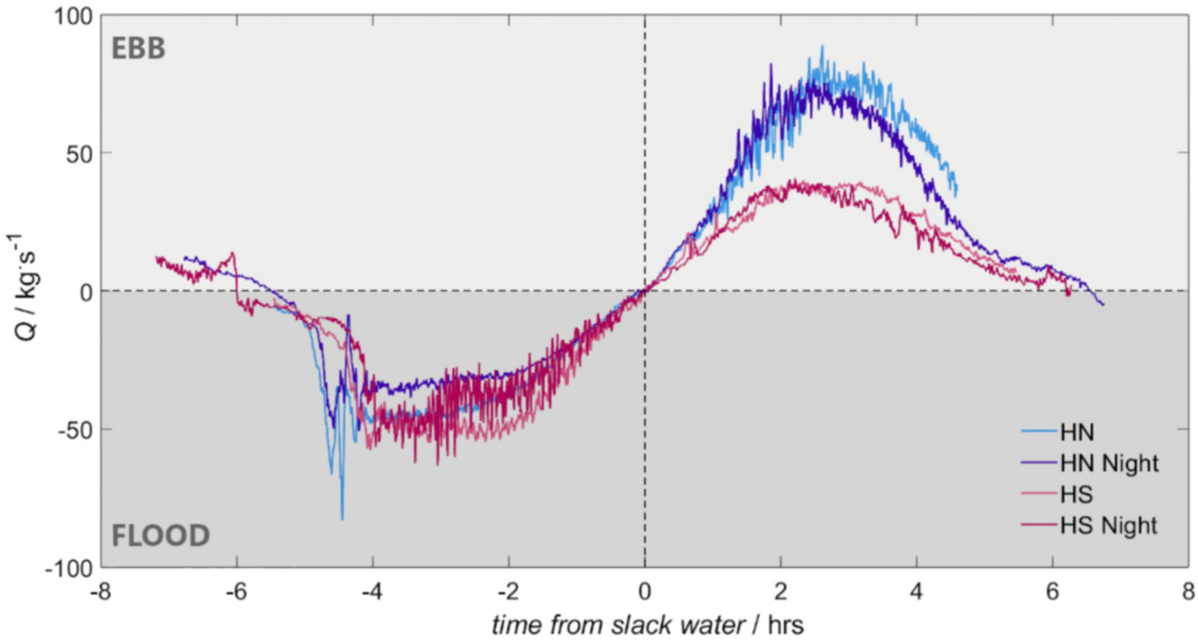

Figure 4.5: ADCP SSC transport data for the flood end ebb flow along the stations along the norther station (blue lines) and the southern stations (magenta lines). Negative hours are showing the flood flow and positive hours the ebb flow, in dependence to the slack water.

In summary, the dynamics of SSC in the Harle tidal inlet are heavily influenced by the hydrodynamic modifications induced by Groyne H. These alterations result in localized variations in sediment mobilization and transport, with stronger currents at the groyne tip playing a critical role in sediment erosion and redistribution.

4.4.2 Grain size distribution

The water depths along the sampling sites of the inlet range from 1.72 m to 7.17 m, with an average depth of 4.60 m ± 2.03 m. Shallower sites are primarily located near the harbor of Harlesiel and at the shallow ends of the inlet channels, including gullies. These regions are characterized by finer grain sizes, with a higher proportion of fine fractions and fine sand. Conversely, deeper sampling sites are situated within the main inlet channels or adjacent to Groyne H, where grain sizes increase, and the sediments are predominant by sand. The average fine fraction content across all sampling sites is 27.33% ± 30.22%, while sand content averages 66.92% ± 29.66%, and shell content accounts for 5.75% ± 13.62% (Tab. 4.1). The considerable variations in grain size distribution are indicative of the high heterogeneity of the tidal inlet, which is an important feature of dynamic systems. In this dynamic system, current velocities are highest near the tip of Groyne H, within the main channels and scours. The construction of Groyne H has influenced hydrodynamic patterns, leading to the formation of vertical and horizontal circulation cells, which cause scouring along the groyne flanks (Albinus et al., 2025, in prep.). The altered flow patterns create zones of high velocity and mixing shear zones south of Groyne H, where transport energy diminishes and sediment deposition occurs (Geßner et al., 2024). This interaction between hydrodynamics and sediment transport underscores the complexity of sedimentary processes within tidal inlets, by controlling their grain size distribution as well as deposition and erosion areas.

Table 4.1: Sediment classification by fractions and by method (sieve analysis and laser-diffraction spectroscopy) of the sediment samples collected from the Harle inlet in March 2023.

			Sieving analysis			**Laser-diffraction analysis**			
Station	**Location**	**Depth [m]**	**Gravel [%]**	**Sand [%]**	**Mud [%]**	**Gravel [%]**	**Sand [%]**	**Silt [%]**	**Clay [%]**
In36_H	North of Groyne H	3.82	0.07	96.86	3.07	0	99.80	0.20	0
In35_H	North of Groyne H	7.15	0.21	96.70	3.08	0	99.70	0.30	0
In34_H	South of Groyne H	5.93	9.71	88.37	1.93	0	100.00	0	0
In18_H	Mixing shear zone	6.54	0.09	96.82	3.09	0	99.95	0.05	0
In14_H	Dove Harle channel	6.95	5.61	13.76	80.63	0	72.21	23.55	4.24
In15_H	Channel flank	4.63	17.27	79.24	3.49	0	99.78	0.22	0
In16_H	Channel flank	5.10	18.70	77.87	3.43	0	99.87	0.13	0
In07_H	Channel flank	6.29	25.85	69.12	5.02	0	99.94	0.06	0
In09_H	Channel	3.06	22.65	72.94	4.40	0	99.95	0.05	0
In03_H	Gully	1.94	3.27	91.57	5.16	0	97.80	2.20	0
HS02	Entrance harbor	2.10	43.22	45.53	11.25	0.01	83.15	13.66	3.18
HS01	Harbor	1.72	0	17.06	82.93	0	13.48	86.52	0
Mean		4.60	12.22	70.49	17.29	0	88.80	10.58	0.62
SD		2.03	13.62	29.66	30.22	0	24.23	23.96	1.40

Considering the siliciclastic, organic- and carbonate-free sediment fractions of all samples analyzed by laser diffraction from the tidal inlet and the salt marsh in direct comparison, the samples are quite heterogeneous and can be assigned to the textural group of mud (clay and silt) and sandy mud, muddy sand as well as sand to slightly gravelly muddy sand. However, when considering the samples from the tidal inlet and the salt marsh separately, it is noticeable that the samples in the area of the tidal inlet are predominantly sandy and coarser (between 13.48% and 100% sand content, i.e., fine to medium sand, 99.79% at the median; Tab. 4.1), while the samples from the salt marsh tend to fall into the fine-grained range (between 68.55% and 91.74% silt content, 89.49% at the median; App. Tab. 14). On average, this means that the grain size of the sediments in the area of the tidal inlet is 206.89 µm (fine sand), while the grain size in the salt marsh sediments is only 20.39 µm (coarse silt).

In the marine offshore area, i.e., in the tidal inlet, results obtained from laser-diffraction spectroscopy revealed that the finest sediments were found in the area of the Harlesiel harbor basin (site HS01, 19.67 µm on average), while the coarsest sediments were documented in the tidal inlet itself (site ln34_H, 366.20 µm on average). Additionally, the sediments in the harbor area (sites HS01 and HS02) tended to be more poorly sorted as well as both coarse (positive) to fine skewed (negative). In contrast, nine of the ten samples further offshore (sites ln03_H to ln36_H) were generally more symmetrical and slightly better sorted (moderate to well sorted) than the harbor samples.

4.4.3 Geochemistry of marine sediments

The primary chemical components of the sediments, in descending order, are SiO_2 (83.10% ± 10.31%), CaO (4.46% ± 3.07%), Al_2O_3 (2.53% ± 1.99%), Fe_2O_3 (0.76% ± 0.97%), Na_2O (0.78% ± 0.37%), K_2O (0.86% ± 0.37%), MgO (0.32% ± 0.41%), TiO_2 (0.23% ± 0.16%), P_2O_5 (0.05% ± 0.07%), and MnO (0.02% ± 0.01%) (Tab. 4.2). These chemical compositions reflect the alteration and weathering of silicates and other minerals (Nesbitt and Young, 1982, 1984, 1989; Fedo and Badechuk, 2023). The chemical profiles provide valuable insights into sediment provenance, transportation pathways, and mineralogical composition. The sediments in this study are predominantly composed of quartz, with associated bivalve fragments, clay minerals, mica, amphibole, feldspar, and pyroxene.

The TOC content is influenced by terrestrial plant and animal decomposition, anthropogenic inputs such as fertilizers and organic-rich waste, and aquatic sources like plankton (Avramidis et al., 2015). In the Harle, TOC values range from 2.35% to 0.5%, with an average of 0.36% ± 0.68%. The highest TOC values correspond to areas with elevated mud content (e.g., site HS01), typically near the mainland where terrigenous organic matter is deposited. Component analysis suggests that plant detritus predominantly accounts for the TOC content in most samples.

Table 4.2: Chemical compound composition in percentages [%] of sediments from the Harle.

Station	TOC [%]	SiO_2	CaO	Al_2O_3	Fe_2O_3	Na_2O	K_2O	MgO	TiO_2	P_2O_5	MnO
In36_H	0.06	92.40	0.68	2.03	0.41	0.69	0.80	0.16	0.25	0.02	0.01
In35_H	0.06	92.90	0.65	1.64	0.31	0.65	0.69	0.13	0.18	0.02	0.01
In34_H	0.05	86.27	5.37	1.01	0.14	0.46	0.50	0.09	0.05	0.02	0
In18_H	0.06	93.61	0.52	1.53	0.20	0.57	0.72	0.09	0.08	0.02	0
In14_H	0.68	72.71	7.16	4.65	1.70	1.20	1.31	0.72	0.33	0.07	0.03
In15_H	-	84.62	5.64	1.59	0.30	0.61	0.68	0.13	0.15	0.02	0.01
In16_H	-	87.07	3.94	1.69	0.32	0.61	0.73	0.12	0.16	0.03	0.01
In07_H	-	83.14	6.36	1.36	0.22	0.60	0.64	0.11	0.09	0.02	0.01
In09_H	0.19	84.45	5.93	1.29	0.23	0.55	0.60	0.10	0.12	0.02	0.01
In03_H	0.12	89.54	1.29	2.52	0.70	0.84	0.90	0.25	0.43	0.03	0.02
HS02	0.70	70.74	10.07	3.1	1.14	0.97	0.96	0.49	0.35	0.11	0.03
HS01	2.35	59.79	5.96	7.99	3.48	1.61	1.84	1.46	0.56	0.24	0.05
Mean	0.36	83.10	4.46	2.53	0.76	0.78	0.86	0.32	0.23	0.05	0.02
SD	0.68	10.31	3.07	1.99	0.97	0.33	0.37	0.41	0.16	0.07	0.01

4.4.4 Heavy metal geochemistry in marine sediments

The concentrations of heavy metals in the sediments are summarized in Table 4.3, with the metals ranked in decreasing concentration as follows: Cr > Zn > As > Cu > Pb.

Aluminum (Al) concentrations range from 0.53% to 4.23%, with an average of 1.40% ± 1.05%. The highest Al concentrations are observed at sites located in the harbor (site HS01) and at site In14_H in the main channel of the Dove Harle, where fine fraction content is also at its peak (80%). Aluminum is a major constituent of clay minerals, and its concentrations correlate strongly with areas of high fine fraction content.

Table 4.3: Heavy metal concentrations in the Harle sediments, reported in parts per million (ppm), except for aluminum (Al), which is expressed as a percentage. For reference, the Effects Range-Low (ERL) thresholds are provided above the corresponding sample values. Concentrations highlighted in bold are higher than the ERL threshold.

Station	Al %	As [ppm]	Cr [ppm]	Cu [ppm]	Pb [ppm]	Zn [ppm]
ERL		8.2	81	34	47	150
In36_H	1.07	**10**	28	2	0	8
In35_H	0.87	**9**	21	2	0	6
In34_H	0.53	8	7	4	0	3
In18_H	0.81	**9**	11	4	0	5
In14_H	2.46	**14**	45	6	5	24
In15_H	0.84	**9**	29	3	1	7
In16_H	0.89	**9**	18	4	1	7
In07_H	0.72	8	13	5	1	5
In09_H	0.68	8	18	3	1	6
In03_H	1.33	**9**	53	4	6	14
HS02	1.64	**12**	49	10	8	29
HS01	4.23	**20**	80	15	24	91
Mean	1.26	10	26	4	3	12
SD	0.55	2	15	1	2	6

Chromium (Cr) concentrations range from 7 ppm to 80 ppm, with an average of 29 ppm ± 22 ppm. The highest values were observed at sites characterized by a higher content of fine-grained sediments. Conversely, Cr concentrations decrease along the channels and their flanks, where the proportion of fine-grained sediments is lower. These Cr values are consistent with the findings of Beck et al. (2013) for the Jade Bay, suggesting a lithogenic origin. This inference aligns with the presence of spinel group minerals, such as chromite, in the southern North Sea, which contain chromium (Kolditz et al., 2011).

Zinc (Zn) concentrations range from 3 ppm to 91 ppm, with an average of 16 ppm ± 25 ppm, reflecting substantial variability across the study area. The highest Zn concentrations are found in the harbor and at stations with finer sediments. Notably, the harbor station exhibits the peak Zn level, though they remain below the threshold set by the OSPAR (2009) guidelines.

Arsenic (As) concentrations peak at 20 ppm in the harbor and drop to 8 ppm in the main tidal channels and the channel flanks, with an average of 11 ppm ± 4 ppm. The average As concentration exceeds the ERL of 8.2 ppm, suggesting potential contamination from anthropogenic activities. Nevertheless, As pollution can originate from both anthropogenic and natural sources. Anthropogenic inputs include industrial processes, agricultural practices (e.g., pesticide use), and medical applications. Natural sources primarily involve the weathering and dissolution of arsenic-bearing minerals (Garelick et al., 2007; Smedley & Kinniburgh, 2002).

Copper (Cu) concentrations vary from 2 ppm to 15 ppm, with an average of 5 ppm ± 4 ppm. The highest Cu levels are observed in the harbor sites, especially at site HS01. Despite the elevated values in the harbor area, Cu concentrations remain below the ERL threshold of 34 ppm.

Lead (Pb) concentrations range from 0 ppm to 24 ppm, with an average of 4 ppm ± 7 ppm. The highest Pb values are again found in the harbor, but overall, the Pb concentrations remain below the ERL guideline of 47 ppm.

In general, most metal concentrations in the Harle inlet are below their respective ERL thresholds, with the exception of As, which exceeds the threshold. The observed spatial variability is closely linked to sediment-grain size, with higher metal concentrations associated with areas of elevated fine-fraction content, particularly in the harbor of Harlesiel.

The harbor is mostly used for freight and passenger transportation to the islands, tourism, sport boats, and traditional boat shipping like fishing, representing here the general human impact. Additionally, potentially polluted waters and particles from the mainland could enter the harbour via a tidal sluice during ebb tide. Notably, site In14_H, located along the main channel of the Dove Harle, also exhibits elevated heavy metal concentrations. This is attributed to the higher fine-fraction content, which forms the matrix within otherwise coarse-grained sediments. Similarly, the heavy metal concentrations at sites in gully sediments are elevated due to their fine-grained nature, resulting from reduced current energies. These findings highlight the critical role of sediment texture and mineralogy in regulating heavy metal distributions within the tidal environment.

4.4.5 Metal enrichment factor and heavy metal sources

The enrichment factor (EF) can reveal whether a metal is depleted or enriched compared to known lithogenic background levels. The EF is a crucial metric for determining the origin of heavy metals in sediments, helping to distinguish between natural lithogenic contributions and anthropogenic influences (Abrahim and Parker, 2008; Almasoud et al., 2015; Li et al., 2021). This information is important for interpreting the impact of human activities and understanding sediment transport mechanisms. Using lithogenic background levels from Beck et al. (2013) for the Jade Bay, a region close to the Harle inlet, EF values for As, Cr, Cu, Pb, and Zn were calculated and analyzed (Tab. 4.4).

Table 4.4: Enrichment factors of heavy metal concentrations at each sampling site, indicating the degree of heavy metal accumulation relative to baseline levels.

	As	**Cr**	**Cu**	**Pb**	**Zn**
Lithogenic background (after Beck et al., 2013)	2.3	16.4	1.8	3.1	8.3
In36_H	4.1	1.6	1.0	0	0.9
In35_H	4.5	1.5	1.3	0	0.8
In34_H	6.5	0.8	4.2	0	0.7
In18_H	4.8	0.8	2.7	0	0.7
In14_H	2.5	1.1	1.4	0.7	1.2
In15_H	4.7	2.1	2.0	0.4	1.0
In16_H	4.4	1.2	2.5	0.4	0.9
In07_H	4.8	1.1	3.9	0.5	0.8
In09_H	5.1	1.6	2.4	0.5	1.1
In03_H	2.9	2.4	1.7	1.5	1.3
HS02	3.2	1.8	3.4	1.6	2.1
HS01	2.1	1.2	2.0	1.8	2.6

The concentrations of heavy metals along the Harle inlet exhibit distinct variability in their EF (Fig. 4.6). Arsenic (As) is the most enriched metal, with EF values ranging from moderate (2.1) to significant (6.5). Higher levels of As enrichment are particularly observed in the sandier regions, both north and south of Groyne H, as well as along the main channels and their flanks. Copper (Cu) also demonstrates notable enrichment across the sites, with EF values varying from minimal (1.0) to moderate (4.2). Chromium (Cr) exhibits slight to moderate enrichment, with EF values ranging from 0.8 to 2.4. Only two sites located along the gullies and channel flanks show moderate enrichment (EF > 2). Zinc (Zn) shows EF values between 0.7 and 2.6, with moderate enrichment observed primarily at the harbor sites. Lead (Pb) is only slightly enriched, with EF values exceeding 1 at just three sites (1.8, 1.6, and 1.5), while the majority of EF values range from 0 to 0.7.

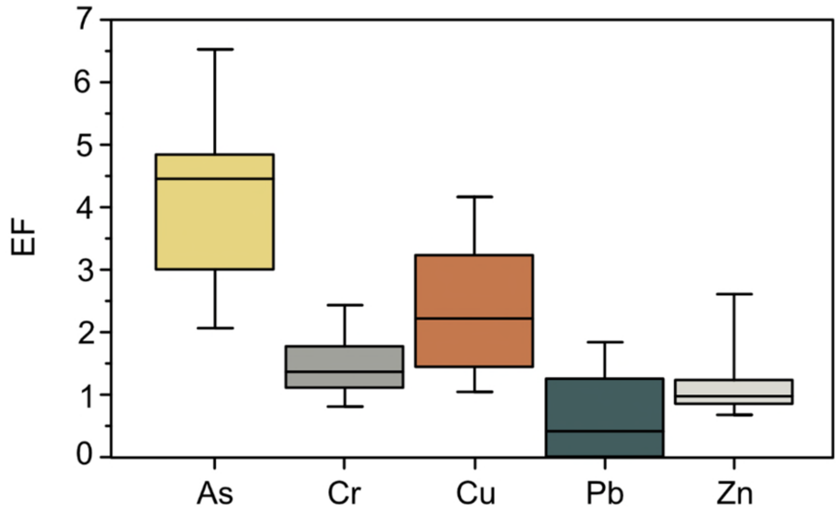

Figure 4.6: Enrichment factors of heavy metals of sediments from the Harle inlet, including arsenic (As), chromium (Cr), copper (Cu), lead (Pb), and zinc (Zn), indicating their relative concentration levels compared to background values.

Enrichment factor values of 1 indicate a natural origin with no elevation above the lithogenic background. Enrichment exceeding a factor of 1 suggests contributions from natural or anthropogenic influences. Factors below 2 are generally considered indicative of no significant contamination from anthropogenic activities (Sutherland, 2000). This implies that most heavy metals in the Harle inlet are slightly enriched, except for select locations where values for Pb, Zn, and Cr exceed 2. Zinc enrichment is limited to harbor areas of Harlesiel, while Cr shows minimal enrichment in gullies and on channel flanks. Critical metals include Cu, which is minimally enriched across the inlet except at specific sites, and As, which is significantly enrichment. This pattern contrasts with the natural occurrence of As and points to anthropogenically driven enrichment. The contamination in this area is moderate, with As concentrations slightly exceeding the ERL threshold. However, compared to the lithogenic background, there is a discernible enrichment, likely induced by the construction of the groyne. The altered hydrodynamic conditions caused by the groyne have led to changes in current velocities and the establishment of new erosion and deposition zones, which may have facilitated the accumulation of As in the region.

Figure 4.7 illustrates the locations of major industrial activities in the region, along with potential sources of pollution. Along the North Sea, the German Bight traffic separation zone runs in a west-east direction, extending eastwards to the Elbe River and the Port of Hamburg. It branches north of the East Frisian Islands toward the Jade and Weser rivers, leading to international trading ports. Wilhelmshaven, situated on the Jade River, hosts the Jade-Weser Port, where 713,000 TEU (Twenty-foot Equivalent Units) were transshipped in 2021, 683,400 TEU in 2022, and 531,000 TEU in 2023. Similarly, the Port of Bremerhaven, on the Weser River, handled 5 million TEU in 2021, 4.6 million TEU in 2022, and 4.2 million TEU in 2023 (Statistisches Bundesamt, 2023). The East Frisian coastline features smaller harbors for recreational boats, cutters, and ferries. Wilhelmshaven is also home to the German Bundeswehr's largest naval base, hosting frigates, supply ships, and tugs. The region experiences heavy maritime traffic, and industrial activities, which further contribute to complex environmental pressures. Notably, an oil refinery north of Wilhelmshaven produces low-sulfur fuel oil. In addition, the mainland supports extensive agricultural activities, particularly livestock farming, grazing land cultivation, and forage crop production (Ministry

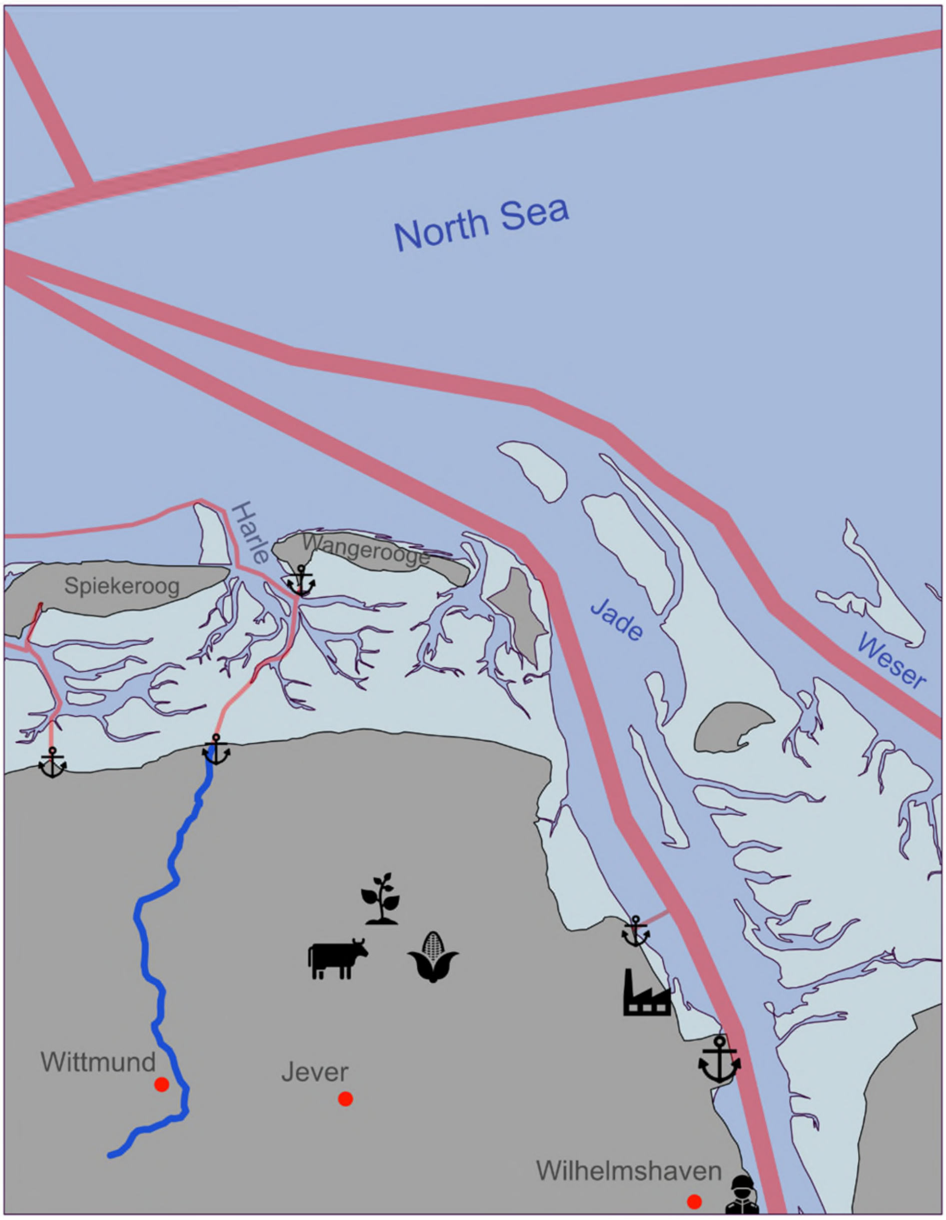

for Food, Agriculture and Consumer Protection of Lower Saxony, 2021).

Figure 4.7: Map of the study area and adjacent mainland, highlighting the locations of ports and harbors (anchor symbols). Near Wilhelmshaven, a military base (military symbol) is located, while an oil refinery (industry symbol) is situated to the north of the city. The mainland is predominantly used for agricultural activities (agricultural symbols). The blue line represents the course of the Harle River, and the red lines indicate designated ship traffic zones.

Additionally, the weathering of natural As sources can contribute to its enrichment in the environment. Pyrite-rich peat is naturally enriched in As due to the incorporation of As into pyrite structures or the formation of stable As sulfides (Dellwig et al., 2002). In the Harle inlet, a peat layer identified by Mascioli et al. (2023) near the tip of Groyne H is likely a major natural source of As and may be of autochthonous origin. Peat layers along the southern North Sea coast were formed during the Holocene and were subsequently buried beneath clastic sediments (Streif, 2004). In the Harle Inlet, this peat layer is subject to accelerated flow and erosion due to high current velocities. This process could facilitate the mobilization and transport of As-rich pyrite into the tidal inlet, contributing to As enrichment in the surrounding environment. Core samples from the mainland, located north of Wilhelmshaven, confirm the presence of pyrite-rich peat layers, which exhibit elevated As concentrations (Dellwig et al., 2002). Streif (2004) provided a detailed geological cross-section of the region, highlighting basal and fen peat layers underlying the tidal-flat sediments of the Wadden Sea. These peat layers act as a natural reservoir of As, likely contributing to the lithogenic background signal. The interaction between this natural As source and anthropogenic inputs leads to considerable As enrichment, particularly along the deposition areas mixing shear layer and to the north and south of Groyne H.

Copper also shows varying degrees of enrichment. While most sites exhibit only slight enrichment, reflecting the lithogenic background, moderate enrichment (EF values of 2–5) is observed near harbors, channels, and channel flanks, as well as south of Groyne H. Anthropogenic sources of Cu include alloys and anti-fouling paints commonly used on vessels and recreational boats (Amara et al., 2018). The distribution of Cu enrichment near channels and harbors strongly suggests contributions from maritime traffic. However, the level of contamination remains minimal, with Cu concentrations consistently below the ERL threshold.

4.4.6 Element interrelation:

A Pearson correlation analysis provides insight into the linear relationships between heavy metal concentrations, sediment properties, and chemical sediment compounds. The results reveal distinct patterns in the association between sediment composition and chemical elements. Most chemical compounds exhibit a negative correlation with sand, except for SiO_2, which shows a positive correlation (Tab. 4.5). Conversely, these compounds display a positive correlation with mud. An exception is CaO, which has an insignificant correlation with mud but shows a moderate positive correlation with the >2 mm fraction. This suggests that SiO_2 dominates the sand fraction, consistent with the predominance of quartz grains in this fraction as confirmed by component analysis. The >2 mm fraction is primarily composed of bivalve fragments and quartz grains. This composition aligns with the observed correlation between CaO and gravel content, reflecting the calcium carbonate contribution from bivalve fragments. Compounds such as Al_2O_3, Fe_2O_3, K_2O, MgO, MnO, Na_2O, P_2O_5, and TiO_2 exhibit a positive correlation with the mud fraction and TOC. This indicates that these compounds are predominantly associated with finer sediments. Aluminum demonstrates a negative correlation with SiO_2 and an insignificant correlation with CaO. Its positive correlation with mud suggests that Al is concentrated in the fine-grained fraction rather than in the sand or gravel fractions. Heavy metals show no significant positive correlation with the sand or gravel content. Instead, they exhibit a negative correlation with both fractions, as well as with SiO_2, and an insignificant correlation with CaO. However, they demonstrate a significant positive correlation with the mud fraction, indicating that heavy metals are predominantly associated with fine-grained sediments. In general, the Pearson correlation analysis highlights that the mud fraction serves as the primary host for most chemical compounds and heavy metals, with their distribution closely tied to fine-grained sediment transport and deposition. SiO_2 is dominant in the sand fraction, reflecting the prevalence of quartz grains. The similarity in correlation patterns among heavy metals suggests that their sources and transport mechanisms are comparable, likely influenced by shared depositional processes in the inlet. These findings emphasize the critical role of sediment texture in controlling the distribution of chemical compounds and heavy metals within the study area (Tab. 4.5-6). Studies from other intertidal regions of the North Sea similarly reveal a strong relationship between grain size, TOC, and Al, attributed to the association between heavy metals and fine-grained sediments. This relationship is primarily driven by the adsorption of metals onto clay minerals and TOC. Aluminum, as a major constituent of clay minerals, serves as a proxy for the fine sediment fraction, further supporting the preferential accumulation of heavy metals in fine-grained deposits (Beck et al., 2013; Du Laing, 2007).

Coastal protection structures significantly influence sediment distribution within the tidal inlet, leading to the formation of new depositional zones while simultaneously creating erosion areas that may remobilize contaminated material, such as heavy metal-enriched sediment layers. However, in highly dynamic environments, strong hydrodynamic forces can prevent the deposition of fine sediments, thereby inhibiting the formation of long-term contaminant sinks. In contrast, under low-energy conditions, fine-grained sediments tend to accumulate, facilitating the sequestration of pollutants and contributing to their long-term retention within the system.

Table 4.5: Statistical correlations (Pearson) between sediment compounds and heavy metal concentrations. Non-significant correlations are displayed in gray.

	Gravel [%]	**Sand [%]**	**Mud [%]**	**TOC [%]**	**Al [%]**	**As (ppm)**	**Cr (ppm)**	**Cu (ppm)**	**Pb (ppm)**	**Zn (ppm)**
SiO_2	0.25	0.97	-0.93	-0.95	-0.95	-0.93	-0.93	-0.96	-0.90	-0.93
Al_2O_3	-0.50	-0.91	0.95	0.97	1.00	0.98	0.98	0.97	0.96	0.99
CaO	0.56	-0.57	0.34	0.34	0.28	0.25	0.28	0.36	0.22	0.26
Fe_2O_3	-0.48	-0.91	0.94	0.97	1.00	0.98	0.97	0.98	0.97	0.99
K_2O	-0.51	-0.92	0.96	0.97	1.00	0.97	0.97	0.96	0.95	0.97
MgO	-0.47	-0.92	0.96	0.98	1.00	0.97	0.97	0.97	0.95	0.98
MnO	-0.42	-0.81	0.84	0.93	0.91	0.84	0.88	0.86	0.85	0.89
Na_2O	-0.43	-0.92	0.94	0.91	0.94	0.94	0.95	0.91	0.86	0.89
P_2O_5	-0.41	-0.90	0.92	0.98	0.98	0.97	0.96	0.98	0.94	0.96
TiO_2	-0.46	-0.86	0.89	0.92	0.94	0.91	0.98	0.90	0.88	0.91

Heavy metal concentrations in the Harle Inlet exhibit distinct spatial variability, with elevated levels strongly associated with fine-grained sediments, particularly in harbor areas and tidal channels, where As concentrations exceed the ERL threshold. Enrichment factor (EF) analysis identified As as the most enriched element, followed by moderate Cu enrichment, while other metals largely remain within lithogenic background levels, indicating a combination of natural and anthropogenic inputs, including maritime traffic and agricultural runoff. Pearson correlation analysis further confirms that heavy metals predominantly accumulate in fine-grained sediments, underscoring the critical role of sediment texture and hydrodynamic processes in controlling their distribution.

Table 4.6: Pearson Correlation matrix between key sediment characteristics and heavy metal concentrations. Non-significant correlations displayed by grayed-out values.

	Gravel [%]	Sand [%]	Mud [%]	TOC [%]	Al [%]	As (ppm)	Cr (ppm)	Cu (ppm)	Pb (ppm)	Zn (ppm)
Gravel	1.00									
Sand	0.25	1.00								
Mud	-0.51	-0.96	1.00							
TOC	-0.46	-0.89	0.92	1.00						
Al [%]	-0.50	-0.91	0.95	0.97	1.00					
As (ppm)	-0.47	-0.90	0.93	0.93	0.98	1.00				
Cr (ppm)	-0.44	-0.88	0.91	0.94	0.98	0.96	1.00			
Cu (ppm)	-0.36	-0.90	0.90	0.94	0.97	0.98	0.95	1.00		
Pb (ppm)	-0.45	-0.84	0.87	0.91	0.96	0.97	0.94	0.97	1.00	
Zn (ppm)	-0.46	-0.87	0.91	0.94	0.99	0.98	0.96	0.98	0.99	1.00

The variability in the isotopic composition of heavy metals could provide valuable insights into their sources, transport pathways, and sinks (Araujo et al., 2019). Further isotopic studies are necessary to quantify the relative contributions of natural and anthropogenic inputs to heavy metal enrichment in the Harle inlet, particularly for As. Its accumulation may result from the weathering and erosion of a peat layer near the tip of the groyne, where scouring enhances As mobilization, or from anthropogenic sources such as maritime traffic and agricultural runoff. However, overall, the Harle inlet does not act as a substantial sink for heavy metals due to their relatively low accumulation in the sediments.

4.4.7 Heavy metal geochemistry of vegetated coasts

Comparative measurements of sediments from a salt marsh in Neßmersiel (Fig. 4.2C), located south of the East Frisian Island of Norderney, indicate that heavy metal concentrations are generally higher in the salt marsh than in the sediments of the tidal inlet. The environmental conditions in the salt marsh differ substantially from those in the tidal inlet. Primarily characterized by the deposition of fine-grained material, the salt marsh is further influenced by resuspension and bioturbation (Bartholdy, 2011). The WNH salt marsh is exposed to relatively hydrodynamically calmer conditions, indicative of a low-energy depositional environment.

Analysis of the mean grain-size distribution of surface samples, determined by laser diffraction, reveals a spatial gradient along the passively restored sites (App. Tab. 14). Finer sediments are concentrated near the dike toe (NMS23-02, 17.99 µm on average), whereas coarser sediments are found at the seaward edge of the salt marsh (NMS23-10, 34.92 µm on average). This pattern is consistent with hydrodynamic sorting mechanisms, where vegetation attenuates current velocity during flooding, thereby reducing the transport capacity for particles at an early stage. Consequently, coarser sediments are deposited at the marsh's seaward edge, while finer particles are transported further inland and deposited in the higher, landward areas (Müller-Navarra et al., 2019). Sediment samples from the actively restored salt marsh, particularly from the rewetted area, exhibit a finer-grained texture, with the lowest mean grain size recorded at site NMS23-08 (14.71 µm). In contrast, the sample from the adjacent tidal-flat area (NMS23-12) exhibits a mean grain size of 19.39 µm, similar to values observed in the Harlesiel harbor basin. Despite the generally finer grain sizes and higher silt and clay content in the salt marsh (App. Tab. 14), the physical and chemical processes governing sediment dynamics in these environments are distinct.

Salt marshes are characterized by high sedimentation rates, which vary according to marsh elevation. Lower elevations, such as the pioneer zone, experience frequent tidal inundation, leading to increased inorganic sediment deposition, while higher zones are primarily affected by storm surges (Christiansen et al., 2000; French and Spencer, 1993; Leonardi et al., 2018). Lead-based age dating by Schimansky, 2023 (unsupported ^{210}Pb) in the WNH salt marsh shows decreasing ^{210}Pb activity with elevation height, indicating sedimentation rates of approximately 0.47 ±0.04 cm yr^{-1} near the toe of the dike and up to 1.33 ±0.17 cm yr^{-1} at more exposed sites. Actively restored areas experience between 100 and 150 inundations per year, with sedimentation rates ranging from 0.55 ±0.14 cm yr^{-1} to 1.20 ±0.6 cm yr^{-1}. However, restoration-related soil disturbances introduce uncertainties in age determination. At site NMS23-12, located at the seaward edge of the marsh, tidal mixing leads to stratigraphic inversion, making ^{210}Pb dating unreliable.

With the exception of Cu, heavy metal concentrations in the salt marsh exceed the Effects Range-Low (ERL) threshold (Tab. 4.7). All metals, except Cr, exhibit enrichment within the salt marsh. The enrichment factor (EF) for Cr (1.08) suggests no significant anthropogenic input. In contrast, Pb and Zn concentrations are markedly elevated in the salt marsh relative to the tidal inlet. Moderate EF values for these metals indicate a notable anthropogenic contribution to their accumulation. One sampling site deviates from this general trend, displaying elevated As concentrations while other heavy metal concentrations remain below ERL levels. This anomaly is likely associated with a former drainage ditch that traversed the salt marsh prior to its renaturation in 2022 (App. Tab. 12).

Table 4.7: The mean concentrations of primary sediment compounds and heavy metals in the salt marsh, alongside their standard deviation (SD), corresponding Enrichment Factors (EF), and the Effects Range-Low (ERL) threshold values.

	salt marsh	**SD**	**ERL**	**EF**
SiO_2 [%]	57.20	6.38		
Al_2O_3 [%]	10.39	1.56		
Mud [%]	88.88	9.04		
TOC [%]	2.81	0.56		
As [ppm]	**24**	4.0	8.2	1.93
Cr [ppm]	**98**	15.0	81	1.08
Cu [ppm]	19	4.0	34	1.92
Pb [ppm]	**54**	16.0	47	3.09
Zn [ppm]	**144**	36.0	150	3.11
Hg [ppm]	**0.35**	0	0.15	1.93

In contrast, the tidal inlet is primarily influenced by tidal dynamics, which govern bidirectional sediment transport. During flood tides, sediments are transported into the tidal basin, where they precipitate in areas with reduced current velocity (Geßner et al., 2024). Fine-grained sediments, however, remain in suspension and are transported further into smaller channel branches and gullies. These areas exhibit slightly elevated heavy metal concentrations due to the finer grain sizes and the strong affinity of contaminants for adsorption onto fine particles and TOC (Siddique and Aktar, 2012). During ebb flow, sediments within the channels are resuspended and transported seaward. Deposition occurs primarily in the gullies, harbor areas, and the mixing shear zone south of Groyne H. The mixing shear zone, characterized by predominantly sandy sediments with limited mud content, does not function as a substantial accumulation area for heavy metals.

The slight enrichment of As and Cu in the tidal inlet is likely attributable to proximity to anthropogenic sources, which introduce localized contaminants, as well as to the natural source of As in the outcropping peat layer at the tip of Groyne H. In contrast, the salt marsh in Neßmersiel experiences higher contamination, primarily due to the high accretion rates of fine-grained sediments and elevated TOC levels, which facilitate the accumulation of heavy metals.

4.5 Conclusion

The Harle tidal inlet exhibits a complex interplay between sedimentary and hydrodynamic processes, significantly influenced by coastal protection measures, particularly the construction of Groyne H. Hydrodynamic measurements and grain size analyses reveal substantial heterogeneity in surface sediments, driven by altered current patterns induced by the groyne. These modifications have led to localized variations in sediment transport, erosion, deposition, and heavy metal distribution.

The construction of Groyne H has accelerated flow dynamics and scouring, particularly at its tip and along the north and south flanks. This process has exposed a peat layer rich in arsenic-bearing pyrite, leading to significant arsenic enrichment in the area, exceeding the ERL threshold. The elevated As concentrations result from both anthropogenic inputs, such as historical pesticide applications, and natural sources, including the mobilization of arsenic-rich pyrite from the exposed peat layer. Other heavy metals, such as Cu, show slight to moderate enrichment, whereas Cr, Zn, and Pb are not enriched, with their distribution closely linked to fine-grained sediment fractions and organic matter.

The absence of substantial mud content and low TOC values along the sandbar, which formed in the mixing shear zone, as well as within the inlet, prevents significant heavy metal accumulation, except for As near Groyne H. Increased current velocities from the bidirectional tidal flow in the Harle inhibit the deposition of fine-grained sediments and organic matter, reducing the potential for heavy metal retention. This contrasts with systems such as the Elbe River, where unidirectional flow and tidal pumping facilitate higher mud and TOC content, creating zones of heavy metal accumulation.

Salt marsh sediments in the region contain higher concentrations of heavy metals than those in the Harle inlet, underscoring the dependence of heavy metal accumulation on sediment texture, TOC content, and depositional environment. This suggests that salt marshes can act as a sink for contaminants, potentially removing heavy metals from the broader system. However, salt marshes are also subject to erosion and dynamic sediment redistribution, which limits their long-term effectiveness as a permanent sink.

Overall, the construction of Groyne H has induced pronounced hydrodynamic changes, leading to the erosion of As-rich peat, the mobilization of heavy metals, and the formation of a sandbar in the mixing shear zone. However, the dynamic tidal conditions of the Harle inhibit the formation of long-term heavy metal sinks due to limited mud and TOC deposition. While salt marshes may temporarily sequester heavy metals, their long-term role as a stable sink remains uncertain due to ongoing erosion and sediment reworking. Future studies, including isotopic analyses, are recommended to better differentiate between anthropogenic and natural As sources and to enhance the understanding of heavy metal dynamics in both salt marshes and tidal inlets.

Chapter 5

Synopsis and conclusion

5.1 General synopsis

Coastal protection measures are fundamental for maintaining coastal resilience and safeguarding areas of considerable cultural, ecological, and socio-environmental significance. As these coastal regions gain importance in the future, they are increasingly threatened by climate change, sea level rise, extreme weather events, and population growth. A diverse range of protection strategies, including soft solutions and hard protection measures, are necessary to mitigate these challenges. Hard protection measures, in particular, have long been implemented as an essential component of coastal defense but are assumed to have negative effects on the environment.

This thesis investigates the long-term effects of hard coastal protection structures on sedimentological and morphological processes to enhance the understanding of interactions between anthropogenic interventions and natural coastal dynamics. The research focuses on the Harle inlet, a tidally dominated system along the German North Sea coast. Characterized by continuously shifting current patterns. Since 1875, the inlet has been subject to hard protection measures, specifically groynes. Subsequent reconstruction efforts have resulted in a significantly reduced exchange zone between the North Sea and the tidal basin since 1940, thereby altering prevailing tidal currents and influencing sediment transport, deposition patterns, and erosion processes.

A core component of this study involved the development of a surface facies map of the Harle inlet to analyze sedimentological changes. To contextualize these findings, a comparative analysis was conducted with the Otzumer Balje inlet, an adjacent system almost unaffected by hard coastal protection measures. This approach enabled the isolation and quantification of anthropogenic impacts. Variations in flow conditions and transport properties were examined, leading to the identification of newly formed deposition and erosion zones and an assessment of heavy metal pollutant distribution.

Chapter 2 presents the methodology for facies mapping in the Harle inlet, interpreting the results in terms of sediment deposition and erosion patterns. A comparative analysis with the Otzumer Balje, based on literature data including Antia (1994), Flemming and Nyandwi (1994), Son et al. (2011), and Valle-Levinson et al. (2018) is also included. Chapter 3 extends this investigation by introducing a facies map of the Otzumer Balje, allowing for a direct comparative analysis that reinforces the inferred impacts of hard coastal protection measures. Chapter 4 shifts focus to sediment transport dynamics and the spatial distribution of heavy metal pollutants within the Harle inlet. Furthermore, this following chapter integrates the previously defined research objectives, as outlined in Chapter 1.3, with the obtained results, providing a thorough discussion and assessment of the findings.

5.2 Conclusion and specific objectives

The primary aim of this thesis is to investigate the complex interactions between hard coastal protection measures and the natural dynamics of a tidal inlet system, using the Harle inlet of Wangerooge Island as a case study. This research provides a comprehensive analysis of the long-term geomorphological, sedimentological, and environmental impacts of hard coastal protection structures within tidal inlets. The findings presented in this study directly address the objectives outlined in Chapter 1.3 and are discussed in detail in the following sections.

> The first objective was to develop a surface facies map of the Harle inlet to systematically characterize the sedimentological properties and spatial distribution of sedimentary facies in its back-barrier area.

The construction of the surface facies map integrated sedimentological characteristics, including grain size distribution and component composition. Through this approach, supported by statistical analysis, seven distinct facies were identified within the Harle inlet. By correlating these sedimentological facies with backscatter data from Mascioli et al. (2022), the facies distribution was extended into a comprehensive facies map, and the identified facies were classified into three distinct realms.

The fist realm, the Wadden realm, consists of facies F1 and F2, which are characterized by fine-grained, organic-rich sediments predominantly found within the intertidal shoal gullies. Second, the channel realm, comprising facies F3, F4, and F5, is composed of fine sand, primarily consisting of silicates and shell debris. These facies are distributed along the channel flanks and within smaller branch channel beds. Third, the main channel realm, is situated within the main channel beds. This realm includes facies F6 and F7, which consist of medium- to coarse-grained sands with shell debris.

The spatial arrangement and composition of these facies provide further insights into sediment transport dynamics and depositional patterns within the Harle. These findings contribute to a deeper understanding of how coastal protection measures influence sediment dynamics and morphological evolution within the tidal inlet system.

> The second objective was to identify deposition and erosion zones along the Harle inlet to analyze the spatial distribution and dynamics of sediment accumulation and loss in response to hydrodynamic modifications induced by the groyne.

Analysis of the spatial distribution of surface facies within the Harle reveals that facies F3, F4, and F5, which constitute the second depositional realm, are also present south of Groyne H, centrally located within the tidal inlet along a sandbar that separates the main channels of the Harle and Dove Harle. This sandbar forms within a mixing shear zone, where reduced current velocities promote sediment deposition. The velocity reduction is primarily induced by the presence of Groyne H. At the tip of the groyne, channel narrowing increases flow velocity, leading to localized shear stress. As the current passes this constricted section, velocities decrease along the mixing shear zone, facilitating sediment deposition.

A recirculation eddy, identified by Albinus et al. (2025, in prep.), forms within the groyne field along Wangerooge during the onset of the flood current. This eddy drives the circular redistribution of channel facies within the groyne field, further influencing sediment transport and deposition patterns.

The semidiurnal tidal cycle, which causes the periodic submergence and emergence of the groyne, contributes to morphological changes within the Harle. Erosion along the groyne flanks is likely driven by vertical circulation cells generated at high tide. Additionally, significant erosion is observed at the tip of the groyne, where increased flow velocities exert higher shear stress, intensifying sediment removal.

Facies F7 is particularly notable for the presence of bryozoans, which are predominantly found on the convex side of bivalve shells, indicating stable positioning. The encrustation of bryozoans suggests a low sedimentation rate in this area, while their orientation implies minimal substrate movement. Facies F7 is located along the main channel of the Dove Harle, where bryozoan-colonized shell beds indicate restricted sedimentation and relatively stable hydrodynamic conditions.

> The third objective was to compare the Harle inlet with a natural, unaltered inlet to identify sedimentological differences attributable to the influence of coastal protection measures.

To assess the impacts of long-standing hard coastal protection measures along the Harle inlet, a comparison with a minimally affected inlet is necessary. The Otzumer Balje inlet, located between the islands of Langeoog and Spiekeroog, provides a suitable reference inlet, as it is only influenced by groynes along its northern coastline, leaving the inlet itself largely unaffected. Additionally, the short distance between the Otzumer Balje and the Harle inlet ensures similar geographical and oceanographic conditions, making it an appropriate natural analogue.

Significant differences in sediment bedforms are observed between the Harle and the more natural system of the Otzumer Balje. In the Otzumer Balje, bedforms are predominantly composed of ripples and megaripples, with occasional subaquatic dunes. A subaquatic dune field, reaching heights of up to 3.5 m and extending 1,280 m in length, has developed in the widest section of the channel, indicating high current velocities (0.6 – 1.5 ms^{-1}). In contrast, the Harle lacks such dunes, instead featuring ripples, megaripples, and sand waves. Water depths in the Otzumer Balje range from 19 m to 25 m, whereas in the Harle, depths are generally less than 10 m, with some localized areas of greater depth and steep slopes. Notably, the Otzumer Balje lacks the F7 sediments with bryozoan colonies that are characteristic of the Harle.

Data on sediment transport near Groyne H remains limited. However, an ebb stream recirculation eddy is likely influencing sediment dynamics in this area. To facilitate a direct and robust comparison between these systems, the development of a comprehensive facies map is essential. Such a map would provide a detailed representation of sediment distribution and surface sedimentary processes across the Otzumer Balje, offering a clearer assessment of the impacts of coastal protection measures on the Harle inlet.

> The fourth objective was to develop such a comparative facies map of the Otzumer Balje inlet, providing a reference for a natural inlet. This map would facilitate a direct comparison with the Harle inlet, enabling the identification of sedimentary differences attributable to coastal protection measures.

In Chapter 3, a comprehensive facies map of the Otzumer Balje inlet is developed using the same methodological approach as in Chapter 2 for the Harle inlet. Sedimentological characteristics were classified through statistical analysis into distinct facies, which were then integrated with hydroacoustic backscatter data to construct a facies map with clearly defined spatial distributions. This approach enhances the comparative potential between the Harle and the Otzumer Balje inlets.

Overall, eight different facies were identified in the Otzumer Balje, with two facies differing from those found within the Harle inlet. Facies F0, composed of clay, represents the characteristic sediment composition of mudflats. Its presence, restricted to March samples and a single location along the western flank of the main channel, suggests that it is not a typical component of the inlet system but rather an allochthonous deposit associated with clay-rich mudflats, transported into the channel by storm activity. During the summer, the sediment composition at the same station shifts, with facies F4 becoming dominant.

Facies F8 occurs in the Otzumer Balje, where a subaqueous dune field has developed. In contrast, facies F7, which is present in the Harle, is absent from the Otzumer Balje. Instead, the Otzumer Balje contains coarse shell sediment, particularly in areas of direct exchange between the North Sea and the backbarrier basin. The relatively small amount of bryozoan colonies in the Otzumer Balje suggests active sediment transport and ongoing reworking processes within the inlet.

The comparative facies map of the Otzumer Balje reveals both general facies differences and variations in facies distribution patterns. The Harle inlet exhibits a circular facies alignment near the groyne fields of Groyne H, Groyne U and Groyne V, shaped by a circular eddy induced by the groynes. In contrast, the Otzumer Balje features elongated facies distributions along its channels and flanks. Additionally, the Otzumer Balje generally has greater water depths throughout its channel system, whereas the Harle inlet is predominantly shallow but contains the deepest depression among the Frisian Island inlets, reaching 34 m within a scour at the tip of Groyne H. This deep depression results from continuous erosion driven by increased flow velocity, which is caused by channel constriction due to Groyne H.

Furthermore, the formation of the secondary channel, the Dove Harle, can be attributed to the scouring effects of past coastal protection measures, which facilitated its connection to a preexisting gully (Lüders, 1952). Key geomorphological distinctions between the two inlets include the presence of the separating sandbar of the Harle and Dove Harle in the inlet, as well as the occurrence of subaqueous dunes in the Otzumer Balje. The absence of dunes in the Harle is attributed to its generally shallow water depths, which inhibit subaqueous dune formation. The development of the sandbar within the Harle inlet, which separates its main channels, is also direct consequence of the construction of Groyne H.

> The fifth objective was to examine sediment transport dynamics within the Harle inlet, with a focus on distinguishing anthropogenically influenced processes from natural transport mechanisms.

The comparative facies maps of the Harle and Otzumer Balje inlets reveal distinct differences in sediment deposition and erosion patterns within the Harle inlet. These differences are primarily attributed to the hydrodynamic alterations induced by the construction of Groyne H, which significantly affects sediment transport processes. Along the Harle inlet, tidal currents intensify at the tip of the groyne, leading to pronounced seafloor scouring. As sediment is transported landward with the flood current, it encounters the narrow passage, where coarser-grained sediments precipitate within the mixing shear zone due to reduced transport energy, forming the sandbar south of Groyne H.

Sediment deposition patterns are governed by grain size and hydrodynamic conditions. Coarser sediment grains settle along the mixing shear layer as flow energy decreases, while finer sediments are transported into the upper parts of the sandbar and the groyne field by eddy circulation and are subsequently deposited. After Ladage and Stephan (2006) flows the predominant ebb tide primarily through the secondary channel, the Dove Harle, near Wangerooge, effectively preventing sedimentation within this channel. Consequently, the main Harle channel experiences a reduction in its drainage area, thereby altering the overall tidal dynamics of the inlet.

The strong ebb currents within the Dove Harle inhibit fine sediment deposition, facilitating the accumulation of shell fragments in a stable configuration where encrusting bryozoans colonize the substrate. The presence of encrusting bryozoans further indicates low sedimentation rates in this area, while the orientation of overgrown disarticulated shells suggests a stable substrate with minimal grain movement. In contrast, the Otzumer Balje features an actively migrating subaqueous dune field, indicating continuous sediment transport and redistribution. This dynamic process ensures the persistent mobility of the dunes, preventing their complete migration out of the inlet system. Structures like a separating sandbar in the center of the inlet or circular aligned facies are not observed in the Otzumer Balje. Indicating no recirculation eddy or current alterations in the backbarrier area.

> The sixth objective was to investigate seasonal variations in sediment composition and distribution across the Harle and Otzumer Balje inlets.

In Chapter 3, seasonal fluctuations in sediment characteristics are examined based on sediment samples collected after the storm season in March and following the fair-weather season in September. Seasonal variability within the study area is influenced by multiple factors, including benthic organism growth, predation, mortality, temperature fluctuations, wind conditions, and hydrodynamic forces. These factors collectively impact the grain size distribution of bioclastic material and the transport properties of sediments.

Overall, the data indicate a general decrease in fine sediment fractions (< 200 µm) and an increase in coarser fractions (> 200 µm) from winter to summer. Additionally, the abundance of bioclastic material increases during the summer months. This seasonal shift is driven by benthic organism growth, as well as predation and mortality, which generate larger shell fragments. Extended transport durations also contribute to mechanical shell fragmentation, producing coarse-grained bioclastic particles during fair weather conditions.

Both inlets exhibit seasonal variations in surface sediments, influenced by biological and physical processes. Benthic activity is particularly pronounced in both systems, but the tubeworm *Lanice conchilega* is more abundant in the Harle inlet, especially during summer. Additionally, encrusting bryozoans are more prevalent in the Harle, particularly in areas of low sedimentation rates within the Dove Harle. The reduced bottom flow velocities in shallower regions, likely influenced by *L. conchilega* patches, promote the establishment of benthic communities while limiting sediment redistribution. Overall, the sediment composition of the Harle inlet is characterized by a more diverse assemblage of bioclastic material compared to the Otzumer Balje.

> The seventh objective was to analyze the concentration and spatial distribution of heavy metals within the Harle inlet, assessing potential heavy metal contamination linked to altered sedimentary processes.

The Harle tidal inlet exhibits a complex interplay between sedimentary and hydrodynamic processes, heavily influenced by anthropogenic modifications, particularly the construction of Groyne H. Hydrodynamic measurements and grain size analyses reveal significant spatial heterogeneity in surface sediments, driven by groyne-induced changes in current patterns. These modifications have led to localized variations in sediment transport, erosion, deposition, and heavy metal enrichment.

The construction of Groyne H has resulted in accelerated flow velocities and enhanced scouring, particularly at the tip and along the northern and southern flanks. This process has exposed a peat layer at the tip of the groyne, which is likely rich in arsenic-bearing pyrite. Core samples from the mainland, north of Wilhelmshaven, confirm the presence of pyrite-rich peat layers with elevated As concentrations (Dellwig et al., 2002). Arsenic concentrations in this region are significantly elevated, exceeding the Effects Range-Low (ERL) threshold. This enrichment is likely a result of both natural and anthropogenic factors, including historical pesticide applications and the mobilization of arsenic-rich pyrite from the exposed peat deposits.

Other heavy metals, such as copper (Cu), exhibit slight to moderate enrichment, whereas chromium (Cr), zinc (Zn), and lead (Pb) show no significant enrichment. The distribution of these metals is closely associated with fine-grained sediment fractions and organic matter content. However, the absence of substantial mud deposits and the low total organic carbon (TOC) values within the sandbar and inlet system inhibit significant heavy metal accumulation, with the exception of arsenic near Groyne H.

> The eighth objective was to identify the sinks and sources of heavy metals to assess the potential of sedimentary deposits to function as sinks, thereby contributing to ecosystem services. Additionally, it aimed to identify potential sources of heavy metal contamination within the inlet.

As discussed, the primary contamination source within the inlet is likely the outcropping peat layer, exposed by groyne-induced intensified currents, leading to the mobilization of arsenic-rich pyrite. Additionally, the bidirectional tidal flow within the Harle Inlet generates strong currents that inhibit the deposition of fine-grained sediments and organic material, thereby limiting the formation of stable heavy metal sinks. In contrast, ecosystems such as salt marshes provide a calmer depositional environment with a higher proportion of fine sediments, resulting in greater heavy metal enrichment. However, processes such as remobilization, erosion, and sediment reworking can temporarily sequester heavy metals, creating uncertainty regarding their long-term stability as sinks.

These findings underscore the critical role of sediment texture, TOC content, and depositional conditions in controlling contaminant distribution. Salt marshes, due to their finer sediments and organic-rich environment, emerge as more effective heavy metal sinks compared to the dynamic inlet system, where heavy metal retention is limited.

5.3 Outlook

The construction of hard coastal protection measures along the island of Wangerooge has altered the natural hydrodynamic and sedimentary conditions of the Harle inlet. The interactions between anthropogenic structures and the natural environment in such a dynamic, tidally dominated system provide critical insights into the impacts of hard coastal protection measures. This understanding is essential for adapting future reconstruction and modification strategies that ensure both effective coastal defense and ecological sustainability.

The influence of Groyne H has introduced both positive and negative effects. On one hand, localized scouring and changes in hydrodynamics have led to erosion, outcropping peat layers and potentially mobilizing contaminants. On the other hand, the structure has facilitated the development of ecological niches, increasing biodiversity interior the inlet. The Dove Harle channel, for instance, has become a stable environment for bryozoan colonization, with encrusting species attaching to disarticulated shells, suggesting a dynamic equilibrium between erosion and deposition.

Additionally, Groyne H has contributed to the formation of depositional zones, particularly within the mixing shear zone, where a sandbar has developed, effectively separating the Harle and Dove Harle channels. The groyne field extending from the western part of Wangerooge has similarly promoted sediment deposition, creating flow-reduced areas that support the establishment of *Lanice conchilega* patches. These biogenic structures, in turn, reduce bottom flow velocities, enhancing habitat suitability for benthic communities (Heuers et al., 1998; Rabaut et al., 2007; Van Hoay, 2006). Sedimentological analyses indicate a higher diversity of benthic organisms in the Harle inlet compared to the naturally evolving Otzumer Balje inlet. Further studies on benthic community structures and long-term biodiversity trends would be valuable for confirming these observations.

Future modifications to Groyne H should be approached with caution, ensuring that any alterations preserve the current hydrodynamic balance while mitigating potential adverse effects. Presently, the Harle inlet appears to have reached a state of relative equilibrium, with no substantial sediment displacement or excessive deepening of depositional zones. However, continuous monitoring is essential to assess whether the system remains stable or if hydrodynamic shifts will lead to a further dominance of ebb currents through the Dove Harle, potentially altering sediment transport dynamics and channel morphology, especially in the Harle channel.

Concerns about arsenic contamination, probably due to the presence of arsenic-bearing pyrite, have been raised by the exposure of a peat layer at the top of Groyne H. Isotopic analyses are necessary to determine whether the peat layer itself is enriched in arsenic or if anthropogenic sources, such as agricultural runoff or maritime activities, contribute to the contamination. Identifying the primary source of pollutants would enable targeted mitigation strategies to reduce further contamination and restore arsenic concentrations to levels below the ERL threshold.

Further investigations should assess the influence of dredging activities along the Harle on sediment transport and potential contaminant dispersion. The fate of dredged material is largely determined by its deposition site. If placed in areas subject to tidal or wave-driven resuspension, fine-grained sediments enriched in heavy metals could be reintroduced into the Harle, increasing contamination in low-energy depositional environments such as harbors, salt marshes, and tidal flats. Alternatively, littoral drift could transport these sediments eastward, affecting adjacent coastal and marine ecosystems. A comprehensive analysis of hydrodynamic conditions, sediment transport pathways, and geochemical interactions is essential for predicting contaminant mobility and informing sustainable dredging and disposal strategies.

Future coastal protection strategies should prioritize adaptive and ecologically integrated approaches. Instead of relying solely on rigid structures, hybrid coastal protection solutions should be explored, combining traditional hard-engineering measures such as groynes with nature-based alternatives that enhance sediment retention and ecological resilience. For instance, incorporating permeable groynes or dynamically adjustable barriers could balance coastal stability with sediment deposition while simultaneously supporting marine biodiversity.

Given the impacts of climate change and rising sea levels, the North Sea islands are becoming increasingly vulnerable. Effective coastal protection is essential for their preservation. According to projections from the IPCC, sea levels are expected to rise by 2100, ranging from 32 cm to 62 cm under lower-emission scenarios to 63 cm to 101 cm under high-emission scenarios (IPCC, 2023). This will significantly alter the natural dynamics of tidal inlets such as the Harle, placing substantial strain on existing coastal defense measures, which will require adaptation. The anticipated increase in extreme weather events, including storm surges, is likely to accelerate coastal erosion and disrupt sediment transport processes in unpredictable ways. Consequently, future protection strategies must not only account for current hydrodynamic conditions but also integrate flexible adaptation mechanisms to accommodate various climate scenarios. A combination of engineering interventions and nature-based solutions, such as targeted sediment replenishment and the promotion of biogenic structures, could enhance long-term resilience to climate change.

Research on Groyne H provides valuable insights into the interaction between anthropogenic structures and natural coastal processes, contributing to the development of sustainable coastal protection concepts in a changing environment. These findings are not only relevant for the studied site but also hold broader applicability for other coastal regions facing similar challenges. By analyzing hydrodynamic responses and sediment transport mechanisms, the outcome can inform groyne design and coastal management strategies in diverse geographical settings, from estuarine environments to open coastlines with varying wave and tidal regimes.

Numerical modeling and experimental studies should be employed to optimize the hydrodynamic performance of Groyne H and comparable structures. Simulations of flow dynamics and in-situ hydraulic experiments can refine groyne designs to achieve more favorable flow conditions while minimizing unintended erosion and sediment displacement. These methodologies can be adapted and applied to different coastal contexts, ensuring that regional variations in wave energy, sediment supply, and tidal influence are adequately considered. Additionally, periodic sediment budget monitoring is necessary to ensure that modifications to coastal structures do not induce sediment deficits in adjacent areas, which could accelerate coastal erosion elsewhere. This aspect is particularly relevant for regions experiencing significant anthropogenic pressures, where unintended sediment imbalances can have far-reaching consequences for both infrastructure and natural habitats.

Implementing an adaptive management framework that integrates flexible design modifications based on real-time monitoring would enable responsive adjustments to coastal protection measures in the face of evolving environmental conditions. Such an approach is critical not only for the long-term resilience of the studied site but also for broader coastal zones facing climate-induced challenges, including rising sea levels, increased storm surge activity, and shifting hydrodynamic patterns. By integrating ecological considerations with advanced engineering techniques, future coastal protection efforts can enhance both shoreline stability and ecosystem sustainability across a wide range of tidally influenced environments. The transferability of these principles underscores the significance of Groyne H research as a model for sustainable coastal engineering in diverse coastal landscapes worldwide.

References

Abrahim, G.M.S., Parker, R.J. (2007): Assessment of heavy metal enrichment factors and the degree of contamination in marine sediments from Tamaki Estuary, Auckland, New Zealand. Environ Monit Assess 136, 227–238.

Adam, P. (2019): Salt marsh restoration. In Coastal Wetlands, eds G. M. E. Perillo, E. Wolanski, D. R. Cahoon and C. S. Hopkinson (Amsterdam: Elsevier), 817–861. DOI: 10.1016/B978-0-444-63893-9.00023-X

Albinus, M. (2021): Circulation in the vicinity of a submerged stream groyne under mesotidal impact (East Frisian Islands, Southern North Sea). [bachelor´s thesis]. [Oldenburg (Nds)]: Carl-von-Ossietzky-Universität Oldenburg.

Albinus, M., Wollschläger, J., Giebel, H.-A., Geßner, A.-L., Herbst, M., Visscher, J., Zielinski, O., Badewien, T. H. (2025): Mesotidal currents reveal a distinct circulation pattern at a submerged stream groyne (Southern North Sea). (in prep).

Allen, J. R. L. (1968): The nature and origin of bed-form hierarchies. Sedimentology 10, 161–182.
DOI: 10.1111/j.1365-3091.1968.tb01110.x.

Allen, J. R. L. (1984): Experiments on the settling, overturning and entrainment of bivalve shells and related models. Sedimentology 31, 227–250.
DOI: 10.1111/j.1365-3091.1984.tb01961.x.

Almasoud, F.I., Usman, A.R., Al-Farraj, A.S. (2015): Heavy metals in the soils of the Arabian Gulf coast affected by industrial activities: analysis and assessment using enrichment factor and multivariate analysis. Arab J Geosci 8, 1691–1703.
DOI: 10.1007/s12517-014-1298-x

Almeida, A. C. S., Souza, F. B. C., Sanner, J., and Vieira, L. M. (2015): Taxonomy of recent Adeonidae (Bryozoa, Cheilostomata) from Brazil, with the description of four new species. Zootaxa 4013, 348.
DOI: 10.11646/zootaxa.4013.3.2.

Almeida, A. C. S., Souza, F. B. C., and Vieira, L. M. (2018a): Malacostegine bryozoans (Bryozoa: Cheilostomata) from Bahia State, northeast Brazil: taxonomy and non-indigenous species. Mar Biodiv 48, 1463–1488.
DOI: 10.1007/s12526-017-0639-x.

Almeida, A., Souza, F., Farias, J., Alves, O., and Vieira, L. (2018b): Bryozoa on disarticulated bivalve shells from Todos os Santos Bay, northeastern Brazil, with the description of two new species. Zootaxa 4434, 401.
DOI: 10.11646/zootaxa.4434.3.1.

Alp, M., Pichon, C.L. (2021): Getting from Sea to Nurseries: Considering Tidal Dynamics of Juvenile Habitat Distribution and Connectivity in a Highly Modified Estuarine Riverscape. Ecosystems 24, 583–601.
DOI: 10.1007/s10021-020-00536-1

Amara I, Miled W, Slama RB, Ladhari N. (2018): Antifouling processes and toxicity effects of antifouling paints on marine environment. A review. Environ Toxicol Pharmacol, 57, 115–30.
DOI: 10.1016/j.etap.2017.12.001

Amini, Z.Z., Adabi, M.H., Burrett, C.F., Quilty, P.G. (2004): Bryozoan distribution and growth form associations as a tool in environmental interpretation, Tasmania, Australia. Sedimentary Geology 167, 1–15.
DOI: 10.1016/j.sedgeo.2004.01.010

Andersen, T.J., Lund-Hansen, L.C., Pejrup, M., Jensen, K.T., Mouritsen, K.N. (2005): Biologically induced differences in erodibility and aggregation of subtidal and intertidal sediments: a possible cause for seasonal changes in sediment deposition. Journal of Marine Systems 55, 123–138.
DOI: 10.1016/j.jmarsys.2004.09.004

Antia, E.E. (1994): The ebb-tidal delta model of shoreface ridge origin and evolution: Appraisal and applicability along the southern North Sea barrier island coast - a discussion. Geo-Marine Letters 14, 59–63.
DOI: 10.1007/BF01204472

Araújo, D.F., Ponzevera, E., Briant, N., Knoery, J., Sireau, T., Mojtahid, M., Metzger, E., Brach-Papa, C. (2019): Assessment of the metal contamination evolution in the Loire estuary using Cu and Zn stable isotopes and geochemical data in sediments. Marine Pollution Bulletin 143, 12–23.
DOI: 10.1016/j.marpolbul.2019.04.034

Arias, M., Pérez-Novo, C., Osorio, F., López, E., Soto, B. (2005): Adsorption and desorption of copper and zinc in the surface layer of acid soils. Journal of Colloid and Interface Science 288, 21–29.
DOI: 10.1016/j.jcis.2005.02.053

Armaly, B. F., Durst, F., Pereira, J. C. F., Schönung, B. (1983): Experimental and theoretical investigation of backward-facing step flow. J. Fluid Mech. 127, 473. DOI: 10.1017/S0022112083002839

Ashley, G.M. (1990): Classification of Large-Scale Subaqueous Bedforms: A New Look at an Old Problem-SEPM Bedforms and Bedding Structures. SEPM JSR Vol. 60, 160-172. DOI: 10.1306/212F9138-2B24-11D7-8648000102C1865D

Avramidis, P., Nikolaou, K., Bekiari, V. (2015): Total Organic Carbon and Total Nitrogen in Sediments and Soils: A Comparison of the Wet Oxidation – Titration Method with the Combustion-infrared Method. Agriculture and Agricultural Science Procedia 4, 425–430.
DOI: 10.1016/j.aaspro.2015.03.048

Badewien, T. H., Zimmer, E., Bartholomä, A., Reuter, R. (2009): Towards continuous long-term measurements of suspended particulate matter (SPM) in turbid coastal waters. Ocean Dynamics 59, 227–238.
DOI: 10.1007/s10236-009-0183-8

Bartholdy, J. 2011. Salt Marsh Sedimentation. In: Davis Jr., R., Dalrymple, R. (Eds): Principles of Tidal Sedimentology. Springer, Dordrecht, pp. 151-86.
DOI: 10.1007/978-94-007-0123-6_8

Bartholomä, A., Ernstsen, V. B., Flemming, B. W., Bartholdy, J. (2004): Bedform dynamics and net sediment transport paths over a flood-ebb tidal cycle in the Grådyb channel (Denmark), determined by high-resolution multi-beam echosounding. Geografisk Tidsskrift-Danish Journal of Geography 104, 45–55.
DOI: 10.1080/00167223.2004.10649503

Bartholomä, A., Kubicki, A., Badewien, T. H., Flemming, B. W. (2009): Suspended sediment transport in the German Wadden Sea—seasonal variations and extreme events. Ocean Dynamics 59, 213–225.
DOI: 10.1007/s10236-009-0193-6

Beck, M., Böning, P., Schückel, U., Stiehl, T., Schnetger, B., Rullkötter, J., Brumsack, H.-J. (2013): Consistent assessment of trace metal contamination in surface sediments and suspended particulate matter: A case study from the Jade Bay in NW Germany. Marine Pollution Bulletin 70, 100–111.
DOI: 10.1016/j.marpolbul.2013.02.017

Becking, L.E., Renema, W., Santodomingo, N.K., Hoeksema, B.W., Tuti, Y., De Voogd, N.J. (2011): Recently discovered landlocked basins in Indonesia reveal high habitat diversity in anchialine systems. Hydrobiologia 677, 89–105.
DOI: 10.1007/s10750-011-0742-0

Behre, K.E., Menke, B. (1969): Pollenanalytische Untersuchungen an einem Bohrkern der südlichen Doggerbank. Beiträge zur Meereskunde 24/25, p.122- 129.

Behre, K.-E. (2004): Coastal development, sea-level change and settlement history during the later Holocene in the Clay District of Lower Saxony (Niedersachsen), northern Germany. Quaternary International 112, 37–53.
DOI: 10.1016/S1040-6182(03)00064-8

Belleney, D., Ehrhold, A., Le Dantec, N., Le Roy, P., Jouet, G. (2022): Multi-temporal analysis of submarine sand dunes morphodynamics (Bay of Brest, Brittany, France): A marker of sediment pathways in a macrotidal environment open to sea swells. Estuarine, Coastal and Shelf Science 274, 107911.
DOI: 10.1016/j.ecss.2022.107911

Beukema, J. (1987): Influence of the predatory polychaete Nephtys hombergii on the abundance of other polychaetes. Marine Ecology-progress Series - MAR ECOL-PROGR SER 40, 95–101.
DOI: 10.3354/meps040095

Biria, H. A., Neshaei, M. A. L., Ghabraei, A., Mehrdad, M. A. (2015): Investigation of sediment transport pattern and beach morphology in the vicinity of submerged groyne (case study: Dahane Sar Sefidrood). Front. Struct. Civ. Eng. 9, 82–90.
DOI: 10.1007/s11709-014-0275-5

Blott, S.J., Croft, D.J., Pye K., Saye, S.E., Wilson, H.E. (2004): Particle size analysis by laser diffraction. Geological Society London, Special Publications, 232, 1, 63-73. DOI: 10.1144/GSL.SP.2004.232.01.08

Boothroyd, J.C. (1985): Tidal Inlets and Tidal Deltas. In Coastal Sedimentary Environments. eds. Davies, R.A. (New York, NY: Springer New York), 445–525.
DOI: 10.1007/978-1-4612-5078-4

Bouwer, L.M. (2019): Observed and Projected Impacts from Extreme Weather Events: Implications for Loss and Damage. In: Mechler, R., Bouwer, L., Schinko, T., Surminski, S., Linnerooth-Bayer, J. (Eds): Loss and Damage from Climate Change. Climate Risk Management, Policy and Governance. Springer, Cham, p. 63-82.
DOI: 10.1007/978-3-319-72026-5_3

Bradl, H.B. (2005): Sources and origins of heavy metals. In: Interface Science and Technology. Elsevier, pp. 1–27.
DOI: 10.1016/S1573-4285(05)80020-1

Brett, C. E., Parsons-Hubbard, K. M., Walker, S. E., Ferguson, C., Powell, E. N., Staff, G., Ashton-Alcox, K.A., Raymond, A. (2011): Gradients and patterns of sclerobionts on experimentally deployed bivalve shells: Synopsis of bathymetric and temporal trends on a decadal time scale. Palaeogeography, Palaeoclimatology, Palaeoecology 312, 278–304.
DOI: 10.1016/j.palaeo.2011.05.019

Bungenstock, F., Hertweck, G., Hochstein, M.L., Wehrmann, A. (2021): Distribution pattern and controls of biosedimentary facies in backbarrier tidal flats of the central Wadden Sea (North Sea). zdgg 172, 409–428.
DOI: 10.1127/zdgg/2021/0248

Burchard, H. Badewien, T.H. (2015): Thermohaline residual circulation of the Wadden Sea. Ocean Dynamics 65, 1717–1730.
DOI: 10.1007/s10236-015-0895-x

Burchard, H., Flöser, G., Staneva, J. V., Badewien, T. H., Riethmüller, R. (2008): Impact of Density Gradients on Net Sediment Transport into the Wadden Sea. Journal of Physical Oceanography 38, 566–587.
DOI: 10.1175/2007JPO3796.1

Carling, P. A., Orr, I. G., Glaister, M. S. (1994): Significance of Dead Zone Flow Structure for Solute and Fine Particle Dynamics. In: Beven, K.J., Chatwin, P.C., Millbank, J.H.T. (Eds.): Mixing and Transport in the Environment. John Wiley & Sons Ltd, 139–157.

Castagno, K.A., Tomiczek, T., Shepard, C.C., Beck, M.W., Bowden, A.A., O´Donnel, K., Scyphers, S.B. (2021): Resistance, resilience, and recovery of salt marshes in the Florida Panhandle following Hurricane Michael. Sci Rep 11, 20381.
DOI: 10.1038/s41598-021-99779-8

Chang, T.S., Flemming, B.W., Tilch, E., Bartholomä, A., Wöstmann, R. (2006): Late Holocene stratigraphic evolution of a back-barrier tidal basin in the East Frisian Wadden Sea, southern North Sea: transgressive deposition and its preservation potential. Facies 52, 329–340.
DOI: 10.1007/s10347-006-0080-2

Christiansen, T., Wiberg, P. L., Milligan, T. G. (2000): Flow and sediment transport on a tidal salt marsh surface. Estuar. Coast. Shelf Sci. 50, 315–331.
DOI: 10.1006/ecss.2000.0548

Coghlan, I., Carley, J., Cox, R., Davey, E., Blacka, M., Lofthouse, J. (2013): Concept Designs for a Groyne Field on the Far North Nsw Coast. In: NSW Coastal Conference. pp. 1–18.

Coleman, F.C., Williams, S.L. (2002): Overexploiting marine ecosystem engineers: potential consequences for biodiversity. Trends in Ecology and Evolution. 17, 1, P40-44.
DOI: 10.1016/S0169-5347(01)02330-8

Costanza, R., Anderson, S.J., Sutton, P., Mulder, K., Mulder, O., Kubiszewski, I., Wang, X., Liu, X., Pérez-Maqueo, O., Luisa Martinez, M., Jarvis, D., Dee, G. (2021): The global value of coastal wetlands for storm protection. Global Environmental Change 70, 102328.
DOI: 10.1016/j.gloenvcha.2021.102328

Cuadrado, D.G., Gómez, E.A. (2011): Morphodynamic characteristics in a tidal inlet: San Blas, Argentina. Geomorphology 135, 203–211.
DOI: 10.1016/j.geomorph.2011.06.038

Currin, C. A., Davis, J., Malhotra, A. (2017): Response of Salt Marshes to Wave energy provides Guidance for Successful Living Shoreline Implementation. In Bilkovic D.M., Mitchell M.M., La Peyre M.K., Toft J.D. (Eds.): Living shorelines: The science and management of nature-based coastal protection. CRC Press, pp. 209–232.
DOI: 10.1201/9781315151465-14

De Blauwe, H. (2006): Bryozoa on shells from the Kwintebank, Southern bight of the North Sea (Belgium). Bulletin Van Het Koninklijk Belgisch Instituut Voor Natuurwetenschappen Biologie, 76, 125–138.

De Blauwe, H. (2020): Bryozoans on disarticulated shells from Pléneuf-Val-André, Brittany, France, Australasian Paleontological Memoirs, 52, 57–65.

De La Vega, C., Schückel, U., Horn, S., Kröncke, I., Asmus, R., Asmus, H. (2018): How to include ecological network analysis results in management? A case study of three tidal basins of the Wadden Sea, south-eastern North Sea. Ocean & Coastal Management 163, 401–416.
DOI: 10.1016/j.ocecoaman.2018.07.019

De Ruig, J.H.M. (1998): Seaward coastal defence: limitations and possibilities. J Coast Conserv 4, 71–78.
DOI: 10.1007/BF02806492

Decho, A., Decho A.W. (2000): Microbial biofilms in intertidal systems: an overview. Cont Shelf Res 20: 1257-1273. Continental Shelf Research 20, 1257–1273.
DOI: 10.1016/S0278-4343(00)00022-4

Deines, K.L. (1999): Backscatter estimation using broadband acoustic Doppler current profilers. Oceans99 MTS/ IEEE Conference Proceedings, 13 – 16 September. The Institute of Electrical and Electronics Engineers, Piscataway, NJ.
DOI: 10.1109/CCM.1999.755249

Dellwig, O., Bottcher, M.E., Lipinski, M. (2002): Trace metals in Holocene coastal peats and their relation to pyrite formation NW Germany.

Denisenko, N. V., Thomsen, E., Tendal, O. S. (2017): Bryozoan epifauna on brachiopods from the Faroe Islands (NE Atlantic). Frit, 96–113.
DOI: 10.18602/fsj.v60i0.9.

Desmond, J.S., Zedler, J.B., Williams, G.D. (2000): Fish use of tidal creek habitats in two southern California salt marshes. Ecological Engineering 14, 233–252.
DOI: 10.1016/S0925-8574(99)00005-1

Dolan, R., Davis, R.E. (1994): Coastal Storm Hazards. Journal of Coastal Research 103–114.

Doughty, S.D., Cleary, W.J., McGinnis, B.A. (2006): The Recent Evolution of Storm-Influenced Retrograding Barriers in Southeastern North Carolina, USA. Journal of Coastal Research. 39, 1, 122-126.

Du Laing G., De Grauwe P., Moors W., Vandecasteele B., Lesage E., Meers E., Tack F.M.G., Verloo M.G. (2007): Factors affecting metal concentrations in the upper sediment layer of intertidal reedbeds along the river Scheldt. J Environ Monitor, 9, 449–455. DOI: 10.1039/B618772B

Durán, O., Moore L.J. (2013): Vegetation controls on the maximum size of coastal dunes, Proc. Natl. Acad. Sci. U.S.A. 110 (43) 17217-17222. DOI: 10.1073/pnas.1307580110

Einstein H.A., Chien, N. (1953): Can the rate of wash load be predicted from the bed-load function? Eos Trans. AGU 34, 876–882. DOI: 10.1029/TR034i006p00876

Eisma, D., Mook, W. G., Laban, C. (1981): An early Holocene tidal flat in the southern Bight. In: Holocene marine sedimentation in the North Sea basin, Wiley, 229–237.

Eitner, V. (1996a): Geomorphological response of the East Frisian barrier islands to sea-level rise: an investigation of past and future evolution. Geomorphology 15, 57–65. DOI: 10.1016/0169-555X(95)00116-M

Eitner, V. (1996b): Morphological and Sedimentological Development of a Tidal Inlet and its Catchment Area (Otzumer Balje, Southern North Sea).

Erftemeijer, P.L.A., Lewis, R.R.R. (2006): Environmental impacts of dredging on seagrasses: A review. Marine Pollution Bulletin, 52, 1553-1572. DOI: 10.1016/j.marpolbul.2006.09.006

Ernstsen, V.B., Noormets, R., Winter, C., Hebbeln, D., Bartholomä, A., Flemming, B.W., Bartholdy, J. (2006): Quantification of dune dynamics during a tidal cycle in an inlet channel of the Danish Wadden Sea. Geo-Mar Lett 26, 151–163. DOI: 10.1007/s00367-006-0026-2

Escapa, M., Perillo, G.M.E., Iribarne, O. (2008): Sediment dynamics modulated by burrowing crab activities in contrasting SW Atlantic intertidal habitats. Estuarine, Coastal and Shelf Science 80, 365–373. DOI: 10.1016/j.ecss.2008.08.020

European Environment Agency (2020): Europe´s seas and coasts. p.11.

Fairley, I., Davidson, M., Kingston, K. (2009): The morpho-dynamics of a beach protected by detached breakwaters in a high energy tidal environment. Journal of Coastal Research, SI 56 (Proceedings of the 10th International Coastal Symposium), Lisbon, Portugal, 607 - 611. ISSN 0749-0258

Feagin, R.A., Smith, W.K., Psuty, N.P., Young, D.R., Martinez, M.L., Carter, G.A., Lucas, K.L., Gibeaut, J.C., Gemma, J.N., Koske, R.E. (2010): Barrier Islands: Coupling Anthropogenic Stability with Ecological Sustainability. Journal of Coastal Research, 26, 987-992. DOI: 10.2112/09-1185.1

Fedo, C.M., Babechuk, M.G. (2023): Petrogenesis of siliciclastic sediments and sedimentary rocks explored in three-dimensional Al2 O3 –CaO* +Na2 O–K2 O–FeO+MgO (A–CN–K–FM) compositional space. Can. J. Earth Sci. 60, 818–838. DOI: 10.1139/cjes-2022-0051

FitzGerald, D. M. (1988): Shoreline erosional-depositional processes associated with tidal inlets. In: (Eds) Aubrey, D.G., Weishar, L.: Lecture Notes on Coastal and Estuarine Studies. Washington, D. C.: American Geophysical Union, 186–225.
DOI: 10.1029/LN029p0186

Fitzgerald, D. M., Penland, S. (1987): Backbarrier dynamics of the East Frisian Islands. Journal of sedimentary petrology, 57, 746–754.

Flemming, B. W. (1978): Underwater sand dunes along the southeast African continental margin — Observations and implications. Marine Geology 26, 177–198.
DOI: 10.1016/0025-3227(78)90059-2

FitzGerald, D. M., Kraus, N. C., Hands, E. B. (2000): Natural Mechanisms of Sediment Bypassing at Tidal Inlets.

Fitzgerald, D. M., Penland, S., Nummedal, D. (1984): Control of barrier island shape by inlet sediment bypassing: East Frisian Islands, West Germany. Marine Geology 60, 355–376.
DOI: 10.1016/0025-3227(84)90157-9

Flemming, B.W. (2000): The role of grain size, water depth and flow velocity as scaling factors.

Flemming, B.W., Davies Jr., R.A. (1994): Holocene Evolution, Morphodynamics and Sedimentology of the Spiekeroog Barrier Island System (Southern North Sea). Senckenbergiana maritima, 24, 117–155.

Flemming, B.W., Nyandwi, N. (1994): Land reclamation as a cause of fine-grained sediment depletion in backbarrier tidal flats (Southern North Sea). Netherlands Journal of Aquatic Ecology 28, 299–307.
DOI: 10.1007/BF02334198

Flockers, H. W. (1722): Kaart van het Dollardgebied met de verdronken dorpen bij de vloed van 1277.

Forstner, U., Wittmann, G. (1983): Metal pollution in the aquatic environment, Springer Verlag Berlin Heidelberg, New York, Tokyo, 486 p.

French JR., Spencer, T. (1993): Dynamics of sedimentation in a tide-dominated backbarrier salt marsh, Norfolk, UK. Marine Geology, 110, 3-4, 315-331.
DOI: 10.1016/0025-3227(93)90091-9

Fritz, H. M., Blount, C., Sokoloski, R., Singleton, J., Fuggle, A., McAdoo, B. G., Moore, A., Grass, C., Tate, B. (2007): Hurricane Katrina storm surge distribution and field observations on the Mississippi Barrier Islands. Estuarine, Coastal and Shelf Science 74, 12–20.
DOI: 10.1016/j.ecss.2007.03.015

Garelick, H., Jones, H., Dybowska, A., Valsami-Jones, E. (2009): Arsenic Pollution Sources, in: Reviews of Environmental Contamination Volume 197, Reviews of Environmental Contamination and Toxicology. Springer New York, New York, NY, pp. 17–60. DOI: 10.1007/978-0-387-79284-2_2

Geßner, A.-L., Wollschläger, J., Giebel, H.-A., Badewien, T.H. (2024): Impact of a submerged stream groyne on morphology and sedimentology on a tidal inlet, Harle (Southern North Sea, Germany). Front. Earth Sci. 12, 1292462.
DOI: 10.3389/feart.2024.1292462

Geßner, A.-L., Albinus, M., Giebel, H.A., Wollschläger, J., Mascioli, F., Badewien, T.H. (2025): Facies Mapping and Seasonal Sediment Shift of Tidal Inlets: Impact of Coastal Protection Measures. Sedimentary Environment. (in review)

Gonzales, R., Eberli, G.P. (1997): Sediment transport and bedforms in a carbonate tidal inlet; Lee Stocking Island, Exumas, Bahamas. Sedimentology, 44: 1015-1030. DOI: 10.1046/j.1365-3091.1997.d01-59.x

Gray, C.W., Mclaren, R.G., Roberts, A.H.C., Condron, L.M. (1999): Solubility, sorption and desorption of native and added cadmium in relation to properties of soils in New Zealand. European J Soil Science 50, 127–137. DOI: 10.1046/j.1365-2389.1999.00221.x

Gregor, C.D. (1972): Solubilization of lead in lake and reservoir sediments by NTA [nitrilotriacetic acid]. Environ. Sci. Technol. 6, 278–279. DOI: 10.1021/es60062a006

Hamilton, E.L. (1980): Geoacoustic modeling of the sea floor. The Journal of the Acoustical Society of America 68, 1313–1340. DOI: 10.1121/1.385100

Hanson, H., Brampton, A., Capobianco, M., Dette, HH., Hamm, L., Laustrup, C., Lechuga, A., Spanhoff, R. (2002): Beach nourishment projects, practices, and objectives - a European overview. Coastal Engineering, 47, 2, 81-111. DOI: 10.1016/S0378-3839(02)00122-9

Hanson, H., Bocamazo, L., Larson, M., Kraus, N. C. (2009): Long-term beach response to groin shortening, Westhampton Beach, Long Island, New York. Coastal Engineering 2008 pp. 1927-1939.

Hayes, M.O. (1979): Barrier island morphology as a function of tidal and wave regime. Academic Press, p. 28.

Hayes, M.O. (1980): General morphology and sediment patterns in tidal inlets. Sedimentary Geology 26, 139–156. DOI: 10.1016/0037-0738(80)90009-3

Henning, M., Hentschel, B. (2013): Sedimentation and flow patterns induced by regular and modified groynes on the River Elbe, Germany. Ecohydrol. 6, 598–610. DOI: 10.1002/eco.1398

Herdiansyah, H., Saiya, H.G., Afkarina, K.I.I., Indra, T.L. (2021): Coastal Community Perspective, Waste Density, and Spatial Area toward Sustainable Waste Management (Case Study: Ambon Bay, Indonesia). Sustainability 13, 10947. DOI: 10.3390/su131910947

Herrling, G., Winter, C. (2014): Morphological and sedimentological response of a mixed-energy barrier island tidal inlet to storm and fair-weather conditions. Earth Surf. Dynam. 2, 363–382. DOI: 10.5194/esurf-2-363-2014

Heuers, J., Jaklin, S., Ziihlke, R., Dittmann, S., Günther, C.-P., Hildenbrandt, H., Grimm, V., (1998): A model on the distribution and abundance of the tube-building polychaete Lanice conchilega (Pallas, 1766) in the intertidal of the Wadden Sea.

Higham, J. E., Brevis, W., Keylock, C. J., Safarzadeh, A. (2017): Using modal decompositions to explain the sudden expansion of the mixing layer in the wake of a groyne in a shallow flow. Advances in Water Resources 107, 451–459.
DOI: 10.1016/j.advwatres.2017.05.010

Hjulström, F. (1935): Studies of the morphological activity of rivers as illustrated by the river fyris, bulletin. Geol. Inst. Upsalsa, 25, 221–527.

Homeier, H. (1973): Die morphologische Entwicklung im Bereich der Harle und ihre Auswirkungen auf das Westende von Wangerooge. Forschungsstelle für Insel- und Küstenschutz.

Hudson, R., Kenworthy, J., Best, M. (Eds) (2021): Saltmarsh Restoration Handbook: UK and Ireland. Environment Agency, Bristol, UK. 112 p.

Hulme, P.E., Bacher, S., Kenis, M., Klotz, S., Kühn, I., Minchin, D., Nentwig, W., Olenin, S., Panov, V., Pergl, J., Pysek, P., Roques, A., Sol, D., Solarz, W., Vila, M. (2008): Grasping at the routes of biological invasions: a framework for integrating pathways into policy. Journal of Applied Ecology, 45, 2, 403-414.
DOI: 10.1111/j.1365-2664.2007.01442.x

Huthnance, J.M. (1991): Physical oceanography of the North Sea. Ocean and Shoeline Management, 16, 3-4, 119-231.
DOI: 10.1016/0951-8312(91)90005-M

Iberall, A., White, D. (1988): Evidence for a long term process scale for social change in modern man settled in place via agriculture and engaged in trade and war. GeoJournal 17.
DOI: 10.1007/BF00181044

Incze, L.S., Lutz, R.A., Watling, L. (1980): Relationships between effects of environmental temperature and seston on growth and mortality of Mytilus edulis in a temperate northern estuary. Mar. Biol. 57, 147–156.
DOI: 10.1007/BF00390733

IPCC (2023): Summary for Policymakers. In: Climate Change 2023: Synthesis Report. Contribution of Working Groups I, II and III to the Sixth Assessment Report of the Intergovernmental Panel on Climate Change. H. Lee and J. Romero (eds.). IPCC, Geneva, Switzerland, pp. 1-34.
DOI: 10.59327/IPCC/AR6-9789291691647.001

Jing, F., Chen, X., Yang, Z., Guo, B. (2018): Heavy metals status, transport mechanisms, sources, and factors affecting their mobility in Chinese agricultural soils. Environ Earth Sci 77, 104.
DOI: 10.1007/s12665-018-7299-4

Karle, M., Bungenstock, F., Wehrmann, A. (2021): Holocene coastal landscape development in response to rising sea level in the Central Wadden Sea coastal region. Netherlands Journal of Geosciences 100, e12.
DOI: 10.1017/njg.2021.10

Kelly, S.M., Horowitz, A.S. (1987): Growth-forms and paleoecology of Missisippian bryozoans: Critical application of Stach´s 1936 model, eastern United States. In: Ross, J.R.P. (Eds.): Bryozoa: Present and Past. Western Washington University, Bellingham, Washington, pp. 137–144.

Kempa, D., Karrasch, L., Schlurmann, T., Prominski, M., Lojek, O., Schulte-Güstenberg, E., Visscher, J., Zielinski, O., Goseberg, N. (2023): Design and Insights Gained in a Real-World Laboratory for the Implementation of New Coastal Protection Strategies. Sustainability, 15, 4623.
DOI: 10.3390/su15054623

Kendon, M., McCarthy, M., Jevrejeva, S., Matthews, A., Williams, J., Sparks, T., West, F. (2023): State of the UK Climate 2022. Intl Journal of Climatology 43, 1–83.
DOI: 10.1002/joc.8167

Khullar, N.K. (2007): Transport of fines/wash load through channels – A review. Hydrology Journal, 30 (3–4), 43–63.

Kolditz, K., Dellwig, O., Barkowski, J., Bahlo, R., Leipe, T., Freund, H., Brumsack, H. (2012): Geochemistry of Holocene salt marsh and tidal flat sediments on a barrier island in the southern North Sea (Langeoog, North-west Germany). Sedimentology 59, 337–355.
DOI: 10.1111/j.1365-3091.2011.01252.x

Kristensen, S. E., Drønen, N., Deigaard, R., Fredsoe, J. (2016): Impact of groyne fields on the littoral drift: A hybrid morphological modelling study. Coastal Engineering 111, 13–22.
DOI: 10.1016/j.coastaleng.2016.01.009

Kröncke, I., Zeiss, B., Rensing, C. (2001): Long-term variability in macrofauna species composition off the island of Norderney (East Frisia, Germany) in relation to changes in climatic and environmental conditions. Senckenbergiana maritima 31, 65–82.
DOI: 10.1007/BF03042837

Kuklinski, P., Barnes, D. (2005): Microhabitat diversity of Svalbard Bryozoa. Journal of Natural History 39, 539–554.
DOI: 10.1080/00222930400001350

Kuklinski, P., Gulliksen, B., Lønne, O. J., Weslawski, J. M. (2005): Composition of bryozoan assemblages related to depth in Svalbard fjords and sounds. Polar Biol 28, 619–630.
DOI: 10.1007/s00300-005-0726-5

Kunz, H. (1997): Groynes on the East Frisian Islands: History and Experiences. in Coastal Engineering 1996 (Orlando, Florida, United States: American Society of Civil Engineers), 2128–2141.
DOI: 10.1061/9780784402429.165

Ladage, F., Stephan, H.-J., Niemeyer, H.D. (2007): Einfluss einer Unterwasserbuhne auf das Seegat Harle. Berichte zur deutschen Landeskunde, 81, 2, 113.

Ladage, F., Stephan, H.-J., (2004): Morphologische Entwicklung im Seegat Harle und seinem Einzugsgebiet 69.

Ladage, F., Stephan, H.-J., Niemeyer, H.D. (2006): Interactions of Large-Scale Groyne and Tidal Inlet Migration, in: Coastal Dynamics 2005. Presented at the Fifth International Conference on Coastal Dynamics, American Society of Civil Engineers, Barcelona, Spain, pp. 1–14.
DOI 10.1061/40855(214)111

Lee, D.-I., Eom, K.-H., Kim, G.-Y., Baeck, G.-W. (2010): Scoping the effective marine environmental assessment of dredging and ocean disposal of coastal sediments in Korea. Marine Policy 34, 1082–1092.
DOI: 10.1016/j.marpol.2010.03.008

Leighton, L., Chojnacki, N., Stafford, E., Tyler, C., Schneider, C. (2016): Categorization of shell fragments provides a proxy for environmental energy and predation intensity. Journal of the Geological Society 173, jgs2015-086.
DOI: 10.1144/jgs2015-086

Leonardi, N., Carnacina, I., Donatelli, C., Ganju, N.K., Plater, A.J., Schuerch, M., Temmerman, S. (2018): Dynamic interactions between coastal storms and salt marshes: A review. Geomorphology 301, 92–107.
DOI: 10.1016/j.geomorph.2017.11.001

Lettmann, K. A., Wolff, J.-O., Badewien, T. H. (2009): Modeling the impact of wind and waves on suspended particulate matter fluxes in the East Frisian Wadden Sea (southern North Sea). Ocean Dynamics 59, 239–262.
DOI: 10.1007/s10236-009-0194-5

Li, Y., Zhou, H., Gao, B., Xu, D. (2021): Improved enrichment factor model for correcting and predicting the evaluation of heavy metals in sediments. Science of The Total Environment 755, 142437.
DOI: 10.1016/j.scitotenv.2020.142437

Linham, M.M., Nicholls, R.J. (2010): Technologies for climate change adaptation: Coastal erosion and flooding. UNEP Riso Centre on Energy, Climate and Sustainable Development, Denmark.

Liu, D., Wang, F., (2019): Typhoon/Hurricane/Tropical Cyclone Disasters: Prediction, Prevention and Mitigation. GEP 07, 26–36.
DOI: 10.4236/gep.2019.75003

Liu, X., Xing, F., Shi, B., Wu, G., Ge, J., Peg, B., Li, M., Wang, Y. (2023): Erosion and accretion patterns on intertidal mudflats of the Yangtze River Estuary in response to storm conditions. Anthropocene Coasts 6, 6.
DOI: 10.1007/s44218-023-00020-y

Lorenzoni, C., Postacchini, M., Brocchini, M., Mancinelli, A. (2016): Experimental study of the short-term efficiency of different breakwater configurations on beach protection. J. Ocean Eng. Mar. Energy 2, 195–210.
DOI: 10.1007/s40722-016-0051-9

Lotze, H.K. (2007): Rise and fall of fishing and marine resource use in the Wadden Sea, southern North Sea. Fisheries Research 87, 208–218.
DOI: 10.1016/j.fishres.2006.12.009

Lubarsky, H.V., Hubas, C., Chocholek, M., Larson, F., Manz, W., Paterson, D.M., Gerbersdorf, S.U. (2010): The Stabilisation Potential of Individual and Mixed Assemblages of Natural Bacteria and Microalgae. PLoS ONE 5, e13794.
DOI: 10.1371/journal.pone.0013794

Luck, G. (1978): Inseln vor der südlichen Nordseeküste. Die Küste, 32, 84-93.

Lüders, V.K. (1952): Die Wirkung der Buhne H in Wangerooge-West auf das Seegat „Harle' 6.

Mascioli, F., Piattelli, V., Cerrone, F., Cinosi, J., Kunde, T., Miccadei, E. (2022): Sediments and bedforms of the Harle tidal inlet (Wadden Sea, Germany). Journal of Maps 19, 2154175.
DOI: 10.1080/17445647.2022.2154175

Mascioli, F., Piattelli, V., Cerrone, F., Gasprino, D., Kunde, T., Miccadei, E. (2021): Feasibility of Objective Seabed Mapping Techniques in a Coastal Tidal Environment (Wadden Sea, Germany). Geosciences, 11, 49.
DOI: 10.3390/geosciences11020049

Masselink, G., Russell, P. (2013): Impacts of climate change on coastal erosion. MCCIP Science Review, p. 16.
DOI: 10.14465/2013.ARC09.071-086

Mather, A.A., Stretch, D.D. (2012): A Perspective on Sea Level Rise and Coastal Storm Surge from Southern and Eastern Africa: A Case Study Near Durban, South Africa. Water 4, 237–259.
DOI: 10.3390/w4010237

Mauelshagen, F. (2007): Flood Disasters and Political Cultura at the German North Sea Coast: A Long-term Historical Perspective. Historical Social Research / Historische Sozialforschung 32, 133–144.

McCave, I.N. (1984): Erosion, transport and deposition of fine-grained marine sediments. SP 15, 35–69.
DOI: 10.1144/GSL.SP.1984.015.01.03

McGregor, G.R., Ferro, C.A.T., Stephenson, D.B. (2005): Projected Changes in Extreme Weather and Climate Events in Europe. In: Kirch, W., Bertollini, R., Menne, B. (Eds): Extreme Weather Events and Public Health Responses. Springer, Berlin, Heidelberg.
DOI: 10.1007/3-540-28862-7_2

McKinney, F. K. (1996): Encrusting organisms on co-occurring disarticulated valves of two marine bivalves: comparison of living assemblages and skeletal residues. Paleobiology 22, 543–567.
DOI: 10.1017/S0094837300016523

Meier, D. (2012): Die Schäden der Sturmflut von 1825 an der Nordseeküste Schleswig-Holsteins 43.

Meier, V.D. (2011): Die Schäden der Weihnachtsflut von 1717 an der Nordseeküste Schleswig-Holsteins 34.

Mejer, J. (1652): Landtcarte Von dem Alten Nortfrieslande, in: C. Danckwerth: Newe Landesbeschreibung der zwey Herzogthümer Schleswig und Holstein, Husum.

Meurer, R. (2000): Wasserbau und Wasserwirtschaft in Deutschland. Vieweg+Teubner Verlag, Wiesbaden.
DOI: 10.1007/978-3-322-80213-2

Miall, A.D. (2022): Stratigraphy: The Modern Synthesis. In: Springer Textbooks in Earth Sciences, Geography and Environment. Springer, 528 p.
DOI: 10.1007/978-3-030-87536-7_7.

Montserrat, F., Van Colen, C., Degraer, S., Ysebaert, T., Herman, P. (2008): Benthic community-mediated sediment dynamics. Mar. Ecol. Prog. Ser. 372, 43–59.
DOI: 10.3354/meps07769

Morris, R.L., Konlechner, T.M., Ghisalberti, M., Swearer, S.E. (2018): From grey to green: Efficacy of eco-engineering solutions for nature-based coastal defence. Global Change Biology 24, 1827–1842.
DOI: 10.1111/gcb.14063

Morss, R.E., Wilhelmi, O.V., Meehl, G.A., Dilling, L. (2011): Improving Societal Outcomes of Extreme Weather in a Changing Climate: An Integrated Perspective. Annu. Rev. Environ. Resour. 36, 1–25.
DOI: 10.1146/annurev-environ-060809-100145

Mouritsen, K.N., Mouritsen, L.T., Jensen, K.T. (1998): Change of topography and sediment characteristics on an intertidal mud-flat following mass-mortality of the amphipod Corophium volutator. Journal of the Marine Biological Association of the United Kingdom 78 (4), 1167–1180.

Mühr, B., Eisenstein, L., Pinto, J.G., Knippertz, P., Mohr, S., Kunz, M. (2022): CEDIM Forensic Disaster Analysis Group (FDA): Winter storm series: Ylenia, Zeynep, Antonia (int: Dudley, Eunice, Franklin) - February 2022 (NW & Central Europe). Karlsruher Institut für Technologie (KIT).
DOI: 10.5445/IR/1000143470

Narayan, S., Beck, M.W., Reguero, B.G., Losada, I.J., Van Wesenbeeck, B., Pontee, N., Sanchirico, J.N., Ingram, J.C., Lange, G.-M., Burks-Copes, K.A. (2016): The Effectiveness, Costs and Coastal Protection Benefits of Natural and Nature-Based Defences. PLoS ONE 11, e0154735.
DOI: 10.1371/journal.pone.0154735

Nesbritt, H. W., Young, G.M. (1982): Early Proterozoic climates and plate motions inferred from major element chemistry of lutites. Nature, 299, 715-717.
DOI: 10.1038/299715a0

Nesbitt, H.W., Young, G.M. (1984): Prediction of some weathering trends of plutonic and volcanic rocks based on thermodynamic and kinetic considerations. Geochimica et Cosmochimica Acta 48, 1523–1534.
DOI: 10.1016/0016-7037(84)90408-3

Nesbitt, H.W., Young, G.M. (1989): Formation and Diagenesis of Weathering Profiles. The Journal of Geology 97, 129–147.
DOI: 10.1086/629290

Neumann, B., Vafeidis, AT., Zimmermann, J., Nicholls, RJ. (2015): Future Coastal Population Growth and Exposure to Sea-Level Rise and Coastal Flooding – A Global Assessment. POLS ONE, 10, 6.
DOI: 10.1371/journal.pone.0131375

Niedersächsisches Ministerium für Ernährung, Landwirtschaft und Verbraucherschutz, 2021. Die niedersächsische Landwirtschaft in Zahlen.

Nielsen, AF., Baun, A., Andresen, SI., Skjollding, LM. (2022): Critical review of the OSPAR risk-based approach for offshore-produced water discharges. Integrated Environmental Assessment and Management. 19, 5, 1172-1187.
DOI: 10.1002/ieam.4715

Niemeyer, H. D. (1995): Long-Term Morphodynamical Development of the East Frisian Islands and Coast. in Coastal Engineering 1994 (Kobe, Japan: American Society of Civil Engineers), 2417–2433.
DOI: 10.1061/9780784400890.176

Niemeyer, HD., Kaiser, R., Knaack, H., Dissanayake, P., Miani, M., Elsebach, J., Berkenbrink, C., Herrling, G., Ritzmann, A. (2011): Evaluation of Coastal Protection Strategies for Lowlands in Respect of Climate Change. In: Proc. 34th IAHR-Congress Brisbane/Australia, p.8.

Niemeyer, H.D. (1990): Morphodynamics of Tidal Inlets.
DOI: 10.13140/RG.2.1.4382.8723

Niemeyer, H.D. (1995): Long-Term Morphodynamical Development of the East Frisian Islands and Coast, in: Coastal Engineering 1994. Presented at the 24t International Conference on Coastal Engineering, American Society of Civil Engineers, Kobe, Japan, pp. 2417–2433.
DOI: 10.1061/9780784400890.176

Niemeyer, H.D., Eiben, H., Rohde, H. (1996): History and Heritage of German Coastal Engineering, in: History and Heritage of Coastal Engineering. Presented at the 25th International Coastal Engineering Conference, American Society of Civil Engineers, Orlando, Florida, pp. 169–213.
DOI: 10.1061/9780784401965.005

Niemeyer, H.D., Kaiser, R. (1994): Ökosystemforschung Wattenmeer: Teilvorhaben Niedersächsisches Wattenmeer, Vorphase; Teilprojekt Hydrodynamik im Ökosystem Wattenmeer; Forschungsbericht 108 02 085/02, Texte. Umweltbundesamt, Berlin.

Niesel, V. (1999): Hydrographic Conditions in the Spiekeroog Backbarrier System. In: Dittmann, S. (Eds.) The Wadden Sea Ecosystem: Stability Properties and Mechanisms. Heidelberg, 1999, p. 26 - 30.

Nijenhuis, W.A.S. (2000): Deposition of Heavy Metals to the Convention Waters of the Oslo and Paris Commissions.

Noormets, R., Ernstsen, V.B., Bartholomä, A., Flemming, B.W., Hebbeln, D. (2006): Implications of bedform dimensions for the prediction of local scour in tidal inlets: a case study from the southern North Sea. Geo-Mar Lett 26, 165–176.
DOI: 10.1007/s00367-006-0029-z

Nummedal, D., Penland, S. (1981): Sediment Dispersal in Norderneyer Seegat, West Germany. In: Nio, SD., Shüttenhelm, RTE., Van Weering, CE (Eds.): Holocene Marine Sedimentation in the North Sea Basin. Blackwell Publishing Ltd.: Oxford, Uk, pp. 187-210.
DOI: 10.1002/9781444303759.ch14

Olariu, C., Steel, R.J., Dalrymple, R.W., Gingras, M.K. (2012): Tidal dunes versus tidal bars: The sedimentological and architectural characteristics of compound dunes in a tidal seaway, the lower Baronia Sandstone (Lower Eocene), Ager Basin, Spain. Sedimentary Geology 279, 134–155.
DOI: 10.1016/j.sedgeo.2012.07.018

Oost, A.P., Hoekstra, P., Wiersma, A., Flemming, B., Lammerts, E.J., Pejrup, M., Hofstede, J., van der Valk, B., Kiden, P., Bartholdy, J., van der Berg, M.W., Vos, P.C., de Vries, S., Wang, Z.B. (2012): Barrier island management: Lessons from the past and directions for the future. Ocean & Coastal Management, 68, 18-38.
DOI: 10.1016/j.ocecoaman.2012.07.010

OSPAR (2008): OSPAR Publication 2008-379 CEMP Assessment Manual: Co-ordinated Environmental Monitoring Programme Assessment Manual for contaminants in sediment and biota.

Pachana, K., Wattanakornsiri, A., Nanuam, J. (2010): Heavy Metal Transport and Fate in the Environmental Compartments. NU Science Journal, 7, 1, 1-11.

Papili, S., Wever, T., Dupont, Y., Van Lancker, V. (2014): Storm influence on the burial of objects in a shallow sandy shelf environment. Marine Geology 349, 61–72.
DOI: 10.1016/j.margeo.2014.01.004

Penland, S., Boyd, R., Suter, J. R. (1988): Transgressive Depositional Systems of the Mississippi Delta Plain: A Model for Barrier Shoreline and Shelf Sand Development.

Perissi, I., Bardi, U., Asmar, TE., Lavacchi, A. (2017): Dynamic patterns of overexploration in fisheries. Ecological Modelling, 359, 285-292.
DOI: 10.1016/j.ecolmodel.2017.06.009

Phillips, E., Hodgson, D.M., Emery, A.R. (2017): The Quaternary Geology of the North Sea Basin. Journal of Quaternary Science, 32 (2). pp. 117-339.
DOI: 10.1002/jqs.2932

Pintilie, S., Branza, L., Betianu, C., Pavel, L.V., Ungureanu, F., Gavrilescu, M. (2007): Modeling and simulation of heavy metals transport in water and sediments. Environ. Eng. Manag. J. 6, 153–161.
DOI: 10.30638/eemj.2007.021

Potter, C. (2014): Global assessment of damage to coastal ecosystem vegetation from tropical storms. Remote Sensing Letters 5, 315–322.
DOI: 10.1080/2150704X.2014.902546

Pranzini, E., Rossi, L., Lami, G., Jackson, N., Nordstrom, K. F. (2018): Reshaping beach morphology by modifying offshore breakwaters. Ocean and Coastal Management, 154, 168-177.
DOI: 10.1016/j.ocecoaman.2018.01.013

Pranzini, E. (2018): Coastal erosion and shore protection: A brief historical analysis. J Coast Conserv 22, 827–830.
DOI: 10.1007/s11852-017-0521-9

Probert, P.K. (1984): Disturbance, sediment stability, and trophic structure of soft-bottom communities. J Mar Res 42, 893–921.
DOI: 10.1357/002224084788520837

Rabaut, M., Guilini, K., Van Hoey, G., Vincx, M., Degraer, S. (2007): A bio-engineered soft-bottom environment: The impact of Lanice conchilega on the benthic species-specific densities and community structure. Estuarine, Coastal and Shelf Science 75, 525–536.
DOI: 10.1016/j.ecss.2007.05.041

Rangel-Buitrago, N., Anfuso, G. (2011): An application of Dolan and Davis (1992) classification to coastal storms in SW Spanish littoral. Journal of Coastal Research, 1891–1895.
ISBN: 0749-0208

Reading, H.G. (1996): Sedimentary environments: processes, facies and stratigraphy, third edition. Blackwell Science, Oxford, 615 p.

Reineck, H.-E., Singh, I.B. (1980): Depositional Sedimentary Environments. Springer Berlin Heidelberg, Berlin, Heidelberg.
DOI: 10.1007/978-3-642-81498-3

Reise, K. (2005): Coast of change: habitat loss and transformations in the Wadden Sea. Helgol Mar Res 59, 9–21.
DOI: 10.1007/s10152-004-0202-6

Reiss, H., Kröncke, I. (2001): Spatial and temporal distribution of macrofauna in the Otzumer Balje (East Frisian Wadden Sea, Germany). Senckenbergiana maritima 31, 283–298.
DOI: 10.1007/BF03043037

Reuter, R., Badewien, T. H., Bartholomä, A., Braun, A., Lübben, A., Rullkötter, J. (2009): A hydrographic time series station in the Wadden Sea (southern North Sea). Ocean Dynamics 59, 195–211.
DOI: 10.1007/s10236-009-0196-3

Robinson, J.E., Newell, R.C., Seiderer, L.J., Simpson, N.M. (2005): Impacts of aggregate dredging on sediment composition and associated benthic fauna at an offshore dredge site in the southern North Sea. Marine Environmental Research 60, 51–68.
DOI: 10.1016/j.marenvres.2004.09.001

Sanchirico, J.N., Albers, H.J., Fischer, C., Coleman, C. (2010): Spatial Management of Invasive Species: Pathways and Policy Options. Environ Resource Econ 45, 517–535.
DOI: 10.1007/s10640-009-9326-0

Sanz-Prada, L., Garcia-Ordiales, E., Flor-Blanco, G., Roqueñí, N., Álvarez, R. (2022): Determination of heavy metal baseline levels and threshold values on marine sediments in the Bay of Biscay. Journal of Environmental Management 303, 114250.
DOI: 10.1016/j.jenvman.2021.114250

Schimansky, J.E.P. (2023): Radiometrische Untersuchungen von Umweltproben einer Salzwiese. Unpublished Bachelor thesis, Institute of Radioecology and Radiation Protection, Gottfried Wilhelm Leibniz Universität Hannover, 61 p.

Schoonees, T., Gijón Mancheño, A., Scheres, B., Bouma, T.J., Silva, R., Schlurmann, T., Schüttrumpf, H. (2019): Hard Structures for Coastal Protection, Towards Greener Designs. Estuaries and Coasts 42, 1709–1729.
DOI: 10.1007/s12237-019-00551-z

Schramkowski, G.P., Schuttelaars, H.M., de Swart, H.E. (2002): The effect of geometry and bottom friction on local bed forms in a tidal embayment. Continental Shelf Research 22, 1821–1833.
DOI: 10.1016/S02784343(02)00040-7

Sello, G., Woebken, C., Schütte, H., Krüger, W. (1966): Geschichte des Jadebusens. Hrsg. Vermessungs- und Katasterverwaltung Oldenburg.

Sha, L.P. (1989): Variation in ebb-delta morphologies along the West and East Frisian Islands, The Netherlands and Germany. Marine Geology, 89, 11-28.
DOI: 10.1016/0025-3227(89)90025-X

Sherene, T. (2010): Mobility and transport of heavy metals in polluted soil environment. Biological Forum, 2, 2, 112-121.
ISSN: 0975-1130

Siddique, M.A.M., Aktar, M. (2012): Heavy metals in salt marsh sediments of Porteresia bed along the Karnafully river coast, Chittagong. Soil Water Res. 7, 117–123. DOI: 10.17221/7/2012-SWR

Sigren, J., Figlus, J., Armitage, A. (2014): Coastal sand dunes and dune vegetation: Restoration, erosion, and storm protection. Shore & Beach, 82(4), 5-12.

Small, C., Nicholls, R.J. (2003): A Global Analysis of Human Settlement in Coastal Zones. Journal of Coastal Research 19, 584–599.

Smedley, PL., Kinniburgh, DG. (2002): A review of the source, behavior and distribution of arsenic in natural waters. Applied Geochemistry, 17, 5, 517-568. DOI: 10.1016/S0883-2927(02)00018-5

Smith, A. M. (1995): Palaeoenvironmental interpretation using bryozoans: a review. SP 83, 231–243. DOI: 10.1144/GSL.SP.1995.083.01.11

Soens, T. (2011): Threatened by the Sea, Condemned by Man? Flood Risk and Environmental Inequalities along the North Sea Coast, 1200–1800. In: Massard-Guilbaud, G., Rodger, R. (Eds.): Environmental and Social Justice in the City: Historical Perspectives. The White Horse Press, pp. 91–112. DOI: 10.3197/9781912186334.ch04

Son, C.S., Flemming, B.W., Bartholomä, A. (2011): Evidence for sediment recirculation on an ebb-tidal delta of the East Frisian barrier-island system, southern North Sea. Geo-Mar Lett 31, 87–100. DOI: 10.1007/s00367-010-0217-8

Sonone, SS., Jadhav, S., Sankhla, MS., Kumar, R. (2021): Water Contamination by Heavy Metals and their Toxic Effect on Aquaculture and Human Health through Food Chain. Letters in Applied NanoBioScience, 10, 2, 2148-2166. DOI: 10.33263/LIANBS102.21482166

Soon, T.K., Zheng, H. (2019): Climate Change and Bivalve Mass Mortality in Temperate Regions. In: de Voogt, P. (Eds): Reviews of Environmental Contamination and Toxicology Volume 251. Reviews of Environmental Contamination and Toxicology, vol 251. Springer, Cham, pp. 109-129. DOI: 10.1007/398_2019_31

Spears, B.M., Saunders, J.E., Davidson, I., Paterson, D.M. (2008): Microalgal sediment biostabilisation along a salinity gradient in the Eden Estuary, Scotland: unravelling a paradox. Mar. Freshwater Res. 59, 313. DOI: 10.1071/MF07164

Spencer, K.L., Cundy, A.B., Croudace, I.W. (2003): Heavy metal distribution and early-diagenesis in salt marsh sediments from the Medway Estuary, Kent, UK. Estuarine, Coastal and Shelf Science 57, 43–54. DOI: 10.1016/S0272-7714(02)00324-4

Stanev, E., Wolff, J.O., Burchard, H., Bolding, K., Flöser, G. (2003): On the circulation in the East Frisian Wadden Sea: numerical modeling and data analysis. Ocean Dynamics 53, 27–51. DOI: 10.1007/s10236-002-0022-7

Stanev, E.V., Brink-Spalink, G., Wolff, J.-O. (2007): Sediment dynamics in tidally dominated environments controlled by transport and turbulence: A case study for the East Frisian Wadden Sea. J. Geophys. Res. 112, C04018.
DOI: 10.1029/2005JC003045

Statistisches Bundesamt (2024): Seeverkehrsstatistik Dezember 2023.

Streif, H. (1990): Das ostfriesische Küstengebiet, 2nd edn, Borntraeger, Berlin Stuttgart. Sammlung Geologischer Führer, 157, pp 1-37.

Streif, H. (1989): Barrier islands, tidal flats, and coastal marshes resulting from a relative rise of sea level in East Frisia on the German North Sea coast. In: Van Der Linden, W. J. M., Cloetingh, S. A. P. L., Kaasschieter, J. P. K., Van De Graaff, W. J. E., Vandenberghe, J., and Van Der Gun, J. A. M. (Eds.): Coastal Lowlands: Geology and Geotechnology, Dordrecht: Springer Netherlands, 213–225.
DOI: 10.1007/978-94-017-1064-0

Streif, H. (2004): Sedimentary record of Pleistocene and Holocene marine inundations along the North Sea coast of Lower Saxony, Germany. Quaternary International 112, 3–28.
DOI: 10.1016/S1040-6182(03)00062-4

Stronkhorst, J., Ariese, F., Van Hattum, B., Postma, J.F., De Kluijver, M., Den Besten, P.J., Bergman, M.J.N., Daan, R., Murk, A.J., Vethaak, A.D. (2003): Environmental impact and recovery at two dumping sites for dredged material in the North Sea. Environmental Pollution 124, 17–31.
DOI: 10.1016/S0269-7491(02)00430-X

Stumpf, R.P. (1983): The process of sedimentation on the surface of salt marsh. Estuarine, coastal and Shelf Science, 17, 5, 495-508.
DOI: 10.1016/0272-7714(83)90002-1

Sukhodolov, A., Engelhardt, C., Krüger, A., Bungartz, H. (2004): Case Study: Turbulent Flow and Sediment Distributions in a Groyne Field. J. Hydraul. Eng. 130, 1–9.
DOI: 10.1061/(ASCE)0733-9429(2004)130:1(1)

Sun, F., Carson, R.T. (2020): Coastal wetlands reduce property damage during tropical cyclones. Proc. Natl. Acad. Sci. U.S.A. 117, 5719–5725.
DOI: 10.1073/pnas.1915169117

Sutherland, R. (2000): Bed sediment-associated trace metals in an urban stream, Oahu, Hawaii. Environmental Geology 39, 611–627.
DOI: 10.1007/s002540050473

Svenson, C., Ernstsen, V.B., Winter, C., Bartholomä, A., Hebbeln, D. (2009): Tide-driven Sediment Variations on a Large Compound Dune in the Jade Tidal Inlet Channel, Southeastern North Sea. Journal of Coastal Research.

Talstra, H., Uijtteewall, W.S.J., Stelling, G.S. (2005): In Research on river dynamics from geological to operational time scales. In: Weerts, H. J. T., Ritsema, I. L., and van Os, A. G. (Eds.): Netherlands Centre for River Studies. 52 – 53.

Taylor-Burns, R., Lowrie, C., Tehranirad, B., Lowe, J., Erikson, L., Barnard, P.L., Reguero, B.G., Beck, M.W. (2024): The value of marsh restoration for flood risk reduction in an urban estuary. Scientific Resports, 14, 6856.
DOI: 10.1038/s41598-024-57474-4

Toso, C., Madricardo, F., Molinaroli, E., Fogarin, S., Kruss, A., Petrizzo, A., Pizzeghello, N.M., Sinapi, L., Trincardi, F. (2019): Tidal inlet seafloor changes induced by recently built hard structures. PLoS ONE 14, e0223240.
DOI: 10.1371/journal.pone.0223240

Turbelin, A.J., Diagne, C., Hudgins, E.J., Moodley, D., Kourantidou, M., Novoa, A., Haubrock, P.J., Bernery, C., Gozlan, R.E., Francis, R.A., Courchamp, F. (2022): Introduction pathways of economically costly invasive alien species. Biol Invasions 24, 2061–2079.
DOI: 10.1007/s10530-022-02796-5

Uddin, M.K. (2017): A review on the adsorption of heavy metals by clay minerals, with special focus on the past decade. Chemical Engineering Journal 308, 438–462.
DOI: 10.1016/j.cej.2016.09.029

Valle-Levinson, A., Stanev, E., Badewien, T.H. (2018): Tidal and subtidal exchange flows at an inlet of the Wadden Sea. Estuarine, Coastal and Shelf Science 202, 270–279.
DOI: 10.1016/j.ecss.2018.01.013

Valsamidis, A., Reeve, D.E. (2020): A new approach to analytical modelling of groyne fields. Continental Shelf Reseach, 211, 104288.
DOI: 10.1016/j.csr.2020.104288

Van Hoey, G., Guilini, K., Rabaut, M., Vincx, M., Degraer, S. (2008): Ecological implications of the presence of the tube-building polychaete Lanice conchilega on soft-bottom benthic ecosystems. Mar Biol 154, 1009–1019.
DOI: 10.1007/s00227-008-0992-1

van Slobbe, E., de Vriend, H. J., Aarninkhof, S., Lulofs, K., de Vries, M., and Dircke, P. (2013): Building with Nature: in search of resilient storm surge protection strategies. Nat Hazards.

Vikas, M., Dwarakish, G.S. (2015): Coastal Pollution: A Review. Aquatic Procedia 4, 381-388.
DOI: 10.1016/j.aqpro.2015.02.051

Vousdoukas, M.I., Mentaschi, L., Voukouvalas, E., Bianchi, A., Dottori, F., Feyen, L. (2018): Climatic and socioeconomic controls of future coastal flood risk in Europe. Nature Clim Change 8, 776–780.
DOI: 10.1038/s41558-018-0260-4

Vuik, V., Borsje, B.W., Willemsen, P.W.J.M., Jonkman, S.N. (2019): Salt marshed for flood risk reduction: Quantifying long-term effectiveness and life-cycle costs. Ocean & Coastal Management. 171, 96-110.
DOI: 10.1016/j.ocecoaman.2019.01.010

Walker, C.H., Sibly, R.M., Sibly, R.M., Peakall, D.B. (2006) Principles of Ecotoxicology. CRC Press, Taylor and Francis Group, Boca Raton, London, New York, p. 275.

Walker, D. J. (1991): Sediment Transport Near Groynes in the Nearshore Zone. Journal of Coastal Research 7.

Wang, Y., Yu, Q., Gao, S., Flemming, B. (2014): Modeling the effect of progressive grain-size sorting on the scale dependence of back-barrier tidal basin morphology. Continental Shelf Research 91, 26–36.
DOI: 10.1016/j.csr.2014.09.006

Wang, Z. B., Hoekstra, P., Burchard, H., Ridderinkhof, H., De Swart, H. E., Stive, M. J. F. (2012): Morphodynamics of the Wadden Sea and its barrier island system. Ocean & Coastal Management 68, 39–57.
DOI: 10.1016/j.ocecoaman.2011.12.022

Wang, Z. B., Louters, T., de Vriend, H. J. (1995): Morphodynamic modelling for a tidal inlet in the Wadden Sea. Marine Geology 126, 289–300.
DOI: 10.1016/0025-3227(95)00083-B

Wang, Z.B., Hoekstra, P., Burchard, H., Ridderinkhof, H., De Swart, H.E., Stive, M.J.F. (2012): Morphodynamics of the Wadden Sea and its barrier island system. Ocean & Coastal Management 68, 39–57.
DOI: 10.1016/j.ocecoaman.2011.12.022

Ward, M. A., Thorpe, J. P. (1989): Assessment of space utilisation in a subtidal temperate bryozoan community. Mar. Biol. 103, 215–224.
DOI: 10.1007/BF00543350

Wasserstraßen- und Schiffahrtsverwaltung des Bundes (WSV). (2021). DGM-W 2012 Außenweser / Jade. https://www.kuestendaten.de [Accessed November 30, 2021].

Wheatcroft, R.A., Goñi, M.A., Richardson, K.N., Borgeld, J.C. (2013): Natural and human impacts on centennial sediment accumulation patterns on the Umpqua River margin, Oregon. Marine Geology 339, 44–56.
DOI: 10.1016/j.margeo.2013.04.015

Wheeler, P., Peterson, J., Gordon-Brown, L. (2010): Long-term bathymetric effects of groyne array emplacement at Lakes Entrance, Victoria, Australia. Applied Geography, 30, 126-140.
DOI: 10.1016/j.apgeog.2009.07.001

Witte, V. H.-H. (1970). Die Schutzarbeiten auf den Ostfriesischen Inseln.

Woo, H.S., Julien, P.Y., Richardson, E.V. (1986): Washload and Fine Sediment Load. J. Hydraul. Eng. 112, 541–545.
DOI: 10.1061/(ASCE)0733-9429(1986)112:6(541)

Wu, T., Qin, J. (2020): Influence of Flow and Sediment Transport Processes on Sedimentation in Groyne Fields. Journal of Coastal Research 95, 304.
DOI: 10.2112/SI95-059.1

Xuemei, Z., Hawkins, S.J. (2002): Interactions of aquaculture and waste disposal in the coastal zone. J Ocean Univ. China 1, 8–12.
DOI: 10.1007/s11802-002-0023-7

Yalin, M.S. (1976): Origin of submarine dunes. Coastal Engineering, 2127-2135.
DOI: 10.1061/9780842620834.124

Yang, L., Peterson, P.J., Williams, W.P., Hou, S., Tan, J. (2002): The Relationship Between Exposure to Arsenic Concentrations in Drinking Water and the Development of Skin Lesions in Farmers from Inner Mongolia, China.

Zhang, X., Yang, L., Li, Y., Li, H., Wang, W., Ye, B. (2012): Impacts of lead/zinc mining and smelting on the environment and human health in China. Environ Monit Assess 184, 2261–2273.
DOI: 10.1007/s10661-011-2115-6

Zhou, Z., Ge, J., Van Maren, D. S., Wang, Z. B., Kuai, Y., Ding, P. (2021): Study of Sediment Transport in a Tidal Channel-Shoal System: Lateral Effects and Slack-Water Dynamics. JGR Oceans 126, e2020JC016334.
DOI: 10.1029/2020JC016334.

Zielinski, O., Pieck, D., Schulz, J., Thölen, C., Wollschläger, J., Albinus, M., Badewien, T.H., Braun, A., Engelen, B., Feenders, C., Fock, S., Lehners, C., Löhmus, K., Lübben, A., Massmann, G., Meyerjügens, J., Nicolai, H., Pollmann, T., Schwalfenberg, K., Stone, J., Waska, H., Winkler, H. (2022): The Spiekeroog Coastal Observatory: A Scientific Infrastructure at the Land-Sea Transition Zone (Southern North Sea). Front. Mar. Sci. 8, 754905.
DOI: 10.3389/fmars.2021.754905.

Żukowska J., Biziuk, M. (2008): Methological Evaluation of Method for Dietary Heavy Metal Intake. Journal of Food Science, 73, 2, R21-R29.
DOI: 10.1111/j.1750-3841.2007.00648.x

Zuschin, M., Stachowitsch, M., Stanton, R.J. (2003): Patterns and processes of shell fragmentation in modern and ancient marine environments. Earth-Science Reviews 63, 33–82.
DOI: 10.1016/S0012-8252(03)00014-X

Authors declaration

I hereby declare that I have written this thesis on my own, indepantly and have not used any sources or aids other than those indicated. Furthermore, I confirm that I have followed the regulations of the good scientific practice of the Carl von Ossietzky University Oldenburg. This dissertation has, neither as a whole, nor in part, been submitted for assessment in a doctoral procedure at another university. No commercial placement or advisory services (promotional advice) have been used within this thesis.

Hamburg, 24.03.2025

Anna-Lena Geßner

Dankessagung

Zuallererst möchte ich mich bei meinem Betreuer Thomas Badewien für seine Unterstützung und sein Verständnis bedanken – dafür, dass er die Betreuung übernommen und mich auf diesem Weg begleitet hat und mir immer die Zeit und den Raum gegeben hat die nötig waren. Außerdem gilt mein Dank meinem weiteren Betreuer Oliver Zielinski, der mich in den ersten Jahren viel unterstützt hat und stets ein offenes Ohr für mich hatte. Ebenso danke ich Katharina Pahnke, die ebenfalls meine Arbeit begutachtet.

Ebenfalls möchte ich mich bei Jochen und Helge bedanken, die mich bei jedem meiner Schritte unterstützt haben und mir immer eine große Hilfe waren. Ich danke euch für die Diskussionen und Gespräche die wir hatten und die Unterstützung beim Verfassen dieser Arbeit.

Ganz besonders danke ich Michelle, Lars, Claudia, Wiebke, Helmo und den Kapitänen der Otzum für ihre tatkräftige Unterstützung bei den Kampagnen, die so manche Herausforderung mit sich brachten. Ohne euch hätten wir in dieser Zeit niemals all die Proben sammeln können. Michelle, ohne deine Zeit, Kraft Mühen und deinen Kopf wäre das nicht möglich gewesen. Ich bin sehr froh, dass keiner Überbord gegangen ist und wir nur arg schmutzig und nicht verletzt im Hafen angekommen sind.

Mein Dank gilt außerdem der Crew der Senckenberg. Und auch der gesamten AG Marine Sensor Systeme.

Dann möchte ich meiner Familie und Freunden von Herzen danken. Ihr habt mich die ganze Zeit über begleitet – auch wenn es bei Weitem nicht immer einfach war. Doch genau das macht eure Unterstützung so besonders. Jede Minute mit euch war unglaublich wertvoll und hat mir die Kraft gegeben, weiterzumachen und niemals aufzugeben. Am Ende zählt nur, was wirklich wichtig ist – und mit euch an meiner Seite wurden alle anderen Probleme klein.

Mama, auch wenn du bis heute nicht genau weißt, was ich während dieser Arbeit eigentlich getan habe, du hast immer an mich geglaubt, mitgefiebert und mich bedingungslos unterstützt. Am liebsten wärst du selbst mitgefahren. Ich bin so froh, dass du und Leon in den letzten Monaten so viel Zeit mit mir verbracht habt. Ihr seid mir eine große Stütze.

Vater, die Zeit mit dir kann mir niemand mehr nehmen, und ich bin unendlich dankbar, dass wir noch so viel davon gemeinsam hatten. Du wirst mir umso mehr fehlen. Deine Unterstützung und alles, was du für mich getan hast, bedeuten mir mehr, als Worte je ausdrücken könnten. Du wirst immer an meiner Seite sein.

Lisa und Marivi, ich danke euch von Herzen. Ihr wart immer da, habt mich unterstützt und mich abgelenkt – selbst in meinen dunkelsten Stunden. Trotz aller Herausforderungen haben wir immer wieder Gründe zum Lachen gefunden, und dafür bin ich euch unendlich dankbar. Es bedeutet mir so viel zu wissen, dass ich jederzeit auf euch zählen kann.

Denis, du hast meine Welt verändert. Ich bin so dankbar, dich an meiner Seite zu haben. In meinen schwersten Momenten hast du mir Kraft gegeben, mich aufgefangen und unterstützt – gerade im letzten Jahr so oft, dass ich es kaum in Worte fassen kann. Ich weiß nicht, wie ich das ohne dich geschafft hätte.

Appendix

Table 1: Stationlist of sedimentological samples

Cruise	Station	Date	Time [UTC]	Latitude	Longitude	Depth [m]
OT202203-1	In01	17.03.2022	08:20	53°44.300' N	7°46.470' E	1.43
OT202203-1	In02	17.03.2022	08:30	53°44.020' N	7°46.500' E	1.54
OT202203-1	In03	17.03.2022	08:50	53°43.500' N	7°46.550' E	0.80
OT202203-1	In04	17.03.2022	09:00	53°43.860' N	7°45.150' E	3.83
OT202203-1	In05	17.03.2022	09:50	53°43.850' N	7°45.190' E	8.77
OT202203-1	In06	17.03.2022	09:30	53°43.810' N	7°45.210' E	5.37
OT202203-1	In07	16.03.2022	10:50	53°43.510' N	7°43.990' E	4.59
OT202203-1	In08	16.03.2022	10:40	53°43.410' N	7°44.000' E	7.33
OT202203-1	In09	16.03.2022	10:20	53°43.300' N	7°44.000' E	3.84
OT202203-1	In10	15.03.2022	07:55	53°43.870' N	7°42.520' E	11.58
SE202203-1	In11	15.03.2022	09:00	53°43.830' N	7°42.410' E	14.72
OT202203-1	In12	15.03.2022	08:20	53°43.810' N	7°42.320' E	2.85
OT202203-1	In13	15.03.2022	08:40	53°44.870' N	7°41.340' E	6.54
OT202203-1	In14	15.03.2022	08:00	53°44.780' N	7°41.320' E	19.31
SE202203-1	In15	15.03.2022	10:10	53°44.690' N	7°41.340' E	11.41
SE202203-1	In16	15.03.2022	08:53	53°44.640' N	7°41.301' E	5.93
OT202203-1	In17	15.03.2022	09:22	53°45.410' N	7°39.661' E	5.18
OT202203-1	In18	15.03.2022	10:50	53°45.340' N	7°39.671' E	7.75
OT202203-1	In19	15.03.2022	14:50	53°45.139' N	7°39.492' E	9.87
OT202203-1	In20	15.03.2022	14:45	53°45.049' N	7°39.321' E	9.02
SE202203-1	In31	15.03.2022	15:38	53°45.588' N	7°38.949' E	21.63
SE202203-1	In32	18.03.2022	16:00	53°45.496' N	7°39.043' E	20.51
SE202203-1	In33	18.03.2022	12:12	53°45.408' N	7°39.116' E	18.98
OT202203-2	In01_H	05.04.2022	14:52	53°45.413' N	7°54.985' E	2.25
OT202203-2	In02_H	05.04.2022	14:32	53°44.848' N	7°54.875' E	2.09
OT202203-2	In03_H	05.04.2022	14:20	53°44.579' N	7°54.681' E	2.03
OT202203-2	In04_H	05.04.2022	13:51	53°45.286' N	7°53.882' E	4.34
OT202203-2	In05_H	05.04.2022	14:00	53°45.264' N	7°53.926' E	6.47
OT202203-2	In06_H	05.04.2022	14:12	53°45.231' N	7°53.942' E	2.88
OT202203-2	In07_H	05.04.2022	13:10	53°45.387' N	7°52.652' E	3.93
OT202203-2	In08_H	05.04.2022	13:17	53°45.340' N	7°52.644' E	7.58
OT202203-2	In09_H	05.04.2022	13:38	53°45.258' N	7°52.615' E	3.25
OT202203-2	In10_H	05.04.2022	12:35	53°45.604' N	7°52.207' E	4.51
OT202203-2	In11_H	05.04.2022	15:15	53°45.565' N	7°52.084' E	7.65
OT202203-2	In12_H	05.04.2022	12:28	53°45.542' N	7°51.998' E	6.44
OT202203-2	In14_H	05.04.2022	15:23	53°46.108' N	7°51.896' E	7.49
OT202203-2	In15_H	05.04.2022	11:56	53°46.015' N	7°51.892' E	3.92
OT202203-2	In16_H	05.04.2022	12:16	53°45.941' N	7°51.857' E	4.94
OT202203-2	In17_H	30.03.2022	11:51	53°46.783' N	7°50.519' E	10.69

Cruise	Station	Date	Time [UTC]	Latitude	Longitude	Depth [m]
OT202203-2	In18_H	30.03.2022	11:32	53°46.678' N	7°50.408' E	6.70
OT202203-2	In19_H	30.03.2022	11:25	53°46.611' N	7°50.287' E	5.24
OT202203-2	In20_H	30.03.2022	11:09	53°46.489' N	7°50.029' E	10.52
OT202209-1	In01	13.09.2022	11:00	53°44.300' N	7°46.470' E	1.43
OT202209-1	In02	13.09.2022	11:12	53°44.020' N	7°46.500' E	1.54
OT202209-1	In03	13.09.2022	11:20	53°43.500' N	7°46.550' E	0.80
OT202209-1	In05	13.09.2022	11:40	53°43.850' N	7°45.190' E	8.77
OT202209-1	In06	13.09.2022	11:50	53°43.810' N	7°45.210' E	5.37
OT202209-1	In07	13.09.2022	12:05	53°43.510' N	7°43.990' E	4.59
OT202209-1	In08	13.09.2022	12:13	53°43.410' N	7°44.000' E	7.33
OT202209-1	In09	13.09.2022	12:27	53°43.300' N	7°44.000' E	3.84
OT202209-1	In10	13.09.2022	12:43	53°43.870' N	7°42.520' E	11.58
SE202209-1	In11	12.09.2022	12:59	53°43.830' N	7°42.410' E	14.72
OT202209-1	In12	13.09.2022	12:56	53°43.810' N	7°42.320' E	2.85
OT202209-1	In13	13.09.2022	13:21	53°44.870' N	7°41.340' E	6.54
SE202209-1	In14	12.09.2022	12:18	53°44.780' N	7°41.320' E	19.31
SE202209-1	In15	12.09.2022	12:36	53°44.690' N	7°41.340' E	11.41
OT202209-1	In16	13.09.2022	13:45	53°44.640' N	7°41.301' E	5.93
OT202209-1	In17	13.09.2022	14:00	53°45.410' N	7°39.661' E	5.18
OT202209-1	In18	12.09.2022	11:46	53°45.340' N	7°39.671' E	7.75
OT202209-1	In19	12.09.2022	11:30	53°45.139' N	7°39.492' E	9.87
OT202209-1	In20	12.09.2022	11:17	53°45.049' N	7°39.321' E	9.02
SE202209-1	In31	12.09.2022	13:54	53°45.588' N	7°38.949' E	21.63
SE202209-1	In32	12.09.2022	12:55	53°45.496' N	7°39.043' E	20.51
SE202209-1	In33	12.09.2022	13:33	53°45.408' N	7°39.116' E	18.98
OT202209-1	In01_H	15.09.2022	14:05	53°45.413' N	7°54.985' E	2.25
OT202209-1	In02_H	15.09.2022	14:00	53°44.848' N	7°54.875' E	2.09
OT202209-1	In03_H	15.09.2022	13:45	53°44.579' N	7°54.681' E	2.03
OT202209-1	In04_H	15.09.2022	13:35	53°45.286' N	7°53.882' E	4.34
OT202209-1	In05_H	15.09.2022	13:25	53°45.264' N	7°53.926' E	6.47
OT202209-1	In06_H	15.09.2022	13:15	53°45.231' N	7°53.942' E	2.88
OT202209-1	In07_H	15.09.2022	13:03	53°45.387' N	7°52.652' E	3.93
OT202209-1	In08_H	15.09.2022	12:51	53°45.340' N	7°52.644' E	7.58
OT202209-1	In09_H	15.09.2022	12:44	53°45.258' N	7°52.615' E	3.25
OT202209-1	In10_H	15.09.2022	12:35	53°45.604' N	7°52.207' E	4.51
OT202209-1	In11_H	15.09.2022	12:23	53°45.565' N	7°52.084' E	7.65
OT202209-1	In12_H	15.09.2022	12:12	53°45.542' N	7°51.998' E	6.44
OT202209-1	In14_H	14.09.2022	13:50	53°46.108' N	7°51.896' E	7.49
OT202209-1	In15_H	14.09.2022	14:17	53°46.015' N	7°51.892' E	3.92
OT202209-1	In16_H	14.09.2022	14:00	53°45.941' N	7°51.857' E	4.94
OT202209-1	In17_H	14.09.2022	13:20	53°46.783' N	7°50.519' E	10.69
OT202209-1	In18_H	14.09.2022	13:00	53°46.678' N	7°50.408' E	6.70
OT202209-1	In19_H	14.09.2022	12:40	53°46.611' N	7°50.287' E	5.24
OT202209-1	In20_H	14.09.2022	12:30	53°46.489' N	7°50.029' E	10.52

Cruise	Station	Date	Time [UTC]	Latitude	Longitude	Depth [m]
OT202303-1	In03_H	17.04.2023	11:10	53°44.579' N	7°54.681' E	2.03
OT202303-1	In07_H	17.04.2023	10:55	53°45.387' N	7°52.652' E	3.93
OT202303-1	In09_H	17.04.2023	10:35	53°45.258' N	7°52.615' E	3.25
OT202303-1	In14_H	17.04.2023	10:05	53°46.108' N	7°51.896' E	7.49
OT202303-1	In15_H	17.04.2023	10:15	53°46.015' N	7°51.892' E	3.92
OT202303-1	In16_H	17.04.2023	10:25	53°45.941' N	7°51.857' E	4.94
OT202303-1	In18_H	17.04.2023	09:45	53°46.678' N	7°50.408' E	6.70
OT202303-1	In34_H	17.04.2023	09:02	53°46.980' N	7°50.220' E	6.30
OT202303-1	In35_H	17.04.2023	09:24	53°47.100' N	7°50.100' E	6.89
OT202303-1	In36_H	17.04.2023	09:30	53°47.160' N	7°49.980' E	3.69
OT202303-1	HS01	17.04.2023	12:00	53°42.420' N	7°48.541' E	1.57
OT202303-1	HS02	17.04.2023	11:50	53°43.079' N	7°48.841' E	2.10

Table 2: Samples provided by Lufi Hannover

Station	Date	Sample from	Latitude	Longitude
NMS-06	04.04.2023	D. Bunzel, LuFi Hannover	53°40.878' N	7°20.649' E
NMS-04	04.04.2023	D. Bunzel, LuFi Hannover	53°40.934' N	7°20.628' E
NMS-06	04.04.2023	D. Bunzel, LuFi Hannover	53°40.970' N	7°20.615' E
NMS-08	04.04.2023	D. Bunzel, LuFi Hannover	53°41.016' N	7°20.596' E
NMS-10	04.04.2023	D. Bunzel, LuFi Hannover	53°41.049' N	7°20.585' E
NMS-12	04.04.2023	D. Bunzel, LuFi Hannover	53°41.079' N	7°20.573' E

Table 3: Grain size analysis of the sediment samples

Cruise	Station	> 2,000 µm [wt %]	2,000 – 1,000 µm [wt %]	1,000- 200 µm [wt %]	200 - 63 µm [wt %]	< 63 µm [wt %]
OT202203-1	In01	0,07	0,05	5,87	78,03	15,99
OT202203-1	In02	0,02	0,01	0,33	80,54	19,11
OT202203-1	In03	0,02	0,01	0,70	93,64	5,63
OT202203-1	In04	0,19	0,07	0,54	88,90	10,30
OT202203-1	In05	0,06	0,18	1,24	49,68	48,84
OT202203-1	In06	0,78	0,03	1,47	95,13	2,59
OT202203-1	In07	0,09	0,01	0,55	82,20	17,15
OT202203-1	In08	0,51	0,15	7,57	41,37	50,40
OT202203-1	In09	0,14	0,06	1,21	80,26	18,33
OT202203-1	In10	0,05	0,04	1,10	96,15	2,67
OT202203-1	In11	0,04	0,11	0,86	84,74	14,25
OT202203-1	In12	0,52	0,06	0,06	4,76	94,60
OT202203-1	In13	9,14	0,41	8,09	75,62	6,74
OT202203-1	In14	10,52	2,61	27,02	54,94	4,91
OT202203-1	In15	1,00	0,11	35,73	57,42	5,74
OT202203-1	In16	3,36	0,95	55,38	36,93	3,38
OT202203-1	In17	0,64	0,27	59,28	37,53	2,28
OT202203-1	In18	0,38	0,51	48,54	46,65	3,92
OT202203-1	In19	0,91	1,51	94,10	2,44	1,03
OT202203-1	In20	0,01	0,03	11,03	80,87	8,05
OT202203-1	In31	28,25	9,84	53,82	6,38	1,71
OT202203-1	In32	0,01	0,00	13,18	84,67	2,14
OT202203-1	In33	1,13	0,52	15,44	81,30	1,60
OT202203-2	In01_H	0,00	0,00	0,53	80,23	19,23
OT202203-2	In02_H	0,05	0,02	1,67	95,99	2,26
OT202203-2	In03_H	0,05	0,03	1,02	63,85	35,04
OT202203-2	In04_H	0,38	0,19	11,34	84,68	3,42
OT202203-2	In05_H	6,52	0,93	30,91	57,69	3,96
OT202203-2	In06_H	0,01	0,01	10,16	87,34	2,48
OT202203-2	In07_H	7,98	0,72	24,83	64,17	2,29
OT202203-2	In08_H	1,32	0,11	8,79	86,20	3,58
OT202203-2	In09_H	11,21	0,78	9,09	76,76	2,16
OT202203-2	In10_H	7,25	0,35	16,36	73,71	2,33
OT202203-2	In11_H	6,39	2,24	62,22	25,69	3,46
OT202203-2	In12_H	0,11	0,01	14,51	81,06	4,31
OT202203-2	In14_H	65,64	1,83	10,32	18,08	4,14
OT202203-2	In15_H	8,42	1,81	47,27	38,94	3,57
OT202203-2	In16_H	0,02	0,03	13,99	83,47	2,49
OT202203-2	In17_H	16,82	0,13	44,96	33,01	5,07
OT202203-2	In18_H	0,02	0,02	23,98	73,34	2,64
OT202203-2	In19_H	0,00	0,00	2,12	96,45	1,42

Cruise	Station	> 2,000 µm [wt %]	2,000 – 1,000 µm [wt %]	1,000- 200 µm [wt %]	200 - 63 µm [wt %]	< 63 µm [wt %]
OT202203-2	In20_H	29,38	9,31	47,92	11,27	2,12
OT202209-1	In01	0,08	0,15	11,45	83,59	4,73
OT202209-1	In02	0,00	0,02	1,70	94,14	4,14
OT202209-1	In03	0,96	0,05	0,55	90,80	7,66
OT202209-1	In05	0,95	0,30	36,43	45,59	16,74
OT202209-1	In06	1,74	0,08	3,02	92,55	2,61
OT202209-1	In07	16,10	1,01	4,10	78,57	0,22
OT202209-1	In08	0,16	0,05	3,16	43,75	52,89
OT202209-1	In09	0,00	0,01	0,30	48,86	50,83
OT202209-1	In10	3,06	0,47	5,15	86,97	4,36
OT202209-1	In11	0,01	0,04	2,68	81,78	15,48
OT202209-1	In12	1,24	0,06	6,75	87,61	4,34
OT202209-1	In13	0,59	0,12	12,04	73,63	13,62
OT202209-1	In14	6,37	0,92	26,65	57,35	8,71
OT202209-1	In15	2,93	0,25	23,25	69,96	3,60
OT202209-1	In16	3,90	0,19	64,27	31,04	0,61
OT202209-1	In17	0,08	0,28	32,98	63,81	2,85
OT202209-1	In18	0,24	0,30	72,72	24,02	2,72
OT202209-1	In19	5,24	0,64	91,54	1,94	0,63
OT202209-1	In20	2,34	2,83	63,61	19,53	11,69
OT202209-1	In31	22,45	7,53	67,69	1,27	1,07
OT202209-1	In32	5,22	2,47	86,52	4,69	1,10
OT202209-1	In33	11,69	10,38	75,43	1,34	1,15
OT202209-1	In01_H	5,31	0,32	3,32	83,69	7,36
OT202209-1	In02_H	0,00	0,01	2,12	94,03	3,85
OT202209-1	In03_H	2,37	0,08	10,64	82,47	4,44
OT202209-1	In04_H	0,13	0,10	26,12	70,01	3,64
OT202209-1	In05_H	7,24	0,12	35,15	54,55	2,94
OT202209-1	In06_H	0,01	0,02	11,95	84,56	3,47
OT202209-1	In07_H	0,00	0,03	9,88	87,44	2,66
OT202209-1	In08_H	9,75	4,30	36,55	43,10	6,30
OT202209-1	In09_H	7,45	0,81	19,00	69,74	3,01
OT202209-1	In10_H	4,48	0,68	33,54	56,68	4,62
OT202209-1	In11_H	1,76	0,19	9,54	85,26	3,24
OT202209-1	In12_H	8,94	0,27	6,48	78,45	5,86
OT202209-1	In14_H	7,30	0,78	9,30	73,24	9,39
OT202209-1	In15_H	19,29	3,12	43,90	30,81	2,88
OT202209-1	In16_H	1,31	0,77	30,26	62,74	4,91
OT202209-1	In17_H	6,89	1,78	68,76	19,79	2,78
OT202209-1	In18_H	0,67	0,26	57,25	38,15	3,66
OT202209-1	In19_H	0,03	0,09	36,63	60,30	2,95
OT202209-1	In20_H	0,00	0,00	13,62	83,23	3,15
OT202303-1	In03_H	3,27	0,09	15,89	75,59	5,16
OT202303-1	In07_H	25,85	2,02	35,68	31,42	5,02

Cruise	Station	> 2,000 µm [wt %]	2,000 – 1,000 µm [wt %]	1,000- 200 µm [wt %]	200 - 63 µm [wt %]	< 63 µm [wt %]
OT202303-1	In09_H	22,65	2,39	42,71	27,84	4,40
OT202303-1	In14_H	5,61	1,82	5,87	6,07	80,63
OT202303-1	In15_H	17,27	2,42	29,87	46,95	3,49
OT202303-1	In16_H	18,70	0,56	17,01	60,30	3,43
OT202303-1	In18_H	0,09	0,16	50,37	46,29	3,09
OT202303-1	In34_H	9,71	4,18	76,03	8,16	1,93
OT202303-1	In35_H	0,21	0,08	51,56	45,06	3,08
OT202303-1	In36_H	0,07	0,06	14,54	82,26	3,07
OT202303-1	HS01	0,00	0,19	1,23	15,64	82,93
OT202303-1	HS02	43,22	7,17	16,53	21,83	11,25
	NMS06	0,16	0,09	0,55	7,04	92,16
	NMS04	0,00	0,00	0,18	7,55	92,27
	NMS08	0,13	0,06	0,70	5,78	93,33
	NMS02	1,19	0,36	1,59	3,87	92,99
	NMS10	0,33	0,16	0,68	28,39	70,45
	NMS12	0,11	0,26	0,43	7,11	92,09

Table 4: ADCP time series measurements

				Start	**End**
Cruise	**Location**	**Latitude**	**Longitude**	**Date & Time [UTC]**	**Date & Time [UTC]**
SE202103-1	Otzumer Balje	53°44.968' N	7°40.448' E	29.06.2021 04:27	30.06.2021 01:53
SE202203-1	Otzumer Balje	53°44.968' N	7°40.448' E	17.03.2022 05:57	17.03.2022 17:15
SE202203-1	Harle (South)	53°46.657' N	7°49.824' E	28.03.2022 09:30	29.03.2022 04:33
SE202206-1	Harle (South)	53°46.657' N	7°49.824' E	28.06.2022 05:09	28.06.2022 16:04
SE202206-1	Harle (North)	53°46.997' N	7°49.519' E	28.06.2022 16:20	29.06.2022 05:52
SE202206-1	Harle (North)	53°46.997' N	7°49.519' E	29.06.2022 05:53	29.06.2022 16:20
SE202206-1	Harle (South)	53°46.657' N	7°49.824' E	29.06.2022 16:27	30.06.2022 05:56

Table 5: Component composition of the sediment samples

Cruise	Station	Grain Size	Components	Abundance
OT202203-1	In01	> 2,000 µm	Bivalve fragments	dominant
			Cardiidae	dominant
OT202203-1	In02	> 2,000 µm	Bivalve fragments	dominant
			Peat	dominant
OT202203-1	In03	> 2,000 µm	Bivalve fragments	dominant
			Cardiidae	dominant
OT202203-1	In04	> 2,000 µm	Bivalve fragments	dominant
OT202203-1	In05	> 2,000 µm	Roots	very abundant
			Bivalve fragments	abundant
			Cardiidae	rare
			Wood	dominant
OT202203-1	In06	> 2,000 µm	Bivalve fragments	dominant
			Cardiidae	dominant
OT202203-1	In07	> 2,000 µm	Roots	abundant
			Bivalve fragments	dominant
			Cardiidae	abundant
			Wood	very abundant
OT202203-1	In08	> 2,000 µm	Bivalve fragments	dominant
			Cardiidae	abundant
			Wood	abundant
OT202203-1	In09	> 2,000 µm	Bivalve fragments	very abundant
			Semelidae	rare
			Lanice fragment	abundant
			Sea Grass	dominant
OT202203-1	In10	> 2,000 µm	*Mytilidae*	dominant
			Silicates	dominant
OT202203-1	In11	> 2,000 µm	Bivalve fragments	dominant
			Plant fragment	dominant
OT202203-1	In12	> 2,000 µm	Bivalve fragments	dominant
OT202203-1	In13	> 2,000 µm	Bivalve fragments	dominant
OT202203-1	In14	> 2,000 µm	Bivalve fragments	dominant
			Mya	rare
			Gastropoda	present
			Bryozoa fragment	dominant
OT202203-1	In15	> 2,000 µm	Bivalve fragments	dominant
			Cardiidae	abundant
			Semelidae	abundant
OT202203-1	In16	> 2,000 µm	Bivalve fragments	dominant
			Cardiidae	abundant
			Semelidae	very abundant
			Mytilidae	rare

Appendix

Cruise	Station	Grain Size	Components	Abundance
			Silicates	very abundant
OT202203-1	In17	> 2,000 µm	Bivalve fragments	dominant
			Mya	present
			Silicates	abundant
OT202203-1	In18	> 2,000 µm	Bivalve fragments	dominant
			Cardiidae	present
			Gastropoda	rare
			Lanice fragment	rare
			Petricolaria p.	present
			Wood	dominant
OT202203-1	In19	> 2,000 µm	Bivalve fragments	dominant
			Cardiidae	rare
			Semelidae	abundant
SE202203-1	In20	> 2,000 µm	Bivalve fragments	dominant
SE202203-1	In31	> 2,000 µm	Roots	present
			Bivalve fragments	dominant
			Cardiidae	abundant
			Semelidae	abundant
			Silicates	present
OT202203-1	In32	> 2,000 µm	Bivalve fragments	dominant
OT202203-1	In33	> 2,000 µm	Bivalve fragments	dominant
			Semelidae	abundant
			Silicates	very abundant
OT202203-2	In01_H	> 2,000 µm	Roots	dominant
OT202203-2	In02_H	> 2,000 µm	Bivalve fragments	dominant
OT202203-2	In03_H	> 2,000 µm	Roots	very abundant
			Bivalve fragments	dominant
OT202203-2	In04_H	> 2,000 µm	Bivalve fragments	dominant
			Cardiidae	dominant
			Mya	very abundant
			Gastropoda	abundant
OT202203-2	In05_H	> 2,000 µm	Bivalve fragments	dominant
			Cardiidae	very abundant
			Mya	present
			Gastropoda	present
OT202203-2	In06_H	> 2,000 µm	Bivalve fragments	dominant
OT202203-2	In07_H	> 2,000 µm	Bivalve fragments	dominant
			Cardiidae	abundant
			Semelidae	abundant
			Bryozoa fragment	present
OT202203-2	In08_H	> 2,000 µm	Bivalve fragments	dominant
			Cardiidae	abundant
			Lanice fragment	very abundant

Cruise	Station	Grain Size	Components	Abundance
OT202203-2	In09_H	> 2,000 µm	Bivalve fragments	dominant
			Cardiidae	rare
			Mya	present
			Bryozoa fragment	rare
			Silicates	rare
OT202203-2	In10_H	> 2,000 µm	Bivalve fragments	dominant
			Cardiidae	abundant
			Semelidae	abundant
			Bryozoa fragment	present
OT202203-2	In11_H	> 2,000 µm	Bivalve fragments	dominant
			Cardiidae	very abundant
			Semelidae	rare
			Mytilidae	present
			Gastropoda	present
			Lanice fragment	rare
			Silicates	present
OT202203-2	In12_H	> 2,000 µm	Silicates	dominant
OT202203-2	In14_H	> 2,000 µm	Bivalve fragments	dominant
			Cardiidae	very abundant
			Mya	rare
			Gastropoda	present
			Bryozoa	dominant
OT202203-2	In15_H	> 2,000 µm	Bivalve fragments	dominant
			Cardiidae	very abundant
			Mytilidae	present
			Lanice fragment	rare
			Feldspat	present
			Silicates	present
OT202203-2	In16_H	> 2,000 µm	Bivalve fragments	dominant
OT202203-2	In17_H	> 2,000 µm	Bivalve fragments	dominant
			Cardiidae	dominant
			Semelidae	abundant
			Gastropoda	abundant
OT202203-2	In18_H	> 2,000 µm	Bivalve fragments	dominant
OT202203-2	In20_H	> 2,000 µm	Bivalve fragments	dominant
			Cardiidae	very abundant
			Semelidae	rare
			Gastropoda	rare
			Silicates	present
OT202209-1	In01	> 2,000 µm	Bivalve fragments	dominant
			Cardiidae	abundant
			Semelidae	abundant
			Echinoid fragment	abundant

Cruise	Station	Grain Size	Components	Abundance
OT202209-1	In03	> 2,000 µm	Bivalve fragments	dominant
			Cardiidae	abundant
			Mya	abundant
			Semelidae	abundant
			Bryozoa fragment	very abundant
OT202209-1	In05	> 2,000 µm	Bivalve fragments	dominant
			Cardiidae	dominant
OT202209-1	In06	> 2,000 µm	Bivalve fragments	dominant
			Semelidae	abundant
			Mytilidae	abundant
OT202209-1	In07	> 2,000 µm	Bivalve fragments	dominant
			Cardiidae	very abundant
			Semelidae	present
			Bryozoa fragment	abundant
			Wood	abundant
OT202209-1	In08	> 2,000 µm	Bivalve fragments	dominant
OT202209-1	In09	> 2,000 µm	Roots	dominant
OT202209-1	In10	> 2,000 µm	Bivalve fragments	dominant
			Mytilidae	very abundant
			Gastropoda	present
OT202209-1	In11	> 2,000 µm	Roots	dominant
			Bivalve fragments	dominant
OT202209-1	In12	> 2,000 µm	Bivalve fragments	dominant
			Cardiidae	dominant
			Semelidae	abundant
			Gastropoda	abundant
OT202209-1	In13	> 2,000 µm	Bivalve fragments	dominant
			Cardiidae	very abundant
			Semelidae	abundant
			Sea Grass	dominant
OT202209-1	In14	> 2,000 µm	Bivalve fragments	dominant
			Cardiidae	dominant
			Mya	rare
			Semelidae	present
			Lanice fragment	abundant
			Silicates	rare
			Sea Grass	present
			Peat	abundant
OT202209-1	In15	> 2,000 µm	Bivalve fragments	dominant
			Cardiidae	very abundant
			Semelidae	rare
			Mytilidae	rare
			Wood	abundant

Cruise	Station	Grain Size	Components	Abundance
OT202209-1	In16	> 2,000 µm	Bivalve fragments	dominant
			Silicates	very abundant
OT202209-1	In17	> 2,000 µm	Bivalve fragments	dominant
			Cardiidae	abundant
			Semelidae	rare
			Silicates	abundant
OT202209-1	In18	> 2,000 µm	Bivalve fragments	dominant
			Mya	abundant
			Silicates	abundant
OT202209-1	In19	> 2,000 µm	Bivalve fragments	dominant
			Cardiidae	dominant
			Silicates	very abundant
OT202209-1	In20	> 2,000 µm	Bivalve fragments	dominant
			Ensis	rare
			Silicates	abundant
			Flint	present
			Echinoid fragment	rare
			Wood	abundant
			Peat	rare
OT202209-1	In31	> 2,000 µm	Bivalve fragments	dominant
			Cardiidae	abundant
			Semelidae	abundant
OT202209-1	In32	> 2,000 µm	Bivalve fragments	dominant
			Cardiidae	very abundant
			Semelidae	rare
OT202209-1	In33	> 2,000 µm	Bivalve fragments	dominant
			Cardiidae	abundant
			Semelidae	rare
			Silicates	dominant
OT202209-1	In01_H	> 2,000 µm	Bivalve fragments	dominant
			Cardiidae	abundant
			Mytilidae	rare
			Silicates	rare
			Crab	rare
OT202209-1	In03_H	> 2,000 µm	Bivalve fragments	dominant
			Cardiidae	abundant
			Wood	abundant
OT202209-1	In04_H	> 2,000 µm	Bivalve fragments	dominant
			Cardiidae	dominant
OT202209-1	In05_H	> 2,000 µm	Bivalve fragments	dominant
			Cardiidae	very abundant
			Mytilidae	abundant
OT202209-1	In06_H	> 2,000 µm	*Cardiidae*	dominant

Cruise	Station	Grain Size	Components	Abundance
OT202209-1	In08_H	> 2,000 µm	Bivalve fragments	dominant
			Cardiidae	abundant
			Gastropoda	rare
			Lanice fragment	dominant
			Flint	present
			Sea Grass	present
OT202209-1	In09_H	> 2,000 µm	Bivalve fragments	dominant
			Cardiidae	very abundant
			Semelidae	rare
OT202209-1	In10_H	> 2,000 µm	Bivalve fragments	dominant
			Cardiidae	very abundant
			Semelidae	present
			Silicates	present
OT202209-1	In11_H	> 2,000 µm	Bivalve fragments	dominant
			Cardiidae	very abundant
			Semelidae	abundant
			Sea Grass	abundant
OT202209-1	In12_H	> 2,000 µm	Bivalve fragments	dominant
			Cardiidae	rare
			Semelidae	present
			Bryozoa fragment	abundant
			Lanice fragment	abundant
			Silicates	present
OT202209-1	In14_H	> 2,000 µm	Bivalve fragments	dominant
			Cardiidae	present
			Mytilidae	dominant
			Bryozoa fragment	abundant
			Lanice fragment	present
OT202209-1	In15_H	> 2,000 µm	Bivalve fragments	dominant
			Cardiidae	dominant
			Semelidae	abundant
			Peat	present
OT202209-1	In16_H	> 2,000 µm	Roots	abundant
			Bivalve fragments	very abundant
			Cardiidae	rare
			Lanice fragment	dominant
			Echinoid fragment	present
OT202209-1	In17_H	> 2,000 µm	Bivalve fragments	dominant
			Cardiidae	abundant
			Semelidae	rare
			Silicates	abundant
			Wood	present
OT202209-1	In18_H	> 2,000 µm	Bivalve fragments	dominant

Cruise	Station	Grain Size	Components	Abundance
			Cardiidae	very abundant
			Semelidae	abundant
OT202209-1	In19_H	> 2,000 µm	Bivalve fragments	dominant
OT202304-1	In03_H	> 2,000 µm	Bivalve fragments	dominant
			Cardiidae	abundant
			Mya	rare
			Mythilidae	rare
OT202304-1	In07_H	> 2,000 µm	Bivalve fragments	dominant
			Cardiidae	very abundant
			Semelidae	very abundant
			Gastopoda fragment	present
OT202304-1	In09_H	> 2,000 µm	Bivalve fragments	dominant
			Cardiidae	rare
			Semelidae	rare
OT202304-1	In14_H	> 2,000 µm	Bivalve fragments	dominant
			Cardiidae	present
			Bryozoa fragment	rare
OT202304-1	In15_H	> 2,000 µm	Bivalve fragments	dominant
			Cardiidae	very abundant
			Semelidae	present
			Mythilidae	present
			Gastropoda	present
			Silicates	present
OT202304-1	In16_H	> 2,000 µm	Bivalve fragments	dominant
			Cardiidae	very abundant
			Semelidae	abundant
			Gastropoda	present
			Bryozoa fragment	present
OT202304-1	In18_H	> 2,000 µm	Bivalve fragments	dominant
OT202304-1	In34_H	> 2,000 µm	Bivalve fragments	dominant
			Cardiidae	abundant
			Mythilidae	present
			Gastropoda	present
			Silicates	abundant
OT202304-1	In35_H	> 2,000 µm	Bivalve fragments	dominant
			Cardiidae	very abundant
OT202304-1	In36_H	> 2,000 µm	Bivalve fragments	dominant
			Silicates	dominant
OT202304-1	HS02	> 2,000 µm	Bivalve fragments	dominant
			Cardiidae	rare
			Gastropoda	abundant
			Silicates	abundant
			Gastopoda fragment	rare

Cruise	Station	Grain Size	Components	Abundance
OT202203-1	In01	2,000 – 1,000 µm	Bivalve fragments	dominant
			Silicates	abundant
			Wood	very abundant
OT202203-1	In02	2,000 – 1,000 µm	Roots	rare
			Plant fragments	dominant
OT202203-1	In03	2,000 – 1,000 µm	Bivalve fragments	dominant
			Semelidae	very abundant
OT202203-1	In04	2,000 – 1,000 µm	Bivalve fragments	dominant
			Cardiidae	rare
			Mytilidae	very abundant
			Plant fragments	very abundant
OT202203-1	In05	2,000 – 1,000 µm	Bivalve fragments	very abundant
			Semelidae	present
			Gastropoda	rare
			Silicates	rare
			Wood	dominant
OT202203-1	In06	2,000 – 1,000 µm	Bivalve fragments	dominant
			Gastropoda	rare
			Silicates	abundant
OT202203-1	In07	2,000 – 1,000 µm	Roots	rare
			Bivalve fragments	very abundant
			Plant fragments	dominant
OT202203-1	In08	2,000 – 1,000 µm	Bivalve fragments	dominant
			Silicates	present
			Plant fragments	very abundant
OT202203-1	In09	2,000 – 1,000 µm	Bivalve fragments	very abundant
			Echinoid spine	rare
			Plant fragments	dominant
OT202203-1	In10	2,000 – 1,000 µm	Bivalve fragments	dominant
			Mytilidae	abundant
			Silicates	dominant
OT202203-1	In11	2,000 – 1,000 µm	Bivalve fragments	dominant
			Plant fragments	dominant
OT202203-1	In12	2,000 – 1,000 µm	Bivalve fragments	dominant
			Gastropoda	abundant
			Echinoid fragment	abundant
SE202203-1	In13	2,000 – 1,000 µm	Bivalve fragments	dominant
			Gastropoda	abundant
			Lanice fragment	present
			Silicates	rare
			Plant fragments	very abundant
OT202203-1	In14	2,000 – 1,000 µm	Bivalve fragments	dominant
			Gastropoda	rare

Cruise	Station	Grain Size	Components	Abundance
			Lanice	present
			Silicates	dominant
			Plant fragments	present
OT202203-1	In15	2,000 – 1,000 µm	Bivalve fragments	dominant
			Gastropoda	present
			Silicates	very abundant
			Plant fragments	abundant
OT202203-1	In16	2,000 – 1,000 µm	Bivalve fragments	dominant
			Semelidae	present
			Gastropoda	abundant
			Silicates	dominant
			Echinoid fragments	rare
OT202203-1	In17	2,000 – 1,000 µm	Bivalve fragments	dominant
			Silicates	very abundant
			Echinoid fragment	rare
SE202203-1	In18	2,000 – 1,000 µm	Bivalve fragments	dominant
			Mytilidae	present
			Gastropoda	rare
			Silicates	present
			Echinoid fragment	very abundant
			Echinoid spine	rare
			Plant fragments	dominant
SE202203-1	In19	2,000 – 1,000 µm	Bivalve fragments	dominant
			Semelidae	present
			Silicates	dominant
			Echinoid fragment	rare
SE202203-1	In20	2,000 – 1,000 µm	Bivalve fragments	dominant
			Silicates	very abundant
			Plant fragments	dominant
SE202203-1	In31	2,000 – 1,000 µm	Bivalve fragments	dominant
			Gastropoda	present
			Silicates	dominant
OT202203-1	In33	2,000 – 1,000 µm	Bivalve fragments	dominant
			Semelidae	present
			Gastropoda	present
			Silicates	dominant
OT202203-2	In01_H	2,000 – 1,000 µm	Peat	dominant
OT202203-2	In02_H	2,000 – 1,000 µm	Bivalve fragments	dominant
			Flint	abundant
OT202203-2	In03_H	2,000 – 1,000 µm	Bivalve fragments	dominant
			Gastropoda	rare
			Echinoid spine	rare
			Wood	very abundant

Cruise	Station	Grain Size	Components	Abundance
			Plant fragments	dominant
OT202203-2	In04_H	2,000 – 1,000 µm	Bivalve fragments	dominant
			Cardiidae	rare
			Gastropoda	rare
			Silicates	very abundant
OT202203-2	In05_H	2,000 – 1,000 µm	Bivalve fragments	dominant
			Cardiidae	rare
			Gastropoda	abundant
			Silicates	rare
			Echinoid fragment	rare
OT202203-2	In06_H	2,000 – 1,000 µm	Bivalve fragments	dominant
OT202203-2	In07_H	2,000 – 1,000 µm	Bivalve fragments	dominant
			Gastropoda	abundant
			Silicates	very abundant
OT202203-2	In08_H	2,000 – 1,000 µm	Bivalve fragments	dominant
			Gastropoda	abundant
			Lanice fragment	present
			Silicates	abundant
			Peat	present
OT202203-2	In09_H	2,000 – 1,000 µm	Bivalve fragments	dominant
			Cardiidae	present
			Gastropoda	rare
			Bryozoa fragment	rare
			Silicates	very abundant
			Echinoid fragment	present
OT202203-2	In10_H	2,000 – 1,000 µm	Bivalve fragments	dominant
			Gastropoda	very abundant
			Bryozoa fragment	present
			Silicates	abundant
			Plant fragments	rare
OT202203-2	In11_H	2,000 – 1,000 µm	Bivalve fragments	dominant
			Semelidae	present
			Gastropoda	abundant
			Bryozoa fragment	present
			Silicates	rare
			Echinoid fragment	rare
			Plant fragments	rare
OT202203-2	In12_H	2,000 – 1,000 µm	Bivalve fragments	dominant
			Gastropoda	dominant
			Plant fragments	very abundant
OT202203-2	In14_H	2,000 – 1,000 µm	Bivalve fragments	dominant
			Gastropoda	rare
			Bryozoa fragment	abundant

Cruise	Station	Grain Size	Components	Abundance
			Plant fragments	rare
OT202203-2	In15_H	2,000 – 1,000 µm	Bivalve fragments	dominant
			Gastropoda	abundant
			Lanice fragment	very abundant
			Silicates	abundant
			Echinoid spine	present
OT202203-2	In16_H	2,000 – 1,000 µm	Bivalve fragments	dominant
			Mytilidae	abundant
OT202203-2	In17_H	2,000 – 1,000 µm	Bivalve fragments	dominant
			Cardiidae	present
			Gastropoda	very abundant
			Silicates	rare
			Flint	present
			Echinoid fragment	rare
OT202203-2	In18_H	2,000 – 1,000 µm	Bivalve fragments	dominant
			Cardiidae	rare
			Echinoid fragment	rare
OT202203-2	In19_H	2,000 – 1,000 µm	Bivalve fragments	dominant
OT202203-2	In20_H	2,000 – 1,000 µm	Bivalve fragments	dominant
			Semelidae	present
			Gastropoda	abundant
			Silicates	very abundant
			Flint	present
OT202209-1	In01	2,000 – 1,000 µm	Bivalve fragments	dominant
			Mya	present
			Semelidae	rare
			Gastropoda	very abundant
			Lanice fragment	rare
			Silicates	present
			Peat	rare
OT202209-1	In02	2,000 – 1,000 µm	Bivalve fragments	dominant
			Peat	abundant
OT202209-1	In03	2,000 – 1,000 µm	Bivalve fragments	dominant
			Semelidae	abundant
			Gastropoda	abundant
			Plant fragments	dominant
OT202209-1	In05	2,000 – 1,000 µm	Bivalve fragments	dominant
			Cardiidae	rare
			Semelidae	rare
			Gastropoda	abundant
			Lanice fragment	present
			Peat	present
OT202209-1	In06	2,000 – 1,000 µm	Bivalve fragments	dominant

Cruise	Station	Grain Size	Components	Abundance
			Mytilidae	rare
			Gastropoda	rare
			Bryozoa fragment	abundant
			Silicates	dominant
			Plant fragments	rare
OT202209-1	In07	2,000 – 1,000 µm	Bivalve fragments	dominant
			Cardiidae	present
			Semelidae	present
			Gastropoda	abundant
			Bryozoa fragment	rare
			Silicates	rare
			Plant fragments	rare
OT202209-1	In08	2,000 – 1,000 µm	Bivalve fragments	abundant
			Cardiidae	present
			Plant fragments	dominant
OT202209-1	In09	2,000 – 1,000 µm	Bivalve fragments	dominant
			Plant fragments	dominant
OT202209-1	In10	2,000 - 1000 µm	Bivalve fragments	dominant
			Mytilidae	abundant
			Gastropoda	rare
			Silicates	rare
OT202209-1	In11	2,000 – 1,000 µm	Bivalve fragments	very abundant
			Gastropoda	present
			Silicates	present
			Plant fragments	dominant
OT202209-1	In12	2,000 – 1,000 µm	Bivalve fragments	dominant
			Cardiidae	rare
			Mytilidae	present
			Gastropoda	very abundant
			Bryozoa fragment	present
			Flint	rare
			Echinoid fragment	rare
			Plant fragments	very abundant
OT202209-1	In13	2,000 – 1,000 µm	Bivalve fragments	very abundant
			Gastropoda	present
			Silicates	present
			Plant fragments	dominant
OT202209-1	In14	2,000 – 1,000 µm	Bivalve fragments	dominant
			Cardiidae	present
			Gastropoda	very abundant
			Lanice fragment	very abundant
			Silicates	very abundant
OT202209-1	In15	2,000 – 1,000 µm	Bivalve fragments	dominant

Cruise	Station	Grain Size	Components	Abundance
			Gastropoda	present
			Silicates	very abundant
			Echinoid fragment	abundant
			Plant fragments	very abundant
OT202209-1	In16	2,000 – 1,000 µm	Bivalve fragments	dominant
			Silicates	dominant
			Echinoid fragment	very abundant
			Echinoid spine	present
OT202209-1	In17	2,000 – 1,000 µm	Bivalve fragments	dominant
			Silicates	very abundant
			Flint	present
OT202209-1	In18	2,000 – 1,000 µm	Bivalve fragments	dominant
			Cardiidae	present
			Mya	present
			Semelidae	rare
			Gastropoda	rare
			Silicates	dominant
			Flint	present
			Echinoid fragment	abundant
OT202209-1	In19	2,000 – 1,000 µm	Bivalve fragments	dominant
			Silicates	dominant
			Flint	rare
			Echinoid fragment	abundant
OT202209-1	In20	2,000 – 1,000 µm	Bivalve fragments	dominant
			Gastropoda	present
			Bryozoa fragment	present
			Silicates	dominant
			Flint	present
			Echinoid fragment	abundant
			Plant fragments	very abundant
OT202209-1	In31	2,000 – 1,000 µm	Bivalve fragments	dominant
			Semelidae	present
			Gastropoda	abundant
			Silicates	very abundant
			Echinoid fragment	abundant
OT202209-1	In32	2,000 – 1,000 µm	Bivalve fragments	dominant
			Cardiidae	present
			Semelidae	present
			Gastropoda	abundant
			Silicates	abundant
			Echinoid fragment	abundant
OT202209-1	In33	2,000 – 1,000 µm	Bivalve fragments	dominant
			Gastropoda	rare

Cruise	Station	Grain Size	Components	Abundance
			Silicates	dominant
			Flint	rare
			Echinoid fragment	rare
OT202209-1	In01_H	2,000 – 1,000 µm	Bivalve fragments	dominant
			Semelidae	present
			Mytilidae	present
			Gastropoda	abundant
			Bryozoa fragment	rare
			Lanice fragment	rare
			Flint	present
			Wood	very abundant
			Plant fragments	abundant
OT202209-1	In02_H	2,000 – 1,000 µm	Bivalve fragments	dominant
OT202209-1	In03_H	2,000 – 1,000 µm	Roots	present
			Bivalve fragments	dominant
			Gastropoda	rare
			Flint	present
			Echinoid spine	present
			Plant fragments	very abundant
OT202209-1	In04_H	2,000 – 1,000 µm	Bivalve fragments	dominant
			Semelidae	abundant
			Gastropoda	rare
			Silicates	rare
OT202209-1	In05_H	2,000 – 1,000 µm	Bivalve fragments	dominant
			Semelidae	present
			Silicates	abundant
OT202209-1	In06_H	2,000 – 1,000 µm	Bivalve fragments	dominant
OT202209-1	In07_H	2,000 – 1,000 µm	Bivalve fragments	dominant
			Cardiidae	abundant
			Semelidae	very abundant
			Mytilidae	abundant
			Silicates	abundant
OT202209-1	In08_H	2,000 – 1,000 µm	Bivalve fragments	dominant
			Cardiidae	present
			Gastropoda	very abundant
			Lanice fragment	dominant
OT202209-1	In09_H	2,000 – 1,000 µm	Bivalve fragments	dominant
			Mya	present
			Gastropoda	dominant
			Silicates	rare
			Flint	present
OT202209-1	In10_H	2,000 – 1,000 µm	Bivalve fragments	dominant
			Gastropoda	rare

Cruise	Station	Grain Size	Components	Abundance
			Silicates	abundant
			Flint	present
OT202209-1	In11_H	2,000 – 1,000 µm	Bivalve fragments	dominant
			Mytilidae	present
			Gastropoda	very abundant
OT202209-1	In12_H	2,000 – 1,000 µm	Bivalve fragments	dominant
			Cardiidae	rare
			Semelidae	present
			Bryozoa fragment	very abundant
			Silicates	abundant
			Plant fragments	very abundant
OT202209-1	In14_H	2,000 – 1,000 µm	Bivalve fragments	dominant
			Semelidae	present
			Mytilidae	very abundant
			Bryozoa fragment	very abundant
			Silicates	abundant
OT202209-1	In15_H	2,000 – 1,000 µm	Bivalve fragments	dominant
			Cardiidae	rare
			Gastropoda	abundant
			Silicates	abundant
			Echinoid spine	present
OT202209-1	In16_H	2,000 – 1,000 µm	Bivalve fragments	dominant
			Cardiidae	present
			Mytilidae	rare
			Gastropoda	present
			Bryozoa fragment	present
			Lanice fragment	dominant
			Plant fragments	present
OT202209-1	In17_H	2,000 – 1,000 µm	Bivalve fragments	dominant
			Semelidae	rare
			Mytilidae	present
			Gastropoda	present
			Silicates	dominant
			Flint	rare
OT202209-1	In18_H	2,000 – 1,000 µm	Bivalve fragments	dominant
			Cardiidae	rare
			Semelidae	rare
			Gastropoda	rare
			Silicates	abundant
			Echinoid fragment	abundant
OT202209-1	In19_H	2,000 – 1,000 µm	Bivalve fragments	dominant
			Mytilidae	rare
			Gastropoda	rare

Cruise	Station	Grain Size	Components	Abundance
			Silicates	abundant
			Echinoid fragment	rare
OT202209-1	In20_H	2,000 – 1,000 µm	Bivalve fragments	dominant
OT202304-1	In03_H	2,000 – 1,000 µm	Bivalve fragments	dominant
			Semelidae	rare
			Gastropoda	abundant
			Bryozoa fragment	abundant
			Gastopoda fragment	rare
OT202304-1	In07_H	2,000 – 1,000 µm	Bivalve fragments	dominant
			Gastropoda	abundant
			Silicates	abundant
OT202304-1	In09_H	2,000 – 1,000 µm	Bivalve fragments	dominant
			Gastropoda	abundant
			Bryozoa fragment	present
			Silicates	abundant
OT202304-1	In14_H	2,000 – 1,000 µm	Bivalve fragments	dominant
			Gastropoda	very abundant
			Silicates	very abundant
OT202304-1	In15_H	2,000 – 1,000 µm	Bivalve fragments	dominant
			Cardiidae	present
			Gastropoda	very abundant
			Silicates	very abundant
OT202304-1	In16_H	2,000 – 1,000 µm	Bivalve fragments	dominant
			Mythilidae	present
			Gastropoda	present
			Silicates	very abundant
			Plant fragments	rare
OT202304-1	In18_H	2,000 – 1,000 µm	Bivalve fragments	dominant
			Semelidae	present
			Silicates	abundant
			Fish scale	present
OT202304-1	In34_H	2,000 – 1,000 µm	Bivalve fragments	dominant
			Gastropoda	abundant
			Silicates	dominant
OT202304-1	In35_H	2,000 – 1,000 µm	Bivalve fragments	dominant
			Silicates	abundant
			Plant fragments	rare
OT202304-1	In36_H	2,000 – 1,000 µm	Bivalve fragments	dominant
			Silicates	dominant
			Echinoid fragment	rare
OT202304-1	HS01	2,000 – 1,000 µm	Bivalve fragments	dominant
			Gastropoda	abundant
			Silicates	very abundant

Cruise	Station	Grain Size	Components	Abundance
			Plant fragments	abundant
OT202304-1	HS02	2,000 – 1,000 µm	Bivalve fragments	dominant
			Gastropoda	dominant
			Silicates	rare
			Gastopoda fragment	very abundant
OT202203-1	In01	1,000 – 200 µm	Bivalve fragments	rare
			Silicates	dominant
			Echinoid spine	abundant
			Plant fragments	present
			Haynesina	present
OT202203-1	In02	1,000 - 200 µm	Bivalve fragments	rare
			Silicates	dominant
			Echinoid fragment	present
			Echinoid spine	very abundant
			Plant fragments	very abundant
			Ammonia	abundant
			Elphididae	rare
			Haynesina	abundant
OT202203-1	In03	1,000 - 200 µm	Bivalve fragments	very abundant
			Gastropoda	present
			Silicates	dominant
			Echinoid fragment	present
			Echinoid spine	rare
			Plant fragments	rare
			Ammonia	rare
			Haynesina	rare
OT202203-1	In04	1,000 - 200 µm	Bivalve fragments	very abundant
			Silicates	dominant
			Echinoid fragment	abundant
			Echinoid spine	very abundant
			Plant fragments	rare
			Ammonia	abundant
			Elphididae	rare
			Haynesina	abundant
OT202203-1	In05	1,000 - 200 µm	Bivalve fragments	abundant
			Silicates	very abundant
			Echinoid fragment	rare
			Echinoid spine	very abundant
			Plant fragments	dominant
			Ammonia	rare
			Elphididae	present
			Haynesina	rare
OT202203-1	In06	1,000 - 200 µm	Bivalve fragments	very abundant

Cruise	Station	Grain Size	Components	Abundance
			Silicates	dominant
			Echinoid spine	present
			Ammonia	present
			Haynesina	present
OT202203-1	In07	1,000 - 200 µm	Bivalve fragments	abundant
			Silicates	very abundant
			Echinoid fragment	rare
			Echinoid spine	very abundant
			Plant fragments	dominant
			Ammonia	rare
			Elphididae	present
			Haynesina	present
OT202203-1	In08	1,000 - 200 µm	Bivalve fragments	rare
			Silicates	dominant
			Plant fragments	very abundant
OT202203-1	In09	1,000 - 200 µm	Bivalve fragments	abundant
			Silicates	rare
			Echinoid spine	very abundant
			Plant fragments	dominant
			Ammonia	present
			Elphididae	present
			Haynesina	present
OT202203-1	In10	1,000 - 200 µm	Bivalve fragments	abundant
			Silicates	dominant
			Echinoid spine	rare
			Pellets	present
			Ammonia	rare
			Elphididae	present
OT202203-1	In11	1,000 - 200 µm	Bivalve fragments	abundant
			Silicates	dominant
			Echinoid fragments	present
			Echinoid spines	very abundant
			Plant fragment	rare
			Ammonia	abundant
			Elphididae	rare
OT202203-1	In12	1,000 - 200 µm	Bivalve fragments	rare
			Silicates	dominant
OT202203-1	In13	1,000 - 200 µm	Bivalve fragments	rare
			Silicates	dominant
			Echinoid spine	rare
			Plant fragments	abundant
OT202203-1	In14	1,000 - 200 µm	Bivalve fragments	rare
			Silicates	dominant

Cruise	Station	Grain Size	Components	Abundance
			Echinoid spines	rare
			Plant fragments	rare
OT202203-1	In15	1,000 - 200 µm	Bivalve fragments	present
			Silicates	dominant
			Plant fragments	present
OT202203-1	In16	1,000 - 200 µm	Bivalve fragments	rare
			Silicates	dominant
OT202203-1	In17	1,000 - 200 µm	Bivalve fragments	present
			Silicates	dominant
OT202203-1	In18	1,000 - 200 µm	Bivalve fragments	rare
			Silicates	dominant
			Plant fragments	rare
OT202203-1	In19	1,000 - 200 µm	Bivalve fragments	rare
			Silicates	dominant
OT202203-1	In20	1,000 - 200 µm	Bivalve fragments	rare
			Silicates	dominant
OT202203-1	In31	1,000 - 200 µm	Bivalve fragments	abundant
			Silicates	dominant
OT202203-1	In32	1,000 - 200 µm	Silicates	dominant
OT202203-1	In33	1,000 - 200 µm	Bivalve fragments	present
			Silicates	dominant
OT202203-2	In01_H	1,000 - 200 µm	Bivalve fragments	abundant
			Silicates	dominant
			Echinoid fragment	rare
			Echinoid spine	very abundant
			Plant fragments	very abundant
			Ammonia	rare
			Elphididae	present
			Haynesina	rare
OT202203-2	In02_H	1,000 - 200 µm	Bivalve fragments	rare
			Silicates	dominant
			Plant fragments	present
OT202203-2	In03_H	1,000 - 200 µm	Bivalve fragments	abundant
			Silicates	dominant
			Echinoid fragment	rare
			Echinoid spine	dominant
			Plant fragments	very abundant
			Elphididae	present
			Haynesina	present
OT202203-2	In04_H	1,000 - 200 µm	Bivalve fragments	abundant
			Silicates	dominant
			Ammonia	present
OT202203-2	In05_H	1,000 - 200 µm	Bivalve fragments	abundant

Cruise	Station	Grain Size	Components	Abundance
			Silicates	dominant
			Ammonia	present
OT202203-2	In06_H	1,000 - 200 µm	Silicates	dominant
OT202203-2	In07_H	1,000 - 200 µm	Bivalve fragments	rare
			Silicates	dominant
OT202203-2	In08_H	1,000 - 200 µm	Bivalve fragments	abundant
			Silicates	dominant
			Echinoid fragment	present
			Echinoid spine	present
OT202203-2	In09_H	1,000 - 200 µm	Bivalve fragments	rare
			Silicates	dominant
OT202203-2	In10_H	1,000 - 200 µm	Bivalve fragments	present
			Silicates	dominant
OT202203-2	In11_H	1,000 - 200 µm	Bivalve fragments	very abundant
			Silicates	dominant
OT202203-2	In12_H	1,000 - 200 µm	Bivalve fragments	present
			Silicates	dominant
OT202203-2	In14_H	1,000 - 200 µm	Bivalve fragments	very abundant
			Silicates	dominant
			Plant fragments	present
OT202203-2	In15_H	1,000 - 200 µm	Bivalve fragments	rare
			Silicates	dominant
OT202203-2	In16_H	1,000 - 200 µm	Silicates	dominant
OT202203-2	In17_H	1,000 - 200 µm	Bivalve fragments	abundant
			Silicates	dominant
			Plant fragments	present
OT202203-2	In18_H	1,000 - 200 µm	Bivalve fragments	rare
			Silicates	dominant
OT202203-2	In19_H	1,000 - 200 µm	Bivalve fragments	abundant
			Silicates	dominant
			Echinoid fragment	present
			Echinoid spine	present
OT202203-2	In20_H	1,000 - 200 µm	Bivalve fragments	very abundant
			Silicates	dominant
OT202209-1	In01	1,000 - 200 µm	Bivalve fragments	abundant
			Silicates	dominant
			Echinoid spine	present
OT202209-1	In02	1,000 - 200 µm	Bivalve fragments	abundant
			Silicates	dominant
			Echinoid spine	rare
			Plant fragments	present
			Ammonia	present
OT202209-1	In03	1,000 - 200 µm	Bivalve fragments	abundant

Cruise	Station	Grain Size	Components	Abundance
			Silicates	dominant
			Echinoid fragment	present
			Echinoid Spine	rare
			Plant fragments	rare
OT202209-1	In05	1,000 - 200 µm	Bivalve fragments	rare
			Silicates	dominant
OT202209-1	In06	1,000 - 200 µm	Bivalve fragments	rare
			Silicates	dominant
OT202209-1	In07	1,000 - 200 µm	Bivalve fragments	very abundant
			Gastropoda	present
			Silicates	dominant
			Echinoid spine	rare
			Plant fragments	rare
OT202209-1	In08	1,000 - 200 µm	Silicates	dominant
			Echinoid fragment	present
			Echinoid spine	abundant
			Plant fragments	dominant
OT202209-1	In09	1,000 - 200 µm	Bivalve fragments	very abundant
			Silicates	rare
			Echinoid fragment	abundant
			Echinoid spine	dominant
			Plant fragments	very abundant
			Ammonia	present
			Elphididae	rare
			Haynesina	rare
OT202209-1	In10	1,000 - 200 µm	Bivalve fragments	very abundant
			Silicates	dominant
			Echinoid spine	rare
			Plant fragments	rare
OT202209-1	In11	1,000 - 200 µm	Bivalve fragments	rare
			Silicates	dominant
			Echinoid fragment	present
			Echinoid spine	rare
			Plant fragments	rare
			Haynesina	present
OT202209-1	In12	1,000 - 200 µm	Bivalve fragments	rare
			Silicates	dominant
			Echinoid fragment	rare
			Echinoid spine	rare
			Plant fragments	present
			Ammonia	present
OT202209-1	In13	1,000 - 200 µm	Silicates	dominant
			Echinoid fragment	present

Cruise	Station	Grain Size	Components	Abundance
			Echinoid spine	very abundant
			Plant fragments	rare
OT202209-1	In14	1,000 - 200 µm	Bivalve fragments	rare
			Silicates	dominant
			Echinoid spine	present
			Plant fragments	present
OT202209-1	In15	1,000 - 200 µm	Bivalve fragments	rare
			Silicates	dominant
			Echinoid fragment	present
OT202209-1	In16	1,000 - 200 µm	Bivalve fragments	present
			Silicates	dominant
OT202209-1	In17	1,000 - 200 µm	Bivalve fragments	abundant
			Silicates	dominant
			Echinoid fragment	present
			Echinoid spine	present
OT202209-1	In18	1,000 - 200 µm	Bivalve fragments	rare
			Silicates	dominant
OT202209-1	In19	1,000 - 200 µm	Bivalve fragments	present
			Silicates	dominant
OT202209-1	In20	1,000 - 200 µm	Bivalve fragments	abundant
			Silicates	dominant
			Echinoid fragment	rare
			Plant fragments	abundant
OT202209-1	In31	1,000 - 200 µm	Bivalve fragments	abundant
			Silicates	dominant
OT202209-1	In32	1,000 - 200 µm	Bivalve fragments	rare
			Silicates	dominant
OT202209-1	In33	1,000 - 200 µm	Bivalve fragments	rare
			Silicates	dominant
OT202209-1	In01_H	1,000 - 200 µm	Bivalve fragments	rare
			Silicates	dominant
			Plant fragments	rare
OT202209-1	In02_H	1,000 - 200 µm	Silicates	dominant
	In03_H	1,000 - 200 µm	Bivalve fragments	present
			Silicates	dominant
OT202209-1	In04_H	1,000 - 200 µm	Bivalve fragments	present
			Silicates	dominant
OT202209-1	In05_H	1,000 - 200 µm	Bivalve fragments	rare
			Silicates	dominant
OT202209-1	In06_H	1,000 - 200 µm	Bivalve fragments	present
			Silicates	dominant
OT202209-1	In07_H	1,000 - 200 µm	Bivalve fragments	rare
			Silicates	dominant

Cruise	**Station**	**Grain Size**	**Components**	**Abundance**
OT202209-1	In08_H	1,000 - 200 µm	Bivalve fragments	very abundant
			Silicates	dominant
			Echinoid spine	present
			Lanice fragment	abundant
OT202209-1	In09_H	1,000 - 200 µm	Bivalve fragments	abundant
			Silicates	dominant
			Echinoid fragment	present
			Ammonia	present
OT202209-1	In10_H	1,000 - 200 µm	Bivalve fragments	rare
			Silicates	dominant
OT202209-1	In11_H	1,000 - 200 µm	Bivalve fragments	rare
			Silicates	dominant
OT202209-1	In12_H	1,000 - 200 µm	Bivalve fragments	rare
			Silicates	dominant
OT202209-1	In14_H	1,000 - 200 µm	Bivalve fragments	abundant
			Cardiidae	abundant
			Silicates	dominant
			Echinoid spine	rare
OT202209-1	In15_H	1,000 - 200 µm	Bivalve fragments	very abundant
			Gastropoda	present
			Silicates	dominant
			Echinoid spine	present
			Ammonia	present
OT202209-1	In16_H	1,000 - 200 µm	Bivalve fragments	rare
			Silicates	dominant
			Echinoid spine	present
			Lanice fragment	rare
OT202209-1	In17_H	1,000 - 200 µm	Bivalve fragments	rare
			Silicates	dominant
OT202209-1	In18_H	1,000 - 200 µm	Bivalve fragments	abundant
			Silicates	dominant
OT202209-1	In19_H	1,000 - 200 µm	Bivalve fragments	present
			Silicates	dominant
OT202209-1	In20_H	1,000 - 200 µm	Bivalve fragments	present
			Silicates	dominant
OT202304-1	In03_H	1,000 - 200 µm	Bivalve fragments	present
			Silicates	dominant
			Echinoid spines	rare
			Plant fragments	rare
OT202304-1	In07_H	1,000 - 200 µm	Bivalve fragments	rare
			Silicates	dominant
OT202304-1	In09_H	1,000 - 200 µm	Bivalve fragments	abundant
			Silicates	dominant

Cruise	Station	Grain Size	Components	Abundance
OT202304-1	In14_H	1,000 - 200 µm	Bivalve fragments	abundant
			Silicates	dominant
			Plant fragments	abundant
OT202304-1	In15_H	1,000 - 200 µm	Bivalve fragments	present
			Silicates	dominant
OT202304-1	In16_H	1,000 - 200 µm	Silicates	dominant
OT202304-1	In18_H	1,000 - 200 µm	Bivalve fragments	present
			Silicates	dominant
OT202304-1	In34_H	1,000 - 200 µm	Bivalve fragments	rare
			Silicates	dominant
OT202304-1	In35_H	1,000 - 200 µm	Silicates	dominant
OT202304-1	In36_H	1,000 - 200 µm	Silicates	dominant
OT202304-1	HS01	1,000 - 200 µm	Bivalve fragments	very abundant
			Silicates	dominant
			Plant fragments	dominant
			Ammonia	abundant
OT202304-1	HS02	1,000 - 200 µm	Bivalve fragments	abundant
			Gastropoda	abundant
			Silicates	dominant
			Echinoid fragments	very abundant
			Ammonia	abundant
OT202203-1	In01	200 - 63 µm	Silicates	dominant
OT202203-1	In02	200 - 63 µm	Silicates	dominant
OT202203-1	In03	200 - 63 µm	Bivalve fragments	rare
			Silicates	dominant
OT202203-1	In04	200 - 63 µm	Bivalve fragments	present
			Silicates	dominant
OT202203-1	In05	200 - 63 µm	Bivalve fragments	rare
			Silicates	dominant
			Echinoid spine	present
			Plant fragments	present
OT202203-1	In06	200 - 63 µm	Silicates	dominant
OT202203-1	In07	200 - 63 µm	Bivalve fragments	present
			Silicates	dominant
OT202203-1	In09	200 - 63 µm	Bivalve fragments	present
			Silicates	dominant
OT202203-1	In10	200 - 63 µm	Silicates	dominant
OT202203-1	In11	200 - 63 µm	Silicates	dominant
			Echinoid spines	present
OT202203-1	In12	200 - 63 µm	Silicates	dominant
OT202203-1	In13	200 - 63 µm	Silicates	dominant
OT202203-1	In14	200 - 63 µm	Silicates	dominant
OT202203-1	In15	200 - 63 µm	Silicates	dominant

Cruise	Station	Grain Size	Components	Abundance
OT202203-1	In16	200 - 63 µm	Silicates	dominant
			Plant fragments	present
OT202203-1	In17	200 - 63 µm	Silicates	dominant
OT202203-1	In18	200 - 63 µm	Silicates	dominant
OT202203-1	In19	200 - 63 µm	Silicates	dominant
OT202203-1	In20	200 - 63 µm	Silicates	dominant
OT202203-1	In31	200 - 63 µm	Bivalve fragments	present
			Silicates	dominant
			Plant fragments	rare
OT202203-1	In32	200 - 63 µm	Silicates	dominant
OT202203-1	In33	200 - 63 µm	Silicates	dominant
OT202203-2	In01_H	200 - 63 µm	Silicates	dominant
OT202203-2	In02_H	200 - 63 µm	Silicates	dominant
OT202203-2	In03_H	200 - 63 µm	Silicates	dominant
OT202203-2	In04_H	200 - 63 µm	Silicates	dominant
OT202203-2	In05_H	200 - 63 µm	Silicates	dominant
OT202203-2	In06_H	200 - 63 µm	Silicates	dominant
OT202203-2	In07_H	200 - 63 µm	Silicates	dominant
OT202203-2	In08_H	200 - 63 µm	Silicates	dominant
OT202203-2	In09_H	200 - 63 µm	Silicates	dominant
OT202203-2	In10_H	200 - 63 µm	Silicates	dominant
OT202203-2	In11_H	200 - 63 µm	Silicates	dominant
OT202203-2	In12_H	200 - 63 µm	Silicates	dominant
OT202203-2	In14_H	200 - 63 µm	Bivalve fragments	rare
			Silicates	dominant
OT202203-2	In15_H	200 - 63 µm	Silicates	dominant
OT202203-2	In16_H	200 - 63 µm	Silicates	dominant
OT202203-2	In17_H	200 - 63 µm	Silicates	dominant
OT202203-2	In18_H	200 - 63 µm	Silicates	dominant
OT202203-2	In19_H	200 - 63 µm	Silicates	dominant
OT202203-2	In20_H	200 - 63 µm	Bivalve fragments	rare
			Silicates	dominant
			Echinoid spine	present
OT202209-1	In01	200 - 63 µm	Silicates	dominant
OT202209-1	In02	200 - 63 µm	Silicates	dominant
OT202209-1	In03	200 - 63 µm	Silicates	dominant
OT202209-1	In05	200 - 63 µm	Silicates	dominant
OT202209-1	In06	200 - 63 µm	Silicates	dominant
OT202209-1	In07	200 - 63 µm	Silicates	dominant
OT202209-1	In09	200 - 63 µm	Silicates	dominant
OT202209-1	In10	200 - 63 µm	Silicates	dominant
OT202209-1	In11	200 - 63 µm	Silicates	dominant
OT202209-1	In12	200 - 63 µm	Silicates	dominant

Appendix

Cruise	Station	Grain Size	Components	Abundance
OT202209-1	In13	200 - 63 µm	Silicates	dominant
OT202209-1	In14	200 - 63 µm	Silicates	dominant
OT202209-1	In15	200 - 63 µm	Silicates	dominant
OT202209-1	In16	200 - 63 µm	Silicates	dominant
OT202209-1	In17	200 - 63 µm	Silicates	dominant
OT202209-1	In18	200 - 63 µm	Silicates	dominant
OT202209-1	In19	200 - 63 µm	Silicates	dominant
OT202209-1	In20	200 - 63 µm	Silicates	dominant
			Plant fragments	present
OT202209-1	In31	200 - 63 µm	Silicates	dominant
OT202209-1	In32	200 - 63 µm	Bivalve fragments	present
			Silicates	dominant
			Plant fragments	present
OT202209-1	In33	200 - 63 µm	Bivalve fragments	present
			Silicates	dominant
			Plant fragments	present
OT202209-1	In01_H	200 - 63 µm	Silicates	dominant
OT202209-1	In02_H	200 - 63 µm	Silicates	dominant
OT202209-1	In03_H	200 - 63 µm	Silicates	dominant
OT202209-1	In04_H	200 - 63 µm	Silicates	dominant
OT202209-1	In05_H	200 - 63 µm	Silicates	dominant
OT202209-1	In06_H	200 - 63 µm	Silicates	dominant
OT202209-1	In07_H	200 - 63 µm	Silicates	dominant
OT202209-1	In08_H	200 - 63 µm	Bivalve fragments	present
			Silicates	dominant
			Echinoid spine	present
			Plant fragments	present
OT202209-1	In09_H	200 - 63 µm	Silicates	dominant
OT202209-1	In10_H	200 - 63 µm	Silicates	dominant
OT202209-1	In11_H	200 - 63 µm	Silicates	dominant
OT202209-1	In12_H	200 - 63 µm	Silicates	dominant
OT202209-1	In14_H	200 - 63 µm	Silicates	dominant
OT202209-1	In15_H	200 - 63 µm	Silicates	dominant
OT202209-1	In16_H	200 - 63 µm	Silicates	dominant
OT202209-1	In17_H	200 - 63 µm	Silicates	dominant
OT202209-1	In18_H	200 - 63 µm	Silicates	dominant
OT202209-1	In19_H	200 - 63 µm	Silicates	dominant
OT202209-1	In20_H	200 - 63 µm	Silicates	dominant
OT202304-1	In03_H	200 - 63 µm	Silicates	dominant
OT202304-1	In07_H	200 - 63 µm	Silicates	dominant
OT202304-1	In09_H	200 - 63 µm	Silicates	dominant
OT202304-1	In14_H	200 - 63 µm	Silicates	dominant
OT202304-1	In15_H	200 - 63 µm	Silicates	dominant

Cruise	Station	Grain Size	Components	Abundance
OT202304-1	In16_H	200 - 63 µm	Silicates	dominant
OT202304-1	In18_H	200 - 63 µm	Silicates	dominant
OT202304-1	In34_H	200 - 63 µm	Silicates	dominant
OT202304-1	In35_H	200 - 63 µm	Silicates	dominant
OT202304-1	In36_H	200 - 63 µm	Silicates	dominant
OT202304-1	HS01	200 - 63 µm	Silicates	dominant
			Echinoid fragments	rare
			Plant fragments	abundant
OT202304-1	HS02	200 - 63 µm	Bivalve fragments	present
			Silicates	dominant
			Echinoid spines	abundant
			Plant fragments	present

Table 6: Chemical compound composition in percentages [%]

Station	Shill [%]	Sand [%]	Mud [%]	TOC	SiO_2	CaO	Al_2O_3	Fe_2O_3	Na_2O	K_2O	MgO	TiO_2	P_2O_5	MnO
In03_H	3.27	91.57	5.16	0.12	89.54	1.29	2.52	0.70	0.84	0.90	0.25	0.43	0.03	0.02
In07_H	25.85	69.12	5.02		83.14	6.36	1.36	0.22	0.60	0.64	0.11	0.09	0.02	0.01
In09_H	22.65	72.94	4.40	0.19	84.45	5.93	1.29	0.23	0.55	0.60	0.10	0.12	0.02	0.01
In14_H	5.61	13.76	80.63	0.68	72.71	7.16	4.65	1.70	1.20	1.31	0.72	0.33	0.07	0.03
In15_H	17.27	79.24	3.49		84.62	5.64	1.59	0.30	0.61	0.68	0.13	0.15	0.02	0.01
In16_H	18.70	77.87	3.43		87.07	3.94	1.69	0.32	0.61	0.73	0.12	0.16	0.03	0.01
In18_H	0.09	96.82	3.09	0.06	93.61	0.52	1.53	0.20	0.57	0.72	0.09	0.08	0.02	0.00
In34_H	9.71	88.37	1.93	0.05	86.27	5.37	1.01	0.14	0.46	0.50	0.09	0.05	0.02	0.00
In35_H	0.21	96.70	3.08	0.06	92.90	0.65	1.64	0.31	0.65	0.69	0.13	0.18	0.02	0.01
In36_H	0.07	96.86	3.07	0.06	92.40	0.68	2.03	0.41	0.69	0.80	0.16	0.25	0.02	0.01
HS01	0	17.06	82.93	2.35	59.79	5.96	7.99	3.48	1.61	1.84	1.46	0.56	0.24	0.05
HS02	43.22	45.53	11.25	0.70	70.74	10.07	3.10	1.14	0.97	0.96	0.49	0.35	0.11	0.03
Mean	10.34	78.33	11.33	0.10	86.67	3.75	1.93	0.45	0.68	0.76	0.19	0.18	0.03	0.01
SD	9.98	24.91	24.37	0.22	6.19	2.69	1.04	0.46	0.21	0.22	0.19	0.12	0.01	0.01

Table 7: Heavy metal concentrations in the Harle sediments

Station	Al [%]	As (ppm)	Cr (ppm)	Cu (ppm)	Pb (ppm)	Zn (ppm)
ERL		8,2	81	34	47	150
In03_H	1.33	9	53	4	6	14
In07_H	0.72	8	13	5	1	5
In09_H	0.68	8	18	3	1	6
In14_H	2.46	14	45	6	5	24
In15_H	0.84	9	29	3	1	7
In16_H	0.89	9	18	4	1	7
In18_H	0.81	9	11	4	0	5
In34_H	0.53	8	7	4	0	3
In35_H	0.87	9	21	2	0	6
In36_H	1.07	10	28	2	0	8
HS01	4.23	20	80	15	24	91
HS02	1.64	12	49	10	8	29
Mean	1.26	10	26	4	3	12
SD	0.55	2	15	1	2	6

Table 8: Statistical correlations (Pearson) between sediment compounds and heavy metal concentrations

	Shill	Sand	Mud	TOC	Al [%]	As (ppm)	Cr (ppm)	Cu (ppm)	Pb (ppm)	Zn (ppm)
SiO_2	0.25	0.97	-0.93	-0.95	-0.95	-0.93	-0.93	-0.96	-0.90	-0.93
Al_2O_3	-0.50	-0.91	0.95	0.97	1.00	0.98	0.98	0.97	0.96	0.99
CaO	0.56	-0.57	0.34	0.34	0.28	0.25	0.28	0.36	0.22	0.26
Fe_2O_3	-0.48	-0.91	0.94	0.97	1.00	0.98	0.97	0.98	0.97	0.99
K_2O	-0.51	-0.92	0.96	0.97	1.00	0.97	0.97	0.96	0.95	0.97
MgO	-0.47	-0.92	0.96	0.98	1.00	0.97	0.97	0.97	0.95	0.98
MnO	-0.42	-0.81	0.84	0.93	0.91	0.84	0.88	0.86	0.85	0.89
Na_2O	-0.43	-0.92	0.94	0.91	0.94	0.94	0.95	0.91	0.86	0.89
P_2O_5	-0.41	-0.90	0.92	0.98	0.98	0.97	0.96	0.98	0.94	0.96
TiO_2	-0.46	-0.86	0.89	0.92	0.94	0.91	0.98	0.90	0.88	0.91

Table 9: Pearson correlation matrix between key sediment characteristics and heavy metal concentrations

	Shill	Sand	Mud	TOC	Al [%]	As (ppm)	Cr (ppm)	Cu (ppm)	Pb (ppm)	Zn (ppm)
Shill		0.25	-0.51	-0.46	-0.50	-0.47	-0.44	-0.36	-0.45	-0.46
Sand	0.25		-0.96	-0.89	-0.91	-0.90	-0.88	-0.90	-0.84	-0.87
Mud	-0.51	-0.96		0.92	0.95	0.93	0.91	0.90	0.87	0.91
TOC	-0.46	-0.89	0.92		0.97	0.93	0.94	0.94	0.91	0.94
Al [%]	-0.50	-0.91	0.95	0.97		0.98	0.98	0.97	0.96	0.99
As (ppm)	-0.47	-0.90	0.93	0.93	0.98		0.96	0.98	0.97	0.98
Cr (ppm)	-0.44	-0.88	0.91	0.94	0.98	0.96		0.95	0.94	0.96
Cu (ppm)	-0.36	-0.90	0.90	0.94	0.97	0.98	0.95		0.97	0.98
Pb (ppm)	-0.45	-0.84	0.87	0.91	0.96	0.97	0.94	0.97		0.99
Zn (ppm)	-0.46	-0.87	0.91	0.94	0.99	0.98	0.96	0.98	0.99	

Table 10: Enrichment factors of heavy metal concentrations

	As	Cr	Cu	Pb	Zn
In03_H	2.93	2.42	1.67	1.45	1.26
In07_H	4.83	1.10	3.86	0.45	0.84
In09_H	5.09	1.61	2.44	0.47	1.06
In14_H	2.47	1.12	1.35	0.66	1.18
In15_H	4.65	2.10	1.98	0.38	1,00
In16_H	4.38	1.23	2.48	0.36	0.94
In18_H	4.83	0.83	2.74	0	0.74
In34_H	6.51	0.80	4.16	0	0.68
In35_H	4.51	1.48	1.28	0	0.83
In36_H	4.05	1.59	1.03	0	0.90
HS01	2.06	1.15	1.97	1.83	2.59
HS02	3.18	1.82	3.39	1.57	2.13
Mean	4.06	1.30	2.21	0.63	1.17
SD	1.26	0.50	1.02	0.66	0.58

Table 11: Metal concentrations in relation to Aluminium (Al)

Station	Hg/Al	As/Al	Cr/Al	Cu/Al	Pb/Al	Zn/Al
In03_H	0.015		39.74	3.00	4.50	10.50
In07_H	0.005	11.12	18.06	6.95	1.39	6.95
In09_H	0.004	11.72	26.37	4.39	1.46	8.79
In14_H	0.004	5.69	18.29	2.44	2.03	9.75
In15_H	0.004	10.70	34.46	3.57	1.19	8.32
In16_H	0.005	10.06	20.13	4.47	1.12	7.83
In18_H	0.003	11.12	13.59	4.94	0	6.18
In34_H	0.005	14.97	13.10	7.48	0	5.61
In35_H	0.004	10.37	24.20	2.30	0	6.91
In36_H	0.004	9.31	26.06	1.86	0	7.45
HS01	0.027	4.73	18.92	3.55	5.68	21.52
HS02	0.027	7.31	29.87	6.10	4.88	17.68

Table 12: Heavy metal concentrations for the salt marsh

Station	Al [%]	As [ppm]	Cr [ppm]	Cu [ppm]	Pb [ppm]	Zn [ppm]
NMS23-02	6.22	4	17	3	9	27
NMS23-04	5.76	5	18	4	12	30
NMS23-06	5.60	4	18	4	9	25
NMS23-08	5.97	5	18	4	10	26
NMS23-10	3.88	4	17	3	6	19
NMS23-12	5.54	5	19	4	11	28

Table 13: Enrichment factors of heavy metal concentrations along the salt marsh

Station	Cr	Cu	Pb	Zn	Hg
ERL	81	34	47	150	0.15
NMS02	106	20	59	166	0.31
NMS04	102	22	69	172	0.58
NMS06	98	20	49	142	0.31
NMS08	107	21	59	154	0.31
NMS10	68	11	23	73	0.11
NMS12	104	21	63	157	0.5
Mean	98	19	54	144	0.35
SD	15	4	16	36	0

Table 14: Laser diffraction measurements

Station	Gravel [%]	Sand [%]	Silt [%]	Clay [%]
In36_H	0	99.80	0.20	0
In35_H	0	99.70	0.30	0
In34_H	0	100.00	0	0
In18_H	0	99.95	0.05	0
In14_H	0	72.21	23.55	4.24
In15_H	0	99.78	0.22	0
In16_H	0	99.87	0.13	0
In07_H	0	99.94	0.06	0
In09_H	0	99.95	0.05	0
In03_H	0	97.80	2.20	0
HS02	0.01	83.15	13.66	3.18
HS01	0	13.48	86.52	0
NMS23-02	0	9.70	90.27	0.03
NMS23-04	0	11.18	88.71	0.10
NMS23-06	0	8.96	91.04	0
NMS23-08	0	8.15	91.74	0.11
NMS23-10	0	31.45	68.55	0
NMS23-12	0	12.41	87.59	0

Table 15: Chemical compound composition in percentages [%] for the salt marsh

Station	Shill [%]	Sand [%]	Mud [%]	TOC	SiO_2	CaO	Al_2O_3	Fe_2O_3	Na_2O	K_2O	MgO	TiO_2	P_2O_5	MnO
NMS23-02	0.16	7.68	92.16	3.41	51.29	7.11	11.75	5.48	1.35	2.36	2.08	0.64	0.27	0.13
NMS23-04	0	7.73	92.27	1.98	59.68	3.91	10.89	4.82	1.41	2.30	1.82	0.60	0.23	0.07
NMS23-06	0.13	6.54	93.33	3.23	55.87	6.10	10.59	4.79	1.45	2.24	1.85	0.61	0.26	0.11
NMS23-08	1.19	5.82	92.99	2.96	54.74	5.85	11.28	5.46	1.73	2.36	1.91	0.64	0.31	0.05
NMS23-10	0.33	29.23	70.45	2.28	68.83	4.92	7.34	2.82	1.11	1.82	1.17	0.49	0.18	0.07
NMS23-12	0.11	7.80	92.09	2.97	52.81	4.43	10.46	4.74	1.68	2.15	1.71	0.60	0.28	0.08
Mean	0.32	10.80	88.88	2.81	57.20	5.39	10.39	4.69	1.46	2.21	1.76	0.60	0.26	0.09
SD	0.44	9.06	9.04	0.56	6.38	1.18	1.56	0.97	0.23	0.20	0.31	0.05	0.05	0.03

Figure 1: ADCP cross groyne transport Harle north

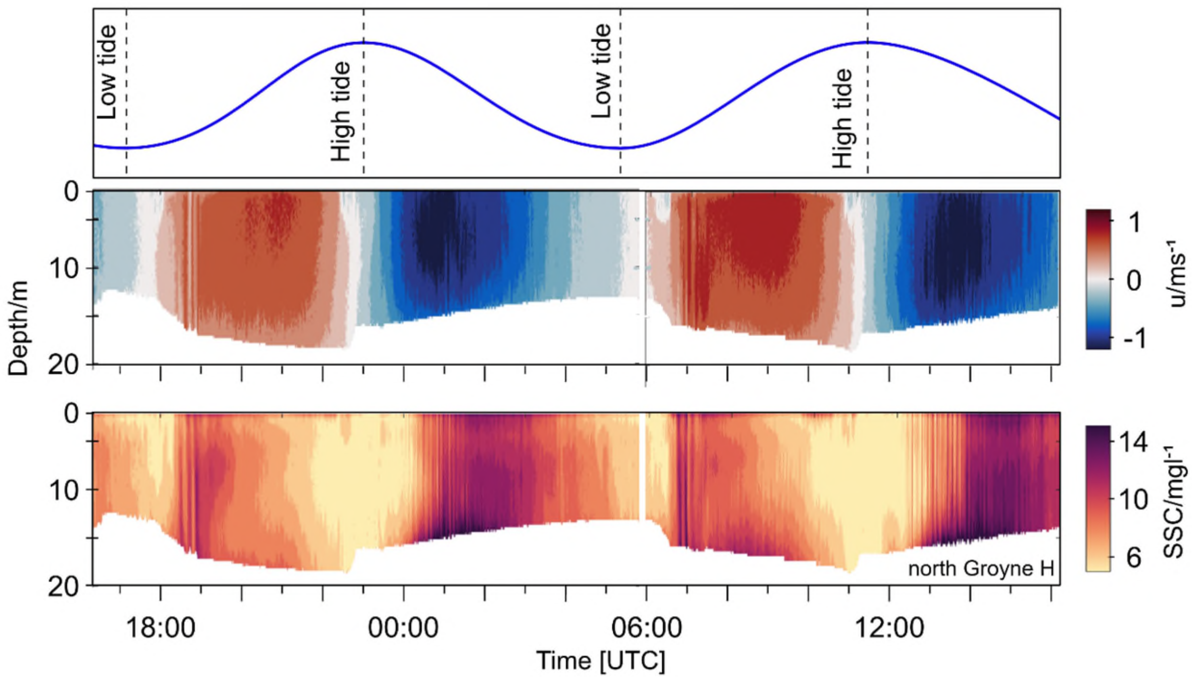

Figure 2: ADCP cross groyne transport Harle south

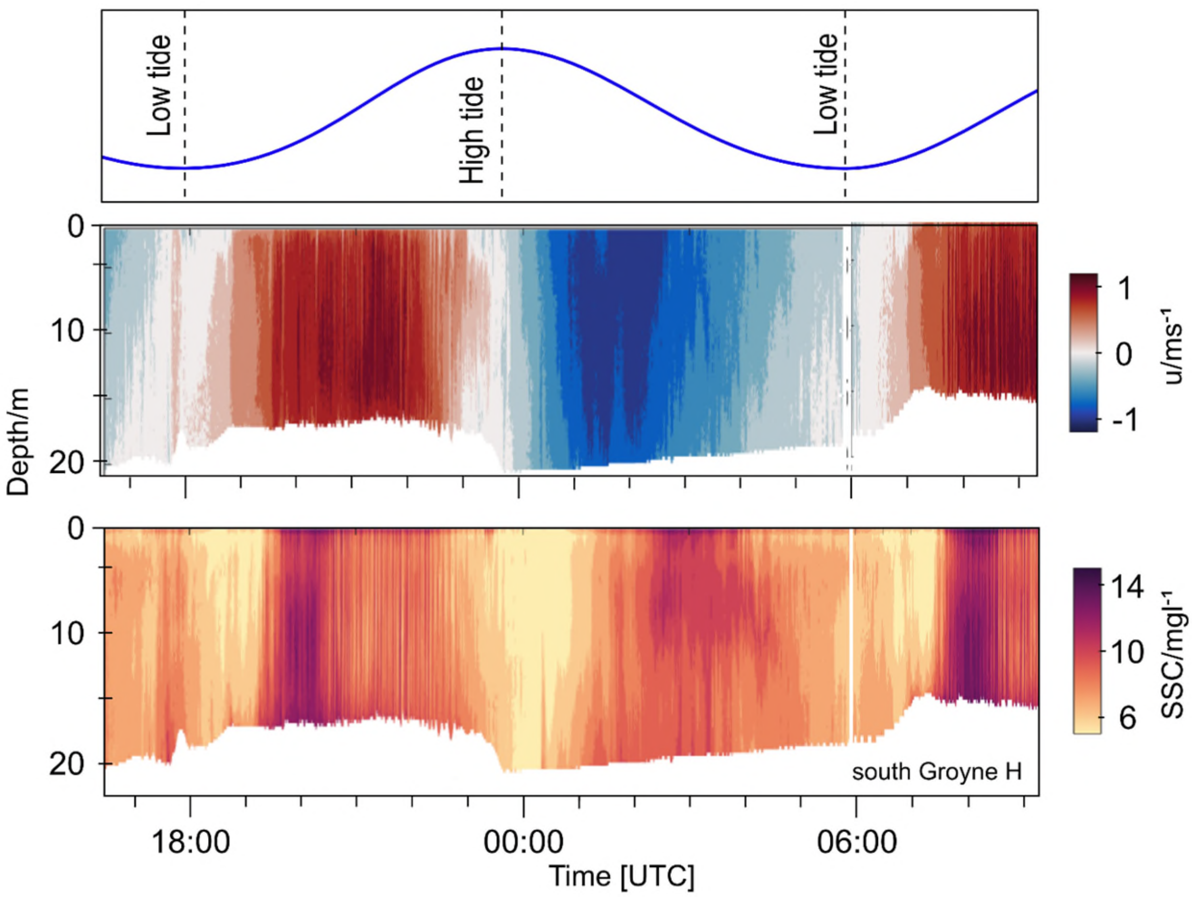

Curriculum vitae

Personal data

Full Name:	**Anna-Lena Geßner**
Date of Birth:	30.05.1996
Place of Birth:	Hamburg (Germany)

Education

10/2015 – 11/2018	Bachelor of Science/ Geosciences (Universität Hamburg)
10/2018 – 03/2021	Master of Science/ Geosciences (Universität Hamburg)

Work experience

Since 05/2021	Scientist at the Institute for Chemistry and Biology of the Marine Environment (ICBM) University of Oldenburg